Systems study for fuel cell powered more electric aircraft

Loughborough University

BAE SYSTEMS

INSPIRED WORK

Systems Study for Fuel Cell Powered More Electric Aircraft

by

Alex Thirkell

A Doctoral Thesis

Submitted in partial fulfilment of the requirements for the award of

Degree of Doctor of Philosophy of Loughborough University

June 2021

Abstract

In response to the increased demand for aircraft electrification and growing interest in fuel cell technology, a comprehensive study has been carried out to assess the suitability of fuel cells for a range of aircraft. Fuel cell systems, whether they are fuelled by gaseous hydrogen or a liquid alcohol must always be treated as a ‘system of systems’ and comprise four well defined, interlinked subsystems: fuel cell stack, fuel, oxidant and thermal management.

The key objectives of this work were to: define a methodology to predict the electrical requirements, propulsive or otherwise of any aircraft based on the highest level design information; critically analyse existing fuel cell technologies and down-select to two technologies; assess the required system of systems for the down-selected fuel cell technologies; and produce and evaluate a dynamic fuel cell system sizing model to assist aircraft designers during an aircraft's preliminary design phase.

Fifteen aircraft categories have been defined based on the aircrafts primary function and propulsion method. A model was then developed which can predict the electrical generation capability and propulsive requirements. Validating the categorisation model against real aircraft data showed a good correlation between the real and modelled data. Generally, an error of less than 5% was obtained by the model. The output of this model was used in the sizing of an appropriate fuel cell system.

A unique challenge to the integration of fuel cell systems in aircraft, the atmosphere was investigated. Three atmospheric models were presented and their usefulness discussed. The challenges to fuel cell system design are primarily ambient temperature and total pressure at altitude. In the field of electrochemistry it is usual to denote the partial pressure of oxygen in the cathode stream as a limiting factor. In reality, it is a combination of both the concentration of oxygen and the total pressure that influence performance. This important distinction is made as these variables can be controlled independently.

Six commercially available fuel cell technologies were reviewed for use in aeronautical applications. Hydrogen fed polymer electrolyte membrane and liquid fed direct methanol fuel cells were down-selected for further study. For each technology, an experimentally validated fuel cell stack model was created to describe the electrochemical reactions between their fuels and oxygen.

Different storage methodologies for molecular hydrogen, methanol and molecular oxygen were compared and optimum solutions in terms of storage efficiency were deduced based on aircraft mission length. A case study was carried out to investigate the system mass variation with altitude. Key variables included the performance derating of the fuel cell as well as the choice of either a compressor based air-breathing design or an air-independent alternative. It was found that an air-breathing solution is preferable for longer mission durations.

Primary thermal management strategies were compared for both fuel cell technologies. For hydrogen fed fuel cells the choice between air-cooling and liquid-cooling is based on the heat generation rate of the fuel cell. If the heat generation rate is less than 4 kW, an air-cooling strategy offers both system mass and volume benefits. For higher power systems, liquid-cooling should be used. Direct methanol fuel cells were shown to offer reduced system complexity from a thermal management perspective as the heat can be rejected to the unused fuel solution in the exhaust.

Four primary submodels, each representing a subsystem of the overall fuel cell system, were combined into a single, dual function dynamic fuel cell sizing model. The first function of this model was to physically size a fuel cell system based on primary design information and a flight profile. Secondary functionality was a dynamic representation of the fuel cell system response to the input current and altitude profiles. Case studies were carried out using the model Skywalker X8 and General Atomics MQ-1 Predator aircraft.

Acknowledgements

I would like to express my utmost thanks to Professor Rui Chen and Professor Lisa Jackson for their support, advice and supervision throughout the project and for providing the opportunity to carry out research in this increasingly competitive area. This work would also not have been possible without the financial support of the Engineering and Physical Sciences Research Council funded Centre for Doctoral Training in Hydrogen Fuel Cells and Their Fuels (Grant number: EP/L015749/1), and my industrial sponsor BAE Systems.

Thank-you to everyone who has helped in some way with my research. Thank-you to all those in the Department of Aeronautical and Automotive Engineering at Loughborough University who have been a part of my education since I started as an undergraduate student in 2011. A special thank-you to Andy Smith and Tom Childs who have helped me more than they know throughout the last four years.

I would also like to thank my family for their support, particularly my parents who continue to offer their encouragement from over 11,000 miles away.

Finally, a special thank-you to my partner Rebecca who has stuck by me through all of the ups and downs. From the times where it looked like there was no end in sight to the times of jubilation when the experiments worked and simulations completed.

Contents

List of Figures

List of Tables

Abbreviations

AFC	-	Alkaline Fuel Cell
APU	-	Auxiliary Power Unit
BoP	-	Balance of Plant
CGH_2	-	Compressed Gaseous Hydrogen
CGO_2	-	Compressed Gaseous Oxygen
CHP	-	Combined Heat and Power
CL	-	Catalyst Layer
conc’	-	Concentration
DI	-	De-Ionised
DMFC	-	Direct Methanol Fuel Cell
GDE	-	Gas Diffusion Electrode
GDL	-	Gas Diffusion Layer
HALE	-	High-Altitude Long-Endurance
HDPE	-	High Density PolyEthylene
HHV	-	Higher Heating Value
IPA	-	IsoPropyl Alcohol
ISA	-	International Standard Atmosphere
$LiCoO_2$	-	Lithium Cobalt Oxide
LH_2	-	Liquid Hydrogen
LHV	-	Lower Heating Value
LO_2	-	Liquid Oxygen
MAE	-	Mean Absolute Error
MALE	-	Medium-Altitude Long-Endurance
MCFC	-	Molten Carbonate Fuel Cell
MEA	-	Membrane Electrode Assembly
MoD	-	Ministry of Defence

MPL	-	Micro Porous Layer
MTOW	-	Maximum Take-Off Weight
$NaBH_4$	-	Sodium Borohydride
NB	-	Narrow Body
OCV	-	Open Circuit Voltage
PAFC	-	Phosphoric Acid Fuel Cell
PEM	-	Polymer Electrolyte Membrane
PEMFC	-	Polymer Electrolyte Membrane Fuel Cell
PTFE	-	PolyTetraFluoroEthylene
RAT	-	Ram Air Turbine
redox	-	REDuction/OXidation
RH	-	Relative Humidity
RMSE	-	Root-Mean-Square-Error
SOC	-	State Of Charge
SOFC	-	Solid Oxide Fuel Cell
UAS	-	Unmanned Aerial System
UAV	-	Unmanned Aerial Vehicle
WB	-	Wide Body
WLT	-	Wet Layer Thickness

Nomenclature

A	-	Cell active area (cm^2)
A_S	-	Surface area (m^2)
a	-	Chemical activity of species in reaction
a_i	-	Chemical activity of species “i” in reaction
C_d	-	Total drag coefficient
C_l	-	Lift coefficient

CPR	-	Compressor Pressure Ratio
c^0	-	Standard-state concentration (mol/dm^3)
c_i	-	Concentration of species "i" in reaction (mol/dm^3)
c_p	-	Specific heat at constant pressure (J/kgK)
D	-	Drag (N)
E_{net}	-	Available energy from fuel (J or kWh)
e	-	Specific energy (J/kg or kWh/kg) OR Error
F	-	Faraday constant (96,485 C/mol)
F_{TR}	-	Thrust force required (N)
$\Delta\overline{g}_{HHV}$	-	Absolute Gibbs free energy change (J/mol)
$\Delta\overline{h}_{HHV}$	-	Absolute enthalpy change (J/mol)
I	-	Current (A)
i	-	Current density (A/cm^2)
i_0	-	Exchange current density (A/cm^2)
i_n	-	Internal current density (A/cm^2)
K	-	Heat transfer coefficient (W/m^{2}K)
k	-	Thermal conductivity (W/mK)
M	-	Number of moles in balanced reaction
M_{air}	-	Molecular mass of air (28.96 g/mol)
M_{CH_3OH}	-	Molecular mass of methanol (42.04 g/mol)
M_{H_2}	-	Molecular mass of hydrogen (2.02 g/mol)
M_{O_2}	-	Molecular mass of oxygen (32 g/mol)
m	-	Mass (kg)
$\dot{m}_i$	-	Mass flow of species "i" (kg/s)
n	-	Number of cells OR Number of values
P_{comp}	-	Compressor power (W)

P_e - Electrical power (W)

P_R - Power required (W)

p_1 - Initial system pressure (Pa)

p_2 - Final system pressure (Pa)

p_{air} - Air pressure (Pa)

p_t - Total pressure (Pa)

$\dot{Q}$ - Heating rate (W)

R - Universal gas constant (8.314 J/molK)

R^2 - Coefficient of determination

S - Wing area (m^2)

$\Delta\bar{s}$ - Absolute entropy change (J/molK)

$\Delta\bar{s}_T$ - Absolute entropy change at temperature "T" (J/molK)

T - Temperature (K)

T_0 - Reference temperature (25°C / 298.15K)

T_1 - Inlet temperature (K)

T_2 - Exit temperature (K)

ΔT - Change in temperature (K)

$\dot{T}_{FC}$ - Rate of change of fuel cell temperature (K/s)

t - Time (s)

u - Energy density (J/m^3 or kWh/L)

V_0 - Reversible open circuit voltage (V)

ΔV_0 - Change in reversible open circuit voltage (V)

$V_{0\,HHV}$ - Reversible potential based on HHV of fuel (V)

$V_{0\,HHV}^{std}$ - Standard-state reversible potential (V)

V_c - Cell voltage (V)

V_{HHV} - Theoretical potential based on HHV of fuel (V)

V_{LHV}	-	Theoretical potential based on LHV of fuel (V)
vol	-	Volume
v_{∞}	-	Free stream air velocity (m/s)
W	-	Aircraft weight (N)
x	-	Mass transport loss empirical constant 1 (V)
y	-	Mass transport loss empirical constant 2 (cm^2/A)
Z	-	Gas deviation factor
z	-	Number of electrons transferred per mole of fuel

Greek

α	-	Charge transfer coefficient
α_t	-	Thermal diffusivity (m^2/s)
γ	-	Specific heat ratio
η_{comp}	-	Compressor efficiency
η_{FC}	-	Real fuel cell efficiency
η_{fuel}	-	Fuel utilisation coefficient
η_{volt}	-	Cell efficiency
λ	-	Stoichiometric factor
ρ_x	-	Density of "x" (kg/m^3)
ϱ_x	-	Partial pressure of "x" in balanced reaction (Pa)
Ω	-	Area specific resistance (Ωcm^2)

Chapter 1 Introduction

1.1 Motivations

Aircraft electrification is seen as the primary driving force towards the goal of significantly reducing aviation industry greenhouse gas emissions by 2050 [1-4]. Military applications would also benefit from increased aircraft electrification as the inherent reduction of both acoustic and thermal emissions would improve an aircraft's stealth.

A tool to quickly and easily predict the electrical generation capacity of existing aircraft has been identified as missing from the current literature. The use of such a tool would enable the requirements of electrical power generation systems to be defined early in the system design stage. Indeed, the need for power system flexibility has been identified as a primary design parameter in the BAE Systems Tempest programme [5].

Traditionally, increased electrification of systems is realised through the use of batteries. Fuel cell systems have been widely reported to offer significant advantages over batteries [6-11] in particular in the area of energy storage density [6]. However, the use of hydrogen as an energy carrier can present a challenge due to the chemical properties of the molecule [12-14]. One potential solution is to use a liquid energy carrier such as methanol. A system of systems comparison between the two technologies would provide interesting insights into the problem and potential solution.

Fuel cell modelling efforts centred around detailed electrochemical principles are the focus of a majority of existing literature [15-25]. Additionally, research has focused on modelling the thermodynamics of fuel cells [26,27] and their transient response under various operating conditions [28-31]. This work will differ from the masses as it will focus on the challenges associated with the fuel cell system. These challenges can be grouped into those associated with each subsystem in the overall system: fuel cell stack, fuel storage and delivery, oxidant and thermal management.

The reduction of harmful emissions from the aviation sector, a key motivation of this work is shared by a large European Consortium Joint Undertaking who published a report at the end of 2020 [1]. This report gives an excellent high-level overview of the economics and climate impact associated with the integration of hydrogen technologies in aviation. The work presented in this Thesis offers additional insight into this field through the development of novel modelling techniques for fuel cell powered more electric aircraft.

1.2 Current Research Aim and Objectives

The aim of this study was to:

Explore the applicability and limitations of utilising fuel cells for the purpose of aircraft electrification

The key objectives of this study were to:

1. Define a methodology to predict the electrical requirements, propulsive or auxiliary of any aircraft based on the highest level design information.
2. Critically analyse existing fuel cell technologies and down-select to two technologies. Assess the required balance of plant necessary for a complete system of systems for the down-selected fuel cell technologies.
3. Produce and evaluate a dynamic fuel cell system of systems sizing model to assist aircraft designers during an aircraft's preliminary design phase.

1.3 Knowledge Contribution

A validated aircraft characterisation model based on a unique database of 519 current (as of 2020) commercial aircraft has been created and published [32]. The model enables the prediction of an aircraft's electrical generation capability or propulsive requirements using readily available, high-level aircraft design information.

A system of systems analysis model was created, presented and published which compared Polymer Electrolyte Membrane (PEMFC) and Direct Methanol Fuel Cell (DMFC) technologies directly [33]. Although the focus of this publication was the automotive market, the same approach was applied to aircraft during this Thesis.

To the authors' knowledge this work represents one of the first documented fuel cell system models to use a ‘system of systems’ approach, account for altitude effects on system design and be suitable for different aircraft types and mission requirements.

1.4 Thesis Outline

This Thesis is written using a paper-style format where each of the Chapters has been designed as a stand-alone item to aid ease of reading whilst contributing to the aim and objectives.

Chapter 2 discusses the need for increased aircraft electrification and details the work carried out and results produced from the aircraft electrical characterisation model.

Chapter 3 provides detailed information on various fuel cell types and the reasoning behind the downselection of polymer electrolyte membrane and direct methanol fuel cell technologies.

Chapter 4 covers the creation of a fuel cell potential equation which accounts for variations in electrical potential as a result of pressure, fluid concentration and temperature.

Chapter 5 compares and contrasts different fuel storage systems for both molecular hydrogen and liquid methanol. Optimum solutions in terms of specific energy and energy density are determined for each fuel type.

Chapter 6 introduces the concepts of air-breathing, air-independant and hybrid designs for fuel cell oxidant systems.

Chapter 7 discusses the four main thermal management strategies for fuel cells along with their typical applications and potential limitations.

Chapter 8 provides a summary of the previous chapters’ contributions to the overall dynamic system of systems fuel cell model. Case studies are then carried out on a range of aircraft to demonstrate the applicability of the model.

1.5 References

[1] McKinsey & Company, Clean Sky 2 JU, Fuel Cells and Hydrogen 2 JU. Hydrogen-powered aviation A fact-based study of hydrogen technology, economics, and climate impact by 2050. 1st ed. McKinsey & Company; 2020. https://doi.org/10.2843/471510.

[2] International Air Transport Association. IATA 2015 Report on Alternative Fuels. Montreal-Geneva: 2015.

[3] Epstein AH, O'Flarity SM. Considerations for reducing aviation's CO2 with aircraft electric propulsion. J Propuls Power 2019;35:572–82. https://doi.org/10.2514/1.B37015.

[4] United Nations. Paris Agreement. 2015. https://doi.org/FCCC/CP/2015/L.9.

[5] Walker N, Garraway A, Brooke-Holland L, Mills C. Combat Air Strategy progress and next steps Compiled by : 2019.

[6] Munoz-ramos K, Pratt JW, Akhil AA, Schenkman, Benjamin L. Klebanoff LE, Curgus DB. Electrical Analysis of Proton Exchange Membrane Fuel Cells for Electrical Power Generation On-Board Commercial Airplanes. IEEE Transp. Electrif. Conf. Expo, 2012, p. 1–6.

[7] Chao CH, Shieh JJ. A new control strategy for hybrid fuel cell-battery power systems with improved efficiency. Int J Hydrogen Energy 2012;37:13141–6. https://doi.org/10.1016/j.ijhydene.2012.03.143.

[8] Wang Y, Chen KS, Mishler J, Cho SC, Adroher XC. A review of polymer electrolyte membrane fuel cells: Technology, applications, and needs on fundamental research. Appl Energy 2011;88:981–1007. https://doi.org/10.1016/j.apenergy.2010.09.030.

[9] Rayment C, Sherwin S. Introduction to Fuel Cell Technology. 2003. https://doi.org/10.1.1.129.3231&rep=rep1&type=pdf.

[10] Larminie J, Dicks A. Fuel Cell Systems Explained. 2nd ed. John Wiley & Sons; 2003. https://doi.org/10.1016/S0378-7753(00)00571-1.

[11] O'Hayre R, Cha S-W, Colella W, Prinz FB. Fuel cell fundamentals. 3rd ed. John Wiley & Sons; 2016.

[12] Tavares S. Aerospace engineering pocket reference. Taylor & Francis; 2015.

[13] National Institute of Standards and Technology. Thermophysical Properties of Fluid Systems. NIST Chem WebBook, SRD 69 2018. https://webbook.nist.gov/chemistry/fluid/ (accessed April 17, 2021).

[14] National Institute of Standards and Technology. Saturation Properties for Hydrogen — Pressure Increments. NIST Chem WebBook, SRD 69 n.d. https://webbook.nist.gov/cgi/fluid.cgi?Action=Load&ID=C1333740&Type=SatT&

Digits=5&PLow=.5&PHigh=1.5&PInc=.1&RefState=DEF&TUnit=K&PUnit=atm&DUnit=kg/m3&HUnit=kJ/mol&WUnit=m/s&VisUnit=uPa*s&STUnit=N/m (accessed June 24, 2020).

[15] Wang C, Hashem Nehrir M, Shaw S. Dynamic models and model validation for PEM fuel cells using electrical circuits. IEEE Trans Energy Convers 2005;20:442–51. https://doi.org/10.1109/pes.2005.1489284.

[16] Monem AA A El, M Azmy A. Dynamic Modelling of Proton Exchange Membrane Fuel Cells for Electric Vehicle Applications. J Pet Environ Biotechnol 2014;5. https://doi.org/10.4172/2157-7463.1000169.

[17] Boccaletti C, Duni G, Fabbri G, Santini E. Simulation models of fuel cell systems. Proc ICEM, Electr Mach … 2006:1–6.

[18] Ko J, Chippar P, Ju H. A one-dimensional, two-phase model for direct methanol fuel cells - Part I: Model development and parametric study. Energy 2010;35:2149–59. https://doi.org/10.1016/j.energy.2010.01.034.

[19] Springer TE. Modeling and Experimental Diagnostics in Polymer Electrolyte Fuel Cells. J Electrochem Soc 1993;140:3513. https://doi.org/10.1149/1.2221120.

[20] Pathapati PR, Xue X, Tang J. A new dynamic model for predicting transient phenomena in a PEM fuel cell system. Renew Energy 2005;30:1–22. https://doi.org/10.1016/j.renene.2004.05.001.

[21] Wilberforce T, El-Hassan Z, Khatib FN, Al Makky A, Baroutaji A, Carton JG, et al. Modelling and simulation of Proton Exchange Membrane fuel cell with serpentine bipolar plate using MATLAB. Int J Hydrogen Energy 2017;42:25639–62. https://doi.org/10.1016/j.ijhydene.2017.06.091.

[22] SALEH IMM, ALI R, ZHANG H. Simplified mathematical model of proton exchange membrane fuel cell based on horizon fuel cell stack. J Mod Power Syst Clean Energy 2016;4:668–79. https://doi.org/10.1007/s40565-016-0196-5.

[23] Abdin Z, Webb CJ, Gray EMA. PEM fuel cell model and simulation in Matlab–Simulink based on physical parameters. Energy 2016;116:1131–44. https://doi.org/10.1016/j.energy.2016.10.033.

[24] Khan F, Nawaz A, Muhammad MA, Khadim MA. Review And Analysis Of MATLAB® Simulink Model Of PEM Fuel Cell Stack. Int J Eng Comput Sci 2013;13:31–4.

[25] Lee JH, Lalk TR, Appleby a. J. Modeling electrochemical performance in large scale proton exchange membrane fuel cell stacks. J Power Sources 1998;70:258–68. https://doi.org/10.1016/S0378-7753(97)02683-9.

[26] Argyropoulos P, Scott K, Taama WM. One-dimensional thermal model for direct methanol fuel cell stacks. Part I. Model development. J Power Sources 1999;79:169–83. https://doi.org/10.1016/S0378-7753(99)00181-0.

[27] Argyropoulos P, Scott K, Taama WM. One-dimensional thermal model for direct methanol fuel cell stacks. Part II. Model based parametric analysis and predicted temperature profiles. J Power Sources 1999;79:184–98. https://doi.org/10.1016/S0378-7753(99)00182-2.

[28] Xu C, Zhao TS, Yang WW. Modeling of water transport through the membrane electrode assembly for direct methanol fuel cells. J Power Sources 2008;178:291–308. https://doi.org/10.1016/j.jpowsour.2007.11.098.

[29] Amphlett JC, Mann RF, Peppley BA, Roberge PR, Rodrigues A. A model predicting transient responses of proton exchange membrane fuel cells. J Power Sources 1996;61:183–8. https://doi.org/10.1016/S0378-7753(96)02360-9.

[30] Kim J, Lee S, Srinivasan S, Chamberlin CE, Kim J, Lee S, et al. Modeling of Proton Exchange Membrane Fuel Cell Performance with an Empirical Equation. J Electrochem Soc 1995;142:2670–4. https://doi.org/10.1149/1.2050072.

[31] Petrinić M, Jakopović Ž. Modeling and simulation of PEM fuel cell - Power converter system. MIPRO 2007 - 30th Jubil Int Conv Proc Microelectron Electron Electron Technol Hypermedia Grid Syst MEE /HGS 2007;1:151–6.

[32] Thirkell A, Chen R, Harrington I. A Fuel Cell System Sizing Tool Based on Current Production Aircraft. Fort Worth, Texas: SAE International; 2017. https://doi.org/10.4271/2017-01-2135.

[33] Thirkell A, Chen R. Comparison of Gaseous and Liquid Fuel Cells for Automotive Applications. In: Razi Nalim M, Vasudevan R, Rahetekar S, editors. Adv. Automot. Technol. 1st ed., Springer Singapore; 2020. https://doi.org/10.1007/978-981-15-5947-1.

Chapter 2 More Electric Aircraft

2.1 The Need for Electrification

Several factors are driving the rapid increase in aircraft electrification and popularity of more electric aircraft such as the Boeing 787. The main driving factor for the whole aviation industry is the pressure to significantly reduce harmful emissions by 2050 [1,2]. The importance of reducing the anthropogenic effects on climate change was demonstrated in 2015 by the signing of the Paris Agreement by nearly 200 countries [3].

When looking at military aviation specifically, the operational environmental impact, although still important, is not the key factor driving the move to increased electrification. The use of increased electrification (or total electrification) has the potential to reduce the observability (both acoustic and thermal) of the aircraft.

The primary sources of both acoustic and thermal emissions from aircraft are concentrated around the motive power plant. Acoustic emissions are most evident from the movement of air by the propulsor, either propeller or fan and the engine exhaust. Thermal emissions are primarily associated with the engine exhaust and can reach over 650 ℃ [4]. Both emissions can be reduced through increased electrification by two means:

1. Engine downsizing, as a result of demands being taken away from the gas turbine engine and being given to an alternative, low-temperature power source. This would result in a more electric aircraft.
2. Engine replacement, using an electrically driven propeller. This is likely to be combined with a reduction in aircraft size and speed requirements. Hypothetically, this could be an ideal scenario for a surveillance High-Altitude Long-Endurance (HALE) Unmanned Aerial Vehicle (UAV). The result of this scenario would be a fully electric aircraft. This aircraft type can also be defined as one with no on-board internal combustion power source.

The main bulk of this Thesis will be centered around the use of low-temperature fuel cells as an alternative electrical power provider onboard more-electric and fully-electric aircraft. In advance of this discussion a grounding must first be set by looking at the existing electrical generation methods and how to predict required capacity.

2.2 Aircraft Electrical Power

In modern aircraft, a majority of electrical power produced onboard is done so using rotating machines. Typically these are driven mechanically from the powerplant or Auxiliary Power Unit (APU) or motored by the freestream airflow around the aircraft in the case of emergency Ram Air Turbines (RAT). Currently, the state of the art power density for an engine driven starter-generator unit coupled with the necessary power conversion unit is 500 W/kg [5].

As the trend towards more-electric and eventually all-electric aircraft, other conventional secondary power systems such as pneumatic, hydraulic and mechanical will need to be converted to either electrically supported or fully electric systems. Currently, these secondary power systems along with existing electrical systems account for approximately 5% of the total flight fuel burn [6]. Therefore, any efficiency increase associated with the change from traditional secondary systems to electrified systems will lead to operational cost savings.

A tool to quickly and easily predict the electrical generation capacity of existing aircraft is missing from the current literature. The understanding which could be gained by someone using such a tool would greatly help with the first step in designing alternative electrical generation methods such as fuel cell systems. This section will centre on a piece of work published as an SAE Technical Paper at the SAE Aerotech International Congress and Exhibition 2017 [7] which details the categorisation of aircraft for the purpose of electrical generation capacity prediction.

2.2.1 Aircraft Categorisation

It was hypothesised that it is possible to relate the electrical generation capability of an aircraft to basic design parameters. The first step in proving this was collating data for 519 aircraft for categorisation [8-18]. The sources used for the collation of this dataset were deemed highly reliable. Five [8-12] were from the Jane's series of aircraft reference books, three [13-15] were aircraft training manuals and the final three [16-18] were direct references from manufacturers' websites.

These aircraft were categorised using a two-step method. Initially, 11 categories were defined based on an aircraft's primary role and easily distinguishable physical characteristics. These categories are summarised in Table 2.1. Each category was further subdivided based on its propulsion method into those propelled by a propeller and those propelled by a jet derived engine. This gave a total of 15 sub-categories for the model to be based on.

Table 2.1: Aircraft category definitions and number included in study

Aircraft Category	**Key Characteristics**	**Number In Dataset**
Fuel cell (propeller)	Primary power source must be a fuel cell. The aircraft can be either manned or unmanned.	6
All-electric (propeller)	Propulsion must be provided by an electric motor and electricity must not be supplied by a fuel cell.	9
Unmanned (propeller)	Any fixed wing aircraft which is either remotely piloted or autonomously controlled and is not all electric or fuel cell.	29
Bomber and surveillance (propeller)	Aircraft designed for the primary role of dropping ordinance or performing surveillance.	20
Fighter and trainer (jet)	A manned aircraft, primary role as a military fighter or trainer. These aircraft typically have a high thrust to weight ratio	35
Fighter and trainer (propeller)		15
Transport (jet)	Typically, a military aircraft for transporting personnel. Aircraft in this category generally have Maximum Take-Off Weight (MTOW) greater than 100,000 kg.	9
Transport (propeller)		21
Airliner and freighter (jet)	Typically, large multi-engine aircraft.	43
Airliner and freighter (propeller)		5
Business (jet)	An aircraft typically designed for transporting small groups of people. This category also includes privatised versions of larger aircraft.	56
Business (propeller)		9
Utility	Typically, a small, general-purpose aircraft for transporting people or freight.	49
Amphibian	More specialised aircraft designed to take-off from and land on water.	30
Lightplane	Any aircraft that does not fit into another category and has a MTOW less than 3,500 kg.	183

2.2.2 UAV Classifications

Unmanned Aerial Vehicles (UAV) are defined by the UK Ministry of Defence (MoD) as “an aircraft that does not carry a human operator, is operated remotely using varying levels of automated functions, is normally recoverable, and can carry a lethal or non-lethal payload” [19]. They are a component of an Unmanned Aerial Systems (UAS) which also includes the ground control elements required for operation.

Unmanned aerial vehicles are generally expected to replace a majority of military manned aircraft operations in the near future [19]. Their adoption into the UK military core equipment programme has been accelerated over the last five years [20], supported by the highest level of government. Both the Prime Minister and Deputy Prime Minister noted in 2010 that “The fast jet fleet will be complemented by a growing fleet of Unmanned Air Vehicles in both combat and reconnaissance roles” [21].

If UAVs are to truly serve a variety of functions in the future of military aviation, then there will need to be as much variety in size and operational capability as there is in the realm of conventional, manned aircraft. Indeed, the classification of UAVs is non-trivial due to their diverse range of capabilities and sizes. However, the MoD has developed a rather elegant methodology which classifies UAVs into three groups based on their gross take-off weight and further subdivides based on primary function and normal operating altitude. A condensed version of the information contained within Joint Doctrine Note 2/11 [19] is shown in Table 2.2.

Table 2.2: Condensed guide to unmanned aerial vehicle classification [19]

Classification	**Category**	**Normal Operating Altitude**	**Example Platforms**
Class I < 150 kg	MICRO < 2 kg	< 200 ft	Black Widow
	MINI 2-20 kg	< 3,000 ft	Scan Eagle, Raven
	SMALL 20-150 kg	< 5,000 ft	Hermes 90, Luna
Class II 150-600 kg	TACTICAL	< 10,000 ft	Aerostar, Watchkeeper
Class III > 600 kg	Medium-Altitude Long-Endurance (MALE)	< 45,000 ft	Heron, Reaper
	High-Altitude Long-Endurance (HALE)	< 65,000 ft	Global Hawk
	STRIKE / COMBAT	< 65,000 ft	N/A

2.2.3 Trend Generation

For each sub-category, with UAVs assumed to be of a single classification, the Maximum Take-Off Weight (MTOW) was related to either the propulsive power or maximum thrust produced by the aircraft. This provided a good correlation as expected from the form of the standard aircraft thrust and power equations (Equation 2.1 and 2.2) which directly relate the thrust or power required to aircraft weight for straight and level flight [22]. These equations are included here for the reader's reference. All modelling carried out as part of this study utilised the generated empirical relationships.

$$F_{TR} = D = \tfrac{1}{2}\rho_\infty v_\infty^2 S C_d = \frac{W}{C_l/C_d} \qquad (2.1)$$

$$P_R = F_{TR} v_\infty = D v_\infty = \frac{W}{C_l/C_d} \bullet v_\infty \qquad (2.2)$$

Where:

C_d - Total drag coefficient

C_l - Lift coefficient

D - Drag (N)

F_{TR} - Thrust force required (N)

P_R - Power required (W)

S - Wing area (m^2)

v_∞ - Free stream air velocity (m/s)

W - Aircraft weight (N)

ρ_∞ - Free stream air density (kg/m^3)

Changes in MTOW were also found to correlate well with the electrical generation capability of each of the aircraft. The electrical generation capability of an aircraft was defined as the total capacity of all engine mounted generators as well as any capability provided by an APU.

Each relationship was refined systematically by curve fitting raw aircraft data using the least squares method to obtain a minimum R^2 value. When considering trendline options in Excel, the focus was on linear and polynomial types as exponential and power lines lead to an inaccurate Coefficient of Determination R^2 [23].

When considering the regression analysis carried out by Excel, R^2 can have a value between zero and one. The larger the value of R^2 the smaller the residual sum of squares and therefore the better fit the trendline is to the data [24]. In some cases, the researched dataset limits the reliability of the empirical relationships. This is because for some aircraft categories the number of aircraft in each MTOW range are not evenly distributed. This can cause some empirical relationships to be sensitive to one or two of the included data points.

Figure 2.1 shows the refined relationships for existing propeller driven bomber and surveillance aircraft. All of the aircraft included in this trend are propelled using propellers, either by a piston engine or turboprop. The refined correlations for both the propulsive power

change with MTOW and on-board electrical generation with MTOW show an excellent fit with the collected real aircraft data. Calculated fits and R^2 values are shown in Table 2.3.

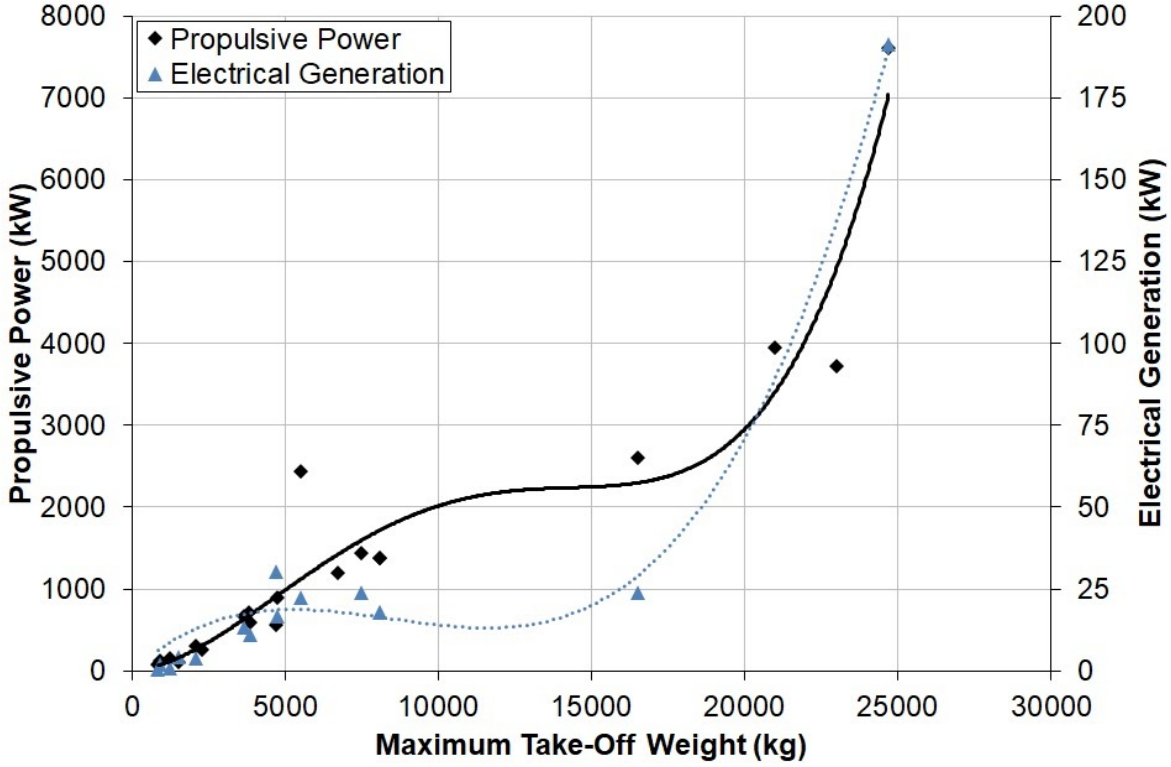

Figure 2.1: Refined correlations for existing propeller driven bomber and surveillance aircraft

Table 2.3: Fits and R^2 values for correlations from Figure 2.1

Plot	**Fitted Correlation (u = MTOW)**	**R^2**
Propulsive power	$P = 1E^{-13}u^4 - 5E^{-9}u^3 + 6E^{-5}u^2 + 3.14E^{-2}u$	0.93
Electrical generation	$P = 5E^{-11}u^3 - 1E^{-6}u^2 + 8.4E^{-3}u$	0.98

Figure 2.2 shows the refined correlations for existing fuel cell powered aircraft. All the aircraft used in the construction of this chart were propelled by a propeller attached to an electric motor. The correlations for the six existing fuel cell aircraft are exceptional. However, the limited amount of data available for these aircraft may be skewing the results.

Calculated fits and R^2 values are shown in Table 2.4. Appendix 2 contains the additional 13 refined correlations.

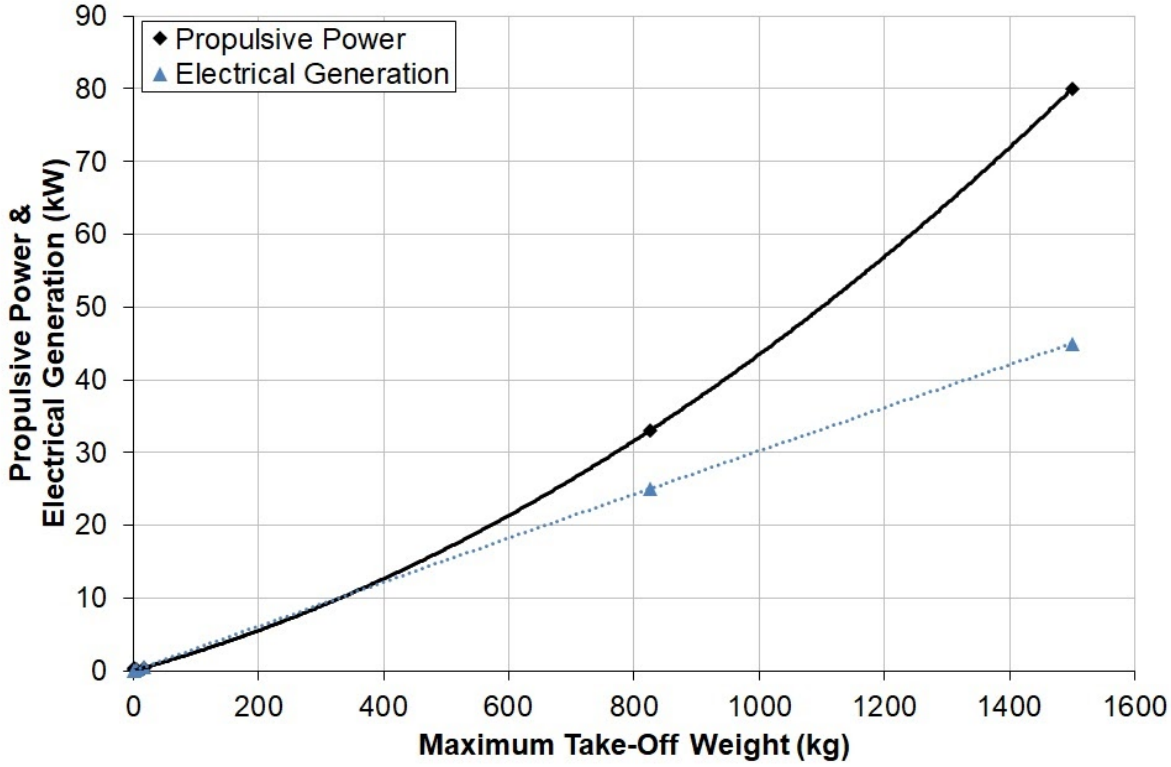

Figure 2.2: Refined correlations for existing fuel cell powered aircraft

Table 2.4: Fits and R^2 values for correlations from Figure 2.2

Plot	**Fitted Correlation (u = MTOW)**	**R^2**
Propulsive power	$P = 2E^{-5}u^2 + 2.37E^{-2}u$	1.0
Electrical generation	$P = -4E^{-7}u^2 + 3.07E^{-2}u$	1.0

2.2.4 Results

Outputs from the aircraft categorisation model were compared with real data for a selection of production aircraft which were excluded from the trend generation. A range of categories were used for validation as each is based on different relationships. Validation results are shown in Table 2.5.

Table 2.5: Model results for aircraft electrical generation prediction

Aircraft	**Electrical Generation Capability Prediction**		
	Real	Model	Error
Lockheed Martin F-35B (fighter & trainer)	60 kW	58 kW	3.3%
Airbus A400M (transport)	225 kW	226 kW	0.4%
Reims F406 (utility)	7 kW	6.6 kW	6.3%
Aviat Husky A-1 (lightplane)	0.98 kW	0.96 kW	2.0%

The results from the validation show a good correlation between the real and modelled data. Generally, an error of less than 5% was obtained by the model. Certain instances were higher than this cut-off. This occurs in cases where a category consists of a small dataset.

Additional application of the model can be made to hypothetical aircraft to provide a preliminary estimation of the power required, with propulsive or auxiliary. For a small Class I UAV with a MTOW of 150 kg, a fuel cell with a power output of 18 kW would be required to provide propulsive duties. Alternatively, a business jet requiring fuel cell auxiliary power and with a MTOW of 50 tonnes would require an 87 kW fuel cell system.

2.3 Aircraft Specific Considerations

In comparison to both the automotive and marine industries, there are several aircraft-specific considerations that directly impact the design of alternative electricity generation systems. Specifically, these can be grouped into two main sections. The first being the extreme operating environment associated with altitude and the second being increased packaging constraints, including more stringent requirements for physical size and mass. In this section

design consideration will be introduced and the implications on the system discussed. This will be expanded into specific effects on performance in later chapters.

2.3.1 Operating Environment

During operation, aircraft operate at an elevated altitude. This can range from just above sea-level for small remotely operated UAV to in excess of 60,000 ft (18,290 m), the certified altitude for a Northrop Grumman RQ-4B Global Hawk [12]. As altitude increases the properties of air change. Of primary concern to the design of a fuel cell system are the temperature and pressure of the air. Another important parameter which must be considered if an air compressor is required is the density of the air. This can be found from the modified ideal gas equation shown in Equation 2.3.

$$\frac{p_{air}}{T_{air}} = \varrho_{air} \frac{R}{M_{air}} \qquad (2.3)$$

Where:

M_{air} - Molecular mass of air (28.96 g/mol)

p_{air} - Air pressure (Pa)

R - Universal gas constant (8.314 J/molK)

T_{air} - Air temperature (K)

ρ_{air} - Air density (kg/m^3)

When considering how the mean air temperature and pressure change with increasing altitude, the first place people turn to for information is the International Standard Atmosphere (ISA) [25]. For the majority of the world land mass the data contained in the ISA is good to use. However, there are regions which have mean average temperatures either substantially higher or lower than those included in the ISA. One of the common standards used for defining the locations of the “hot” and “cold” regions is shown in Figure 2.3, taken from MIL-STD-210C, contained within MIL-HDK-310 [26].

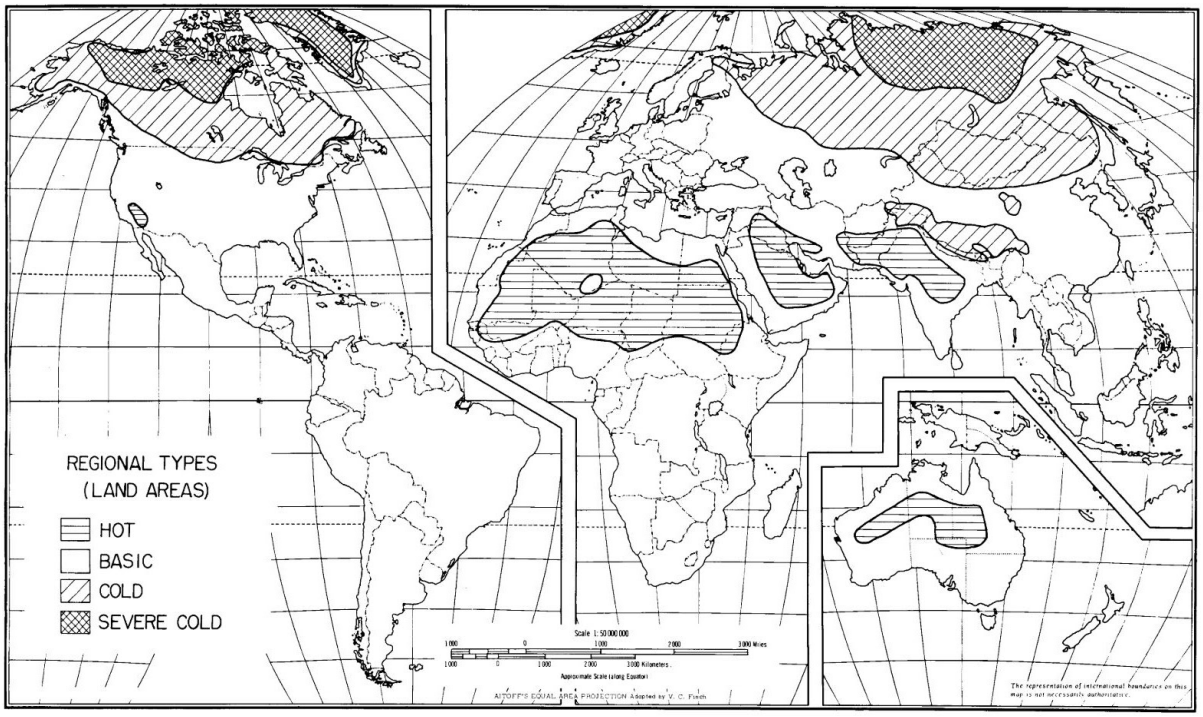

Figure 2.3: Location of Climatic Regional Types for the Land Areas of the World [26]

Using Figure 2.3 as a reference, “Basic” type land areas are suitably covered by the data contained within the ISA [25]. Data for “Hot” type land areas was taken from Table 5.3.1.1.2 and for “Cold” type land areas, Table 5.3.1.2.2 both from MIL-HDBK-310 [26]. Both sets of data provide temperatures expected 1% of the time which suitably covers the requirement of any system to cope with extreme environments. All three plots of temperature variation with altitude are included in Figure 2.4.

As mentioned earlier, in addition to the variation in air temperature, the variation in air pressure with increasing altitude is also of crucial importance to the design of a fuel cell system for an aircraft. This is because air compressor performance is directly related to the pressure and temperature of the inlet air.

Unlike temperature, the three atmospheric models (ISA, MIL-HDBK-310 Hot and MIL-HDBK-310 Cold) all show the same mean air pressure variation with increasing altitude. Figure 2.5 shows the variation of pressure with altitude.

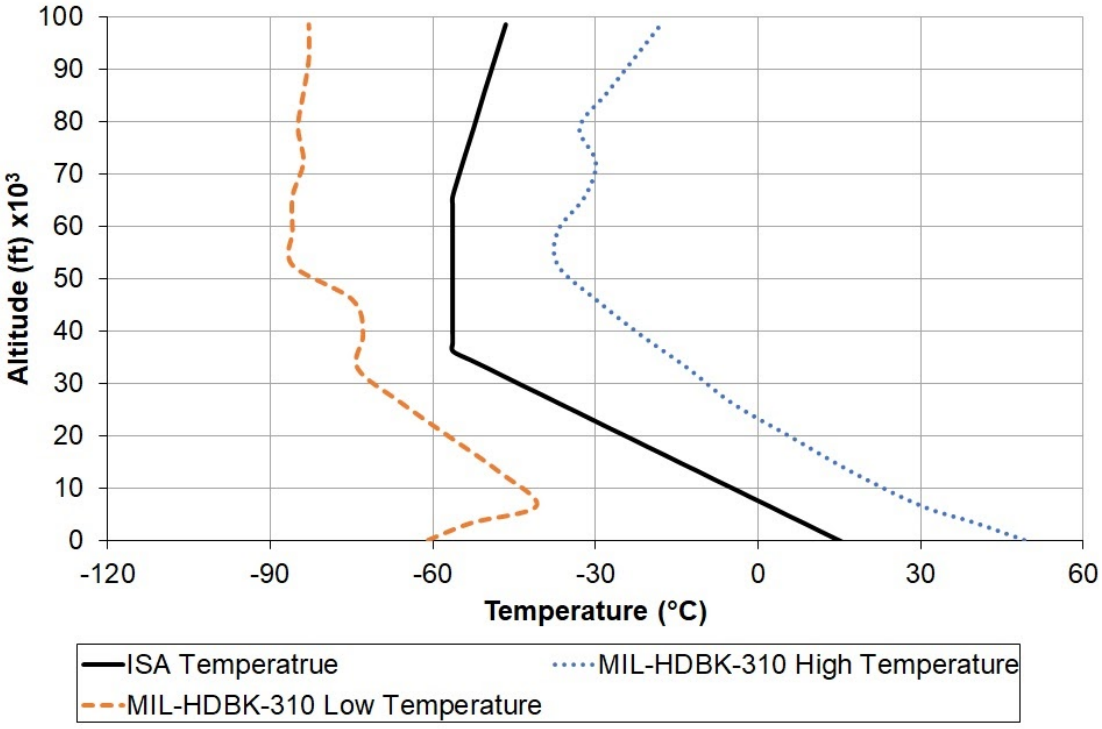

Figure 2.4: Temperature variation with altitude based on the International Standard Atmosphere [25] and MIL-HDBK-310 [26]

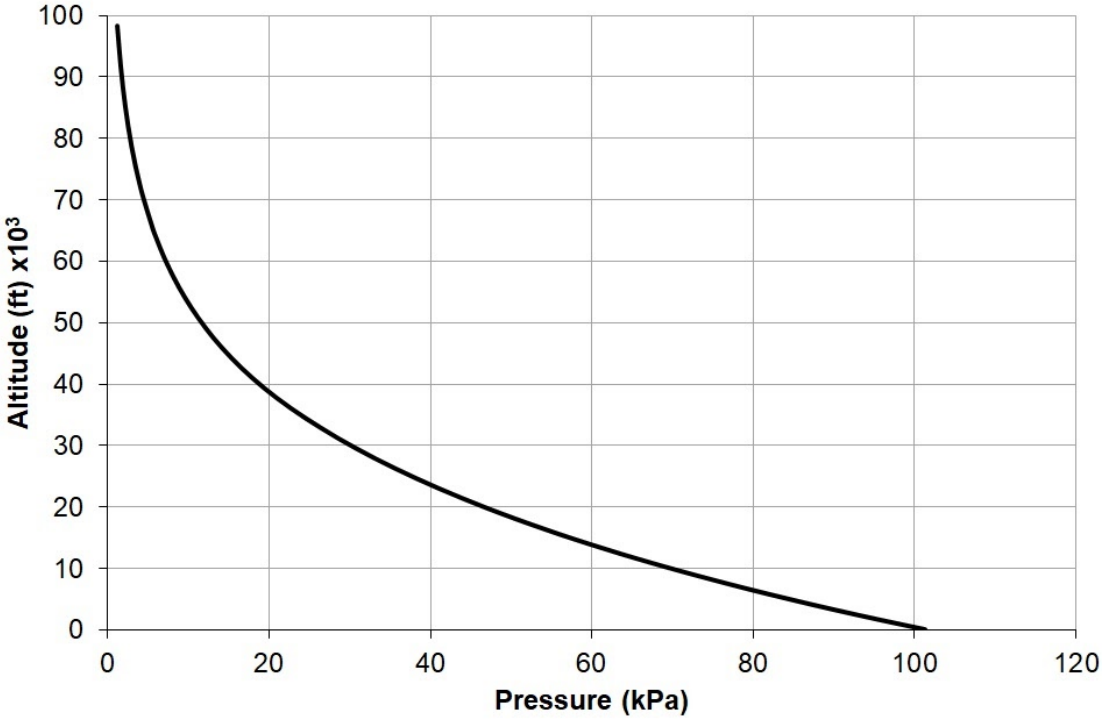

Figure 2.5: Pressure variation with altitude [25,26]

2.3.2 System Packaging

The term “system packaging” can be divided into three key elements: mass, size (volume) and subsystem arrangement. Unlike many other industries, such as the automotive and marine sectors, in the aeronautical environment, all three of these elements are mission critical.

This Thesis will cover the optimisation of system mass and volume for different arrangements of fuel cell technology. The specific arrangement of the subsystems or components are beyond the scope of this work as they would be covered in the detailed design phase of a project.

However, the author would like to emphasise that the flexibility to arrange and rearrange the components and subsystems of the complete fuel cell system must still be given consideration at this early stage or all preliminary design work would be wasted.

2.4 Summary

The rate of aircraft electrification is increasing and combined with the ever present environmental pressures, a greater focus is being made on the research and development of novel (to aircraft) electrical generation technologies. To enable efficient preliminary design decisions on fuel cell systems for aeronautical applications, a predictive tool was constructed to quickly estimate the peak electrical demand of the user's aircraft.

Fifteen aircraft categories have been defined based on the aircrafts primary function and propulsion method. A model was then developed which can predict the electrical generation capability and propulsive requirements. Validating the categorisation model against real aircraft data showed a good correlation between the real and modelled data. Generally, an error of less than 5% was obtained by the model. Certain instances, higher than this cut-off percentage arose when the model was based on a small dataset.

When designing the subsystems required to support the operation of a fuel cell (Chapters 5-7) there are considerations specific to aeronautical applications which must be considered. Of primary concern is the extreme operating environment (low temperature and pressure) provided by high-altitude flight. Three atmospheric models have been introduced and will be used when modelling the fuel cell subsystems.

2.5 References

[1] International Air Transport Association. IATA 2015 Report on Alternative Fuels. Montreal-Geneva: 2015.

[2] Epstein AH, O'Flarity SM. Considerations for reducing aviation's CO2 with aircraft electric propulsion. J Propuls Power 2019;35:572–82. https://doi.org/10.2514/1.B37015.

[3] United Nations. Paris Agreement. 2015. https://doi.org/FCCC/CP/2015/L.9.

[4] DeSilva U, Bunce RH, Claussen H. Novel gas turbine exhaust temperature measurement system. ASME Turbo Expo, vol. 4, 2013, p. 1–8. https://doi.org/10.1115/GT2013-95152.

[5] Astronics. COREPOWER 1425 400 Amp Power Conversion Unit n.d. https://www.astronics.com/docs/default-source/aes-docs/tier-iii/data-sheets/1425-pcu.pdf?sfvrsn=6f2eab58_12 (accessed March 24, 2020).

[6] Moir I, Seabridge A, Jukes M. Electrical Systems. Civ. Avion. Syst. 2nd ed., John Wiley & Sons; 2013, p. 235–90.

[7] Thirkell A, Chen R, Harrington I. A Fuel Cell System Sizing Tool Based on Current Production Aircraft. Fort Worth, Texas: SAE International; 2017. https://doi.org/10.4271/2017-01-2135.

[8] Gunston B, Willis D, Munson K, Peacock L, Jackson P, Bushell S, editors. Jane's all the world's aircraft: development & production 2016-2017. IHS; 2016.

[9] Gunston B, Willis D, Munson K, Peacock LT, Jackson P, Bushell S, editors. Jane's all the world's aircraft: development & production 2015-2016. IHS; 2015.

[10] Gunston B, Willis D, Munson K, Peacock LT, Jackson PA, Bushell S, editors. Jane's all the world's aircraft: development & production 2014-2015. IHS; 2014.

[11] Endres GG, Gething MJ. Jane's aircraft recognition guide. 5th ed. Collins; 2007.

[12] Streetly M, editor. Jane's all the world's aircraft: unmanned 2015-2016. IHS; 2015.

[13] Airbus Training. A320-Electrical n.d.:38. http://www.smartcockpit.com/docs/A320-Electrical.pdf (accessed March 8, 2017).

[14] Airbus Training. A330-Electrical n.d.:44, http://www.smartcockpit.com/docs/A330-Electrical.pdf (accessed March 8, 2017).

[15] Airbus Training. A340-Electrical n.d.:46, http://www.smartcockpit.com/docs/FCOM_A340-Electrical.pdf (accessed March 8, 2017).

[16] General Atomics - Aeronautical Systems Inc. MQ-9 Reaper/Predator 2015:2, http://www.ga-asi.com/Websites/gaasi/images/products/aircraft_systems/pdf/MQ9Reaper_Predator_B_032515.pdf (accessed March 8, 2017).

[17] General Atomics - Aeronautical Systems Inc. Predator B 2015:2, http://www.ga-asi.com/Websites/gaasi/images/products/aircraft_systems/pdf/Predator_B021915.pdf (accessed March 8, 2017).

[18] Boeing. F-15 Strike Eagle 2016, http://www.boeing.com/defense/f-15-strike-eagle/ (accessed March 8, 2017).

[19] Ministry of Defence. Joint Doctrine Note 2/11 the UK Approach To Unmanned Aircraft. 2011.

[20] Ministry of Defence. Joint Doctrine Publication 0-30.2: Unmanned Aircraft Systems. 2017.

[21] Ministry of Defence. Securing Britain in an Age of Uncertainty : The Strategic Defence and Security Review Securing Britain in an. 2010.

[22] Tavares S. Aerospace engineering pocket reference. Taylor & Francis; 2015.

[23] Middleton M. Better Exponential Curve Fitting Using Excel. Decis. Sci. Inst. Annu. Meet. 41st, San Diego: 2010.

[24] Microsoft. LINEST function 2017. https://support.office.com/en-us/article/LINEST-function-84d7d0d9-6e50-4101-977a-fa7abf772b6d?NS=EXCEL&Version=16&SysLcid=1033&UiLcid=1033&AppVer=ZXL160&HelpId=xlmain11.chm60097&ui=en-US&rs=en-US&ad=US (accessed March 10, 2017).

[25] Technical Committee ISO/TC20. ISO 2533:1975 Standard Atmosphere. 1975.

[26] U.S. Department of Defense. Department of Defense Handbook: Global Climatic Data for Developing Military Products MIL-HDBK-310. vol. MIL-STD-31. 1997.

Chapter 3 Zero Emission Aircraft Propulsion

3.1 Why Fuel Cells?

Several methods exist for reducing the environmental impact of the aeronautical industry. One solution is to replace the existing fossil based fuelling infrastructure with one based around either biofuels or synthetic fuels [1]. Alternatively, aircraft systems including propulsion could be electrified and energy provided by either batteries or fuel cell systems.

Possible biofuels such as methanol and ethanol [2] are derived from plant-based feedstocks. Therefore, their use as the sole alternative fuel for the aviation industry would not be possible due to the excessive requirement of arable land [3]. Unlike biofuels, synthetic fuels can be a direct drop-in replacement for traditional Jet A-1 [2]. However, current synthetic fuels are still a product of non-renewable hydrocarbon feedstocks [2,4] and therefore do not classify as a zero emission propulsion method.

Aircraft electrification, either fully or partially, in the case of more electric aircraft is a particularly promising route to emissions reduction and even elimination. Given that power electronics and electric motors are commonalities between all electro-mechanical systems, the key differentiation comes from the energy source used. Two energy sources have gained significant traction, batteries and fuel cells.

Lithium Cobalt Oxide ($LiCoO_2$) batteries have been proven effective in recent more electric aircraft such as the Boeing 787 [5]. However, their poor energy density with respect to fuel cell systems, shown by Figure 3.1 [6] severely limits their application to anything more than a supporting role to traditional fuel burning systems.

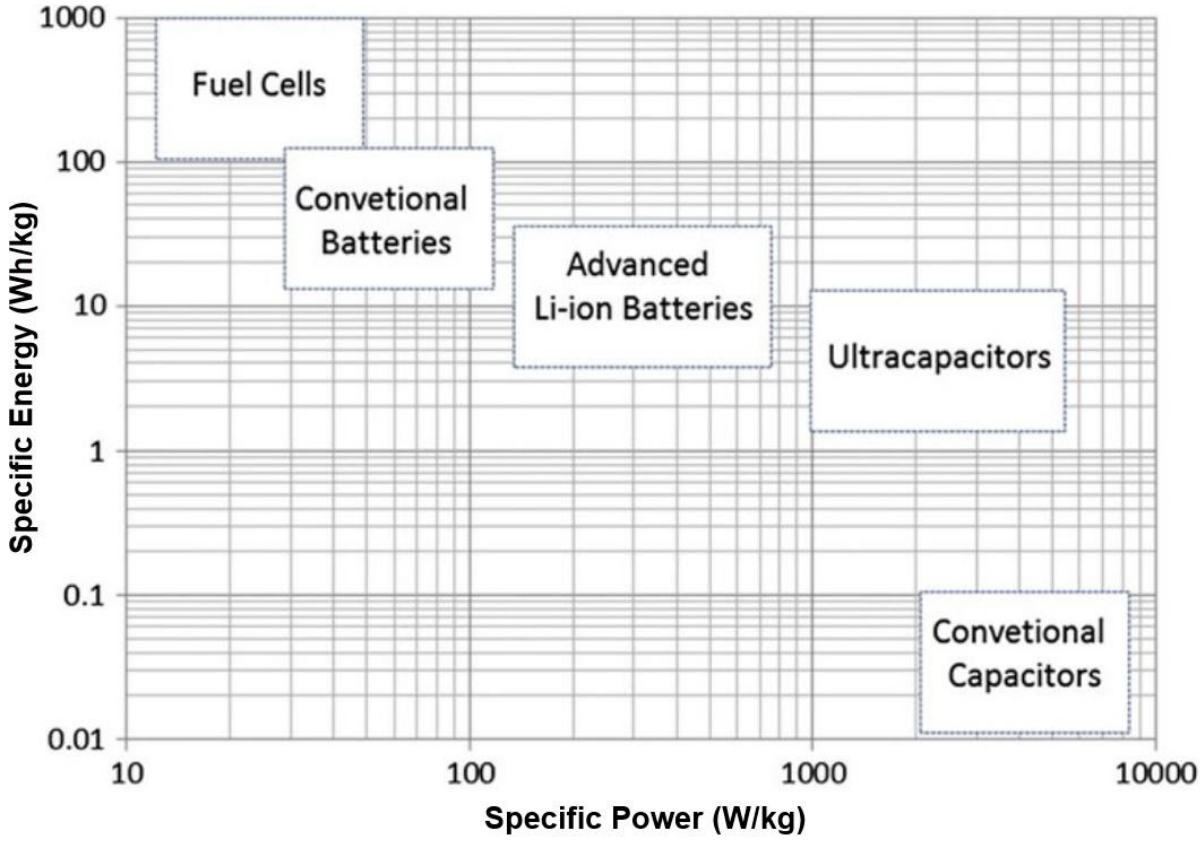

Figure 3.1: Specific Energy vs. Specific Power for various energy storage technologies, including fuel cells and advanced Li-ion batteries [6] reproduced with permission from Elsevier (Licence: 4927150372144)

Fuel cells are high-efficiency electrochemical energy conversion devices. They convert chemical energy into electrical energy and heat through a catalytically supported REDuction/OXidation (redox) reaction between a fuel and an oxidant.

Since its first inception by William Grove in 1839, fuel cell technology has undergone significant research and development in the ever present quest for higher energy and power densities. This has led to the evolution of several discrete fuel cell technologies. These fuel cell technologies all operate on the basic principle however, they utilise a range of fuel types and operating temperature to achieve the electrochemical reaction. In this Chapter each of these technologies will be compared and contrasted and down selected to the specific technologies which will be the focus of the research undertaken in this work.

3.2 Polymer Electrolyte Membrane Fuel Cells

Polymer Electrolyte Membrane Fuel Cells (PEMFC) produce electricity as the product of an exothermic electrochemical reaction between a fuel and oxygen in the presence of a platinum electrocatalyst. The main by-products of this chemical reaction are heat and water [7].

When we talk about 'fuel cells', the primary component or 'cell' refers to a sub-assembly called the Membrane Electrode Assembly (MEA) [8]. The MEA consists of a Polymer Electrolyte Membrane (PEM) sandwiched by an anode and cathode Gas Diffusion Electrode (GDE). Gas diffusion electrodes are themselves an assembly of a Gas Diffusion Layer (GDL) layered with a Catalyst Layer (CL). Figure 3.2 shows the general arrangement of a PEMFC.

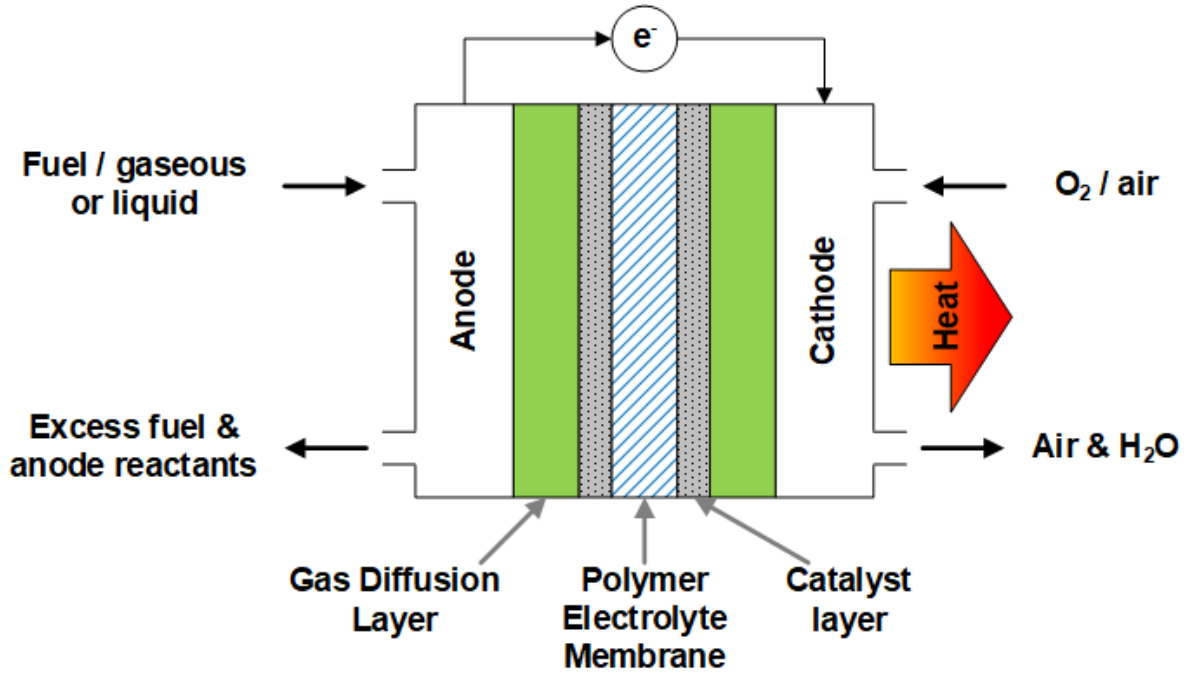

Figure 3.2: General single cell construction for a polymer electrolyte membrane fuel cell

3.2.1 Hydrogen Fuel Cell

Hydrogen fuelled PEMFCs are low temperature fuel cells with a typical operating temperature in the range of 30-100 °C. They are one of the more common fuel cell types and are usually used in mobile and motive applications, although they are also sometimes used in smaller Combined Heat and Power (CHP) systems. The primary advantage of hydrogen fuelled PEMFCs is that they benefit from the highest power density of all fuel cell technologies [9,10]

Using Figure 3.2 as a reference, hydrogen enters the fuel cell at the anode and diffuses through the GDL. The GDL allows direct, uniform access of the fuel and oxidant to the catalyst layer [11]. Utilising hydrogen as an energy carrier for consumption in a PEMFC comes with inherent advantages and disadvantages. The main advantage being that hydrogen has the highest gravimetric energy density possible of any fuel. However, the same physical characteristics of hydrogen that lend to its high gravimetric energy density (its low molecular mass, $M_{H2} = 2.016\ g/mol$) also gives way to its main problem, in that it is very difficult to contain. However, this will be covered in more detail in Chapter 5.

After diffusing through the GDL, the hydrogen-oxidation reaction, described by Equation 3.1 takes place at the anode catalyst layer.

$$H_2 \rightarrow 2H^+ + 2e^- \tag{3.1}$$

As the protons (hydrogen cations) diffuse through the proton exchange membrane, the electrons flow through the electrical load connected to the fuel cell. These constituent parts then combine with oxygen at the cathode to produce water. This is described by the oxygen-reduction reaction shown in Equation 3.2.

$$\tfrac{1}{2}O_2 + 2H^+ + 2e^- \rightarrow H_2O \tag{3.2}$$

The full redox reaction as described by Equation 3.3 is common to all fuel cells utilising hydrogen as the fuel. This also shows the 'HEAT' component of the overall reaction.

$$2H_2 + O_2 \rightarrow 2H_2O + HEAT \qquad (3.3)$$

3.2.2 Methanol Fuel Cell

Acidic Direct Methanol Fuel Cells (DMFC) are similar in construction to hydrogen fed PEMFCs and have a similar low operating temperature but differ in several areas. The key differentiating factor is the ability to utilise liquid methanol directly as a fuel without the need for prior reformation. This leads to the elimination of the key problem associated with the hydrogen fed PEMFCs, the storage of hydrogen.

However, the complex composition (relative to hydrogen) of methanol means that it cannot be oxidised in a single step at the anode catalyst sites. The resultant six-step methanol oxidation reaction is one of the main causes of lower DMFC performance when compared to PEMFC. Figure 3.3 is a useful summary of the different stages of the multistep methanol oxidation reaction. If the reader would like a detailed explanation of these processes, then the author would like to recommend an article by Hamnett, A [12] who provides excellent information on this topic.

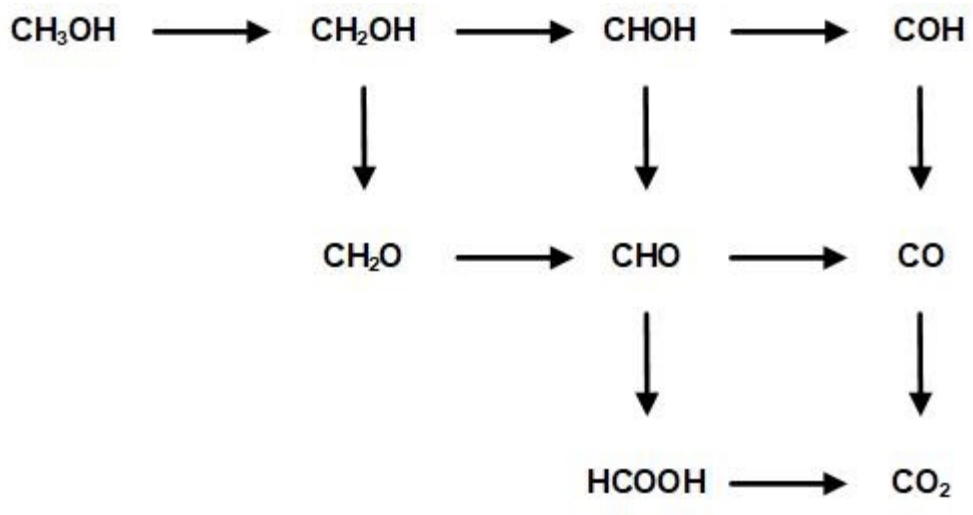

Figure 3.3: Methanol oxidation stages at a direct methanol fuel cell anode [9]

For the purpose of this work, the oxidation reaction will be assumed possible in a single step. Therefore, the complete methanol oxidation reaction, described by Equation 3.4 takes place at the anode catalyst layer. Unlike with hydrogen fed PEMFCs, DMFCs require water on the anode side of the MEA. This is nearly always injected as a constituent of the dilute methanol solution.

$$CH_3OH + H_2O \rightarrow 6H^+ + 6e^- + CO_2 \qquad (3.4)$$

As the protons diffuse through the proton exchange membrane, the electrons flow through the electrical load connected to the fuel cell. These constituent parts then combine with oxygen at the cathode to produce water. This is described by the oxygen-reduction reaction shown in Equation 3.5.

$$1\tfrac{1}{2}O_2 + 6H^+ + 6e^- \rightarrow 3H_2O \qquad (3.5)$$

The full redox reaction is described by Equation 3.6. This also shows the 'HEAT' component of the overall reaction.

$$2CH_3OH + 2H_2O + 3O_2 \rightarrow 6H_2O + 2CO_2 + HEAT \qquad (3.6)$$

3.3 Alkaline Fuel Cell

Alkaline electrolyte Fuel Cells (AFC) differ in their construction when compared to the two PEMFC designs discussed in the previous sections. One key difference is the state of the electrolyte used. For PEMFCs, a solid, acidic electrolyte is used. In comparison, in AFCs an alkaline liquid electrolyte such as potassium hydroxide is used.

The other main difference between the two technologies is the mobile ion available in the electrochemical reactions. The movement of the hydroxide anion is clearly demonstrated by the anode and cathode half reactions as shown by Equation 3.7 and 3.8 respectively. The full redox reaction is the same as that for a PEMFC due to the common use of hydrogen as a fuel.

$$H_2 + 2OH^- \rightarrow 2H_2O + 2e^- \quad (3.7)$$

$$\tfrac{1}{2}O_2 + 2e^- + 2H_2O \rightarrow 2OH^- \quad (3.8)$$

Main advantages of AFCs over PEMFCs are typically centered around cost. Although there are many different possible internal architectures for AFCs, generally they do not require bipolar plates and the liquid electrolytes used are considerably cheaper than the solid types used in PEMFCs [9]. However, the current state-of-the-art current density for atmospheric AFCs was shown by a review paper written by McLean, GF to be in the order of 400 mA/cm^2 [13] this is approximately 80% less than the current state of the art for PEMFCs [14].

3.4 Phosphoric Acid Fuel cell

Phosphoric Acid Fuel Cells (PAFC) operate on the same electrochemical principle as PEMFCs, utilising hydrogen as a fuel and oxygen as the oxidant. As such, the half cell reactions described by Equations 3.1 and 3.2 hold. However, unlike PEMFCs, PAFCs utilise a liquid phosphoric acid electrolyte to allow transport of the hydrogen ions. As the pure phosphoric acid electrolyte must remain in a liquid state to allow ion conduction, the operating temperature must remain above 42 ℃ (the freezing point of phosphoric acid). This also avoids serious stress issues related to repeated freeze-thaw cycles [10]. In reality, to maintain optimal performance, it is common to operate PAFCs at much higher temperatures than PEMFCs, usually in the region of 180-210 ℃.

Operating at this higher temperature does lead to certain advantages and disadvantages. The positives related to higher temperature operation include a greater CHP efficiency and improved tolerance to fuel impurities. Although, the use of platinum as an electrocatalyst does mean that it is still susceptible to carbon monoxide poisoning. The main disadvantage of operating at the elevated temperature is an increased evaporation rate of the liquid electrolyte. This does lead to a requirement for the electrolyte to be continually added during operation.

Phosphoric acid fuel cells are commonly used in CHP systems (200 kW +) [9]. However, they are not suitable for motive applications, either on the ground or in the air. This is because the requirement of a PAFC to continually maintain an elevated temperature would not be possible to achieve during the non-operation sections of a vehicle's drive/flight profile.

3.5 Molten Carbonate Fuel Cell

Some analogies can be made between AFC and Molten Carbonate Fuel Cell (MCFC) technologies. These are the use of a liquid electrolyte and an electrochemical reaction dominated by an anion instead of the cation lead PEMFC designs. A binary mixture of molten alkali carbonates, typically, lithium and potassium based are used as the electrolyte.

The relatively high operating temperature of MCFCs, typically on the order of 650 °C allows for fuel flexibility and the absence of platinum in the electrode construction means that unlike the low temperature fuel cell designs discussed earlier, MCFCs are not susceptible to carbon monoxide poisoning. Although able to run on simple hydrocarbon fuels, these are reformed internally, therefore, the electrochemical half-cell reactions only involve hydrogen [9,10]. Equation 3.9 shows the anode half-cell reaction for an MCFC using pure hydrogen as a fuel. This reaction shows that in addition to the production of water, carbon dioxide is also produced.

$$H_2 + CO_3^{2-} \rightarrow H_2O + CO_2 + 2e^- \qquad (3.9)$$

The carbon dioxide produced at the anode has to be recirculated to the cathode where it is combined with oxygen to produce the mobile carbonate anion, as described by Equation 3.10. The recirculation of carbon dioxide from anode to cathode is done with the aid of a burner to combust any excess fuel to produce a carbon dioxide/steam mixture [10]. The added benefit of this process is the addition of heat at the cathode inlet, helping to maintain the higher operating temperature of the MCFC.

$$\tfrac{1}{2}O_2 + CO_2 + 2e^- \rightarrow CO_3^{2-} \qquad (3.10)$$

Molten carbonate fuel cells are a very popular option for CHP systems and are frequently used in megawatt scale installations. However, their high operating temperature and intolerance to freeze-thaw cycles means that they are not suitable for mobile applications.

3.6 Solid Oxide Fuel Cell

With a typical operating temperature range of 600 ℃ to 1,000 ℃, the Solid Oxide Fuel Cell (SOFC) is currently the highest temperature fuel cell technology. Unlike MCFCs, SOFCs are solid-state devices utilising ceramic electrolytes and specialised metallic interconnects between cells. Different materials are used for the anode and cathode due to the extreme high-temperature and highly reducing and oxidising environments [10].

The anode half-cell reaction (Equation 3.11), aided by a yttria-stabilised zirconia supported nickel catalyst shows how the water is produced from the hydrogen fuel and the superoxide anion from the cathode half-cell reaction (Equation 3.12).

$$H_2 + O^{2-} \rightarrow H_2O + 2e^- \qquad (3.11)$$

$$\tfrac{1}{2}O_2 + 2e^- \rightarrow O^{2-} \qquad (3.12)$$

This type of fuel cell has similar advantages to that of a MCFC, in the sense that the elevated temperature allows fuel flexibility. However, as the fuel cells require heating to this temperature before the reaction can take place and the brittle nature of the ceramic electrolytes precludes their use in motive applications.

3.7 Previous Aeronautical Fuel Cell Research

Generally, fuel cells are viewed as an interesting proposition for electrical production onboard aircraft, both manned and unmanned. Existing literature can be generalised into two main categories based on their content, pure theoretical and those which include experimental work.

Theoretically, both SOFC [15] and PEMFC [16-21] technologies have been considered for use in aeronautical applications. Aguiar P, 2008 [15] modelled various configurations of a SOFC / gas turbine system for a High-Altitude Long-Endurance (HALE) Unmanned Aerial

Vehicle (UAV) with a goal of maximising efficiency to increase range. The three configurations considered by Aguiar differed primarily on the number of fuel cell stacks connected electrically in parallel. The hypothesis was that increasing the number of parallel stacks would decrease their individual operating current and therefore the cooling demand. A key limitation of Aguiar's work is that throughout the system configuration study the change in aircraft mass from adding additional fuel cells was not considered.

An in-depth but limited case study was carried out by Pratt JW, 2013 [16] on the application of a PEMFC system on board a more-electric Boeing 787. This study focused on using the fuel cell to support the main engine generators in meeting the high electrical demands of this aircraft. The limitations of this study were that it only considered a single aircraft in the case study and that altitude effects on fuel cell performance did not appear to have been taken account of.

Using a fuel cell as a complete replacement for an internal combustion engine in a Class I mini UAV was the subject of a paper published by Renau J, 2015 [17]. In this case, the study was purely theoretical and seemed to be the early stages of a larger project. In this case, the information provided was limited and did not discuss the thermal management strategy employed. However, their work looked promising and may have led to fuel cell powered flight.

A study performed by Sliwinksi J, 2017 [18] also looked at the potential for replacing the traditional internal combustion engine of a small UAV with some form of system derived from fuel cell technology. In this case they considered hybridising the electrical technologies with the internal combustion engine as a stepping stone to fully electrified. Unfortunately, little detail was provided in this work on the modelling methodology used for the fuel cell system.

A NASA study [19] along with two review style papers [20,21] although not contributing new information directly, all add credence to the application of fuel cells in aircraft. The recent study prepared by McKinsey & Company for the Clean Sky 2 and Fuel Cells and Hydrogen 2 joint undertakings [22] was in good agreement with the findings of the review by Roth B, 2010 [20].

The Clean Sky 2 report's overall conclusion is that hydrogen propulsion has the potential to be a major part of the future aircraft propulsion technology mix. Based on the technical developments resulting from the joint undertakings, hydrogen propulsion is suggested for commuter, regional, short-range, and medium-range aircraft.

In addition to the aforementioned theoretical studies [15-22], several have also been published which took a more experimental approach to the use of fuel cells in aircraft [23-30]. Renouard-Vallet G, 2012 [23] carried out experimental studies on a 10 kW fuel cell test rig to determine production rates of water and inerting gas with an oxygen concentration of < 12%. Their intention was the application of these two products of fuel cell operation in civil aircraft however, this intention was only hypothesised. The actual usage of fuel cells to produce water and inert gas was not explored.

Lapeña-Rey N, 2008 [24] in collaboration with Intelligent Energy Ltd published the results of preflight bench testing of an Intelligent Energy fuel cell system for a Boeing demonstrator aircraft. Two air-breathing fuel cell stacks were electrically connected in series with a system net power output of 20 kW at 200 V. The paper describes the system architecture and experimental work however, it does not discuss scalability or altitude effects on fuel cell performance.

Several published works [25-28] have integrated fuel cell systems into small UAVs and performed flight tests with varying degrees of success. Ward TA, 2010 [25] and Dudek M, 2013 [26] both integrated air-cooled fuel cells produced by Horizon Energy Systems into custom airframes. Both used compressed gaseous hydrogen as a fuel and hybridised the fuel cell with a battery to account for peak loads. Varying degrees of success were achieved with Ward completing a < 30 s flight on fuel cell power and Dudek flying for around 30 min. In both cases, the primary limitations of their studies were that because small, remotely operated UAVs were used and flown at low altitude, it's effect on performance was not demonstrated.

Bradley T, 2007 [27] also used a small (circa' 500 W) fuel cell, in this case provided by BCS Technology Inc to provide propulsive power to a UAV. This study differed from those previously discussed as the fuel cell was liquid-cooled using de-ionised water instead of relying on air-cooling. Although this may not have been necessary for the quantity of heat produced in this study, it was an interesting insight on how this type of thermal management system could be integrated into a small UAV.

Another interesting study into integrating a fuel cell into a UAV was carried out by Herwerth C, 2007 [28]. In this work, a customised fuel cell with doughnut shaped cells was created to allow better integration into the aircraft's aerodynamic fuselage. No flight test resulted from this study however, it is an excellent example of the multitude of configurations possible for hydrogen fuel cells and how they could be integrated into the aircraft environment,

Sodium Borohydride ($NaBH_4$) when exposed to water in the presence of a catalyst releases hydrogen along with a waste product, sodium metaborate. Two studies, Kim K, 2011 [29] and Kim T, 2012 [30] have used $NaBH_4$ as a hydrogen source for PEMFC fuel cells as it has a higher energy density than the more common molecular hydrogen storage used in other studies. Both publications have reported impressive flight times of nearly two hours. However, due to complexities in waste material handling and recycling, at this current time $NaBH_4$ is not suitable for larger aeronautical applications.

Pratt JW, 2012 [31] performed both experimental and theoretical research on operating fuel cells at subatmospheric pressures. It was shown that there is a clear decrease in PEMFC performance with reduced total pressure. Total pressure and concentration effects were separated out from partial pressure. It was discovered that total pressure effects were greater than concentration effects. However, this work has limited scope as a short fuel cell stack (23 cells) was used and this may not fully account for the effects of total pressure and concentration in larger fuel cells.

A majority of the previous studies have focussed their efforts on polymer electrolyte membrane fuel cell technology [16-30], citing high power density and low operating temperature as the deterministic characteristics. However, they have generally agreed that the use of pure hydrogen gas as a fuel led to difficulties and limitations in system performance due to its poor volumetric energy density. One potential solution to this problem would be to use a similar fuel cell technology which utilises a liquid fuel such as a direct methanol fuel cell. Both PEMFCs and DMFCs are similar in that they both incorporate a polymer electrolyte membrane to conduct the mobile hydrogen ion. They also share commonalities in their low operating temperature (< 100 °C) and have relatively short startup times when compared to high-temperature fuel cell technologies.

3.8 Summary

An overview of the various commercially viable fuel cell technologies have been given in this Chapter. The primary distinguishing factors (mobile ion and operating temperature) along with some typical applications are summarised in Table 3.1.

Table 3.1: Overview information of different fuel cell technologies [9,32-34]

Fuel Cell Technology	**Mobile Ion**	**Operating temperature**	**Traditional Applications or Fuel?**
Direct Methanol	H^+	20-90 °C	Portable electronics, low power and long run time.
Polymer Electrolyte Membrane	H^+	30-100 °C	Vehicles, mobile applications and lower power Combined Heat and Power (CHP) systems.
Alkaline	OH^-	60-200 °C	Space vehicles, e.g. Apollo and Shuttle.
Phosphoric Acid	H^+	≈ 200 °C	Large numbers of 200kW+ CHP systems in use.
Molten Carbonate	CO_3^{2-}	≈ 650 °C	Medium to large scale CHP systems up to 1MW in capacity.
Solid Oxide	O^{2-}	600-1,000 °C	All sizes of CHP system, 2kW to multi-MW capacity.

The hydrogen fuelled polymer electrolyte membrane fuel cell, commonly referred to as just 'PEMFC' is, at the time of writing the most widely utilised fuel cell technology in active use with over 900 MW of installed capacity [35]. The preference of PEMFC technology over other types of fuel cell has been increasing year to year as shown by Figure 3.4. This is most likely the result of the introduction of several new products in the automotive sector.

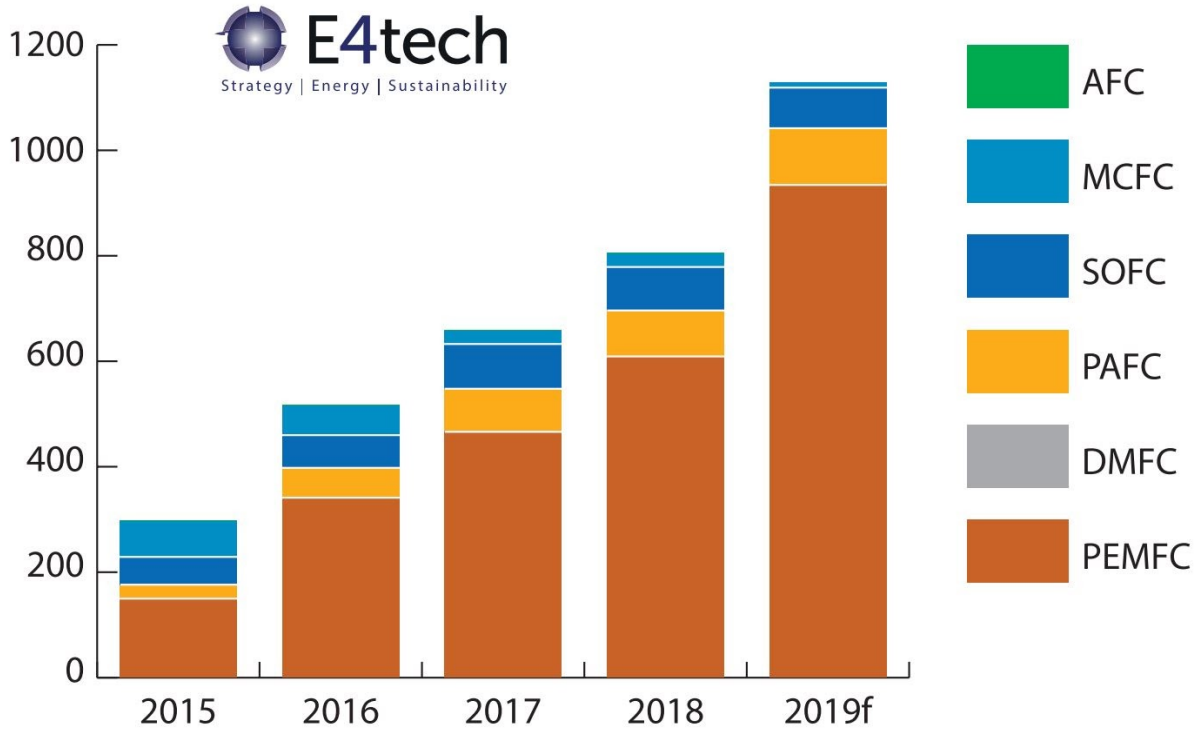

Figure 3.4: Megawatts by fuel cell type 2015-2019, 2019f includes real data for Jan-Sept and forecast for Oct-Dec [35]

Based on the advantages described in Section 3.2, primarily the advanced power density and the maturity of the technology evidenced by Figure 3.4, PEMFCs have been judged by the author and the bulk of existing literature to be the most suitable for application to the aeronautical environment. One of the primary concerns with this technology, the storage of hydrogen, is a topic that still requires a great deal of investigation.

Unfortunately, the scope of this work does not include the detailed experimental studies which would be required to increase hydrogen storage technology to certification levels. As DMFCs alleviate this problem entirely with the use of a liquid fuel, and are similar in operation and construction to hydrogen fuelled PEMFCs, they will also feature heavily in this work. It is important to note that although the use of PEMFCs has been considered and indeed implemented in a small number of aircraft, the use of DMFCs has received little to no attention in the published literature due to their relatively low specific-power.

3.9 References

[1] Scheelhaase J, Maertens S, Grimme W. Synthetic fuels in aviation - Current barriers and potential political measures. Transp Res Procedia 2019;43:21–30. https://doi.org/10.1016/j.trpro.2019.12.015.

[2] Daggett D, Hadaller O, Hendricks R, Walther R. Alternative fuels and their potential impact on aviation. 25th Congr. Int. Counc. Aeronaut. Sci. 2006, vol. 5, Hamburg: 2006, p. 2888–97.

[3] Kandaramath Hari T, Yaakob Z, Binitha NN. Aviation biofuel from renewable resources: Routes, opportunities and challenges. Renew Sustain Energy Rev 2015;42:1234–44. https://doi.org/10.1016/j.rser.2014.10.095.

[4] Braun-Unkhoff M, Riedel U. Alternative fuels in aviation. CEAS Aeronaut J 2014;6:83–93. https://doi.org/10.1007/s13272-014-0131-2.

[5] Boeing. Batteries and Advance Airplanes 2013. http://787updates.newairplane.com/787-Electrical-Systems/Batteries-and-Advanced-Airplanes (accessed March 7, 2018).

[6] Chao CH, Shieh JJ. A new control strategy for hybrid fuel cell-battery power systems with improved efficiency. Int J Hydrogen Energy 2012;37:13141–6. https://doi.org/10.1016/j.ijhydene.2012.03.143

[7] Wang Y, Chen KS, Mishler J, Cho SC, Adroher XC. A review of polymer electrolyte membrane fuel cells: Technology, applications, and needs on fundamental research. Appl Energy 2011;88:981–1007. https://doi.org/10.1016/j.apenergy.2010.09.030.

[8] Rayment C, Sherwin S. Introduction to Fuel Cell Technology. 2003. https://doi.org/10.1.1.129.3231&rep=rep1&type=pdf.

[9] Larminie J, Dicks A. Fuel Cell Systems Explained. 2nd ed. John Wiley & Sons; 2003. https://doi.org/10.1016/S0378-7753(00)00571-1.

[10] O'Hayre R, Cha S-W, Colella W, Prinz FB. Fuel cell fundamentals. 3rd ed. John Wiley & Sons; 2016.

[11] Mehta V, Cooper JS. Review and analysis of PEM fuel cell design and manufacturing 2002;114.

[12] Hamnett A. Mechanism and electrocatalysis in the direct methanol fuel cell. Catal Today 1997;38:445–57. https://doi.org/10.1016/S0920-5861(97)00054-0.

[13] McLean GF, Niet T, Djilali N. An assessment of AFC technology. Int J Hydrogen Energy 2002;27:507–26.

[14] Kongkanand A, Subramanian NP, Yu Y, Liu Z, Igarashi H, Muller DA. Achieving High-Power PEM Fuel Cell Performance with an Ultralow-Pt-Content Core-Shell Catalyst. ACS Catal 2016;6:1578–83. https://doi.org/10.1021/acscatal.5b02819.

[15] Aguiar P, Brett DJL, Brandon NP. Solid oxide fuel cell/gas turbine hybrid system analysis for high-altitude long-endurance unmanned aerial vehicles. Int J Hydrogen Energy 2008;33:7214–23. https://doi.org/10.1016/j.ijhydene.2008.09.012.

[16] Pratt JW, Klebanoff LE, Munoz-Ramos K, Akhil AA, Curgus DB, Schenkman BL. Proton exchange membrane fuel cells for electrical power generation on-board commercial airplanes. Appl Energy 2013;101:776–96. https://doi.org/10.1016/j.apenergy.2012.08.003.

[17] Renau J, Lozano A, Barroso J, Miralles J, Martin J, Sanchez F, et al. Use of fuel cell stacks to achieve high altitudes in light unmanned aerial vehicles. Int J Hydrogen Energy 2015;40:14573–83. https://doi.org/10.1016/j.ijhydene.2015.02.071.

[18] Sliwinski J, Gardi A, Marino M, Sabatini R. Hybrid-electric propulsion integration in unmanned aircraft. Energy 2017;140:1407–16. https://doi.org/10.1016/j.energy.2017.05.183.

[19] Guynn MD, Freh JE, Olson ED. Evaluation of a hydrogen fuel cell powered blended-wing-body aircraft concept for reduced noise and emissions. NASA 2004;NASA/TM-20.

[20] Roth B, Iii RG. Fuel cell hybrid propulsion challenges and opportunities for commercial aviation 2010:1–15. https://doi.org/doi:10.2514/6.2010-6537.

[21] McConnell VP. Military UAVs claiming the skies with fuel cell power. Fuel Cells Bull 2007;2007:12–5. https://doi.org/10.1016/S1464-2859(07)70438-8.

[22] McKinsey & Company, Clean Sky 2 JU, Fuel Cells and Hydrogen 2 JU. Hydrogen-powered aviation A fact-based study of hydrogen technology, economics, and climate impact by 2050. 1st ed. McKinsey & Company; 2020. https://doi.org/10.2843/471510.

[23] Renouard-Vallet G, Saballus M, Schumann P, Kallo J, Friedrich KA, Müller-Steinhagen H. Fuel Cells for Civil Aircraft Application: On-Board Production of Power, Water and Inert Gas. Chem Eng Res Des 2012;90:3–10. https://doi.org/10.1016/j.cherd.2011.07.016.

[24] Lapeña-Rey N, Mosquera J, Bataller E, Ortí F, Dudfield C, Orsillo A. Environmentally friendly power sources for aerospace applications. J Power Sources 2008;181:353–62. https://doi.org/10.1016/j.jpowsour.2007.11.045.

[25] Ward TA, Jenal N. Design and initial flight tests of a hydrogen fuel cell powered unmanned air vehicle (UAV). Electrochem Soc 2010;26:433–44. https://doi.org/10.1149/1.3429016.

[26] Dudek M, Tomczyk P, Wygonik P, Korkosz M, Bogusz P, Lis B. Hybrid fuel cell - battery system as a main power unit for small unmanned aerial vehicles (UAV). Int J Electrochem Sci 2013;8:8442–63.

[27] Bradley TH, Moffitt BA, Mavris DN, Parekh DE. Development and experimental characterization of a fuel cell powered aircraft. J Power Sources 2007;171:793–801. https://doi.org/10.1016/j.jpowsour.2007.06.215.

[28] Herwerth C, Chiang C, Ko A, Matsuyama S, Choi SB, Mirmirani M, et al. Development of a small long endurance hybrid PEM fuel cell powered UAV. SAE Tech Pap 2007. https://doi.org/10.4271/2007-01-3930.

[29] Kim K, Kim T, Lee K, Kwon S. Fuel cell system with sodium borohydride as hydrogen source for unmanned aerial vehicles. J Power Sources 2011;196:9069–75. https://doi.org/10.1016/j.jpowsour.2011.01.038.

[30] Kim T, Kwon S. Design and development of a fuel cell-powered small unmanned aircraft. Int J Hydrogen Energy 2012;37:615–22. https://doi.org/10.1016/j.ijhydene.2011.09.051.

[31] Pratt JW, Brouwer J, Samuelsen GS. Performance of Proton Exchange Membrane Fuel Cell at High-Altitude Conditions. J Propuls Power 2012;23:437–44. https://doi.org/10.2514/1.20535.

[32] Guynn MD, Freh JE, Olson ED. Evaluation of a hydrogen fuel cell powered blended-wing-body aircraft concept for reduced noise and emissions. NASA 2004;NASA/TM-20.

[33] Kumar L, Jain S. Electric propulsion system for electric vehicular technology: A review. Renew Sustain Energy Rev 2014;29:924–40. https://doi.org/10.1016/j.rser.2013.09.014.

[34] Faghri A, Guo Z. Challenges and opportunities of thermal management issues related to fuel cell technology and modeling. Int J Heat Mass Transf 2005;48:3891–920. https://doi.org/10.1016/j.ijheatmasstransfer.2005.04.014.

[35] E4tech. The Fuel Cell Industry Review 2019. 2019.

Chapter 4 PEMFC Modelling

4.1 Defining Performance

The term “performance” is defined as “how well a person, machine, etc. does a piece of work or an activity” by the Cambridge Dictionary [1]. The performance of a fuel cell and a fuel cell system are also two different things, and therefore will be covered separately. In this section, the performance and modelling of that performance will be covered for the fuel cell only.

Before considering how to define or calculate fuel cell performance there are some terminologies which require explanation to ensure a full understanding of the following work. These are Higher Heating Value (HHV) and Lower Heating Value (LHV) whose definitions can be found in Table 4.1.

Table 4.1: Definitions of Higher Heating Value and Lower Heating Value

Term	**Definition**
Higher Heating Value	Higher calorific value of a fuel, determined by bringing all of the products of combustion of that fuel with oxygen back to their original temperature and condensing all water vapour produced into liquid [2,3].
Lower Heating value	Lower calorific value of a fuel and is found by subtracting the latent heat of vapourisation of water from the HHV [2,3].

Both HHV and LHV are important concepts to grasp as the calculated performance metrics of fuel cells, such as efficiency, are heavily influenced by which heating value is used. In general, for low temperature Polymer Electrolyte Membrane Fuel Cells (PEMFC) (both hydrogen and methanol fed) operating below 100 °C, the HHV of the fuel/oxygen reaction should always be used. This is because it is highly likely that a majority of the water produced by the reaction inside the fuel cell will be in liquid form [2,3].

The story of modelling fuel cell performance is fairly long and complex. The following subsections will attempt to present this information in a logical and easily digestible fashion. We will start by defining idealised potentials before moving on to dealing with losses and irreversibilities. Finally, we will conclude the "performance" section by introducing and explaining the "Polarisation Curve" and its significance in the design of fuel cell systems.

4.1.1 Ideal Potential

Although it has no physical meaning to the operation of a fuel cell, the imagined **ideal** potential, V_{HHV}, is extremely useful for calculating the heat release from a fuel cell during operation [3]. The calculation of the ideal potential is based on the assumption that all of the energy contained in the fuel (i.e. its heating value or enthalpy of formation) is transformed into electrical energy as shown by Equation 4.1 [2]. In other words, it assumes the electrochemical reaction taking place within the fuel cell is 100% efficient. Typical values for the enthalpy change and ideal potential for both PEMFC and Direct Methanol Fuel Cells (DMFC) are shown in Table 4.2.

$$V_{HHV} = \frac{\Delta\bar{h}}{zF} \qquad (4.1)$$

Where:

F - Faraday constant (96,485 C/mol)

$\Delta\bar{h}$ - Absolute enthalpy change (J/mol)

V_{HHV} - Theoretical potential based on the HHV of fuel (V)

z - Number of electrons transferred per mole of fuel

Table 4.2: Typical values for fuel HHV and ideal potential for PEMFC and DMFC

Fuel Cell Type	**Fuel Higher Heating Value**	**Ideal Potential (HHV)**
PEMFC	-285.66 kJ/mol	1.48 V
DMFC	-736.92 kJ/mol	1.27 V

The variation of absolute enthalpy change, $\Delta\bar{h}$ with temperature for both the PEMFC and standard DMFC reactions are shown in Figure 4.1. A temperature range of 298 K - 360 K was chosen as this would ensure that water is always in a liquid state, therefore the HHV of $\Delta\bar{h}$ is quoted in this plot. Linear trend lines, with excellent fit were generated for both sets of data to allow the small variance of $\Delta\bar{h}$ with temperature to be included in the modelling effort.

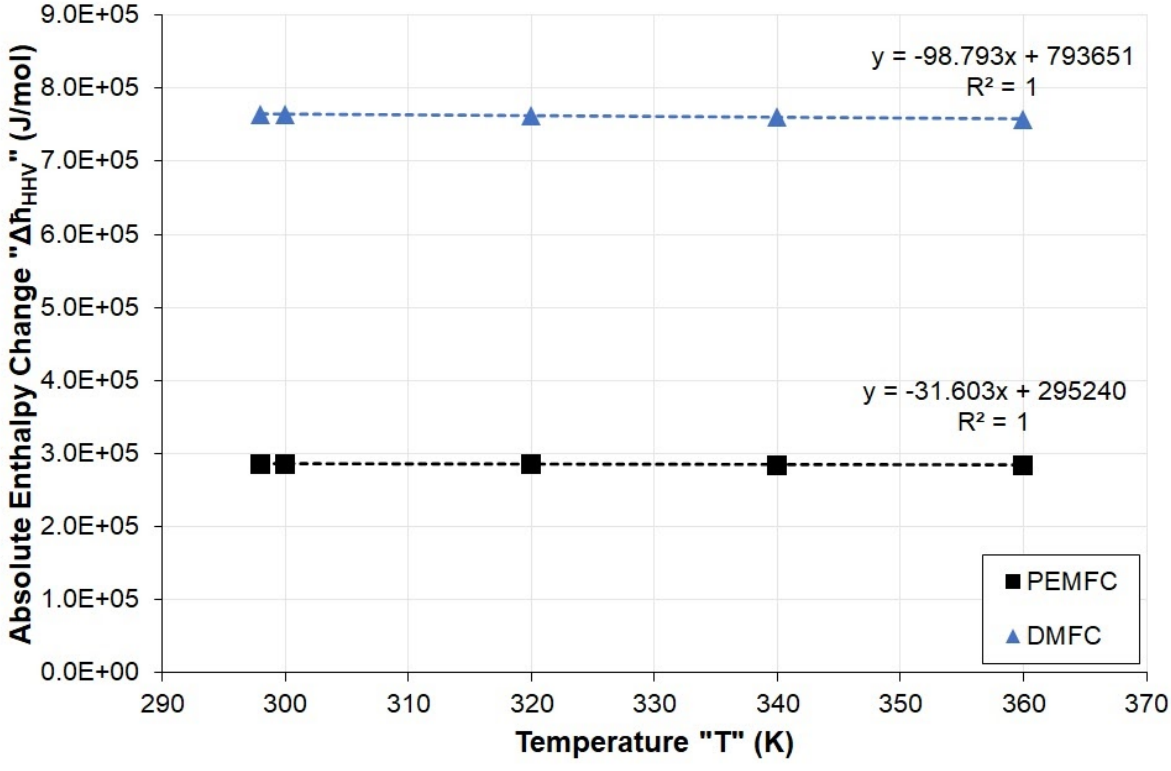

Figure 4.1: Variation of the absolute enthalpy change of reaction for both a PEMFC and DMFC between temperatures of 298 K and 360 K assuming liquid water

4.1.2 Thermodynamic Reversible Potential

The thermodynamic **reversible** potential, $V_{0\,HHV}$ of a polymer electrolyte membrane fuel cell is defined by the ratio between the Gibbs free energy and the product of the number of electrons involved in the reaction and the Faraday constant, as shown by Equation 4.2. This is a theoretical maximum potential and is not achievable due to irreversibilities in the reaction [2].

$$V_{0\,HHV} = \frac{\Delta\bar{g}}{zF} \tag{4.2}$$

Where:

F - Faraday constant (96,485 C/mol)

$\Delta\bar{g}$ - Absolute Gibbs free energy change (J/mol)

$V_{0\,HHV}$ - Reversible potential based on the HHV of fuel (V)

z - Number of electrons transferred per mole of fuel

The main difference between the “Ideal Potential” discussed earlier and the “Thermodynamic Reversible Potential” is the use of Gibbs free energy, or the work potential of the fuel instead of the enthalpy of reaction (heat potential of the fuel). The “Thermodynamic Reversible Potential” will always be less than the “Ideal Potential” due to the very definition of Gibbs free energy. The definition, demonstrated by Equation 4.3 shows that the Gibbs free energy change will always be less than the Enthalpy change as they are related by subtracting an Entropy term, which due to the Second Law of Thermodynamics, must always be positive.

$$\Delta\bar{g} = \Delta\bar{h} - T\Delta\bar{s} \tag{4.3}$$

Where:

$\Delta\bar{g}$ - Absolute Gibbs free energy change (J/mol)

$\Delta\bar{h}$ - Absolute enthalpy change (J/mol)

$\Delta\bar{s}$ - Absolute entropy change (J/molK)

T - Temperature (K)

Typical values for the Gibbs free energy change (at 298 K) and corresponding thermodynamic reversible potentials for both PEMFC and DMFCs are shown in Table 4.3. Appendix 2 contains further chemical information which can be used to calculate the values for $\Delta\overline{g}$ and therefore $V_{0\,HHV}$ at a range of temperatures.

Table 4.3: Typical values for Gibbs free energy change and thermodynamic reversible potential for PEMFC and DMFC

Fuel Cell Type	**Gibbs Free Energy Change at 298 K**	**Thermodynamic Reversible Potential (HHV)**
PEMFC	-237.2 kJ/mol	1.23 V
DMFC	-706.5 kJ/mol	1.22 V

The variation of absolute Gibbs free energy change, $\Delta\overline{g}$ with temperature for both the PEMFC and standard DMFC reactions are shown in Figure 4.2. A temperature range of 298 K - 360 K was chosen as this would ensure that water is always in a liquid state, therefore the HHV of $\Delta\overline{g}$ is quoted in this plot. Linear trend lines, with excellent fit were generated for both sets of data to allow the variance of $\Delta\overline{g}$ with temperature to be included in the modelling effort.

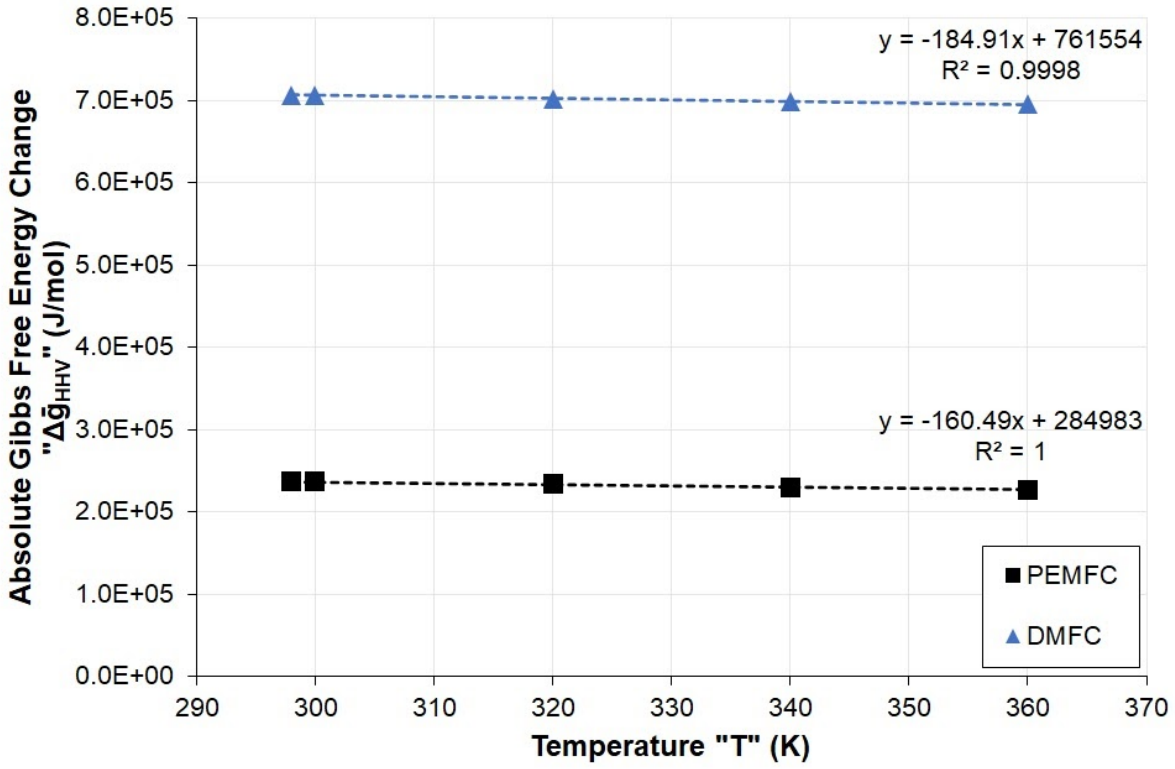

Figure 4.2: Variation of the absolute Gibbs free energy change of reaction for both a PEMFC and DMFC between temperatures of 298 K and 360 K assuming liquid water

4.1.3 Efficiency

It is widely agreed that defining efficiency as a relationship between electrical energy produced and the work potential of the fuel (change in Gibbs free energy) is rarely done as irrespective of the conditions used, the efficiency limit would be 100% [2].

The determination of real fuel cell efficiency is approached slightly differently by the two main sources of fundamental fuel cell knowledge, Larminie, D (2003) [2] and O'Hayre, R (2016) [3]. Both sources agree that its calculation is based on several factors and despite different approaches, both achieve very similar results.

For the purpose of modelling fuel cell efficiency in this work, the approach taken by Larminie, D (2003) [2] will be followed. In their approach, the real fuel cell efficiency, η_{FC} is defined as the product of the cell efficiency, η_{volt} and the fuel utilisation coefficient, η_{fuel} as shown by Equation 4.4.

$$\eta_{FC} = \eta_{volt} \cdot \eta_{fuel} \quad (4.4)$$

Where:

η_{FC} - Real fuel cell efficiency

η_{fuel} - Fuel utilisation coefficient

η_{volt} - Cell efficiency

Cell efficiency, η_{volt} is the ratio of the actual cell voltage of the fuel cell to the ideal potential found from the heating value of the fuel as demonstrated by Equation 4.5. It is possible to define cell efficiencies on either the HHV or LHV of the fuel. However, it is common practice to define the efficiency based on the HHV of the fuel as this gives a more realistic value and allows direct comparison to heat engines.

$$\eta_{volt} = V_c / V_{HHV} \times 100\% \quad (4.5)$$

Where:

V_c - Cell voltage (V)

V_{HHV} - Theoretical potential based on the Higher Heating Value (HHV) of fuel

η_{volt} - Cell efficiency

The fuel utilisation coefficient, η_{fuel} is the ratio of mass of fuel reacted in the fuel cell to the mass of fuel fed to the fuel cell as shown by Equation 4.6. This value is also related to another important parameter in fuel cell system design, stoichiometry. More information on this parameter will be discussed later on in this chapter.

$$\eta_{fuel} = \frac{mass\ of\ fuel\ reacted\ in\ cell}{mass\ of\ fuel\ input\ to\ cell} \times 100\% \quad (4.6)$$

Where:

η_{fuel} - Fuel utilisation coefficient

4.1.4 Fuel Cell Irreversibilities

Due to the highly interdisciplinary nature of fuel cells, there are several different sets of terminology used when describing the irreversibilities responsible for differences between a real fuel cell voltage and the predicted theoretical potentials discussed earlier. When discussing the operation of fuel cells it is difficult to stick to a single term. Therefore, throughout this Thesis the following list of terms, which all have the same meaning when related to fuel cell potentials will be used interchangeably:

- Irreversibility / irreversibilities
- Overpotential / overvoltage
- Voltage drop
- Loss / losses
- Polarisation

Operational fuel cell voltage can be found by combining the four major irreversibilities: activation, fuel crossover, resistance and concentration losses and subtracting them from the thermodynamic reversible potential defined by Equation 4.2. Definitions of these irreversibilities can be found in Table 4.4.

Table 4.4: Definitions of fuel cell irreversibilities [2,3]

Irreversibility	**Definition**
Activation losses	Overpotential associated with driving the reaction forward at the catalyst surface on the electrode. The voltage drop associated with this loss is highly nonlinear.
Fuel crossover	Losses associated with the fuel wastage which occurs as it passes through the electrolyte. This irreversibility is generally very small for PEMFCs and only has a noticeable effect on the Open Circuit Voltage (OCV) of low temperature fuel cells. For DMFCs this irreversibility is more substantial.
Ohmic losses	Voltage drop associated with the resistance to the flow of electrons through the electrode materials and the various interconnects, as well as the flow of ions through the electrolyte.
Mass transport and concentration losses	Losses resulting from the change in concentration of the reactants at the surface of the electrodes as the fuel is used. These irreversibilities are most prevalent at higher current densities.

The Nernst equation, first developed by Walther Nernst in 1887 is well established as one of the most cited electrochemical equations in history [4,5]. The Nernst equation has been expanded to several different forms of an empirical full cell equation [2,3,6] which is used to describe how these irreversibilities are combined to find the cell voltage of a single cell from the thermodynamic reversible voltage. It also shows how increasing current density leads to a lower cell potential. The numerical form of the full cell equation, utilising the empirical parameters i_0, i_n, Ω, x & y is shown in Equation 4.7.

$$V_c = V_{0\,HHV} - \frac{RT}{z\alpha F} ln\left(\frac{i + i_n}{i_0}\right) - i\Omega - xexp\,(yi) \qquad (4.7)$$

Where:

F - Faraday constant (96,485 C/mol)

i - Current density (A/cm^2)

i_0 - Exchange current density (A/cm^2)

i_n - Internal current density (A/cm^2)

R - Universal gas constant (8.314 J/molK)

T - Temperature (K)

$V_{0\,HHV}$ - Theoretical potential based on the Higher Heating Value (HHV) of hydrogen

V_c - Cell potential (V)

x - Mass transport loss empirical constant 1 (V)

y - Mass transport loss empirical constant 2 (cm^2/A)

z - Number of electrons transferred per mole of fuel

α - Charge transfer coefficient

Ω - Area specific resistance (Ωcm^2)

The hydrogen/oxygen redox reaction occurs at all times when the reactants are in both in the presence of a suitable catalyst. Under a no-load condition, the reduction and oxidation reactions are in equilibrium. The resulting flow of electrons generates a current density,

commonly referred to as the exchange current density, i_0 [2]. This reversible equilibrium current can also be thought of as the "idle" current at the electrode [7]

Overvoltage associated with i_0 is a combination of the overvoltage at the cathode and that at the anode. For a hydrogen fuelled PEMFC, the cathodic overvoltage is substantially higher than that at the anode. Therefore, the anodic overvoltage is typically considered negligible [2]. Direct methanol fuel cells, on the other hand, have a much larger anodic overvoltage due to the complex methanol oxidation reaction. For both fuel cell technologies, the exchange overvoltage can be minimised by increasing the exchange current density by either increasing the cell temperature or increasing the catalyst site occupancy through elevating the pressure or increasing the reactant purity [2].

Internal current density, i_n is used as an approximation of the voltage drop associated with the crossover of fuel from the anode to the cathode. Fuel crossover is a term commonly given to the phenomena of fuel diffusing across the polymer membrane and reacting directly with the oxidant at the cathode. This process is more prevalent in DMFCs than PEMFCs [2,3,8] and removes electrons from the anode side of the fuel cell before they can be utilised by a connected electronic load.

Ohmic losses are represented in Equation 4.7 by the area specific resistance, Ω. This parameter represents the electrical losses due to material resistances. Each cell component contributes in part to the overall electrical resistance. However, the polymer electrolyte has by far the largest contribution [2].

Finally, there are two empirical constants, x, y (sometimes m, n)which are used to estimate the losses associated with mass transport. Although there is no real theoretical grounding, this approach is widely used in the fuel cell community as it tends to give the best fit [9,10].

4.1.5 The Polarisation Curve

Graphically, fuel cell irreversibilities are best represented by a polarisation curve. This type of performance figure is usually represented as a plot of decreasing cell potential with increasing current density. As fuel cells are highly scalable electrochemical devices, the use of current density instead of just current is preferred as it enables more straightforward comparisons between different fuel cells. An example polarisation plot for a generic low

temperature fuel cell is shown in Figure 4.3. This exemplar diagram clearly shows how the primary losses affect the fuel cell voltage.

As shown by Figure 4.3, activation losses are most prominent in the low current density portion of the polarisation curve whereas the high current density region is dominated by mass transport losses. It is preferable to operate a fuel cell in the ohmic region of the polarisation curve as the voltage response to a current demand is the most predictable.

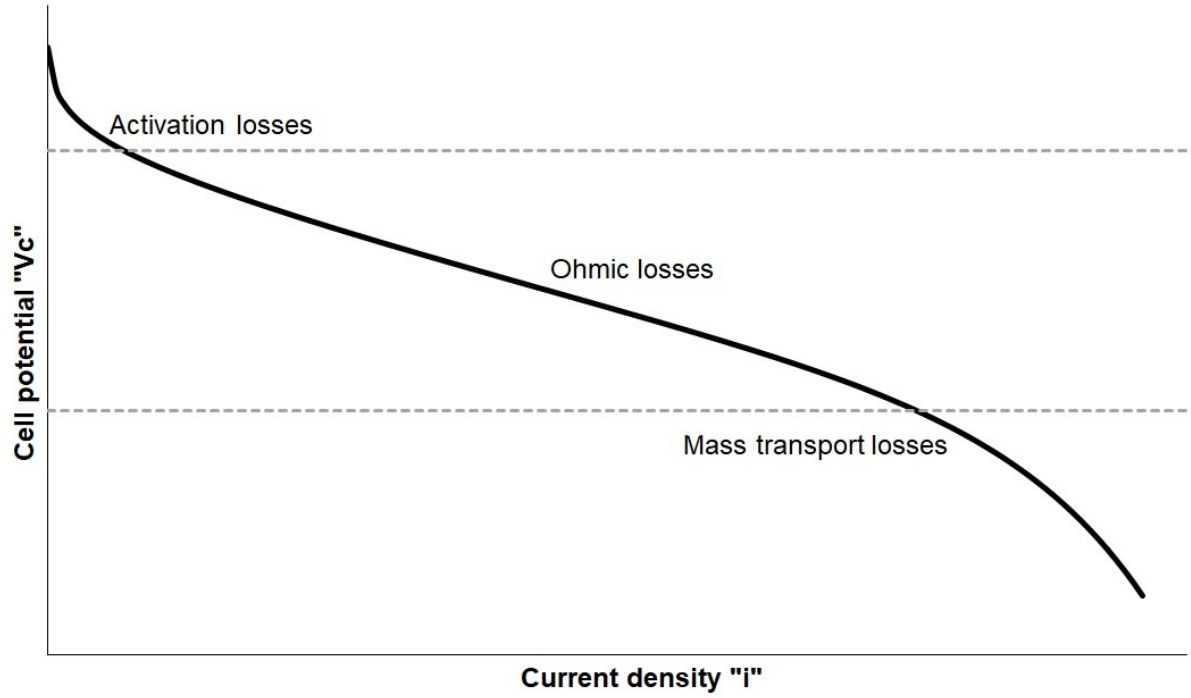

Figure 4.3: Fuel cell irreversibilities illustrated on a generic polarisation curve

Membrane electrode assemblies were purchased commercially from https://www.fuelcellstore.com/ for both fuel cell technologies so that experimental polarisation results could be obtained. Theoretical polarisation curves were then fitted to the experimental data by modifying the empirical constants from Equation 4.7. Technical specifications for both MEAs are contained in Table 4.5.

Table 4.5: Technical specifications for PEMFC and DMFC MEAs used in experimental work

	PEMFC MEA	**DMFC MEA**
Active area	25 cm^2	25 cm^2
Anode catalyst and loading	0.5 mg/cm^2 Pt/C	4.0 mg/cm^2 Pt.Ru
Cathode catalyst and loading	0.5 mg/cm^2 Pt/C	0.5 mg/cm^2 Pt/C
Membrane	Nafion™ 212	Nafion™ 117
Gas diffusion layer	Carbon cloth with MPL	Carbon cloth with MPL

The polymer electrolyte MEA was operated at a temperature of 70 ℃ with pure hydrogen as a fuel and humidified air as the oxidant. Experimental conditions were varied slightly for the DMFC MEA compared with the PEMFC. An operating temperature of 60 ℃ was used due to rig limitations. Humidified air was used as the oxidant and dilute methanol as the fuel. Full details of the experimental setups used are discussed in Chapter 8.

Literature derived [2,3,6,9] ranges were used as the starting point for the iterative determination of fit parameters for the full cell equation (Equation 4.7). These starting points were: $i_0 = 3.0E^{-6} \rightarrow 6.7E^{-5}\ A/cm^2$, $i_n = 0.003 \rightarrow 0.02\ A/cm^2$, $\Omega = 0.01 \rightarrow 0.245\ \Omega cm^2$, $x = 3.0E^{-4}\ V$, $y = 9.45\ cm^2/A$, and $\alpha = 0 \rightarrow 1$. It is expected that the values required to fit the experimental data may differ slightly from these ranges due in part to the age of available references and the experimental nature of the tested fuel cells.

Empirical parameters used to fit the full cell equation to experimental data for the PEMFC were: $i_0 = 1.0E^{-5}\ A/cm^2$, $i_n = 0.07\ A/cm^2$, $\Omega = 0.35\ \Omega cm^2$, $x = 3.5E^{-4}\ V$, $y = 11\ cm^2/A$ and the charge transfer coefficient, α was set at 0.29. Figure 4.4 contains the experimental and theoretical polarisation curves.

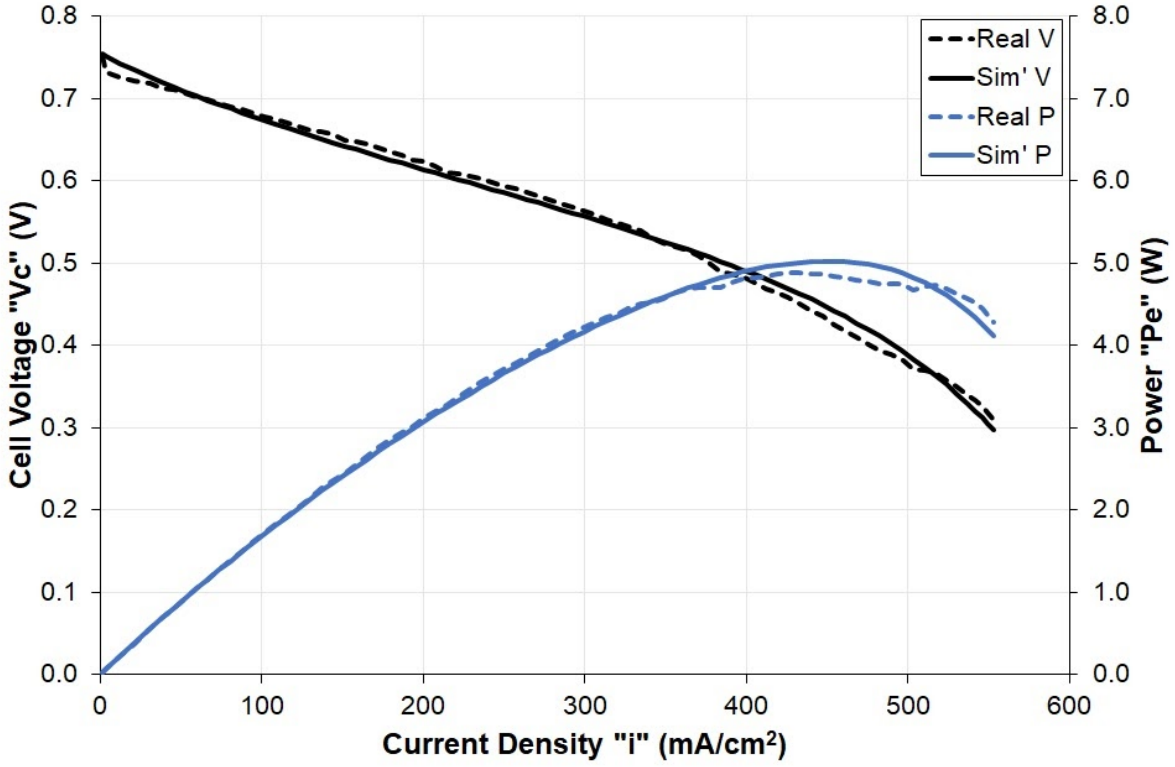

Figure 4.4: Comparison of theoretical and experimental results for a single cell 25cm² polymer electrolyte membrane fuel cell

Experimental conditions were varied slightly for the DMFC MEA compared with the PEMFC. An operating temperature of 60 °C was used due to rig limitations. Humidified air was used as the oxidant and dilute methanol as the fuel. Full details of the experimental setup used to obtain these results is discussed in Chapter 8. A theoretical polarisation curve was fitted to the experimental data using the following empirical parameters: $i_0 = 2.5E^{-7}\ A/cm^2$, $i_n = 0.0045\ A/cm^2$, $\Omega = 0.37\ \Omega cm^2$, $x = 1.5E^{-4}\ V$, $y = 28.9\ cm^2/A$ and $\alpha = 0.074$. Figure 4.5 contains the corresponding experimental and theoretical polarisation curves.

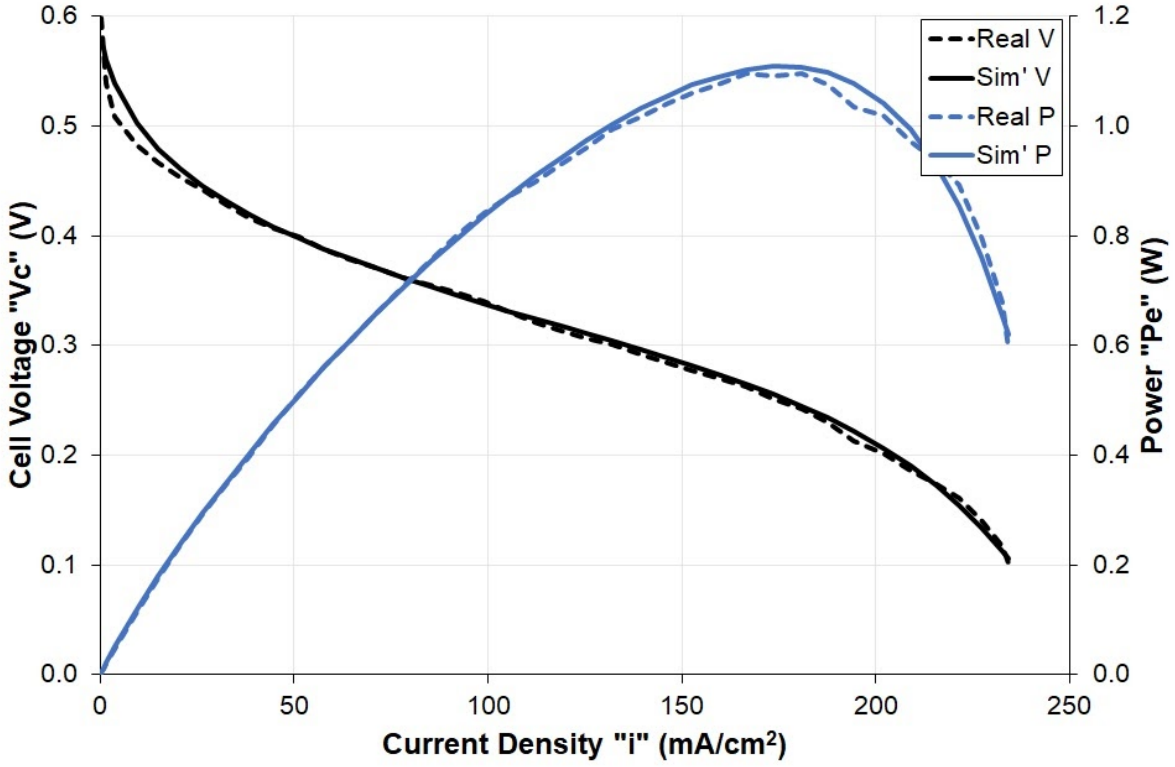

Figure 4.5: Comparison of theoretical and experimental results for a single cell 25cm² direct methanol fuel cell

A common measurement of error between experimental and modelled results is the Mean Absolute Error (MAE) as described by Equation 4.8 where an error, e is defined as the difference between modelled and real values (Equation 4.9). It is described as the "most natural measure of average error magnitude" [11] because it does not have a weighted error bias and relies purely on the absolute differences between measured and modelled values.

$$MAE = n^{-1} \sum_{i=1}^{i} |e_i| \tag{4.8}$$

$$e = x_{model} - x_{real} \tag{4.9}$$

Where:

e - Error

n - Sample size

However, an alternative error measurement which is generally regarded as being more suitable for calculating model error sensitivities is the Root-Mean-Square Error (RMSE) [12]. The key benefits of RMSE over MAE are that it applies a heavier weighting to larger errors and does not rely on the absolute difference between experimental and modelled results. Both these traits allow it to provide a more realistic interpretation of model performance. Equation 4.10 shows the principal calculation behind RMSE.

$$RMSE = n^{-1}\sqrt{\sum_{i=1}^{i} e_i^2} \qquad (4.10)$$

Where:

e - Error

n - Sample size

For the PEMFC model a RMSE of 9.52 mV is achieved whereas 8.72 mV was achieved for the DMFC model. Both of these errors are small and represent less than 1% of the thermodynamic reversible potentials for each fuel cell technology respectively.

4.2 Effect of Operating Conditions on Performance

Several factors, which can be defined as operating conditions can influence the electrical performance of a fuel cell. Specifically, the effects of pressure, temperature and anode and cathode reactant concentrations will be highlighted.

In reality these parameters will change the value of the reversible open circuit voltage. It is therefore important to first define the standard-state reversible potential, $V_{0\,HHV}^{std}$ which will provide the reference point for any change. The standard-state reversible potential is defined as the thermodynamically reversible potential of a fuel cell under standard temperature and pressure conditions of 298.15 K and 100 kPa respectively [3]. The standard-state reversible potentials for a PEMFC and DMFC are 1.23 V and 1.22 V respectively.

Most changes to the reversible open circuit voltage can be characterised by one of the more common forms for the Nernst equation [2,3]. As demonstrated by Equation 4.11a, this form of the Nernst equation relates the chemical activity of the reactants and products to the standard-state potential. The modified reversible open circuit voltage, V_0 produced by the Nernst equation can also be referred to as the "Nernst Voltage". As we are only interested in the change in voltage, this can be simplified to Equation 4.11b.

$$V_0 = V_{0\,HHV}^{std} + \frac{RT}{zF} ln \left(\frac{\Pi a_{reactants}^{M}}{\Pi a_{products}^{M}} \right) \qquad (4.11a)$$

$$\Delta V_0 = \frac{RT}{zF} ln \left(\frac{\Pi a_{reactants}^{M}}{\Pi a_{products}^{M}} \right) \qquad (4.11b)$$

Where:

a	-	Chemical activity of species in reaction
F	-	Faraday constant (96,485 C/mol)
M	-	Number of moles in balanced reaction
R	-	Universal gas constant (8.314 J/molK)
T	-	Temperature (K)
V_0	-	Reversible open circuit potential (V)
$V_{0\,HHV}^{std}$	-	Standard-state reversible potential (V)
ΔV_0	-	Change in reversible open circuit voltage (V)
z	-	Number of electrons transferred per mole of fuel

4.3 Liquid Reactant Considerations

Direct methanol fuel cells can be fed with liquid methanol fuel at almost any concentration. Experimental studies have been carried out with concentrations of methanol ranging from 0.25mol/dm^3 [13] to pure methanol [14]. Methanol dilution should always be carried out with deionised water to prevent potential catalyst poisoning when used as a fuel in a DMFC.

Generally, dilute aqueous solutions of methanol and deionised water are used to fuel DMFCs. Solution concentrations vary from publication to publication and between commercial systems however, they are generally low and in the range of 1.0 → 4.0 mol/dm^3 [15-21].

4.3.1 Nernstian Effect

Chemical activity and liquid reactant solution concentration are directly related through Equation 4.12 [3]. Substitution of this relationship into Equation 4.11b and assigning the standard-state concentration, c^0 a value of 1.0 mol/dm^3 it is possible to draw a direct relationship between the concentration of the anode reactant and the change in reversible open circuit voltage as shown by Equation 4.13. According to the mathematics, as anode reactant concentration increases, the reversible open circuit voltage will also increase.

$$a_i = c_i / c^0 \qquad (4.12)$$

$$\Delta V_0 = \frac{RT}{zF} ln\,(c_{methanol}) \qquad (4.13)$$

Where:

a_i - Chemical activity of species "i" in reaction

c^0 - Standard-state concentration (mol/dm^3)

c_i - Concentration of species "i" in reaction (mol/dm^3)

$c_{methanol}$ - Concentration of methanol solution (mol/dm^3)

F - Faraday constant (96,485 C/mol)

R - Universal gas constant (8.314 J/molK)

T - Temperature (K)

ΔV_0 - Change in reversible open circuit voltage (V)

z - Number of electrons transferred per mole of fuel

If the effects of crossover are negated, then the result of changing the methanol feed concentration on DMFC would be that demonstrated by Figure 4.6. The experimental and validated 1.0 M plots are from the model validation undertaken in Section 4.1.5. Lines of 0.5 M, 1.5M, 2.0 M and 4.0 M are modelled results by applying Equation 4.11b with Equation 4.12 substituting for the chemical activity term. This represents only the change in Nernst voltage.

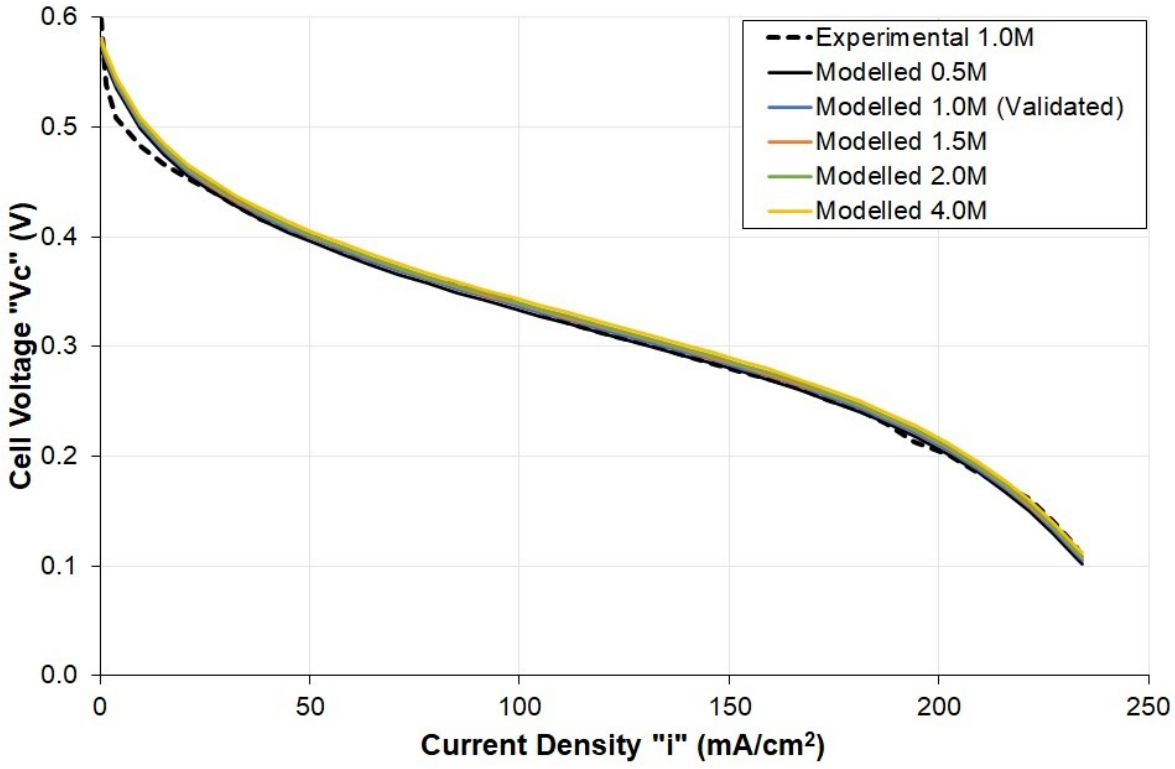

Figure 4.6: Modelled effect on DMFC performance as a result of changing the methanol feed concentration. Effect shown is that on the Nernst voltage, mass transport effects are assumed to be negligible.

As can be seen by the results, the Nernstian effect of increasing the methanol feed concentration is a slight increase in voltage as predicted. However, the results also show that the effect is negligible. In reality, increasing methanol feed concentration will raise the performance of a DMFC by a greater extent. This is because the increased concentration will greatly increase activity at the catalyst sites. This represents a limitation with the current modelling strategy which could be further improved with detailed electrochemical modelling of the processes.

4.3.2 The Problem with Crossover

The expected result of increasing methanol concentration; increasing electrical performance is not a continuous process. This is due to complex and conflicting interactions between methanol crossover and changes in the Nernst voltage.

The rate at which methanol crosses over from the anode to the cathode has been shown to be roughly proportional to the methanol concentration [15]. It has also been shown that the overall efficiency of a DMFC decreases as the methanol concentration increases [8,16]. This suggests that the crossover effects on DMFC electrical performance are more prevalent than the change in Nernst voltage.

Exemplar results, shown in Figure 4.7 from an experimental investigation into the effects of changing methanol feed concentration on DMFC performance have been reproduced with kind permission from Thiagarajan, V [17].

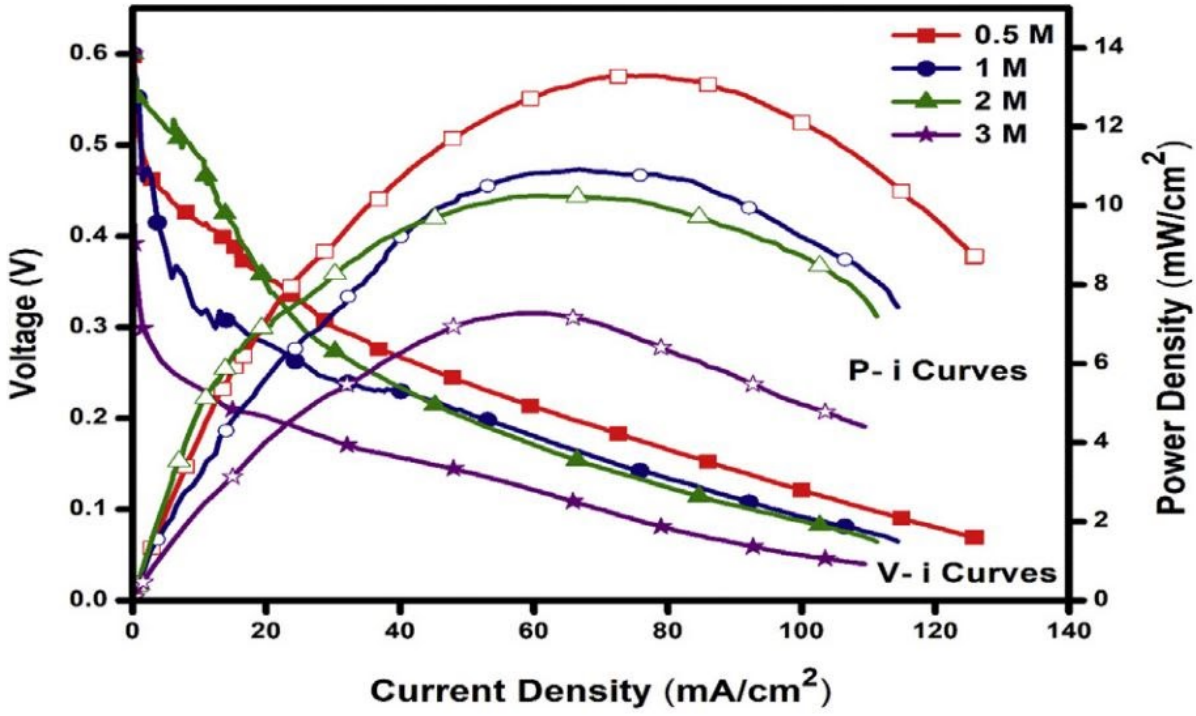

Figure 4.7: Polarisation (V-i) and power density (P-i) curves of the DMFCs for different molar concentrations of methanol. Reproduced with kind permission from Thiagarajan, V. 2019 [17].

These results clearly show a greater change in performance as the methanol feed concentration is varied, most likely linked to the dominant nature of methanol crossover as the general trend is for reducing performance as concentration is increased. Similar results are shown by [18-21].

4.4 Gaseous Reactant Considerations

Hydrogen fuelled PEMFCs are highly sensitive to the concentration, or purity of the hydrogen fuel used. Ideally, pure hydrogen should be used to maximise fuel cell electrical performance and minimise degradation [2,3]. However, due to the current primary hydrogen production method being the reformation of some light hydrocarbon fuel, it is inevitable that some impurities will also be produced as byproducts. One particular impurity which can have a highly adverse effect on the electrical performance of a PEMFC is carbon monoxide. Carbon monoxide particles poison the noble metal catalyst layer [22] by occupying the active platinum sites [2].

Due to the polluting nature of fossil fuel reformation, it will not be welcome in a future world with ever increasing environmental pressures. Hydrolysis is the process of splitting water into its constituent elements, hydrogen and oxygen. This process is carried out by supplying electrical energy to what is in essence a reverse PEMFC. If this electrical energy is generated in a renewable, zero-emission way using technologies such as solar and wind then the generated hydrogen is commonly given the name ‘green hydrogen’ [23,24]. When green hydrogen is used as a fuel in a hydrogen fuel cell, it is considered completely zero emissions.

Unlike their different fuel requirements, both PEMFC and DMFC technologies require oxygen to be reduced at the cathode. Reduced oxygen anions are then available to bond with the hydrogen cations being transported through the polymer electrolyte membrane. It is usually assumed that air is used as a source of oxygen due to the simple, low cost implementation. However, it is possible and arguably desirable to use an oxidant supply with a higher concentration of oxygen, even up to pure oxygen in air-independent designs.

As discussed in Chapter 2, aircraft operating at altitude where the air density is lower means that there will be less oxygen available to the fuel cell per unit volume of air injected. It stands to reason that this will also adversely affect the chemical activity of the air. This relationship warrants further investigation, which will be detailed below.

4.4.1 Partial Pressure, the Traditional Solution

As the cathode for both fuel cell technologies is gaseous, it is very common both in the literature and the teaching of fuel cell fundamentals to use the partial pressure form of the Nernst equation [2,3,25,26]. The partial pressure form is made by equating the chemical activity terms in Equation 4.8a to the partial pressures of the same species. Equation 4.11 demonstrates the partial pressure form of the Nernst equation specifically for a hydrogen fed PEMFC [2,3,25,26]. The full form of the partial pressure Nernst equation is based on the LHV of products and reactants [2]. If a calculation based on the HHV is desired, Equation 4.14 can be simplified by setting $\varrho_{H_2O} = 1,000\ kg/m^3$ as liquid water would be produced at the cathode. [3]

$$V_0 = V_{0\,HHV}^{std} + \frac{RT}{2F} ln\left(\frac{\varrho_{H_2} \bullet \varrho_{O_2}^{1/2}}{\varrho_{H_2O}}\right) \qquad (4.14)$$

Where:

F - Faraday constant (96,485 C/mol)

R - Universal gas constant (8.314 J/molK)

T - Temperature (K)

V_0 - Reversible open circuit potential (V)

$V_{0\,HHV}^{std}$ - Standard-state reversible potential (V)

ϱ_{H_2} - Partial pressure of hydrogen in balanced reaction (Pa)

ϱ_{H_2O} - Partial pressure of water in balanced reaction (Pa)

ϱ_{O_2} - Partial pressure of oxygen in balanced reaction (Pa)

4.4.2 Concentration and Total Pressure

For most applications, the partial pressure form of the Nernst equation, which is in itself an approximation, is more than adequate at representing the Nernstian effects on fuel cell voltage. However, when systems are operated at altitude, such as in aircraft, this approximation can break down as partial pressure is actually a function of both species concentration and total pressure, as per Equation 4.15 [25]. This relationship is particularly important as the cathode oxygen concentration can be varied independently of total pressure by either supplementing an air supply or injecting pure oxygen directly into the fuel cell.

$$\varrho_i = c_i \, p_t \qquad (4.15)$$

Where:

c_i - Concentration of species "i" in reaction (mol/dm^3)

p_t - Total system pressure (Pa)

ϱ_i - Partial pressure of species "i" in balanced reaction (Pa)

During a flight, total cathode inlet pressure will vary as a function of the changing altitude pressure as discussed in Chapter 2 and the form of system compression used. Air composition, and therefore oxygen concentration remains fairly consistent up to an altitude of around 100 km (> 300,000 ft) [27], far above that of any aircraft past or present [28-30]. Oxygen concentration is defined as the molar ratio, mol_{O_2}/mol_{air}, this is equivalent to the percentage composition by volume which is 20.95% for oxygen.

Oxygen concentration is related to the Nernst voltage using the same equation that was used for dealing with changes in methanol concentration (Equation 4.13). In addition to the improvement in Nernst voltage, using pure oxygen instead of air as an oxidant reduces activation losses and greatly reduces mass transport losses in a PEMFC [2]. The effect is similar for a DMFC, however, mass transport losses can never be fully eliminated due to the presence of methanol crossover [8,16].

Figure 4.8 shows the result of changing the oxidant feed from air to pure oxygen in the developed fuel cell model. The general upwards translation of the oxygen polarisation curve is as a result of the improved Nernst voltage.

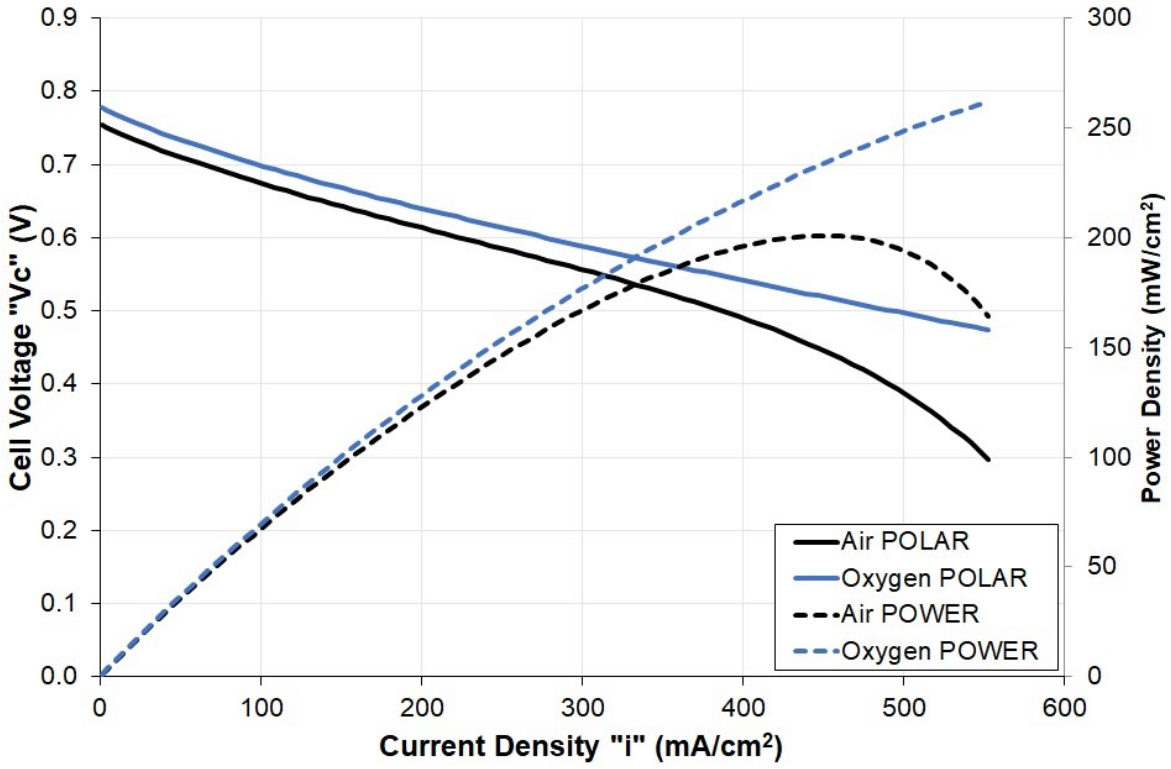

Figure 4.8: Modelled comparison of air-breathing and air-independent PEMFC polarisation and power curves

The key benefit of using pure oxygen as demonstrated by Figure 4.8 is the 30% increase in peak power due to the elimination of mass transport losses at high current densities. Further verification of the applicability of the developed fuel cell model comes from Prater, K [31] who also noted a 30% performance increase as a result of switching from air to oxygen.

Although the benefit to fuel cell performance is clear when changing from air to oxygen, the benefit to system performance is not quite as obvious. This is because, utilising oxygen as the cathode oxidant would require an aircraft to carry all of the oxygen it requires for completing its mission. A full trade-off study from the perspectives of mass, volume and parasitic load will be carried out in Chapter 6 to compare the system level efficiencies of air-breathing vs. air-independent designs. Additionally, hybrid air/oxygen systems will also be discussed.

Equation 4.16 [2] is a common representation that shows how the Nernstian cell voltage of the fuel cell increases with increasing operating pressure. It is assumed that the anode and cathode are kept under the same pressure. This assumption is generally expected as the pressures would have to be equilibrated to ensure excessive gas diffusion and mass transport don't happen.

$$\Delta V_0 = \frac{RT}{4F} ln\left(\frac{p_2}{p_1}\right) \qquad (4.16)$$

Where:

F - Faraday constant (96,485 C/mol)

p_1 - Initial system pressure (Pa)

p_2 - Final system pressure (Pa)

R - Universal gas constant (8.314 J/molK)

T - Temperature (K)

ΔV_0 - Change in reversible open circuit voltage (V)

Pressure related voltage increases are primarily a result of the cathode activation overvoltage being reduced [2]. Additional benefits on cell performance from increasing the pressure include increased exchange current density and the potential for a reduction in mass transport losses [2].

However, assuming air is used as an oxidant the parasitic load associated with driving a compressor to increase the cathode inlet pressure means that generally the gross system performance is reduced as pressure is increased [32,33] despite the net fuel cell performance increase [34].

As with concentration, the Nernstian effects of changing pressure are negligible. However, the effect of increasing total pressure has been shown to dramatically improve the performance of both PEMFCs and DMFCs. Increasing the total pressure from 100 kPa to 400 kPa has been shown to increase power density (mW/cm^2) of PEMFCs by over 50% [35] and by 20% for DMFCs [36].

This explanation is backed up by Heinzel, A [8] who noted that experimental works have shown significant performance improvements in DMFCs as a result of increasing the cathode inlet pressure. These performance gains could not be predicted by the thermodynamic or kinetic behaviour.

Performance gains resulting from increases in total pressure are due to the associated rise in chemical activity. This occurs as the elevated pressure has the effect of increasing the availability of reactants to the catalyst sites. However, the pressure cannot be raised indefinitely due to physical design constraints. Of particular note are the potential issues of gas passage sealing and the mass and volume increases resulting from the increased structure required to resist the mechanical stresses of elevated pressure operation.

Finally, the effects of altering both the concentration and total pressure of the cathode oxidant supply can be summarised by substituting Equation 4.16 into Equation 4.11b as shown by Equation 4.17.

$$\Delta V_0 = \frac{RT}{zF} ln \left(\frac{\Pi c^M_{reactants}}{\Pi c^M_{products}} \right) + \frac{RT}{4F} ln \left(\frac{p_2}{p_1} \right) \qquad (4.17)$$

Where:

c - Concentration of species in reaction (mol/dm^3)

F - Faraday constant (96,485 C/mol)

p_1 - Initial system pressure (Pa)

p_2 - Final system pressure (Pa)

R - Universal gas constant (8.314 J/molK)

T - Temperature (K)

ΔV_0 - Change in reversible open circuit voltage (V)

z - Number of electrons transferred per mole of fuel

4.5 Effects of Operating Temperature

Fuel cell operating temperature is a function of the heat generation rate by the exothermic electrochemical reaction and the heat rejection rate. This process will be covered in detail in Chapter 7 where the modelling of fuel cell thermal management systems will be discussed. For now, the effects of operating temperature specifically on the electrical performance of PEMFCs will be discussed.

It is well documented for both hydrogen fuelled PEMFCs [37,38] and DMFCs [17,39,40] increasing the operating temperature up to 80 ℃ of the fuel cell will increase the electrical performance. For PEMFCs, increases in peak electrical power output of around 30% have been observed as a result of increasing the operating temperature from 40 ℃ to 80 ℃ for fuel cells fuelled with humidified hydrogen and air [37,38].

A more varied rise in peak electrical power has been observed for DMFCs as the operating temperature was increased. Values have ranged from 16% → 38% for air-breathing test setups [39,40] and 28% → 43% for tests using pure oxygen as the oxidant [17,40] all with a temperature rise of approximately 20 ℃. The discrepancy in the results for the DMFCs is most likely a result of the high variance in catalytic compositions of the electrodes used. In comparison, the understanding of PEMFC electrode catalytic loading (and materials) is more developed and therefore the published works all use similar test setups.

In addition to the published experimental results, it is also possible to estimate the effect of changing the fuel cell operating temperature on electrical performance. If you refer back to Equation 4.2, the thermodynamic reversible voltage was shown to be a function of the change in Gibbs free energy, $\Delta\bar{g}$. In turn, $\Delta\bar{g}$ was shown by Equation 4.3 to be a function of temperature. Through the combination of these predefined formulations, an empirical approximation was made using Equation 4.18 [41].

$$\Delta V_0 = \frac{\Delta \bar{s}_T}{zF} \ (T - T_0) \qquad (4.18)$$

Where:

F - Faraday constant (96,485 C/mol)

$\Delta\bar{s}_T$ - Absolute entropy change at temperature “T” (J/mol.K)

T - Temperature (K)

T_0 - Reference temperature (25°C / 298.15 K)

ΔV_0 - Change in reversible voltage (V)

z - Number of electrons

As operating temperature increases the thermodynamically reversible voltage for the oxidation of hydrogen decreases (1.23 V @ 25 °C → ≈ 1.18 V @ 100 °C). In contrast, as operating temperature increases the thermodynamically reversible voltage for the oxidation of methanol increases (1.17 V @ 25 °C → ≈ 1.18 V @ 100 °C).

However, as has been shown in published experimental works typically, real fuel cell performance increases with an increase in temperature [17,37-40]. This is despite the fact that the thermodynamically reversible voltage decreases for the hydrogen oxidation reaction. This discrepancy is due to the raised temperature increasing the chemical activity of the reactants and allowing greater accessibility to the catalyst sites.

One final consideration to make is that the upper-limit for the operating temperature for a PEMFC is 100 °C. This limit is imposed for non-pressurised systems in an effort to ensure the presence of liquid water in the polymer membrane. Dehydrated polymer electrolyte membranes have been shown to consistently produce less electrical power than their hydrated (humidified) counterparts in the same cell setup [34,42,43].

4.6 Stacking

As it is common to specify fuel cell performance using current density, it is also important to know what the active area of each cell is. Knowing these two values allows the calculation of the gross fuel cell current using Equation 4.19. In order to increase the total current production potential of a fuel cell, either the current density must be improved, or the cell must be physically larger so that that active area is greater. Generally, it is easier and cheaper to increase the active area of a fuel cell as complex materials research is usually required to improve current density. However, the mass and volume limitations associated with the aeronautical industry may limit the maximum active area possible for any given application.

$$I = iA \tag{4.19}$$

Where:

A - Cell active area (cm^2)

I - Current (A)

i - Current density (A/cm^2)

Fuel cell stacks are an assembly of multiple individual fuel cells, literally stacked one on top of another. Typically, the cells share common fuel and oxidant feeds as this maintains simplicity and helps reduce the mass and volume of the stack. One of the primary benefits of fuel cell technology is the flexibility afforded in the electrical configuration. Each of the cells can be electrically connected either in series or parallel with any number of other cells to produce the current and voltage profiles stipulated by the customer. Electrical power produced by a fuel cell stack is a function of the cell potential, current and number of cells as described by Equation 4.20.

$$P_e = V_c In \tag{4.20}$$

Where:

I - Current (A)

n - Number of cells

P_e - Electrical power (W)

V_c - Cell potential (V)

4.7 Summary

Creation of a validated electrical fuel cell stack model has been detailed step-by-step throughout this chapter. Two common idealised fuel cell voltages were defined, where the thermodynamic reversible voltage, $V_{0\,HHV}$ bears more importance than the ideal potential, V_{HHV} in the prediction of fuel cell electrical behaviour. Whereas, V_{HHV} is used in the calculation of fuel cell efficiency.

Primary fuel cell irreversibilities: activation, fuel crossover, ohmic and mass transport have been defined, both theoretically and empirically. An empirical form of the Nernst equation was used to predict the performance of both a single cell PEMFC and DMFC. The model results were validated against experimental data for both fuel cell technologies. Model prediction root-mean-square errors of 9.52 mV and 8.72 mV were achieved for PEMFC and DMFC respectively.

Combining Equations 4.2, 4.7, 4.17 and 4.18 gives the final full cell equation (Equation 4.21) used for the modelling study. It combines the effects of reactant concentration, pressure, temperature and validated irreversibilities on the temperature dependent reversible thermodynamic voltage.

$$V_c = \frac{\Delta\bar{g}_{HHV}}{zF} + \frac{RT}{zF} ln\left(\frac{\Pi c^{M}_{reactants}}{\Pi c^{M}_{products}}\right) + \frac{RT}{4F} ln\left(\frac{p_2}{p_1}\right) + \frac{\Delta\bar{s}_T}{zF}(T - T_0) - \\ - \frac{RT}{z\alpha F} ln\left(\frac{i + i_n}{i_0}\right) - i\Omega - xexp(yi) \qquad (4.21)$$

A summary of the effects of changing several operating parameters covered in Equation 4.21 on real fuel cell performance is given in Table 4.6.

Table 4.6: Influence of increasing different operating parameters on methanol crossover and fuel cell performance [8]

Parameter	**Methanol Crossover (DMFC only)**	**PEMFC / DMFC Performance**	
		Low Current Density	**High Current Density**
Cell temperature	Favourable	Favourable	Favourable
Cathode pressure	Unfavourable	Favourable	Favourable
Fuel concentration	Favourable	Unfavourable	Favourable
Current density	Unfavourable	Unfavourable	Unfavourable

4.8 References

[1] Cambridge Dictionary. performance. Cambridge Dict n.d. https://dictionary.cambridge.org/dictionary/english/performance (accessed April 23, 2020).

[2] Larminie J, Dicks A. Fuel Cell Systems Explained. 2nd ed. John Wiley & Sons; 2003. https://doi.org/10.1016/S0378-7753(00)00571-1.

[3] O'Hayre R, Cha S-W, Colella W, Prinz FB. Fuel cell fundamentals. 3rd ed. John Wiley & Sons; 2016.

[4] Feiner AS, McEvoy AJ. The Nernst Equation. J Chem Educ 1994;71:493–4. https://doi.org/10.1021/ed071p493.

[5] Vidal-Iglesias FJ, Solla-Gullón J, Rodes A, Herrero E, Aldaz A. Understanding the Nernst equation and other electrochemical concepts: An easy experimental approach for students. J Chem Educ 2012;89:936–9. https://doi.org/10.1021/ed2007179.

[6] Barbir F. PEM Fuel Cells Theory and Practice. Elsevier Academic Press; 2005.

[7] Bard AJ, Faulkner L. Electrochemical methods: fundamentals and applications. 2nd ed. New York, London: Wiley-Interscience; 2000.

[8] Heinzel A, Barragán VM. Review of the state-of-the-art of the methanol crossover in direct methanol fuel cells. J Power Sources 1999;84:70–4. https://doi.org/10.1016/S0378-7753(99)00302-X.

[9] Kim J, Lee S, Srinivasan S, Chamberlin CE, Kim J, Lee S, et al. Modeling of Proton Exchange Membrane Fuel Cell Performance with an Empirical Equation. J Electrochem Soc 1995;142:2670–4. https://doi.org/10.1149/1.2050072.

[10] Laurencelle F, Chahine R, Hamelin J, Agbossou K, Fournier M, Bose TK, et al. Characterization of a Ballard MK5-E Proton Exchange Membrane Fuel Cell Stack. Fuel Cells 2001;1:66–71. https://doi.org/10.1002/1615-6854(200105)1:1<66::AID-FUCE66>3.0.CO;2-3.

[11] Willmott CJ, Matsuura K. Advantages of the mean absolute error (MAE) over the root mean square error (RMSE) in assessing average model performance. Clim Res 2005;30:79–82. https://doi.org/10.3354/cr030079.

[12] Chai T, Draxler RR. Root mean square error (RMSE) or mean absolute error (MAE)? -Arguments against avoiding RMSE in the literature. Geosci Model Dev 2014;7:1247–50. https://doi.org/10.5194/gmd-7-1247-2014.

[13] Xu C, Zhao TS. A new flow field design for polymer electrolyte-based fuel cells. Electrochem Commun 2007;9:497–503. https://doi.org/10.1016/j.elecom.2006.10.031.

[14] Halim FA, Hasran UA, Masdar MS, Kamarudin SK. Study on a Passive Vapor Feed Direct Methanol Fuel Cell with High Methanol Concentration. J Clean Energy Technol 2013;1:292–4. https://doi.org/10.7763/JOCET.2013.V1.66.

[15] Guo Z, Faghri A. Vapor feed direct methanol fuel cells with passive thermal-fluids management system. J Power Sources 2007;167:378–90. https://doi.org/10.1016/j.jpowsour.2007.02.024.

[16] Liu J, Zhao T, Chen R, Wong C. The effect of methanol concentration on the performance of a passive DMFC. Electrochem Commun 2005:288–94. https://doi.org/10.1016/j.elecom.2005.01.011.

[17] Thiagarajan V, Karthikeyan P, Thanarajan K, Neelakrishnan S, Manoharan R, Chen R, et al. Experimental investigation on DMFCs using reduced noble metal loading with NiTiO3 as supportive material to enhance cell performances. Int J Hydrogen Energy 2019;44:13415–23. https://doi.org/10.1016/j.ijhydene.2019.03.244.

[18] Kang K, Lee G, Gwak G, Choi Y, Ju H. Development of an advanced MEA to use high-concentration methanol fuel in a direct methanol fuel cell system. Int J Hydrogen Energy 2012;37:6285–91. https://doi.org/10.1016/j.ijhydene.2011.06.114.

[19] Pan YH. Advanced air-breathing direct methanol fuel cells for portable applications. J Power Sources 2006;161:282–9. https://doi.org/10.1016/j.jpowsour.2006.03.048.

[20] Zhao TS, Xu C, Chen R, Yang WW. Mass transport phenomena in direct methanol fuel cells. Prog Energy Combust Sci 2009;35:275–92. https://doi.org/10.1016/j.pecs.2009.01.001.

[21] Nakagawa N, Xiu Y. Performance of a direct methanol fuel cell operated at atmospheric pressure. J Power Sources 2003;118:248–55. https://doi.org/10.1016/S0378-7753(03)00090-9.

[22] Pilatowsky I, Romero RJ, Isaza CA, Gamboa SA, Sebastian PJ, Rivera W. Thermodynamics of Fuel Cells. Cogener. Fuel Cell - Sorption Air Cond. Syst. 1st ed., London: Springer-Verlag; 2011, p. 25–36. https://doi.org/10.1007/978-1-84996-028-1.

[23] Dincer I. Green methods for hydrogen production. Int J Hydrogen Energy 2012;37:1954–71. https://doi.org/10.1016/j.ijhydene.2011.03.173.

[24] Clark WW, Rifkin J. A green hydrogen economy. Energy Policy 2006;34:2630–9. https://doi.org/10.1016/j.enpol.2005.06.024.

[25] Pratt JW, Brouwer J, Samuelsen GS. Performance of Proton Exchange Membrane Fuel Cell at High-Altitude Conditions. J Propuls Power 2007;23:437–44. https://doi.org/10.2514/1.20535.

[26] Monem AA A El, M Azmy A. Dynamic Modelling of Proton Exchange Membrane Fuel Cells for Electric Vehicle Applications. J Pet Environ Biotechnol 2014;5. https://doi.org/10.4172/2157-7463.1000169.

[27] Reid A. The Composition of Earth's Atmosphere With Elevation. MrReidOrg 2014. http://wordpress.mrreid.org/2014/08/01/the-composition-of-earths-atmosphere-with-elevation/ (accessed June 15, 2020).

[28] Gunston B, Willis D, Munson K, Peacock L, Jackson P, Bushell S, editors. Jane's all the world's aircraft: development & production 2016-2017. IHS; 2016.

[29] Gunston B, Willis D, Munson K, Peacock LT, Jackson P, Bushell S, editors. Jane's all the world's aircraft: development & production 2015-2016. IHS; 2015.

[30] Gunston B, Willis D, Munson K, Peacock LT, Jackson PA, Bushell S, editors. Jane's all the world's aircraft: development & production 2014-2015. IHS; 2014.

[31] Prater K. The renaissance of the solid polymer fuel cell. J Power Sources 1990;29:239–50. https://doi.org/10.1016/0378-7753(90)80023-7.

[32] Qin Y, Du Q, Fan M, Chang Y, Yin Y. Study on the operating pressure effect on the performance of a proton exchange membrane fuel cell power system. Energy Convers Manag 2017;142:357–65. https://doi.org/10.1016/j.enconman.2017.03.035.

[33] Cunningham JM, Hoffman MA, Friedman DJ. A Comparison of High-Pressure and Low-Pressure Operation of PEM Fuel Cell Systems. SAE Tech Pap Ser 2010;1. https://doi.org/10.4271/2001-01-0538.

[34] Wang L, Husar A, Zhou T, Liu H. A parametric study of PEM fuel cell performances. Int J Hydrogen Energy 2003;28:1263–72. https://doi.org/10.1016/S0360-3199(02)00284-7.

[35] Yan Q, Toghiani H, Causey H. Steady state and dynamic performance of proton exchange membrane fuel cells (PEMFCs) under various operating conditions and load changes. J Power Sources 2006;161:492–502. https://doi.org/10.1016/j.jpowsour.2006.03.077.

[36] Im JY, Kim BS, Choi HG, Cho SM. Effect of pressure for direct fuel cells using DME-based fuels. J Power Sources 2008;179:301–4. https://doi.org/10.1016/j.jpowsour.2007.12.046.

[37] Amirinejad M, Rowshanzamir S, Eikani MH. Effects of operating parameters on performance of a proton exchange membrane fuel cell. J Power Sources 2006;161:872–5. https://doi.org/10.1016/j.jpowsour.2006.04.144.

[38] Coppo M, Siegel NP, Spakovsky MR von. On the influence of temperature on PEM fuel cell operation. J Power Sources 2006;159:560–9. https://doi.org/10.1016/j.jpowsour.2005.09.069.

[39] Ko J, Chippar P, Ju H. A one-dimensional, two-phase model for direct methanol fuel cells - Part I: Model development and parametric study. Energy 2010;35:2149–59. https://doi.org/10.1016/j.energy.2010.01.034.

[40] Vasile NS, Monteverde Videla AHA, Simari C, Nicotera I, Specchia S. Influence of membrane-type and flow field design on methanol crossover on a single-cell DMFC: An experimental and multi-physics modeling study. Int J Hydrogen Energy 2017;42:27995–8010. https://doi.org/10.1016/j.ijhydene.2017.06.214.

[41] Colleen Spiegel. PEM Fuel Cell: Modeling and Simulation using MATLAB. ElsevierAcademic Press; 2008. https://doi.org/10.1016/B978-012374259-9.50006-9.

[42] Chen C-CC, Shaw D, Hsueh K-LL. Optimization of the electrodes humidification temperature and clamping pressure to achieve uniform current density in a commercial-sized proton exchange membrane fuel cell. Int J Hydrogen Energy 2017;42:3185–96. https://doi.org/10.1016/j.ijhydene.2016.09.178.

[42] Kim S, Hong I. Effects of humidity and temperature on a proton exchange membrane fuel cell (PEMFC) stack. J Ind Eng Chem 2008;14:357–64. https://doi.org/10.1016/j.jiec.2008.01.007

Chapter 5 Fuel System Analysis

5.1 Introduction

When considering primary galvanic cells of which fuel cells are a type, the anode refers to the electrode from which electrons are produced [1]. Therefore, electrically speaking a fuel cell anode is negative which is contrary to the popular convention of electrically positive anodes for electrolytic cells i.e. electrolysers.

A fuel cell anode system is defined for the purpose of this study as all of the equipment required to store and supply fuel to the anode inlet port of the fuel cell stack as well as items which may exist on an anode exhaust. The internal fuel pathway from the anode inlet, through the flow field and gas diffusion layer to the anode electrode catalyst site was considered separately as being part of the fuel cell itself.

As previously discussed, the two fuel cell technologies focussed on in this study have very different fuel requirements. Polymer Electrolyte Membrane Fuel Cells (PEMFC) require pure hydrogen gas to be fed to the anode, typically under pressure [1,2]. Whereas Direct Methanol Fuel Cells (DMFC) require methanol as a fuel, typically fed to the anode as a liquid solution [1,2].

Fuel cells can typically have one of three macro-scale anode designs: dead-ended, open-ended and semi-dead-ended. In a dead-ended design there is no anode exhaust. Therefore, all of the fuel provided at the inlet must be reacted through the fuel cell. This is only possible in fuel cell designs where the inlet fuel is pure as any impurities are unlikely to pass through the polymer electrolyte membrane.

Alternatively, open-ended and semi-dead-ended designs are able to utilise impure fuel stock, assuming the impurities don't interfere with the electrochemical reaction or poison the catalyst sites. This is particularly important with DMFC's where the fuel is a diluted solution [1,2]. An open-ended design is as it sounds, the anode has an exhaust which is always open (although it can be restricted to increase back-pressure). The primary disadvantage of this design is poor fuel utilisation.

Semi-dead-ended designs have a valve on the anode exhaust. This is normally in the closed position, allowing dwell times for the fuel to react at the catalyst sites. Periodically, the valve is opened to remove excess fuel and any products which may have been produced or crossed over to the anode. This process is called purging [3] and the associated purge strategies are a whole topic of research in themselves and therefore will not be covered in this work.

For semi-dead-ended designs incorporating some form of purging, it is also possible to recirculate the anode exhaust stream between purge events. Benefits of implementing anode recirculation are reported to include: improved fuel utilisation, reduced cell-to-cell voltage variation across a stack, and increased membrane humidification for gas fed fuel cells [4-6]. However, due to the complex multi-phase interactions associated with anode recirculation it will not be considered for use with PEMFCs in this work.

In this Chapter, anode system design considerations for both fuel cell technologies will be analysed. In addition to fulfilling the fuel flow rate and inlet pressure requirements, key design priorities for anode fuel systems intended for use in aeronautical must include mass and volume. As fuel cells are fundamentally energy conversion devices, the most suitable way of analysing these systems would be to use specific energy, $e_{FCS}\,(J/kg)$ and energy density, $u_{FCS}\ (J/m^3)$.

5.2 Hydrogen

Hydrogen is a colourless, odourless gas which is utilised in its pure molecular form as a fuel in PEMFCs. It is generally not found as an isolated molecule in nature (on Earth) but is present in many common chemical compounds. As such, it must be extracted and isolated through an energy consuming process. As a result, it is common to refer to hydrogen as an energy carrier rather than a fuel. Properties of molecular hydrogen which are pertinent to the design and analysis of storage and delivery systems are contained within Table 5.1. Additional thermodynamic data for hydrogen can be found in Appendix 3.

Table 5.1: Properties of molecular hydrogen [1,2,7-9]

Property	**Value**
Molecular weight	2.016 g/mol
Boiling point	20.4 K
Calorific value (Higher Heating Value) at 298 K	141.8 MJ/kg (39.38 kWh/kg)
Gaseous density at 100kPa and 298 K	0.0899 kg/m^3
Liquid density at 100kPa and 20.4 K	70.85 kg/m^3

A range of advantages and disadvantages are presented by hydrogen's physical properties. The low molecular mass of hydrogen can be seen to be a big advantage, especially considering the mass sensitive nature of aeronautical applications. However, when coupled with the incredibly low density of pure gaseous hydrogen, the volumetric energy density is somewhat lower than other common fuel types.

There are three common metrics used in the literature when comparing different methods of hydrogen storage to each other and to other fuel storage solutions. These are weight percentage, gravimetric energy density and volumetric energy density. Weight percentage, *wt*.% is a useful metric for comparing different storage technologies for the same fuel as it avoids any confusion with which heating value was used (higher or lower). It is defined as the mass of hydrogen stored divided by the total mass of the hydrogen and the storage vessel.

Both gravimetric and volumetric energy densities can be used to compare different fuel types in addition to different hydrogen storage methods. Gravimetric energy density (specific energy), e is found using the fuel calorific value and the mass of the fuel and storage vessel, common units are kWh/kg. Volumetric energy density, u is found using the fuel calorific value and the volume of the fuel and storage vessel, common units are kWh/L.

Figure 5.1 shows the gravimetric and volumetric storage densities of various hydrogen storage options. As aerospace applications tend to be more mass sensitive than volume sensitive, metal hydride hydrogen storage would be the least suitable solution. Ideally, light hydrides would be used, however, they are generally more difficult to re-fuel due to their availability. This leaves Liquid Hydrogen (LH_2) and high pressure Compressed Gaseous Hydrogen (CGH_2) as remaining storage options.

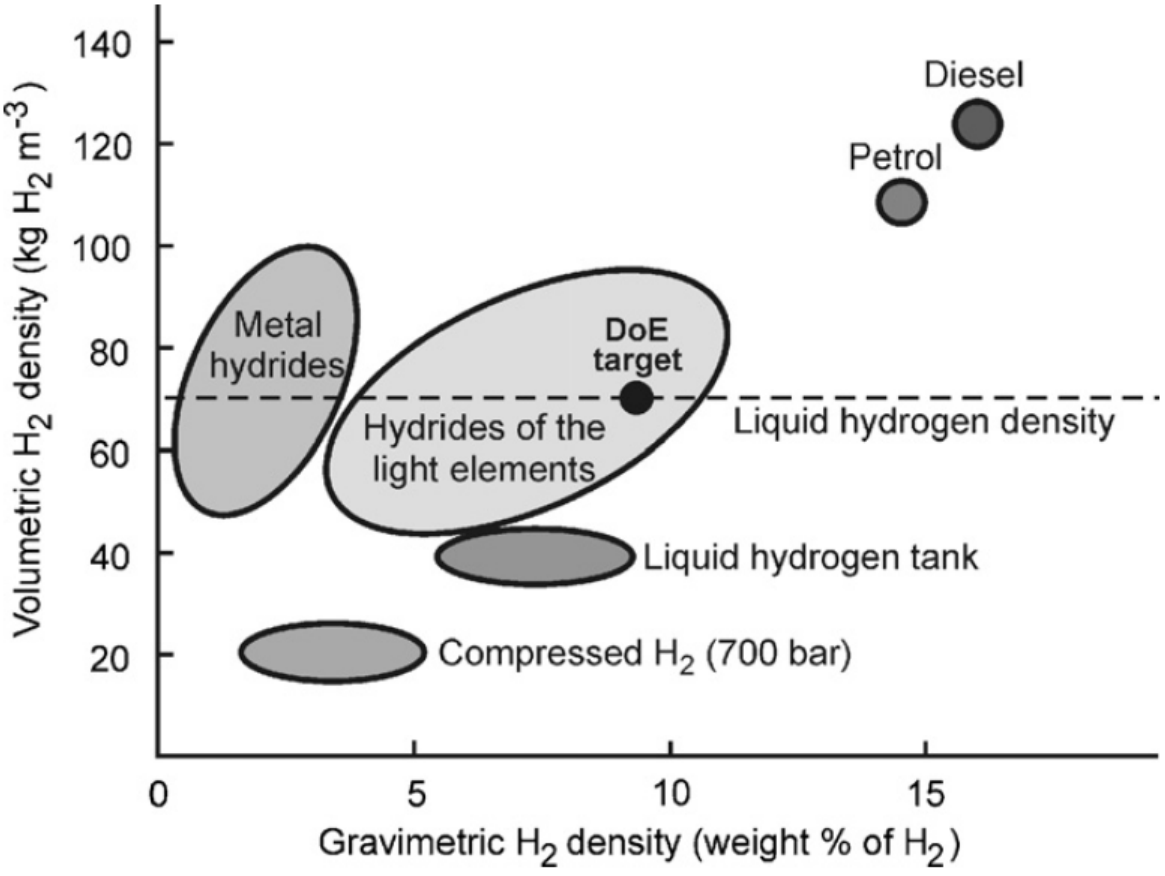

Figure 5.1: Gravimetric and volumetric densities of various hydrogen storage options. 'DoE target' represents the US Department of Energy target for hydrogen storage material [10] (Open access CC BY-NC-ND license)

5.2.1 Gaseous Storage

Molecular hydrogen is commonly stored as a compressed gas at around 200 bar g [1,11] and is commercially available as an industrial fuel gas [12]. Energy density of CGH_2 storage is improved by increasing the storage pressure of the molecular hydrogen. The pressure can be raised either using a mechanical piston based compressor or using non-mechanical compression techniques such as electrochemical and metal-hydride compression [11,13]. Of the different compression techniques available, non-mechanical methods are preferred when compressing hydrogen intended for use in fuel cells as the guarantee that the gas is not contaminated with the lubricating oil required in mechanical compressors [11].

Although regularly treated as an ideal gas due to small size and weak intermolecular forces, this assumption breaks down as the pressure is increased [14]. Compressibility factor, sometimes gas deviation factor, Z is used to describe the deviation between the ideal gas assumption and the behaviour of a real gas whilst being compressed. The variation of compressibility factor for hydrogen is shown in Figure 5.2

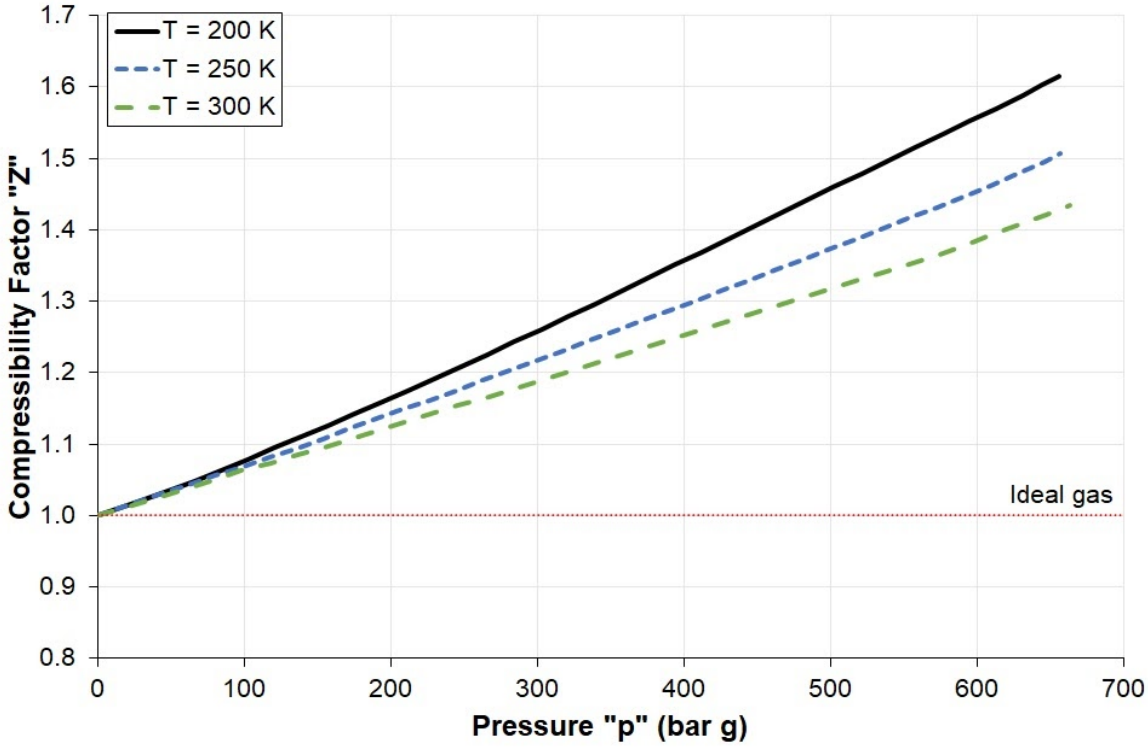

Figure 5.2: Variation of compressibility factor of hydrogen with increasing pressure at temperatures of 200, 250 ad 300 K [14]

As demonstrated by Figure 5.2, changing storage temperature leads to deviations in the rate of change of compressibility factor with increasing pressure. Up to a storage pressure of around 100 bar g, the compressibility factor for molecular hydrogen is fairly consistent in the temperature range of 200 K to 300 K. Above this pressure, increasing the temperature leads to a decreasing rate of change in gas deviation factor. Factoring this observation into the determination of gas density change with increasing pressure leads to the results shown in Figure 5.3.

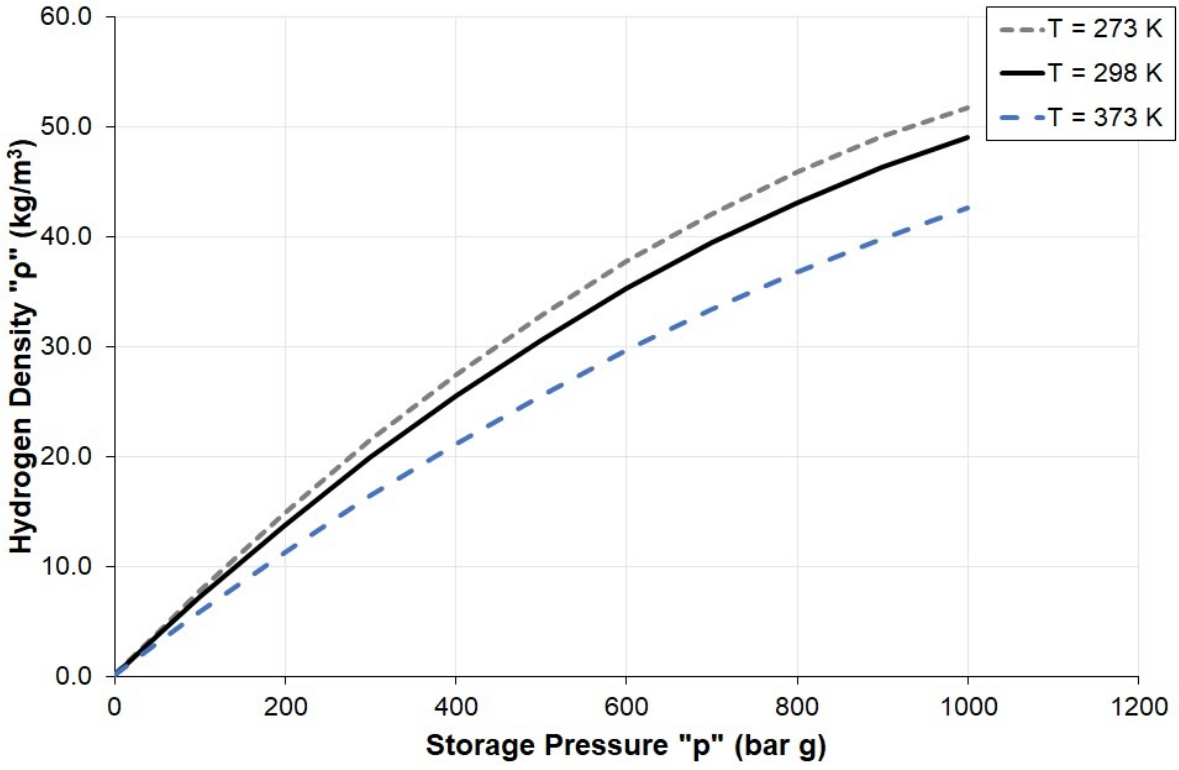

Figure 5.3: Density evolution of molecular hydrogen with respect to storage pressure for temperatures of 273, 298 and 373 K [11,15]

An interesting observation from Figure 5.3 which is particularly relevant to the storage of molecular hydrogen at very high pressures (> 500 bar g) is the evolving nonlinearity of density evolution with increasing pressure. It is important that the model developed as part of this work is able to account for this deviation as it will lead to variations in the gravimetric and volumetric storage efficiencies.

In addition to the non-ideal density evolution of molecular hydrogen, the physical characteristics of the storage vessel will play an important role in determining the hydrogen storage efficiency. Due to the potentially high pressures associated with hydrogen storage, the pressure vessel material choice is one of the most important considerations when designing CGH_2 systems [16]. In addition to being capable of withstanding the high pressure, chosen materials must also be resistant to hydrogen embrittlement [17]. Typically, austenitic stainless steels, aluminium and high-density polymers such as HDPE are used.

Currently, there are four commercially available CGH_2 storage cylinders, Type I → Type IV [14,18,19]. Information relating to the construction materials and capabilities of each cylinder type are given in Table 5.2 with key differences graphically represented in Figure 5.4.

Table 5.2: Materials and pressure ranges of Type I, II, III and IV cylinders [14,18-20]

Cylinder Classification	**Typical Storage Pressure**	**Construction Materials**
Type I	150 - 300 bar g	All steel construction
Type II	< 1,000 bar g	Load-bearing metallic liner hoop wrapped with resin impregnated composite
Type III	< 450 bar g	Non-load-bearing metallic liner axially and hoop wrapped with resin impregnated composite
Type IV	Up to 700 bar g	High-density polymer liner, axially and hoop wrapped with resin impregnated composite

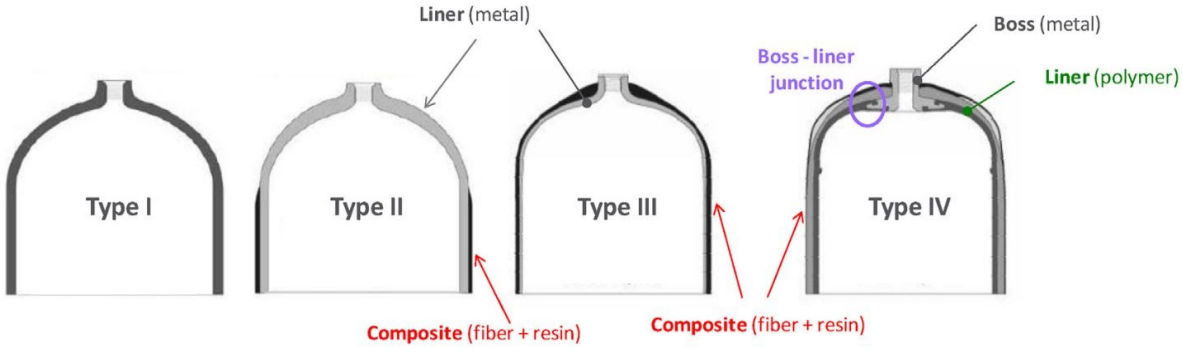

Figure 5.4: Representation of Type I, II, III and IV compressed gas cylinders [19] reproduced with permission from Elsevier (Licence: 4860680258275)

Although Type II cylinders currently have the highest storage pressure possible [19,20], their reliance on load-bearing metallic liners means that the fully polymer and composite construction of Type IV cylinders gives a distinct weight advantage. This is shown by plotting the specific energy and energy density averages for current commercially available CGH_2 cylinders at their peak storage pressures, Figure 5.5 [21-26]. Specific energy and energy density values were found using non-ideal density evolution at 298 K demonstrated by Figure 5.3 in addition to the physical mass and liquid volume of the empty cylinders. These results are valid for CGH_2 tanks capable of storing up to 10 kg of hydrogen in a single tank.

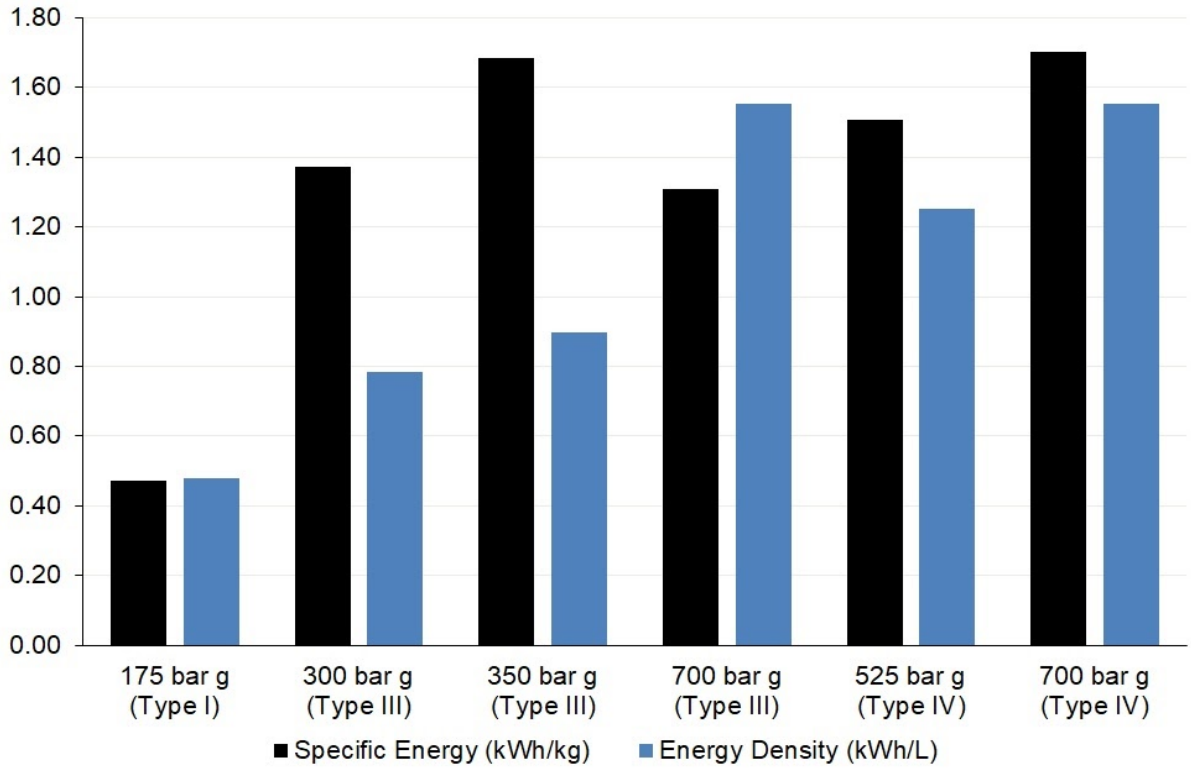

Figure 5.5: Specific energy and energy density variation with storage pressure and cylinder type for existing commercially available CGH_2 storage cylinders (data for several cylinders has been averaged to produce each plot) [21-26]

The analysis from Figure 5.5 clearly shows general improvements in both specific energy and energy density as the cylinder technology is advanced from Type I to Type IV. Although certain Type III cylinders come close to matching the performance of Type IV either on specific energy or energy density, Type IV cylinders show the best balance.

As well as knowledge of the energy density and specific energy, collectively storage efficiency of different CGH_2 technologies; it would also be beneficial to have direct relationships between the quantity of hydrogen stored and the physical characteristics of the vessel, in particular its mass and volume. Commercial CGH_2 cylinder data [21-26] was used to produce the relationships for mass (Figure 5.6) and volume (Figure 5.7). For each plot, a linear trendline was generated with the equations for mass plots given in Table 5.3 and those for volume in Table 5.4. Data for 175 bar g hydrogen storage was limited to two cylinder types from BOC therefore, the inclusion of this information is meant only for reference.

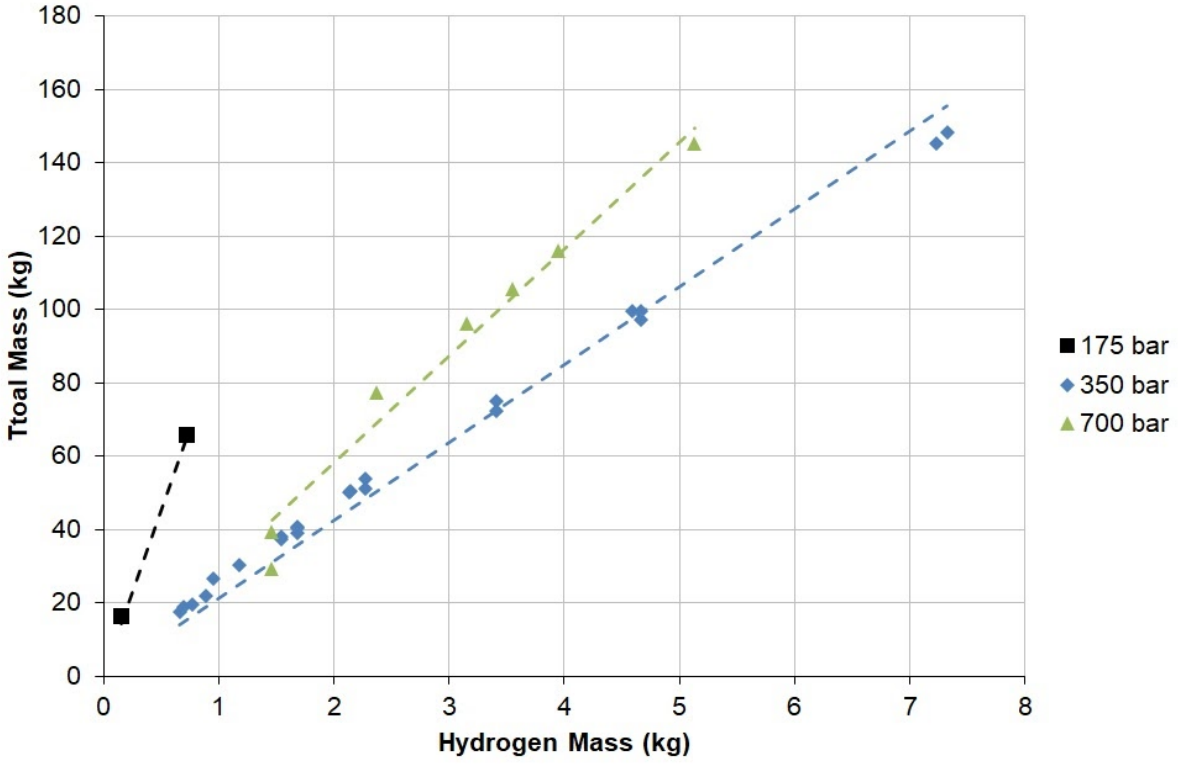

Figure 5.6: Change in total mass of hydrogen and vessel with increasing mass of hydrogen stored for 175, 350 and 700 bar g storage pressures [21-26]

Table 5.3: Fits through origin and R^2 values for correlations from Figure 5.6

Plot	**Fitted Correlation (u = mass of hydrogen stored (kg))**	**R^2**
175 bar g	$mass = 90.592u$	1
350 bar g	$mass = 29.13u$	0.99
700 bar g	$mass = 21.228u$	0.99

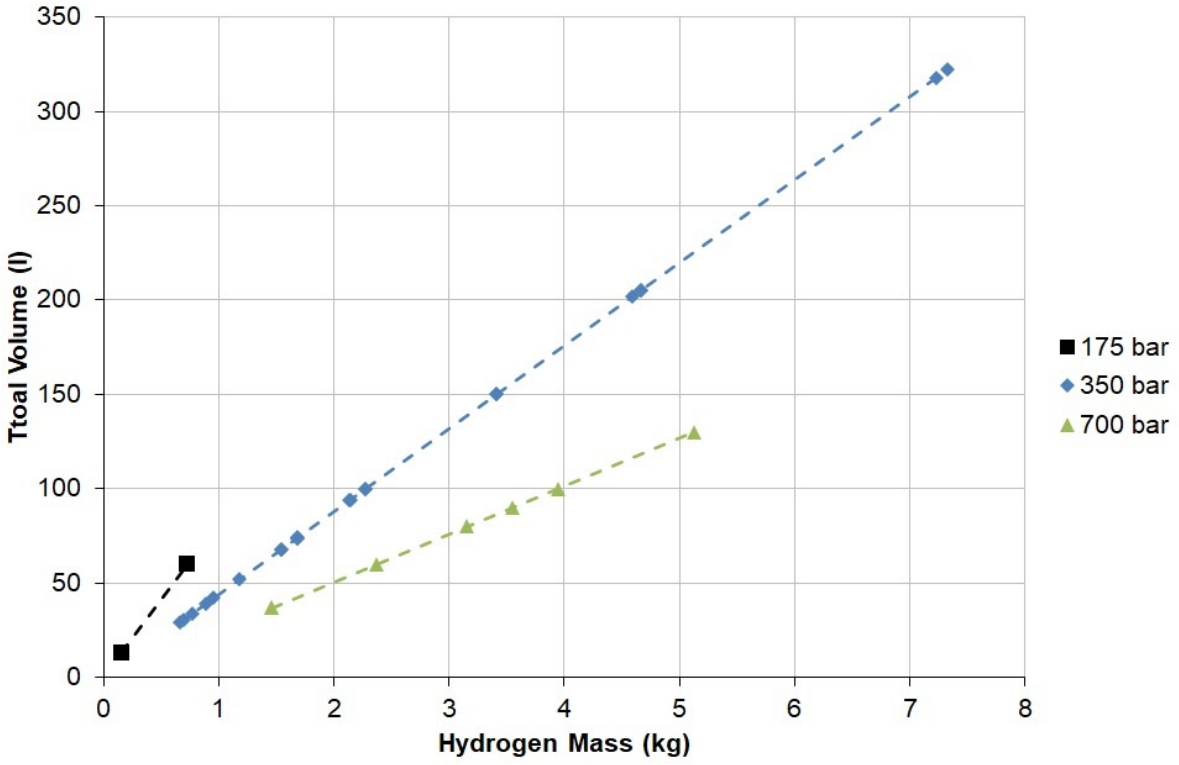

Figure 5.7: Change in total volume of storage vessel with increasing mass of hydrogen stored for 175, 350 and 700 bar g storage pressures [21-26]

Table 5.4: Fits through origin and R^2 values for correlations from Figure 5.7

Plot	**Fitted Correlation (u = mass of hydrogen stored (kg))**	**R^2**
175 bar g	$vol = 82.199u$	1
350 bar g	$vol = 43.958u$	1
700 bar g	$vol = 23.356u$	1

All of the presented data and relationships for CGH_2 storage methodologies clearly shows beneficial traits for storing hydrogen at either 350 bar g or 700 bar g. In the case of 350 bar g CGH_2, the lower storage pressure allows for a lighter tank design when compared to 700 bar g options. However, the volume advantage of storing at 700 bar g is more influential due to the greater slope difference between the two technologies.

5.2.2 Liquid Storage

Molecular hydrogen can be stored cryogenically as a liquid if it is cooled below its boiling point (20.4 K). Although the requirement for this extremely low temperature may dissuade some from this storage technique, the major benefit of LH_2 must be considered. This is that the density of LH_2 under atmospheric pressure is still 79% higher than the density of gaseous hydrogen which has been compressed to 700 bar g. The second, is that it is much more efficient to store the potentially large quantities of hydrogen required for aviation as a liquid than a compressed gas [27-29].

The extremely low temperatures required for LH_2 storage present some unique design challenges when compared to other hydrogen storage methods. In particular, the internal vessel temperature should not be allowed to exceed 20.4 K, above which liquid hydrogen will boil. Given that the density of gaseous hydrogen is over 48 times smaller than liquid hydrogen (along the saturation line at 1.1 bar absolute) [30] any vaporisation will cause the vessel internal pressure to rise significantly. Although there are several different insulation strategies which can be implemented, more on these later, a combination of a significant temperature difference and inherent inefficiencies of any physical system mean that there will always be some heat leakage into the LH_2 tank. This energy transfer will always cause a small amount of unavoidable LH_2 evaporation, a phenomena commonly referred to as “Boil off” [27-40] which must be managed.

Typical cryogenic storage vessels (cryostat) used to store LH_2 have a double wall construction and are insulated using a combination of a high-vacuum inter-wall cavity and advanced multi-layer reflective insulation [18,36]. They are also designed as low-pressure storage vessels, typically expecting a range of ambient to 1,000 kPa [33,36,42].

In addition to a highly efficient insulation design, it is best practice to only partially fill LH_2 tanks to around 85% to 95% [41]. The remaining 5% to 15% of available volume is known as ullage and is present to accommodate some of the space taken up by the expansion of liquid to gaseous hydrogen. Despite the additional volume requirement not directly dedicated to storing fuel, as shown by Figure 5.8, the mass and volume of LH_2 storage is still less than that of state-of-the-art CGH_2 storage.

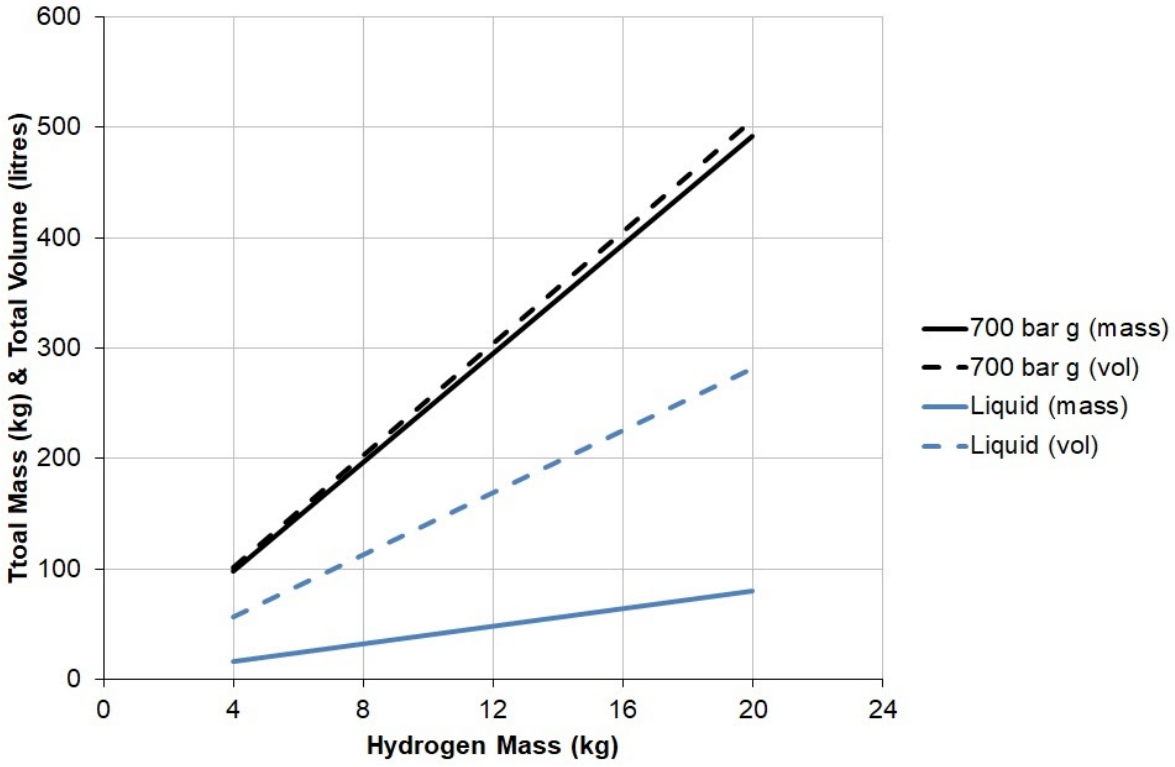

Figure 5.8: Total mass and volume variation for advanced CGH_2 and LH_2 storage vessels (data for several vessels has been averaged to produce each plot) [21,23,24,26,43]

The main advantage of LH_2 over CGH_2 storage, a far superior specific energy is also demonstrated by Figure 5.8. Therefore, for larger aircraft designs and/or extended missions, LH_2 should be the preferred choice for storing hydrogen in aircraft.

5.2.3 Delivery

Hydrogen, regardless of whether it is stored as a gas or liquid, needs to be supplied to the fuel cell anode inlet in gaseous form and at a regulated pressure. For CGH_2 storage solutions, this is achieved relatively simply through the use of valves and pressure regulators. Although, it should be noted that it is common to have more than one regulator to ensure that the low anode inlet pressure, typically < 3 bar gauge [44-46] can be maintained across the wide range of possible storage pressures.

For LH_2 storage solutions, fuel delivery is more complicated as it requires the liquid hydrogen to be vaporised (and pressure allowed to rise) before it can be fed to the fuel cell. This can be achieved through careful design of the tank insulation to control boil-off and use of an electric heater.

Regardless of the method chosen to store hydrogen, the fuel cell is always going to require a certain mass flow to allow the electrochemical reaction to move forward. Based on the fundamental electrochemical reaction in a PEMFC as described chemically in Chapter 3 it can be shown that two electrons are transferred for each molecule of hydrogen reacted. Therefore, the hydrogen usage can be calculated from Equation 5.1. The full derivation of this equation is shown by Larminie, J [1].

$$\dot{m}_{H_2} = \frac{M_{H_2} In}{2F} = \frac{M_{H_2} P_e}{2V_c F} \qquad (5.1)$$

Where:

F - Faraday constant (96,485 C/mol)

I - Current (A)

M_{H_2} - Molecular mass of hydrogen (2.02 g/mol)

$\dot{m}_{H_2}$ - Hydrogen mass flow rate (kg/s)

n - Number of cells

P_e - Electrical power (W)

V_c - Cell potential (V)

Obtaining the desired mass flow calculated from Equation 5.1 whilst also maintaining the specified inlet pressure can generally be achieved by one of two methods. For open-ended anode designs, a mass flow controller should be used to control the flow of hydrogen into the fuel cell. Storage pressure will need to be regulated down to the specified inlet pressure of the mass flow controller to ensure correct function. In the case of our experimental setup, this is 2 bar g. The effective anode pressure in the fuel cell should be controlled by a back-pressure valve on the anode exhaust. Alternatively, for both dead-ended and semi-dead-ended designs, the anode pressure is regulated directly from the storage solution and the mass-flow is roughly equal to the rate of consumption by the fuel cell.

For open-ended designs where the mass flow is controlled and an exhaust flow is expected, it is paramount that the hydrogen mass flow into the anode is greater than the rate of consumption. The ratio of actual fuel mass flow to rate of consumption is termed the stoichiometric ratio, λ [1,2]. It is common to run a PEMFC with a hydrogen stoichiometry greater than one. Actual hydrogen flow rate from the storage solution can be found from Equation 5.2.

$$\dot{m}_{H_2\ in} = \dot{m}_{H_2}\lambda \qquad (5.2)$$

Where:

$\dot{m}_{H_2}$ - Hydrogen mass flow rate (kg/s)

$\dot{m}_{H_2\ in}$ - Hydrogen mass flow into fuel cell (kg/s)

λ - Stoichiometry

5.3 Methanol

Unlike hydrogen fed PEMFCs where the hydrogen fuel must have no impurities, DMFCs are able to operate using a methanol feed of varying concentration. Typically, the literature prefers using a methanol concentration of 1.0 mol/dm^3 [47-50]. However, it is not uncommon for applications to use a concentration much higher than this, even up to pure methanol [51]. To obtain different methanol solutions for use as a fuel in a fuel cell, it is critically important that it is diluted using De-Ionised (DI) water. This is to avoid potential contamination from impurities in the water supply. Properties of pure methanol, CH_3OH are shown in Table 5.5 [52,53].

Table 5.5: Properties of pure methanol [52,53]

Property	**Value**
Molecular weight	32.04 g/mol
Boiling point	337.7 K
Freezing point	175 K
Calorific value (Higher Heating Value) at 298 K	22.66 MJ/kg (6.29 kWh/kg)
Density at 100kPa and 298 K	791 kg/m^3

When compared to hydrogen (either gaseous or liquid), methanol has some significant advantages. Indeed, the density of pure methanol, as illustrated in Table 5.5 is over ten times greater than that of liquid hydrogen leading to a much higher volumetric energy density. Additionally, under standard conditions methanol is a liquid which is significantly easier to store than either CGH_2 or LH_2 [54].

When dealing with liquid in applications expected to operate at sub-ambient temperatures; aircraft flying at altitude being an excellent example, the freezing point of the liquid in question becomes of great importance. For pure methanol, this shouldn't be an issue with a freezing point around ten degrees less than the coldest temperatures expected during normal flight [55,56]. However, this is not the case for methanol solutions diluted with DI water as demonstrated by Figure 5.9 [57,58].

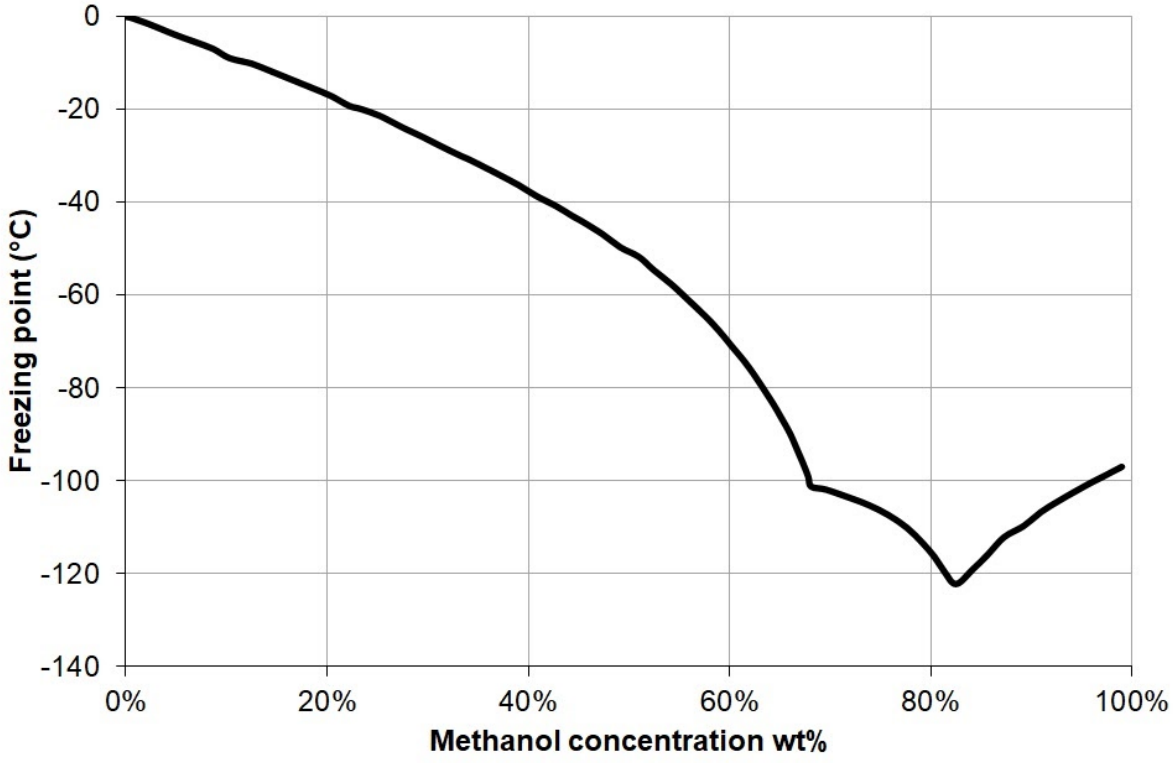

Figure 5.9: Methanol solution freezing point variation with concentration [57,58]

The shape of Figure 5.9 is a result of the interactions between pure methanol and water in a binary mixture. For the methanol / water mixture, the location of the first vertex close to -100 °C is likely a result of a change in crystalline structure of ice at this temperature. The minimum freezing point (eutectic temperature) of a binary mixture occurs at the eutectic concentration which is around 82 - 88 wt% depending on data source [57,58].

At the lowest temperature expected at the ceiling of a Global Hawk Unmanned Aerial Vehicle (UAV) as defined by MIL-HDBK-310, 187 K (-86 °C) [56] solution concentrations of less than 18 mol/dm^3 (0.65 wt% methanol) will freeze. Therefore, careful consideration will need to be made to the design of methanol storage solutions for aircraft specification DMFC systems.

5.3.1 Anode Configurations

Analogies can be made between the two common DMFC anode designs, active and passive to the previously discussed dead/open-ended. However, the two sets of terminology can not be used interchangeably. This is because fuel is actively fed to the fuel cell in both dead- and open-ended cases whereas, in a passive DMFC design a fixed tank of methanol solution is located in the anode side end plate of the fuel cell as shown in Figure 5.10. This type of DMFC also implements a porous diffusion layer in place of a more traditional flow field.

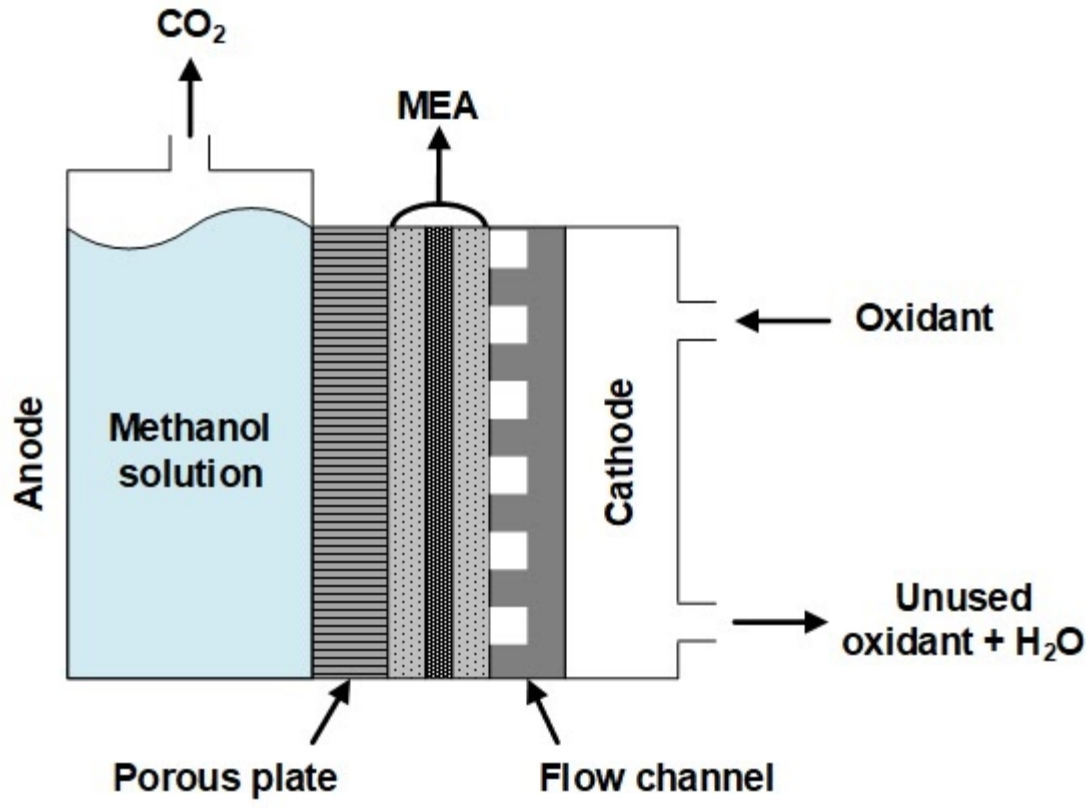

Figure 5.10: Example layout for a passive DMFC, highlighting the fixed methanol solution tank and porous anode flow plate

For passive DMFC designs, the optimum methanol concentration has been shown to be around twice that of an active design (≈ 4.0 mol/dm^3) as the access of the fuel to the active sites is only by diffusion [59,60]. Performance results for passive designs are also significantly lower than those achieved for active designs. This combined with limited refuelling ability excludes their use in aeronautical applications.

Active DMFCs are most analogous to an open-ended PEMFC design as they are designed to allow the methanol based fuel to flow through the anode flow fields. This increases the availability of fuel to the reactive sites whilst also allowing lower concentrations to be used [61,62], reducing the inefficiencies caused by crossover. An example layout for an active DMFC, highlighting the anode flow channels can be seen in Figure 5.11.

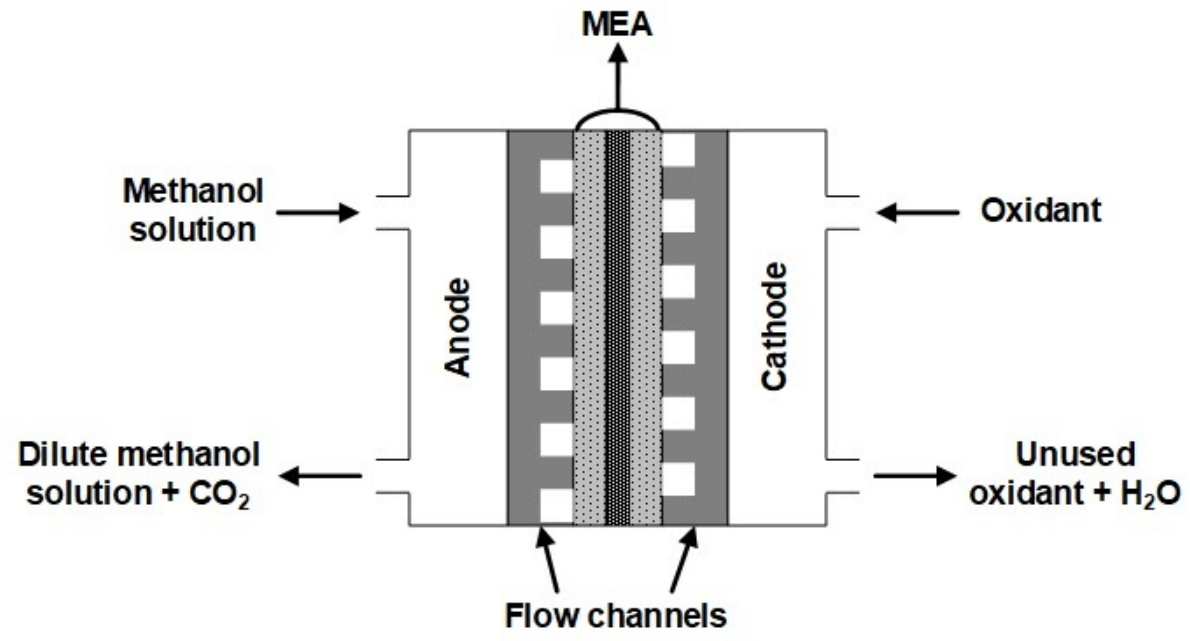

Figure 5.11: Example layout for an active DMFC, highlighting the flow channels on both anode and cathode and the flowing methanol solution through the anode end plate

5.3.2 Storage

Compared to hydrogen, the storage of methanol is fairly trivial. In large part this is because it has a liquid state for the full environmental regime of most aircraft. However, the density of liquid methanol changes with both temperature and concentration. Both are important factors and should be considered when designing the storage system for a DMFC.

From a materials perspective, methanol can be stored readily in most polymer and ferrous metal containers and is also compatible with several elastomer seal materials [63,64]. In order to avoid potential contamination which may leach from wetted materials entering the fuel cell, it is general practice to use materials such as High Density PolyEthylene (HDPE), PolyTetraFluoroEthylene (PTFE) and austenitic stainless steels such as 316 and 316L.

Density evolution of methanol with changing temperature is an important consideration in the design of any type of storage vessel as pure methanol will expand by up to 10 % when chilled from 50 ℃ to -50 ℃ [8]. The density evolution is also non-linear with the density increasing at a slower rate at lower temperatures. This relationship is demonstrated in Figure 5.12.

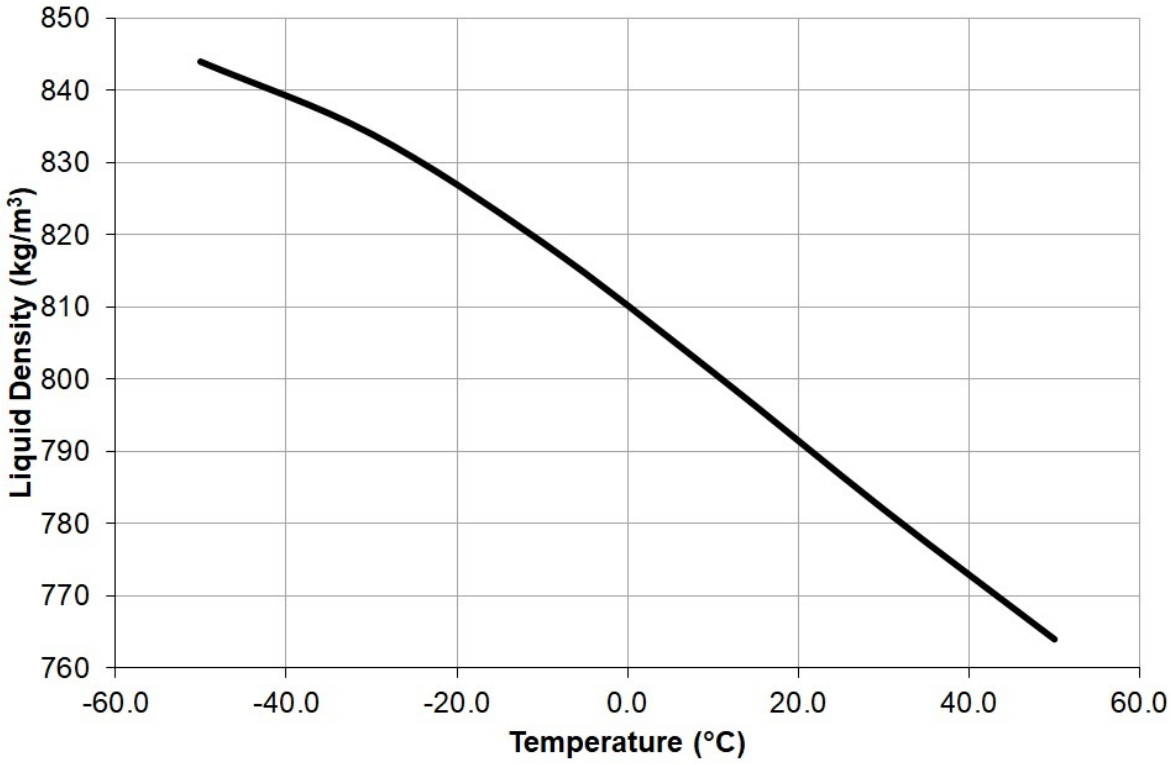

Figure 5.12: Density variation of pure liquid methanol with temperature [8]

As mentioned, the density of a methanol solution also varies with concentration in addition to temperature as demonstrated at both 0 ℃ and 20 ℃ in Figure 5.13 [65]. As the concentration of a methanol solution decreases from 100 wt% to 1.0 mol/dm^3 (3.6 wt%) the liquid density increases by 25% under a constant temperature of 20 ℃ ($\rho = 791.7\ kg/m^3$ @ 100 *wt*% & $\rho = 991.8\ kg/m^3$ @ 3.6 *wt*%).

The two different density evolution trends of liquid methanol, one with temperature and the other with concentration have shown that the fuel storage subsystem of a DMFC is much more sensitive to the concentration of the fuel stored than it is to temperature. This leads to some interesting design concepts for achieving the highest storage efficiency for methanol fuel. One solution, and the simplest in terms of number of components and control logic would be to scale up a typical lab setup where there is a single storage vessel containing a premixed dilute methanol solution. This would be fed to the fuel cell using an appropriately sized positive displacement pump and the exhaust flow to atmosphere. An example of this design concept can be seen in Figure 5.14.

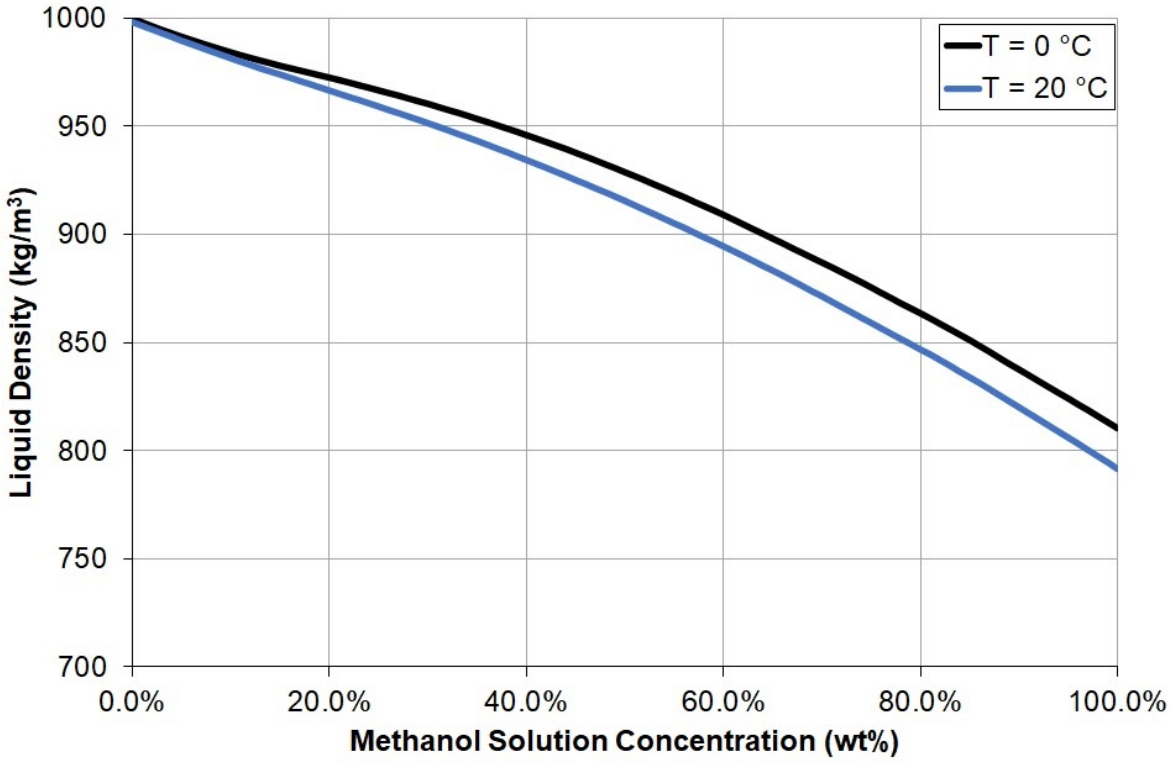

Figure 5.13: Change in liquid density with methanol solution concentration at 0 ℃ and 20 ℃ [65]

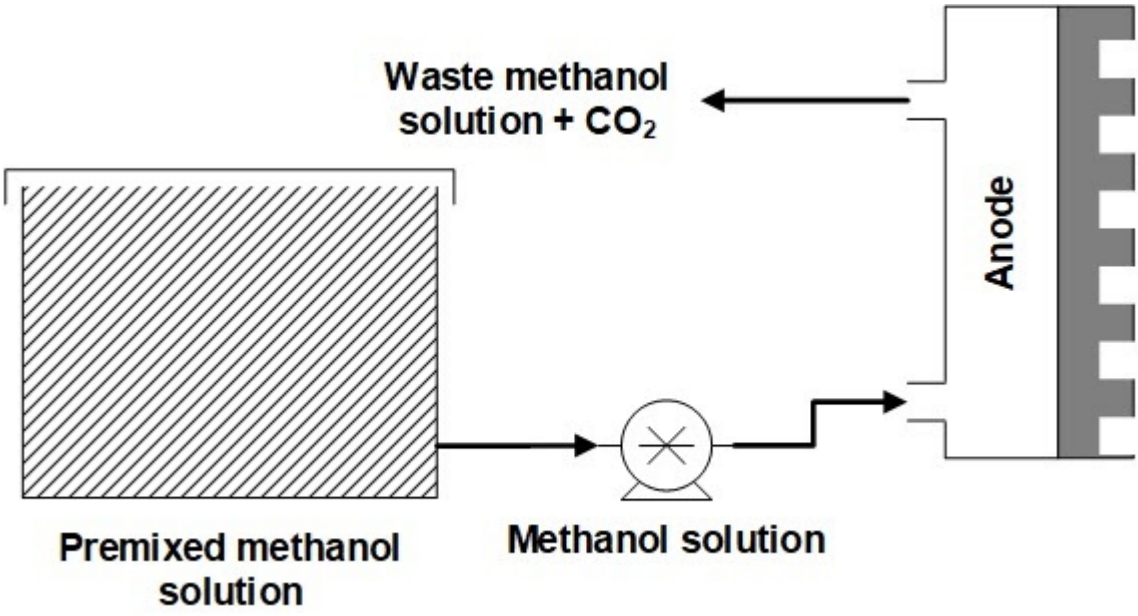

Figure 5.14: Concept design for single tank active DMFC anode system

A more advanced concept would involve the use of multiple (as little as two) storage vessels. One would be purposed with storing pure methanol for maximum energy density whereas, the second tank would be an intermediary for diluting the pure methanol prior to injection into the fuel cell. An example schematic for such a system is highlighted in Figure 5.15.

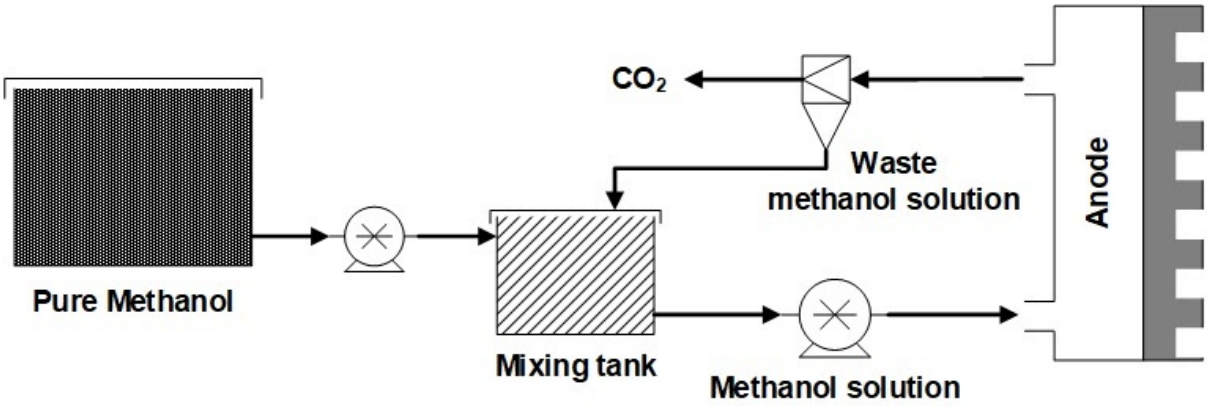

Figure 5.15: Concept design for multi-tank active DMFC anode system

5.3.3 Delivery

Delivering a methanol solution to the anode inlet of an active DMFC is trivial in comparison to using hydrogen with a PEMFC. However, positive displacement pumps are preferred over other types to allow the flow rate of methanol solution to be carefully controlled. We have already discussed the material compatibility of methanol and fortunately it shares many properties with other hydrocarbon fuels. Therefore, nearly all automotive rated fuel pumps will be suitable for use with methanol.

Based on the fundamental electrochemical reaction in a DMFC as described in Chapter 3 it can be shown that six electrons are transferred for each molecule of methanol reacted. Therefore, the methanol usage can be calculated from Equation 5.3.

$$\dot{m}_{CH_3OH} = \frac{M_{CH_3OH} In}{6F} = \frac{M_{CH_3OH} P_e}{6 V_c F} \qquad (5.3)$$

Where:

F - Faraday constant (96,485 C/mol)

I - Current (A)

M_{CH_3OH} - Molecular mass of methanol (32.04 g/mol)

$\dot{m}_{CH_3OH}$ - Methanol mass flow rate (kg/s)

n - Number of cells

P_e - Electrical power (W)

V_c - Cell potential (V)

For active DMFC designs where the mass flow is controlled and an exhaust flow is expected, it is paramount that the methanol mass flow into the anode is greater than the rate of consumption. The ratio of actual fuel mass flow to rate of consumption is termed the stoichiometric ratio, λ [1,2]. It is common to run a DMFC with a methanol stoichiometry greater than one. Actual pure methanol flow rate from the storage solution can be found from Equation 5.4.

$$\dot{m}_{CH_3OH\ in} = \dot{m}_{CH_3OH}\lambda \tag{5.4}$$

Where:

$\dot{m}_{CH_3OH}$ - Methanol mass flow rate (kg/s)

$\dot{m}_{CH_3OH\ in}$ - Methanol mass flow into fuel cell (kg/s)

λ - Stoichiometry

Unlike hydrogen, as discussed it is common to use a dilute concentration of methanol fuel in a DMFC. Therefore, the methanol flow rate calculated by Equations 5.3 and 5.4 is just that for the active methanol component of a solution. In order to size fuel pumps and storage vessels, the gross solution flow rate is required. This is calculated by dividing the methanol mass flow rate into the fuel cell by the solution concentration expressed as a weight percentage. This is described in Equation 5.5.

$$\dot{m}_{Fuel\ in} = \dot{m}_{CH_3OH\ in} / conc' \tag{5.5}$$

Where:

$conc'$ - Methanol solution concentration

$\dot{m}_{CH_3OH\ in}$ - Methanol mass flow into fuel cell (kg/s)

$\dot{m}_{Fuel\ in}$ - Fuel mass flow rate into fuel cell (kg/s)

5.4 Sub-System Energy Density

When designing alternative energy systems such as fuel cells and batteries, in particular those systems destined for aeronautical applications; the ability of that system to store energy efficiently is crucial. In the literature, a multitude of different methods are used to try and describe the storage efficiency of a fuel cell system. Unfortunately, a majority of these seem to only focus on the storage vessel itself and not the additional balance of plant required. They also seem to prefer expressing storage efficiencies as weight percentages, a ratio of the mass of fuel stored to the total storage mass, and similarly for volume.

So that the reader may make easier comparisons with more traditional fuel types, this work will use specific energy, e and energy density, u to compare and contrast the relative storage efficiencies of the different fuel storage technologies previously discussed for both hydrogen and methanol.

5.4.1 Efficiency Calculation

Specific energy or energy per unit mass, e, Equation 5.6 is often used to define the gravimetric storage efficiency of a system. The SI units for specific energy are J/kg however, due to the scales involved, it is more common to see it expressed in kWh/kg. The conversion from J to kWh is: $3.6 \times 10^6\ J\ =\ 1\ kWh$.

$$e_{FCS} = \frac{E_{net}}{m_{FCS}} \tag{5.6}$$

Where:

E_{net} - Available energy from fuel (J)

e_X - Specific energy of X (J/kg)

m_X - Mass of X (kg)

Energy density or energy per unit volume, u, Equation 5.7 is often used to define the volumetric storage efficiency of a system. The SI units for specific energy are J/m^3 however, due to the scales involved, it is more common to see it expressed in kWh/L. The conversion from J/m^3 to kWh/L is: $3.6 \times 10^9\ J/m^3\ =\ 1\ kWh/L$.

$$u_{FCS} = \frac{E_{net}}{vol_{FCS}} \tag{5.7}$$

Where:

E_{net} - Available energy from fuel (J)

u_X - Energy density of X (J/m^3)

vol_X - Volume of X (m^3)

5.4.2 Hydrogen Storage

For hydrogen storage, the physical size and mass of the storage tank(s) will be significantly higher than that of supporting balance of plant (regulators and heaters) except in very small hand-held Unmanned Aerial Vehicles (UAV). Therefore, the estimations of specific energy and energy density of the fuel storage system were performed solely on the storage vessel. To carry out this analysis data from multiple commercial sources [21,23,24,26,43] was used.

For each storage technology, the mass of hydrogen stored was used to calculate the energy availability of each storage technology. Specific energy values were calculated by dividing this energy by the total mass of the hydrogen stored and the storage vessel, note that for the LH_2 case this mass includes the required insulation. To calculate the energy density the energy content was divided by the total physical volume of the storage vessel. Results are shown in Figure 5.16.

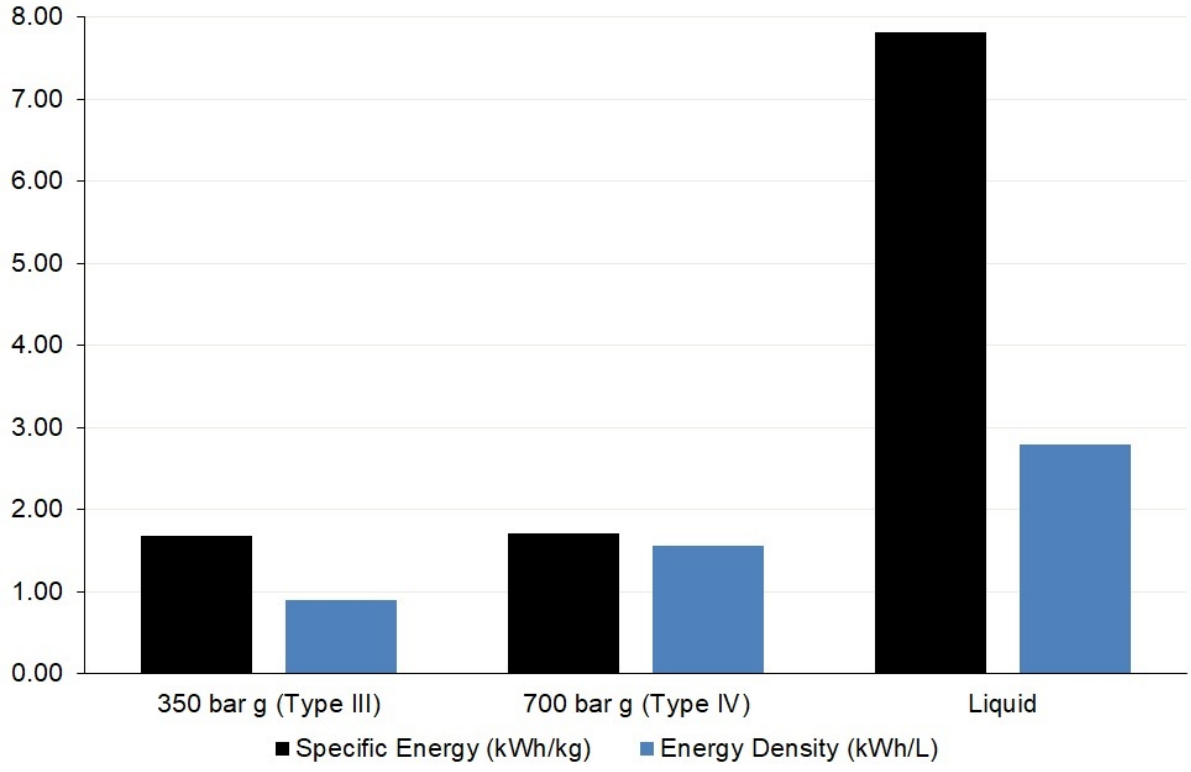

Figure 5.16: Specific energy and energy density variation for advanced CGH_2 and LH_2 storage vessels (data for several vessels has been averaged to produce each plot) [21,23,24,26,43]

Figure 5.16 demonstrates the relative improvements in specific energy and energy density as the storage technology was advanced from 350 bar g Type III cylinders through to LH_2. The results show similar specific energy for both CGH_2 storage technologies with an improvement of over 4x for the LH_2 case.

Compressed gaseous storage options are however separated by their relative energy densities, with the higher pressure Type IV cylinders performing better than the lower pressure Type III. However, LH_2 storage also outperforms both gaseous options, but by a smaller margin than the specific energy case. This is a result of the still relatively low density of liquid hydrogen (70.85 kg/m^3) and the additional bulk associated with cryogenic insulation.

Despite the fact that from a storage efficiency perspective, LH_2 has been shown here to outperform all types of CGH_2, it is not necessarily the best case for every application. This is due to the complexities of creating and storing cryogenic liquid hydrogen as discussed earlier.

5.4.3 Methanol Storage - Single vs' Twin Tank Case Study

In order to evaluate the storage efficiency of the two different active DMFC anode systems discussed earlier, a single pre-diluted tank (Figure 5.14) and a multi tank system consisting of a pure methanol tank and a separate mixing tank (Figure 5.15).

To define the operating requirements on the anode feed system, the validated single-cell DMFC model created in Chapter 4 was used. The model was scaled by increasing the fuel cell active area, A from 25 cm^2 to 100 cm^2 to increase the current output and the number of cells was increased to raise the voltage. A fixed current density, i of 153 mA/cm^2, chosen because of its location at the lower end of the ohmic region of the validated polarisation curve. These points gave a steady state operation case of $I = 15.3\,A$, $V = 65.5\,V$ and $P_e = 1,001\,W$. This corresponded to a (pure) methanol inlet flow rate of around 15 cc/min using Equation 5.3.

Liquid fuel pumps [66,67] were chosen based on their material compatibility with pure methanol and sized to deliver over the desired flow rates to allow for derating over time. Fuel tank sizing assumed spherical HDPE vessels with an assumed wall thickness of 5 mm. An overview of the system operating setpoint and component selection has been included in Table 5.6. The component selections in Table 5.6 are specific to the size of fuel cell specified with the exception of the storage vessels where a conversion factor from volume of fuel required is given.

Table 5.6: Overview of designs and system operating setpoint used in case study

Overview of Two Design Schematics	
Single Tank Case	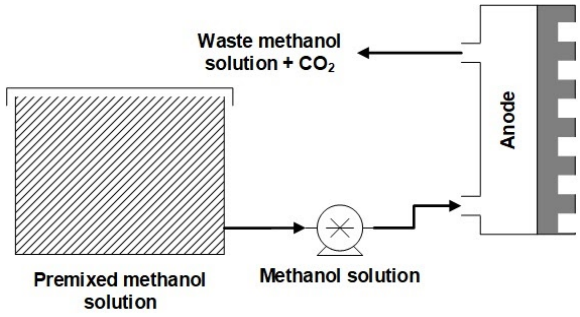
Twin Tank Case	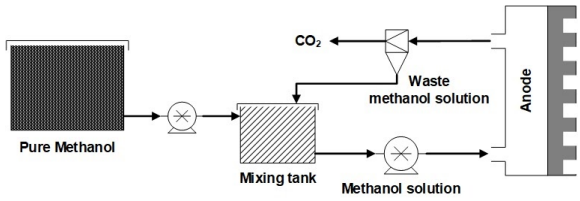
Component Selection for Case Study and Relevant Sizes	
Methanol storage tanks can be made from HDPE [68] which has a density of 0.97 g/cm^3 (storage vessels assumed spherical)	Tank material mass = $0.251 \times liquid\ vol^{0.657}$ (kg) Tank material volume = $0.2587 \times liquid\ vol^{0.657}$ $(litres)$
Solution pump is a Flojet Triplex design [66]	Pump mass = 3.5 kg Pump volume = 1.97 L
Concentrated methanol pump is a RS-Pro micropump [67]	Pump mass = 0.05 kg Pump volume = 0.024 L
Liquid separator data is estimated	Mass = 1.0 kg Volume = 2.0 L

System Operating Point for 1,001 W Electrical Power	
Current density, i	0.153 A/cm^2
Active area, A	100 cm^2
Stack current, I	15.3 A
Number of cells, n	233
Stack voltage, V	65.5 V

To provide a range of system operating cases the anode inlet stoichiometry of 1.5 was assumed along with a two hour run time. Methanol concentration at the inlet to the fuel cell varied from 1.0 mol/dm^3 to 15.0 mol.dm^3. The results of this case study are shown in Figure 5.17.

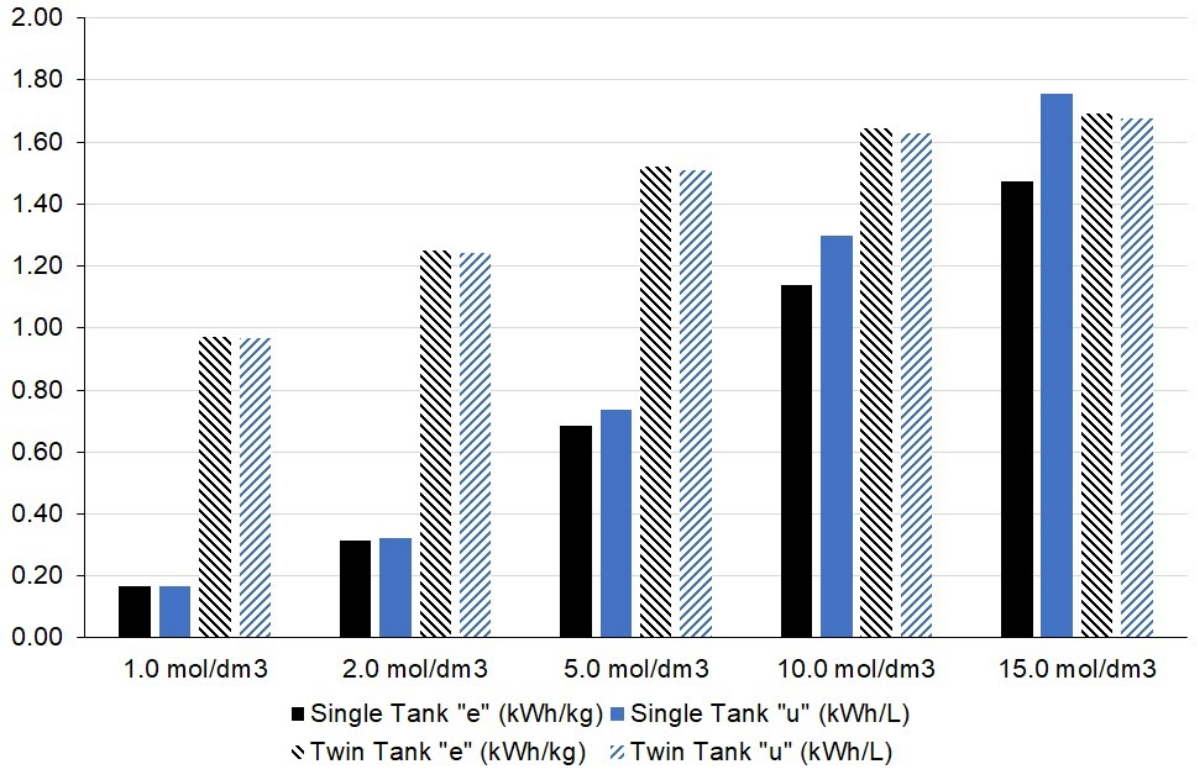

Figure 5.17: Energy density and specific energy results for methanol storage cases study at varying methanol feed concentrations

As would be expected, both the system specific energy and energy density are improved by feeding the DMFC with a higher concentration methanol solution. It was also shown that the storage efficiency improvement is much more prominent for the single tank case. This is because the increase in energy content of a more concentrated solution is the largest contributor to the size of the pre-dilute tank in that design.

Overall, it is clear that a twin tank design with a pure methanol container and a separate mixing tank will give both higher system specific energy and energy density, unless highly concentrated methanol could be fed to the DMFC without prior dilution. Given the current mass transport limitations discussed in Chapter 4, it is highly likely that any DMFC system would either need to store pre-diluted fuel or incorporate an on-demand dilution system.

5.4.4 Technology Comparison

To compare the gravimetric and volumetric storage efficiencies of hydrogen to methanol, specific energy and energy density values were calculated for just the storage vessel for each of the cases outlined in Figure 5.18. For the methanol cases, a single tank with the respective concentrations shown was assumed. Just the fuel and storage vessels were considered as they scale with mission duration for both fuel cell technologies whereas. The additional associated componentry for hydrogen systems (regulators, valves) does not scale whereas pumps required for methanol systems will. The storage efficiency parameters are all based on the associated fuel cell (PEMFC or DMFC) operating under the conditions described earlier in 5.4.3.

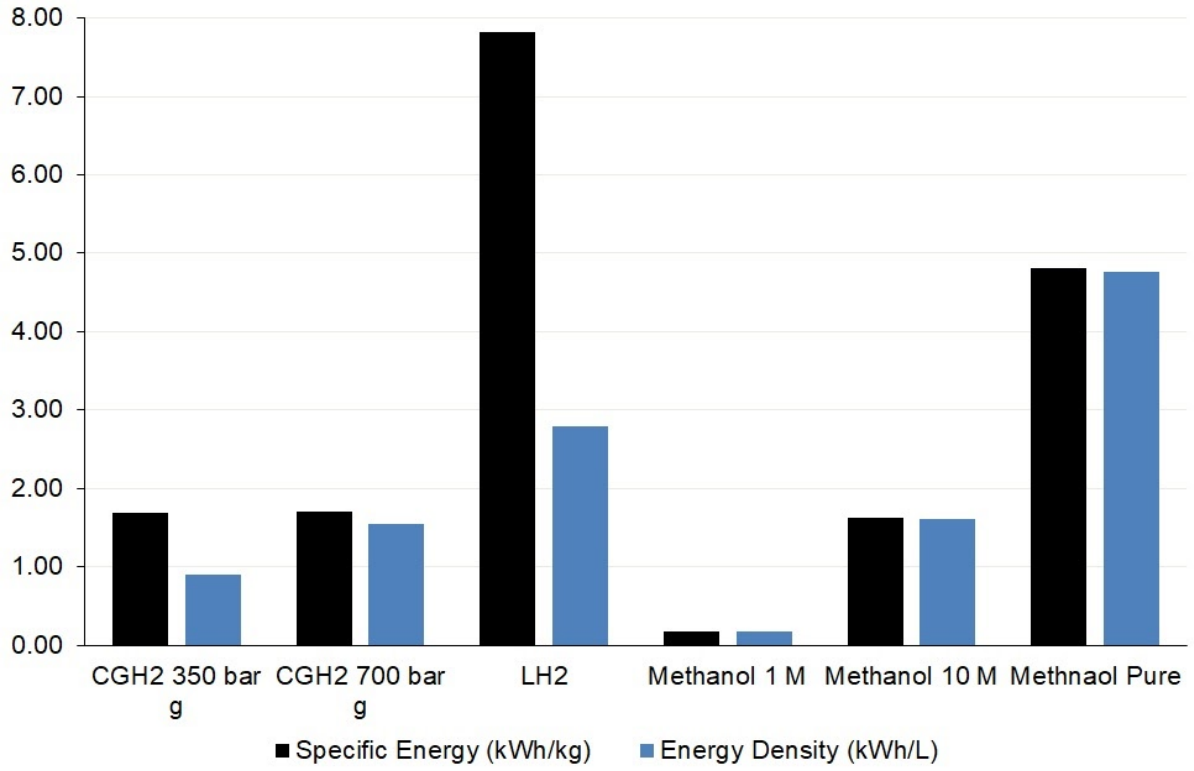

Figure 5.18: Specific energy and energy density averages for commercial hydrogen and methanol storage solutions [21,23,24,26,43,68]

Firstly, the results highlight the excellent scope available from advanced LH_2 storage, both in terms of energy density and specific energy. However, it should be noted that an increased energy density can be achieved with very high concentration or pure methanol. Additionally, storing pure methanol is comparatively very simple when compared to LH_2.

Methanol storage at lower concentrations of around 10.0 $mol.dm^3$ shows comparable performance to highly pressurised hydrogen. Again, also without the added complexities and difficulties of storing hydrogen.

For use in the aviation industry, military or civil, the use of methanol as a fuel would result in very few changes to existing infrastructure and cost models. This could be the key factor in the wide adoption of fuel cell technology in the aeronautical industry despite the higher power of similarly sized hydrogen fuel cell systems. It's current limitation is the requirement for lower power density DMFCs to utilise the fuel.

5.5 Summary

In this Chapter, the anode subsystems of both PEMFCs and DMFCs have been analysed in detail from the perspective of possible integration into an aircraft. Based purely on the material properties of both hydrogen and methanol, the primary fuel sources for the aforementioned fuel cells, interesting comparisons have been made based on the extremely high specific energy of hydrogen and the comparatively high density of methanol.

It has been shown that anode subsystem specific energy and energy density both improve for hydrogen as the storage pressure is increased, cylinder type advanced and with liquefaction. A similar trend has also been shown with methanol storage with increasing specific energy and energy density with increasing methanol concentration.

A case study was carried out to determine whether a single or multi tank methanol storage solution would be optimal for a DMFC anode feed system. It was found that although the performance of the single tank system improved dramatically with increasing methanol concentration, the twin tank design cases had higher specific energy and energy density at the same inlet feed concentration.

Finally, hydrogen and methanol storage solutions were directly compared. Liquid hydrogen was found to be the most energy dense fuel cell fuel storage configuration considered. However, pure and high concentration methanol storage both showed similar performance to those for LH_2 and CGH_2. Given that the material properties favoured methanol from a cost and ease of storage perspective, the potential benefits of DMFCs over PEMFCS for aviation have been shown.

5.6 References

[1] Larminie J, Dicks A. Fuel Cell Systems Explained. 2nd ed. John Wiley & Sons; 2003. https://doi.org/10.1016/S0378-7753(00)00571-1.

[2] O'Hayre R, Cha S-W, Colella W, Prinz FB. Fuel cell fundamentals. 3rd ed. John Wiley & Sons; 2016.

[3] Kim K, Kim T, Lee K, Kwon S. Fuel cell system with sodium borohydride as hydrogen source for unmanned aerial vehicles. J Power Sources 2011;196:9069–75. https://doi.org/10.1016/j.jpowsour.2011.01.038.

[4] Barbir F, Görgün H. Electrochemical hydrogen pump for recirculation of hydrogen in a fuel cell stack. J Appl Electrochem 2007;37:359–65. https://doi.org/10.1007/s10800-006-9266-0.

[5] Toghyani S, Baniasadi E, Afshari E. Performance analysis and comparative study of an anodic recirculation system based on electrochemical pump in proton exchange membrane fuel cell. Int J Hydrogen Energy 2018;43:19691–703. https://doi.org/10.1016/j.ijhydene.2018.08.194.

[6] Shen KY, Park S, Kim YB. Hydrogen utilization enhancement of proton exchange membrane fuel cell with anode recirculation system through a purge strategy. Int J Hydrogen Energy 2020;45:16773–86. https://doi.org/10.1016/j.ijhydene.2020.04.147.

[7] Tavares S. Aerospace engineering pocket reference. Taylor & Francis; 2015.

[8] National Institute of Standards and Technology. Thermophysical Properties of Fluid Systems. NIST Chem WebBook, SRD 69 2018. https://webbook.nist.gov/chemistry/fluid/ (accessed April 17, 2021).

[9] National Institute of Standards and Technology. Saturation Properties for Hydrogen — Pressure Increments. NIST Chem WebBook, SRD 69 n.d. https://webbook.nist.gov/cgi/fluid.cgi?Action=Load&ID=C1333740&Type=SatT&Digits=5&PLow=.5&PHigh=1.5&PInc=.1&RefState=DEF&TUnit=K&PUnit=atm&DUnit=kg/m3&HUnit=kJ/mol&WUnit=m/s&VisUnit=uPa*s&STUnit=N/m (accessed June 24, 2020).

[10] Edwards PP, Kuznetsov VL, David WIF, Brandon NP. Hydrogen and fuel cells: Towards a sustainable energy future. Energy Policy 2008;36:4356–62. https://doi.org/10.1016/j.enpol.2008.09.036.

[11] Makridis SS. Hydrogen storage and compression. In: Carriveau R, Ting DS-K, editors. Methane Hydrog. Energy Storage. 1st ed., IET Digital Library; 2016. https://doi.org/10.1049/pbpo101e_ch1.

[12] BOC. Hydrogen. Factsheet 2017. https://www.boconline.co.uk/en/legacy/attachment?files=tcm:t410-116758,tcm:410-116758,tcm:10-116758 (accessed June 29, 2020).

[13] Rohland B, Eberle K, Ströbel R, Scholta J, Garche J. Electrochemical hydrogen compressor. Electrochim Acta 1998;43:3841–6. https://doi.org/10.1016/S0013-4686(98)00144-3.

[14] Hirscher M, editor. Handbook of Hydrogen Storage: New Materials for Future Energy Storage. Wiley-VCH; 2010. https://doi.org/10.1002/9783527629800.

[15] Air Liquide (Paris). Division Scientifique. Encyclopedie des gaz. Amsterdam, New York: Elsevier; 1976.

[16] Durbin DJ, Malardier-Jugroot C. Review of hydrogen storage techniques for on board vehicle applications. Int J Hydrogen Energy 2013;38:14595–617. https://doi.org/10.1016/j.ijhydene.2013.07.058.

[17] Zuttel A. Materials for hydrogen storage. Mater Today 2003;6:24–33. https://doi.org/10.1016/S1369-7021(03)00922-2.

[18] Tzimas E, Filiou C, Peteves SD, Veyret J. Hydrogen Storage : State-of-the-Art and Future Perspective. 2003.

[19] Barthelemy H, Weber M, Barbier F. Hydrogen storage: Recent improvements and industrial perspectives. Int J Hydrogen Energy 2017;42:7254–62. https://doi.org/10.1016/j.ijhydene.2016.03.178.

[20] FIBA Technologies. High Pressure Hydrogen Type II Vessel 2018. https://www.fibatech.com/2014/11/24/type-2-hydrogen-vessel/#:~:text=Our new%2C Type 2%2C hoop,on board hydrogen-fueled vehicles. (accessed July 12, 2020).

[21] Luxfer Gas Cylinders. G-Stor H2 Fuel Cell Vehicle Cylinders. Prod Specific Sheet 2018.https://www.luxfercylinders.com/img/luxfer/products_upload/G-Stor-H2-spec-sheet-2018.pdf (accessed July 12, 2020).

[22] Horizon Fuel Cell Technologies. Ultra-light composite cylinder (E-Series) 2017. http://www.fuelcellstore.com/hydrogen-equipment/hydrogen-storage/composite-storage-cylinders/ultra-light-composite-storage-cylinder-e-series (accessed January 5, 2017).

[23] Luxfer Gas Cylinders. G-StorTM H2 hydrogen-storage cylinders 2015. http://www.luxfercylinders.com/products/alternative-fuel/gstorh2 (accessed January 5, 2016).

[24] Mahytec. Hydrogen storage solutions 2016. http://www.mahytec.com/en/our-solutions/ (accessed January 5, 2017).

[25] Steelhead Composites. Hydrogen gas storage 2016. http://steelheadcomposites.com/products/gas-cylinders/hydrogen/ (accessed January 5, 2017).

[26] Villalonga S, Nony F, Magnier C, Yvernes JL, Thomas C, Delmas B, et al. Composite 700 Bar-Vessel for on-Board Compressed Gaseous Hydrogen Storage. ICCM17, Edinburgh: International Committee on COmposite Materials; 2009.

[27] Preuster P, Alekseev A, Wasserscheid P. Hydrogen Storage Technologies for Future Energy Systems. Annu Rev Chem Biomol Eng 2017;8:445–71. https://doi.org/10.1146/annurev-chembioeng-060816-101334.

[28] Mills GL, Buchholtz BW, Olsen A. Design, fabrication and testing of a liquid hydrogen fuel tank for a long duration aircraft. AIP Conf Proc 2012;1434:773–80. https://doi.org/10.1063/1.4706990.

[29] Garceau NM, Kim SY, Lim CM, Cho MJ, Kim KY, Baik JH. Performance test of a 6 L liquid hydrogen fuel tank for unmanned aerial vehicles 2015;101. https://doi.org/10.1088/1757-899X/101/1/012130.

[30] Winnefeld C, Kadyk T, Bensmann B, Krewer U, Hanke-Rauschenbach R. Modelling and Designing Cryogenic Hydrogen Tanks for Future Aircraft Applications. Energies 2018;11:105. https://doi.org/10.3390/en11010105.

[31] Plachta DW, Johnson WL, Feller JR. Zero Boil-Off System Testing. Cryogenics (Guildf) 2016;74:88–94. https://doi.org/10.1016/j.cryogenics.2015.10.009.

[32] Plachta DW, Guzik MC. Cryogenic Boil-Off Reduction System. Cryogenics (Guildf) 2014;60:62–7. https://doi.org/10.1016/j.cryogenics.2013.12.006.

[33] Notardonato WU, Swanger AM, Fesmire JE, Jumper KM, Johnson WL, Tomsik TM. Zero boil-off methods for large-scale liquid hydrogen tanks using integrated refrigeration and storage. IOP Conf Ser Mater Sci Eng 2017;278. https://doi.org/10.1088/1757-899X/278/1/012012.

[34] Barsi S, Kassemi M. Numerical and Experimental Comparisons of the Self-Pressurization Behavior of an LH2 Tank in Normal Gravity. Cryogenics (Guildf) 2008;48:122–9. https://doi.org/10.1016/j.cryogenics.2008.01.003.

[35] Zhang J, Fisher TS, Ramachandran PV, Gore JP, Mudawar I. A Review of Heat Transfer Issues in Hydrogen Storage Technologies. J Heat Transfer 2005;127:1391. https://doi.org/10.1115/1.2098875.

[36] Haberbusch MS, Hui TY, Lobo S. No-Vent ™ Liquid Hydrogen Storage System. AIAA/ASME/SAE/ASEE Jt. Propuls. Conf. Exhib., Denver: AIAA; 2009, p. 1–8. https://doi.org/10.2514/6.2009-5331.

[37] Haberbusch MS, Nguyen CT, Stochl RJ, Hui TY. Development of No-VentTM Liquid Hydrogen Storage System for Space Applications. Cryogenics (Guildf) 2010;50:541–8. https://doi.org/10.1016/j.cryogenics.2010.02.025.

[38] Babac G, Sisman A, Cimen T. Two-Dimensional Thermal Analysis of Liquid Hydrogen Tank Insulation. Int J Hydrogen Energy 2009;34:6357–63. https://doi.org/10.1016/j.ijhydene.2009.05.052.

[39] Klell M, Kindermann H, Jogl C. Thermodynamics of gaseous and liquid hydrogen storage. Proc. Int. Hydrog. Energy Congr. Exhib. IHEC 2007, Istanbul: 2007, p. 13–5.

[40] Schlapbach L, Züttel a. Hydrogen-storage materials for mobile applications. Nature 2001;414:353–8. https://doi.org/10.1038/35104634.

[41] Ahluwalia RK, Peng JK. Dynamics of Cryogenic Hydrogen Storage in Insulated Pressure Vessels for Automotive Applications. Int J Hydrogen Energy 2008;33:4622–33. https://doi.org/10.1016/j.ijhydene.2008.05.090.

[42] Hasan MM, Balasubramaniam R. Analysis of the pressure rise in a partially filled liquid tank in microgravity with low wall heat flux and simultaneous boiling and condensation. 50th AIAA Aerosp Sci Meet Incl New Horizons Forum Aerosp Expo 2012. https://doi.org/10.2514/6.2012-760.

[43] lapesa. Horizontal Cryogenic Tanks n.d.:10–1. www.lapesa.es/descargar.php?f=/sites/default/files/documentos/gnli_1011.pdf (accessed January 5, 2017).

[44] Santarelli MG, Torchio MF. Experimental analysis of the effects of the operating variables on the performance of a single PEMFC. Energy Convers Manag 2007;48:40–51. https://doi.org/10.1016/j.enconman.2006.05.013.

[45] Tang Y, Yuan W, Pan M, Wan Z. Experimental investigation on the dynamic performance of a hybrid PEM fuel cell/battery system for lightweight electric vehicle application. Appl Energy 2011;88:68–76. https://doi.org/10.1016/j.apenergy.2010.07.033.

[46] Yan Q, Toghiani H, Causey H. Steady state and dynamic performance of proton exchange membrane fuel cells (PEMFCs) under various operating conditions and load changes. J Power Sources 2006;161:492–502. https://doi.org/10.1016/j.jpowsour.2006.03.077.

[47] McGrath KM, Surya Prakash GK, Olah G a. Direct Methanol Fuel Cell. J Ind Eng Chem 2004;10:1063–80.

[48] Bresciani F, Rabissi C, Casalegno A, Zago M, Marchesi R. Experimental investigation on DMFC temporary degradation. Int J Hydrogen Energy 2014;39:21647–56. https://doi.org/10.1016/j.ijhydene.2014.09.072.

[49] Inoue M, Iwasaki T, Sayama K, Umeda M. Effect of conditioning method on direct methanol fuel cell performance. J Power Sources 2010;195:5986–9. https://doi.org/10.1016/j.jpowsour.2009.11.015.

[50] Gwak G, Kim D, Lee S, Ju H. Studies of the methanol crossover and cell performance behaviors of high temperature-direct methanol fuel cells (HT-DMFCs). Int J Hydrogen Energy 2018;43:13999–4011. https://doi.org/10.1016/j.ijhydene.2017.11.029.

[51] Nakagawa N, Tsujiguchi T, Sakurai S, Aoki R. Performance of an active direct methanol fuel cell fed with neat methanol. J Power Sources 2012;219:325–32. https://doi.org/10.1016/j.jpowsour.2012.07.062.

[52] Sigma-Aldrich. Methanol Safety Data Sheet 2018. https://www.sigmaaldrich.com/MSDS/MSDS/DisplayMSDSPage.do?country=GB&language=en&productNumber=322415&brand=SIAL&PageToGoToURL=https%3A%2F%2Fwww.sigmaaldrich.com%2Fcatalog%2Fproduct%2Fsial%2F322415%3Flang%3Den (accessed August 17, 2018).

[53] McAllister S, Chen J-Y, Fernandez-Pello AC. Fundamentals of Combustion Processes. 1st ed. New York: Springer-Verlag; 2011. https://doi.org/10.1007/978-1-4419-7943-8.

[54] Thirkell A, Chen R. Comparison of Gaseous and Liquid Fuel Cells for Automotive Applications. In: Razi Nalim M, Vasudevan R, Rahetekar S, editors. Adv. Automot. Technol. 1st ed., Springer Singapore; 2020. https://doi.org/10.1007/978-981-15-5947-1.

[55] Technical Committee ISO/TC20. ISO 2533:1975 Standard Atmosphere. 1975.

[56] U.S. Department of Defense. Department of Defense Handbook: Global Climatic Data for Developing Military Products MIL-HDBK-310. vol. MIL-STD-31. 1997.

[57] Methanol Institute. Freezing Points of Methanol. Methanol Prop 2016. http://www.methanol.org/wp-content/uploads/2016/06/FreezingPointsMethanol-WaterSolutions.pdf (accessed March 25, 2020).

[58] Dougherty AJ, Bartholet ZT, Chumsky RJ, Delano KC, Huang X, Morris DK. The Liquidus Temperature for Methanol-Water Mixtures at High Pressure and Low Temperature, With Application to Titan. J Geophys Res Planets 2018;123:3080–7. https://doi.org/10.1029/2018JE005707.

[59] Han J, Park ES. Direct methanol fuel-cell combined with a small back-up battery. J Power Sources 2002;112:477–83. https://doi.org/10.1016/S0378-7753(02)00441-X.

[60] Park GG, Yang TH, Yoon YG, Lee WY, Kim CS. Pore size effect of the DMFC catalyst supported on porous materials. Int J Hydrogen Energy 2003;28:645–50. https://doi.org/10.1016/S0360-3199(02)00140-4.

[61] Scott K, Taama WM, Argyropoulos P. Engineering aspects of the direct methanol fuel cell system. J Power Sources 1999;79:43–59. https://doi.org/10.1016/S0378-7753(98)00198-0.

[62] Wei Z, Wang S, Yi B, Liu J, Chen L, Zhou WJ, et al. Influence of electrode structure on the performance of a direct methanol fuel cell. J Power Sources 2002;106:364–9. https://doi.org/10.1016/S0378-7753(01)01023-0.

[63] Methanol Institute. Compatibility of Elastomers in Neat Methanol. 2016

[64] Methanol Institute. Compatibility of Metals & Alloys in Neat Methanol Service. 2016.

[65] Green DW, Perry RH. Perry's Chemical Engineers' Handbook. 8th ed. London: McGraw-Hill; 2008.

[66] Flojet Triplex Series Pump Datasheet. RS-Online Datasheet 2013. https://docs.rs-online.com/a85f/0900766b8144b750.pdf (accessed July 31, 2020).

[67] Datasheet Micropumps. RS-Online Datasheet n.d. https://docs.rs-online.com/facd/0900766b815814c9.pdf (accessed July 31, 2020).

[68] Pressol HDPE Jerrycan. RS-Online Datasheet 2010:2010. https://docs.rs-online.com/ab22/0900766b80e0f376.pdf (accessed July 31, 2020).

Chapter 6 Oxidant System Analysis

6.1 Introduction

Oxidant, generally oxygen, can either be extracted from the ambient air in an air-breathing system or stored on-board in pure form in an air-independent system. The main aircraft specific consideration for which system should be used is flight altitude. As a result of the temperature and pressure fluctuations associated with altitude, only closed-cathode fuel cell designs are deemed suitable. A closed-cathode design refers to one where one where forced convection through the cathode flow channels is required.

The first step in system design, common to both air-breathing and air-independent systems is the calculation of the required oxidant flow rate to maintain the chemical reaction. The mass flow rate of oxygen required to maintain the electrochemical reaction is defined by Equation 6.1 [1].

$$\dot{m}_{O2} = \frac{M_{O2} In}{4F} = \frac{M_{O2} P_e}{4 V_c F} \qquad (6.1)$$

Where:

F - Faraday constant (96,485 C/mol)

I - Current (A)

M_{O_2} - Molecular mass of oxygen (32 g/mol)

$\dot{m}_{O_2}$ - Oxygen mass flow rate (kg/s)

n - Number of cells

P_e - Electrical power (W)

V_c - Cell potential (V)

6.2 Air-Breathing

A majority of existing commercially available Polymer Electrolyte Membrane Fuel Cell (PEMFC) and Direct Methanol Fuel Cell (DMFC) systems implement an air-breathing design [2-9]. This is done because for a majority of fuel cell use cases: automotive, portable, an air-breathing design is cheaper to implement as there is no need for onboard oxidant storage. Although, technically a fuel cell system would still be considered “air-breathing” if stored compressed air was used, in practice this would not happen due to the increased performance seen whilst running on oxygen [10]. Figure 6.1 shows a typical schematic diagram for the cathode side of an air-breathing low-temperature fuel cell design.

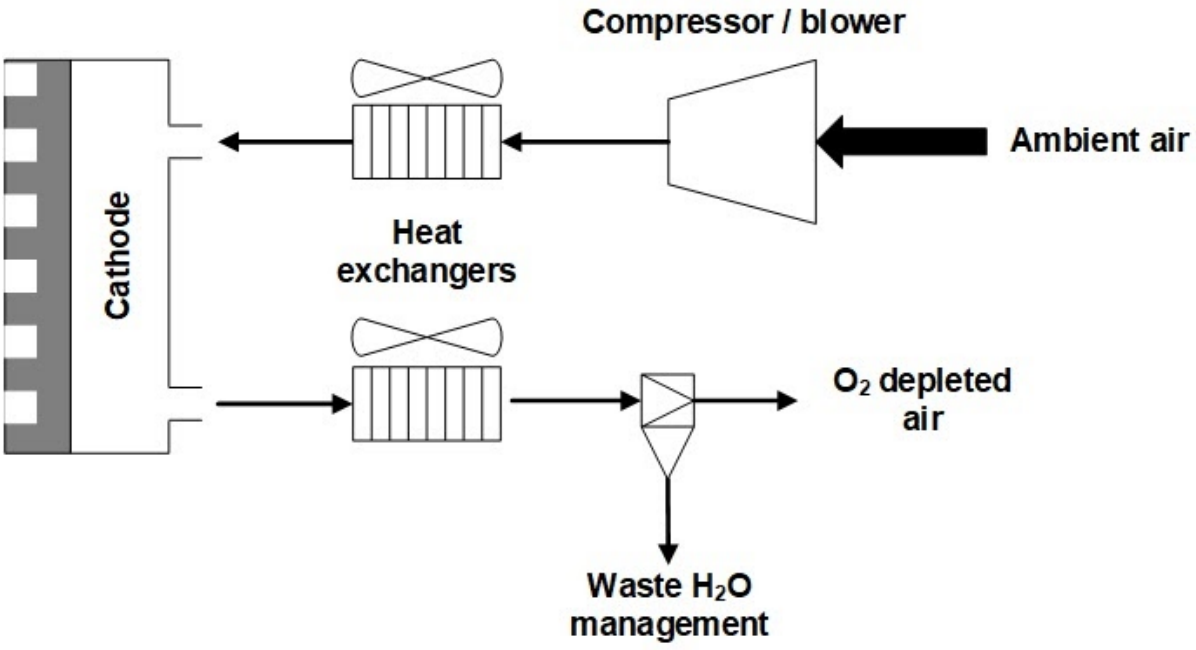

Figure 6.1: Example schematic for the cathode side of a typical air-breathing low-temperature fuel cell

In this system configuration, the oxygen required by the fuel cell to maintain the reaction is supplied in the form of air. Compressor air mass flow rate can be used for sizing a compressor for a fuel cell system, regardless of altitude because even though the partial pressure of oxygen reduces (a direct result of the total pressure reducing) the concentration of oxygen in air remains constant. The mass flow rate of air required is calculated in a similar manner to that of oxygen. The calculation for air is described by Equation 6.2 [1]. Where "0.21" refers to the volume fraction of oxygen in air.

$$\dot{m}_{air} = \frac{M_{air} In}{0.21 \cdot 4F} = \frac{M_{air} P_e}{0.21 \cdot 4 V_c F} \qquad (6.2)$$

Where:

F - Faraday constant (96,485 C/mol)

I - Current (A)

M_{air} - Molecular mass of air (28.96 g/mol)

$\dot{m}_{air}$ - Air mass flow rate (kg/s)

n - Number of cells

P_e - Electrical power (W)

V_c - Cell potential (V)

6.2.1 Compressor Design

The intolerance of low temperature fuel cells to contaminants in either the fuel or oxidant stream is well documented [1,11-14]. As a result, the design and manufacture of dry compressors utilising air bearing technology has progressed in recent years. At current technology levels, fuel cell compatible air compressors have an average gravimetric power efficiency of 0.45 kW/kg and volumetric power efficiency of 0.39 kW/l [14-19].

In addition to the mass and space occupied by the additional component, a compressor or blower is going to present as a parasitic power draw on the fuel cell system. It is therefore very important that a compressor is sized such that it can be as small and efficient as possible whilst still delivering the required oxygen mass flow. Operating fuel cell systems in an aeronautical environment presents particular challenges for the cathode system due to the reduced air pressure and lower availability of oxygen at altitude.

To investigate the effect of increasing altitude on the operation of an air breathing fuel cell system, the power required to compress the necessary inlet air was calculated over a range of altitudes. The power of a fuel cell suitable compressor can be found from Equation 6.3 [1,20].

$$P_{comp} = \frac{c_p \dot{m}_{air} T_1}{\eta_{comp}} \left(\left(\frac{p_2}{p_1} \right)^{\frac{\gamma-1}{\gamma}} - 1 \right) \qquad (6.3)$$

Where:

c_p - Specific heat at constant pressure (J/kgK)

$\dot{m}_{air}$ - Air mass flow rate (kg/s)

P_{comp} - Compressor power (W)

p_1 - Compressor inlet pressure (Pa)

p_2 - Compressor exit pressure (Pa)

T_1 - Temperature at compressor inlet (K)

γ - Specific heat ratio

η_{comp} - Compressor efficiency

Air pressure and temperature both vary with altitude as discussed in Chapter 2 [21]. Data from the International Standard Atmosphere (ISA) [21] was used to calculate the compressor power requirement for a two stoichiometry flow at a range of altitudes as a percentage of net fuel cell power. The results, shown in Figure 6.2 are independent of fuel cell power. There are many fuel cell subsystems which may require electrical power. The power that these subsystems consume is deemed to be parasitic and the largest is the compressor or blower required in an air-breathing cathode design. It would not be unreasonable to impose a limit of 20% of the net fuel cell rated power as an upper limit for any individual system component [22].

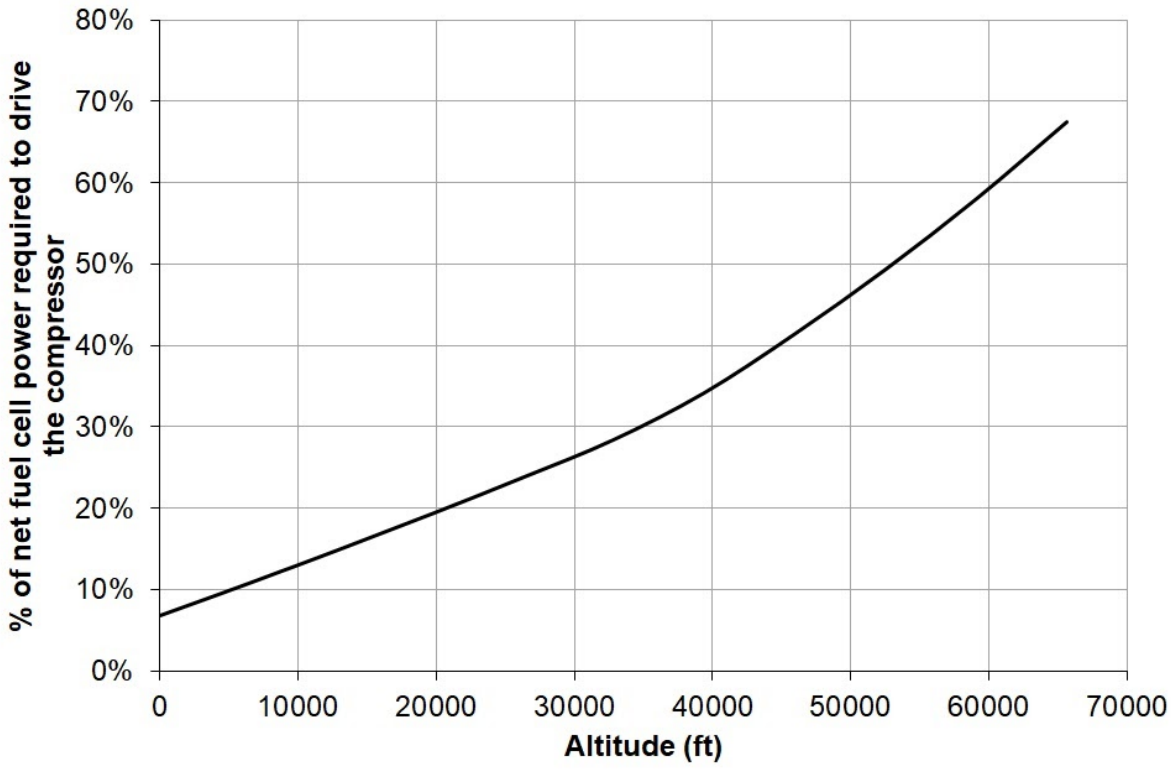

Figure 6.2: Compressor power variation with altitude as a percentage of net fuel cell power. Assumes fuel cell operating at 2.5 air stoichiometries and a compressor efficiency of 67%

At an altitude of ≈ 20,000 ft the power required by the compressor to meet the inlet air mass flow requirement was 20% of that produced by the fuel cell. This is an excessive parasitic load for an aircraft fuel cell therefore, an air independent system will be required for any aircraft operating at an altitude above 20,000 ft. An air breathing design will be used for altitudes less than 20,000 ft.

An alternative compressor design which could be considered for use in this application is a turbo compressor. For this design, some of the energy contained within the cathode exhaust is used to help compress and feed oxygen to the inlet. This type of compressor has not been considered here as it would require a separate detailed study on the behaviour of turbine wheels in fully humidified and super-saturated flows.

6.2.2 Additional Balance of Plant

In addition to the air compressor, other Balance of Plant (BoP) components demonstrated in Figure 6.1 such as heat exchangers and water separation need to be considered. Depending on the operating environment and specific fuel cell requirements, the air flow exiting the compressor may need to be cooled prior to inlet into the fuel cell. It is well documented that an operating temperature of around 80 °C is favourable for low temperature fuel cells [23-27]. Specifics on the different thermal management systems required to maintain this temperature will be detailed in Chapter 7. For now it is sufficient to note that low power fuel cells (< 5 kW) are typically air cooled and higher power fuel cells have a separate dedicated cooling system

Based on this understanding and the knowledge that fuel cells are generally insensitive to changes in cathode inlet temperature [28] as long as it is below the maximum limit, determination of compressor exit temperature variation with altitude will reveal any requirement of inlet charge cooling. The first step in this determination is to apply the isentropic pressure / temperature relationship to a compressor using the standard NASA equation, Equation 6.4 [20].

$$CPR = \frac{p_{t_2}}{p_{t_1}} = \left(\frac{T_2}{T_1}\right)^{\frac{\gamma}{\gamma-1}} \qquad (6.4)$$

Where:

CPR - Compressor pressure ratio

p_{t_1} - Total inlet pressure (Pa)

p_{t_2} - Total exit pressure (Pa)

T_1 - Compressor inlet temperature (K)

T_2 - Compressor exit temperature (K)

γ - Specific heat ratio

Rearranging Equation 6.4 for T_2, using a standardised compressor exit pressure of 500 mbar gauge along with a specific heat ratio of $\gamma = 1.4$ it is possible to calculate the change in compressor exit temperature based on the changing ambient pressure and temperature with altitude. Standardised ISA data [21] was used to provide the ambient temperature and pressure variation.

The results, shown in Figure 6.3 demonstrate how the compressor exit temperature increases with increasing altitude. This is a result of the increasing pressure ratio required to maintain the same exit pressure at altitude. Up to a flight altitude of 24,000 ft the compressor exit temperature remains below 80 °C, if it is assumed that the compressor inlet is at ambient. Above this altitude it would be necessary to implement a heat exchange system between the compressor exit and fuel cell inlet.

For system configurations that require the compressor exit air to be cooled, the amount of heat rejection required to lower the temperature should be calculated. This is achieved through the implementation of Equation 6.5 [20]. The results, also included in Figure 6.3 demonstrate a more linear response to heat generation rate with altitude than simply exit temperature.

$$\dot{Q} = \dot{m}\, c_p \Delta T \qquad (6.5)$$

Where:

- c_p - Specific heat at constant pressure (J/kgK)
- $\dot{m}$ - Mass flow rate (kg/s)
- $\dot{Q}$ - Heating rate (W)
- ΔT - Change in temperature (K)

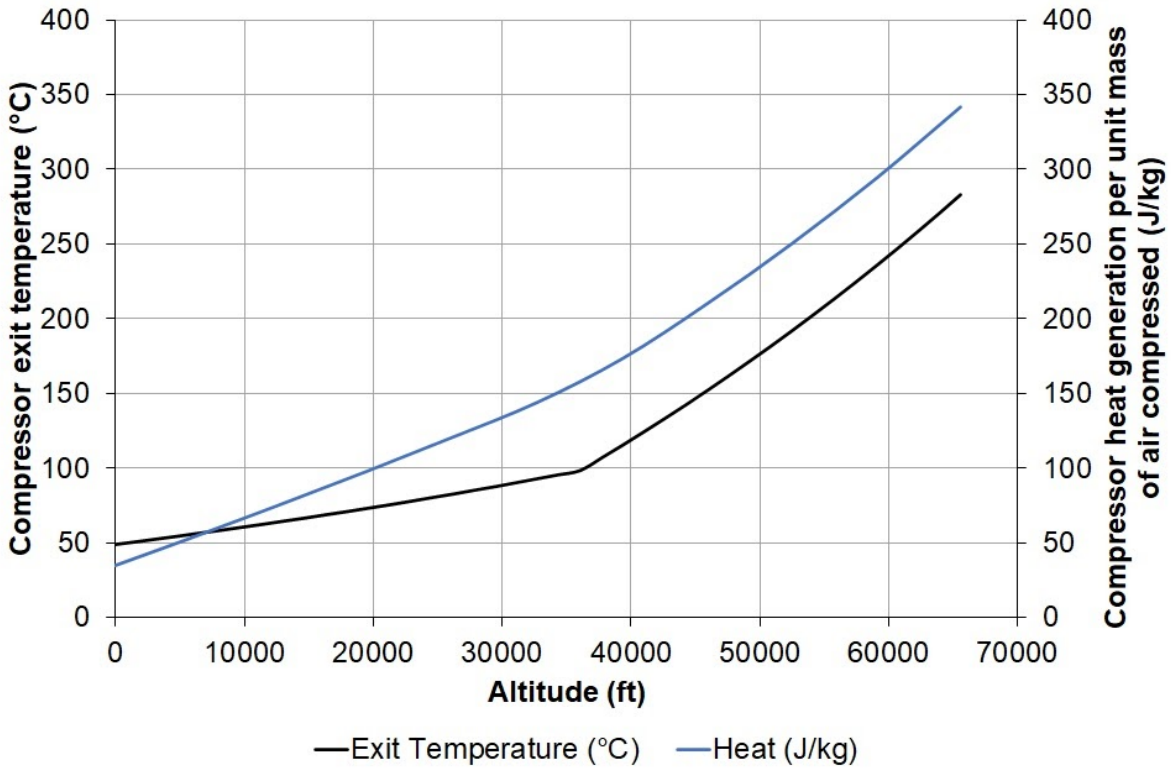

Figure 6.3: Compressor exit temperature variation and heat generation per unit mass with altitude

6.3 Air-Independent

Air-independent fuel cell cathode systems are characterised by their isolation from the atmosphere. The main component of an air independent system is a method of storing pure oxygen on-board the aircraft in a sufficient quantity to meet the desired endurance and cooling requirements. An example layout of an air-independant low-temperature fuel cell system is given in Figure 6.4.

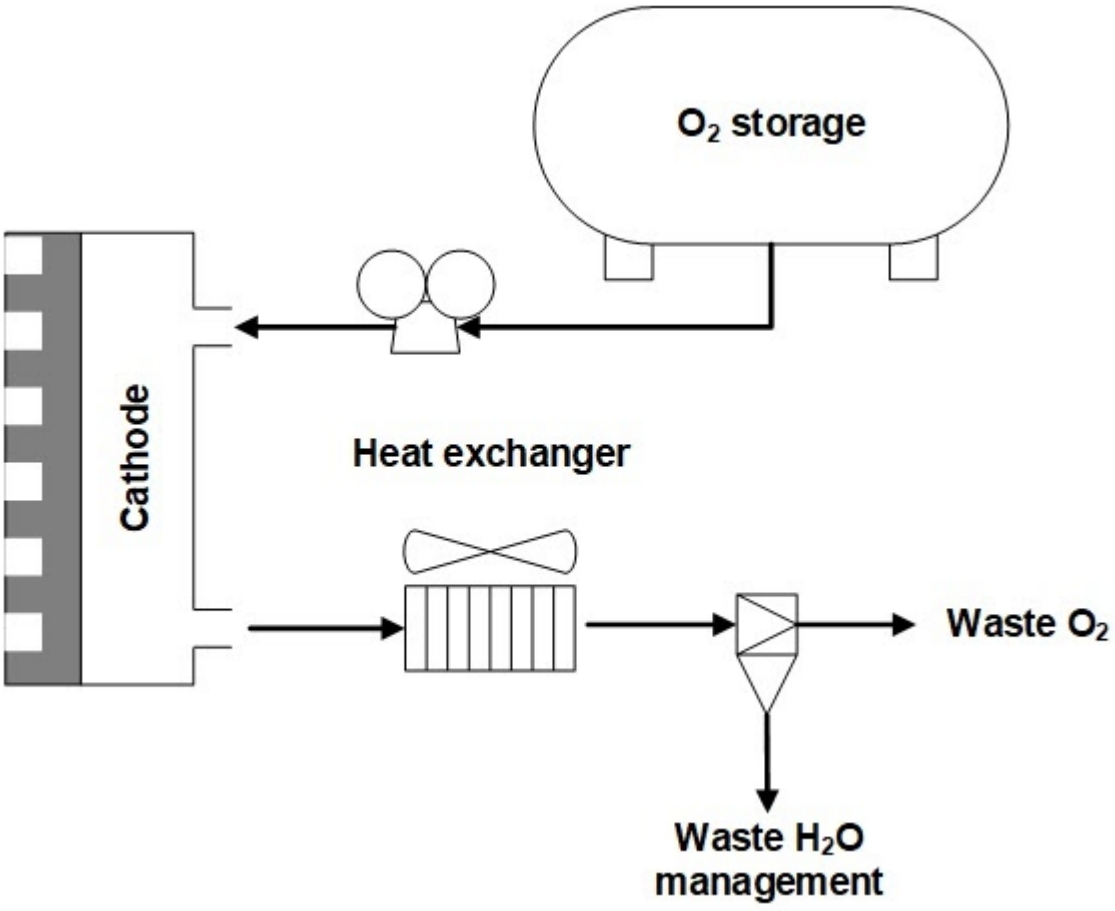

Figure 6.4: Example schematic for the cathode side of a typical air-independent low-temperature fuel cell

The requirement of an air-independent system to store all of the oxidant required for the mission should not be underestimated as the total mass and volume of the oxidant system will vary based on mission requirements. Whereas, an air-breathing design will be sized for the fuel cell in use and operating environment of the mission.

6.3.1 Oxygen Storage

Storing pure oxygen in large quantities either under pressure as a gas or at low temperature as a liquid, although technically more straight forward than hydrogen, poses a greater risk to the user due to its unique properties. Pure oxygen is an excellent oxidising agent and if present in sufficient concentration in combination with certain materials can cause violent reactions and spontaneous combustion [29,30]. For reference, the properties of molecular oxygen used in this study have been included in Table 6.1.

Table 6.1: Properties of molecular oxygen [30,31]

Property	**Value**
Molecular weight	32 g/mol
Boiling point	90.2 K
Gaseous density at 100kPa and 298 K	1.33 kg/m^3
Liquid density at 100kPa and 20.4 K	1,142 kg/m^3

The same methodology that was used for hydrogen storage in Chapter 5 was used to find the most suitable oxygen storage method between Compressed Gaseous Oxygen (CGO_2) and Liquid Oxygen (LO_2). Data from commercially available storage cylinders was gathered and analysed for the purpose of comparison [32-39]. The results of this analytical comparison are shown in Figure 6.5.

Unlike hydrogen, the total storage mass of gaseous oxygen isn't improved by increasing the storage pressure for current tank technologies. However, liquefaction is still an effective method of increasing the gravimetric storage efficiency of oxygen. The evolution of volumetric storage efficiency of oxygen storage does follow the same trend as for hydrogen with the efficiency increasing as the gaseous storage pressure is increased and further still as a result of liquefaction.

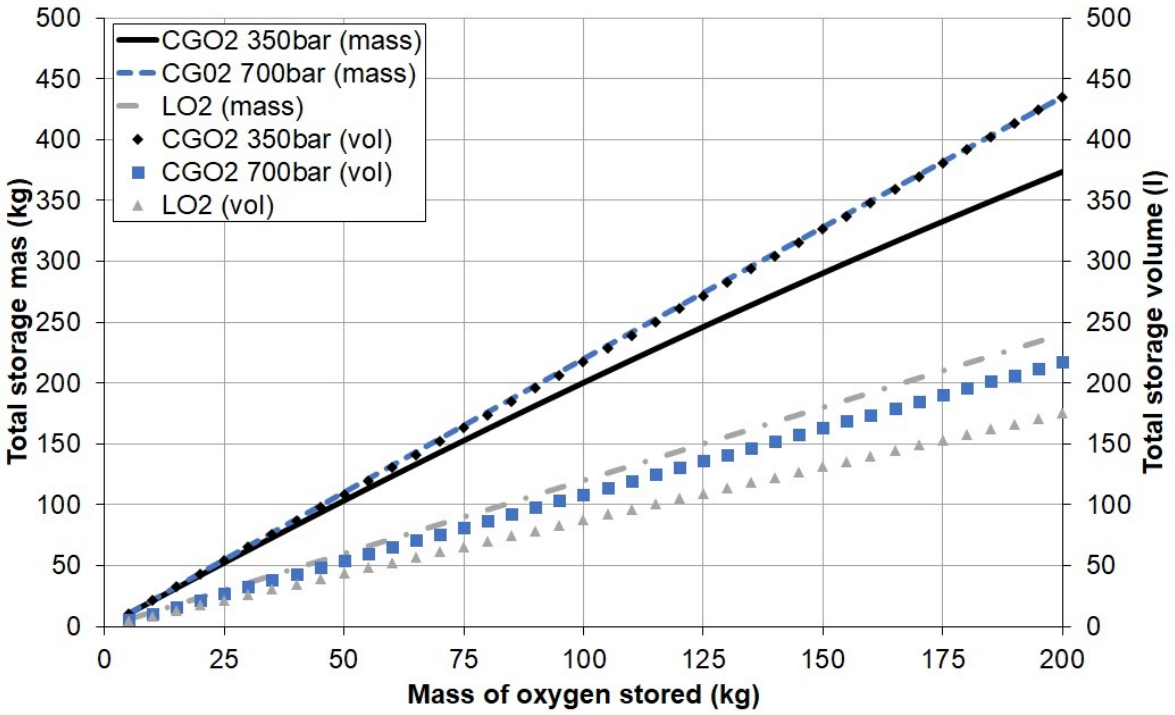

Figure 6.5: Comparison of molecular oxygen storage methods [32-39]

Overall, based on the total mass and volume of the storage systems, LO_2 outperforms both compressed gas options. This is because the higher (relative to hydrogen) boiling point of oxygen as shown in Table 6.1 allows for a simpler, more lightweight tank insulation design. However, if weight isn't the limiting factor in the system design, storing oxygen as a compressed gas at a pressure of 700 bar gauge provides similar volumetric storage efficiency.

6.4 Hybrid, Semi-Independent

To minimise the parasitic current draw on the fuel cell system and the amount of on-board oxygen required it is hypothesised that a hybrid system combining both a compressor and on-board "top-up" oxygen storage could be used. An example schematic for this type of system has been included as Figure 6.6.

Another potential use of this type of cathode system configuration would be to supply supplemental oxygen to the fuel cell under periods of high-altitude operation. This would allow greater mission flexibility from a singular system design.

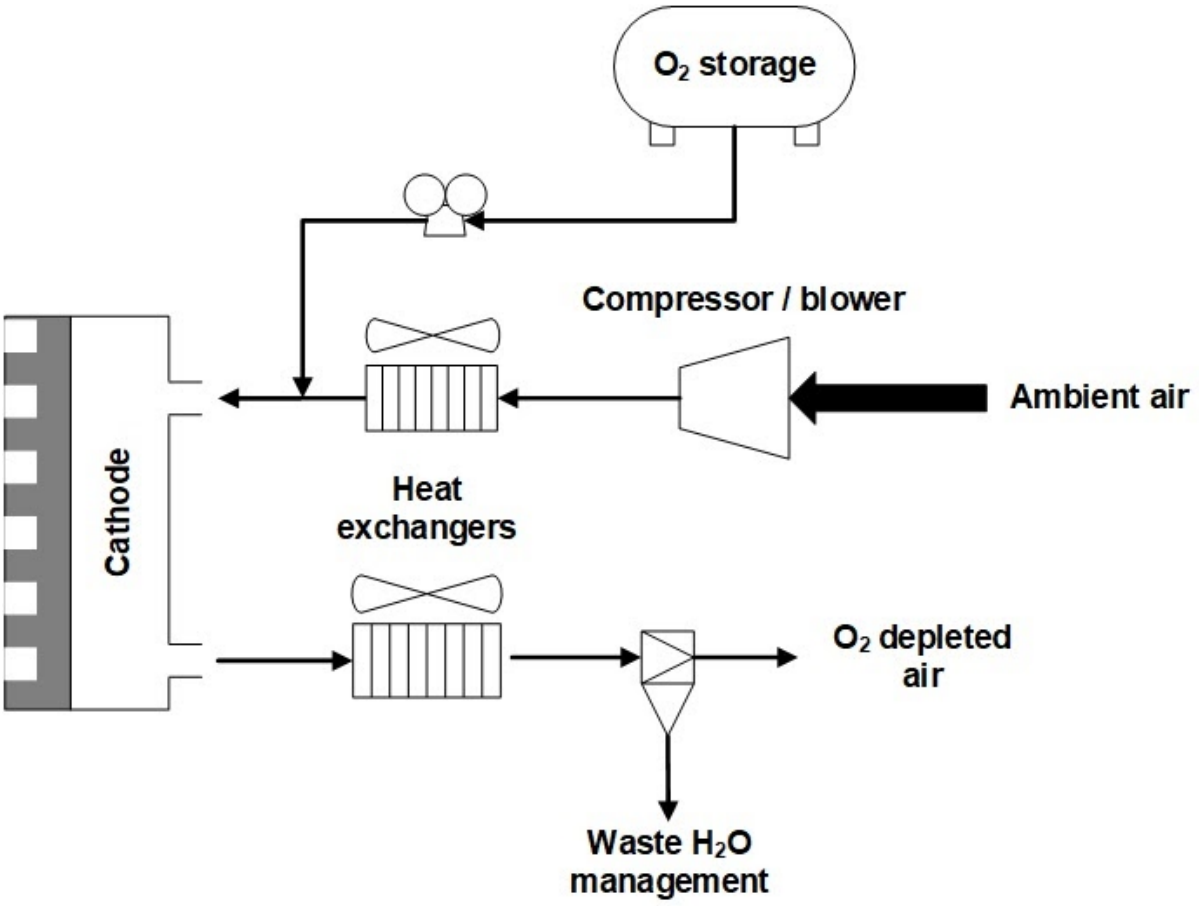

Figure 6.6: Example schematic for the cathode side of a hybrid semi-independent low-temperature fuel cell

6.5 System Comparison

An investigation was carried out into the potential advantage of implementing a hybrid semi-independent system, analogous to the one discussed in Section 6.4. Results were achieved by derating the compressor component of the system to reduce the airflow rate into the fuel cell and then calculating the additional oxygen required to bring the cathode stoichiometry, λ back up to 2.0. The study was conducted for the system configurations shown in Table 6.2 over a range of altitudes from 0 ft to 65,600 ft and range of flight times from 30 minutes to ten hours.

Table 6.2: Cathode system configurations for system comparison study

Configuration	**% O_2 from Compressor**	**% O_2 from LO_2 Storage**
Air-breathing	100%	0%
Hybrid	75%	25%
	50%	50%
	25%	75%
Air-independent	0%	100%

The primary outputs of this study were comparisons of the mass and volume of air-breathing, hybrid and air-independent cathode systems for a fuel cell operating over a range of altitudes and for a variety of mission durations. The first step was to define an operating map for the compressor based on parasitic power draw. Using Equation 6.2 for cathode airflow with a stoichiometry of 2.0 and Equation 6.3 the variation of compressor power with altitude is expressed as a function of net fuel cell power in Figure 6.7. Compressor flow rates required to deliver 25%, 50%, 75% and 100% of the 2.0 stoichiometry flow rate are included to represent the system configurations from Table 6.2.

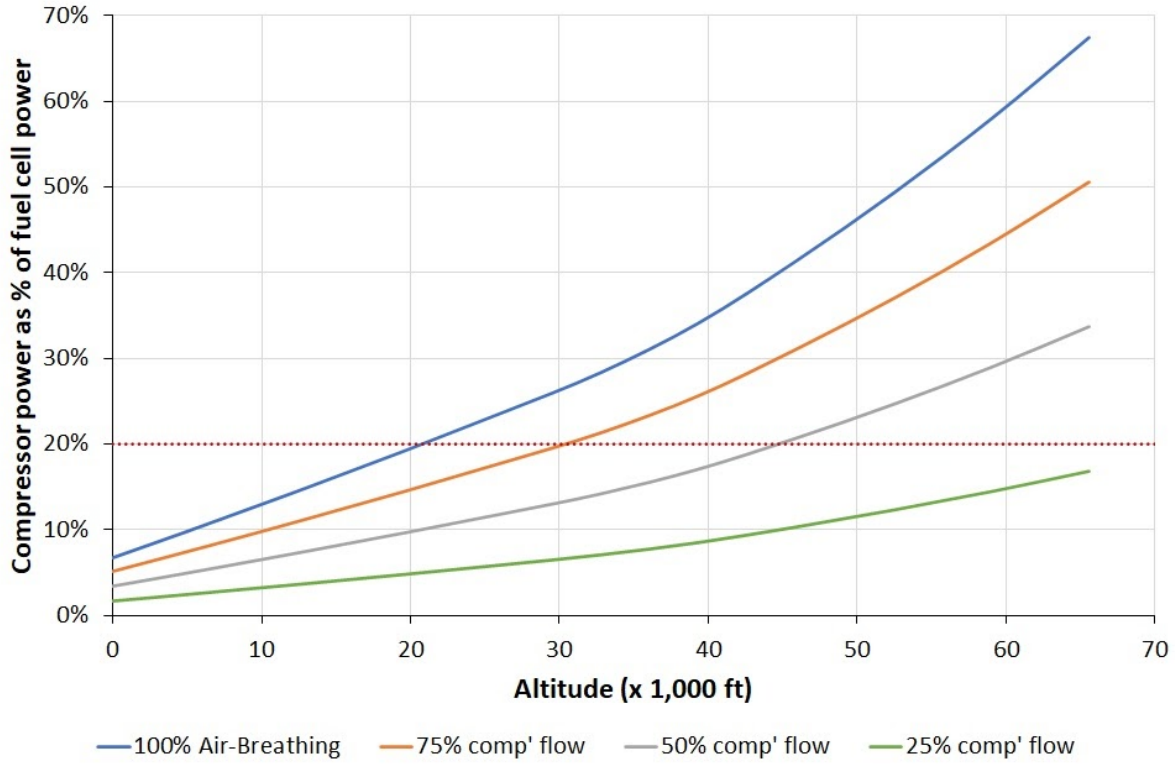

Figure 6.7: Compressor power as a percentage of net fuel cell power

A dotted line on Figure 6.7 represents a compressor power draw of 20% of net fuel cell power. As this has already been deemed excessive, only case studies in which the compressor power draw is below this limit were considered in the study.

Three flight times; 30 minutes, one hour and ten hours were used to demonstrate the sensitivity of system configuration to mission duration. As all design points have been normalised to an air-independent case and compressor power normalised to fuel cell power it was found that the results presented were insensitive to fuel cell power. Mass and volume of the compressor and liquid oxygen storage were calculated using the relationships derived during this Chapter.

Figure 6.8 shows the system configuration comparison for a 30 minute flight time. The red dotted line represents the mass and volume of a fully air-independent system using LO_2 storage. Each of the solid lines represent the mass of a system configuration as a percentage of the air-independent system. The dashed lines show the same relationship for volume. The lengths of each line represents the maximum altitude possible for each configuration before the compressor power exceeds 20% of the fuel cell power.

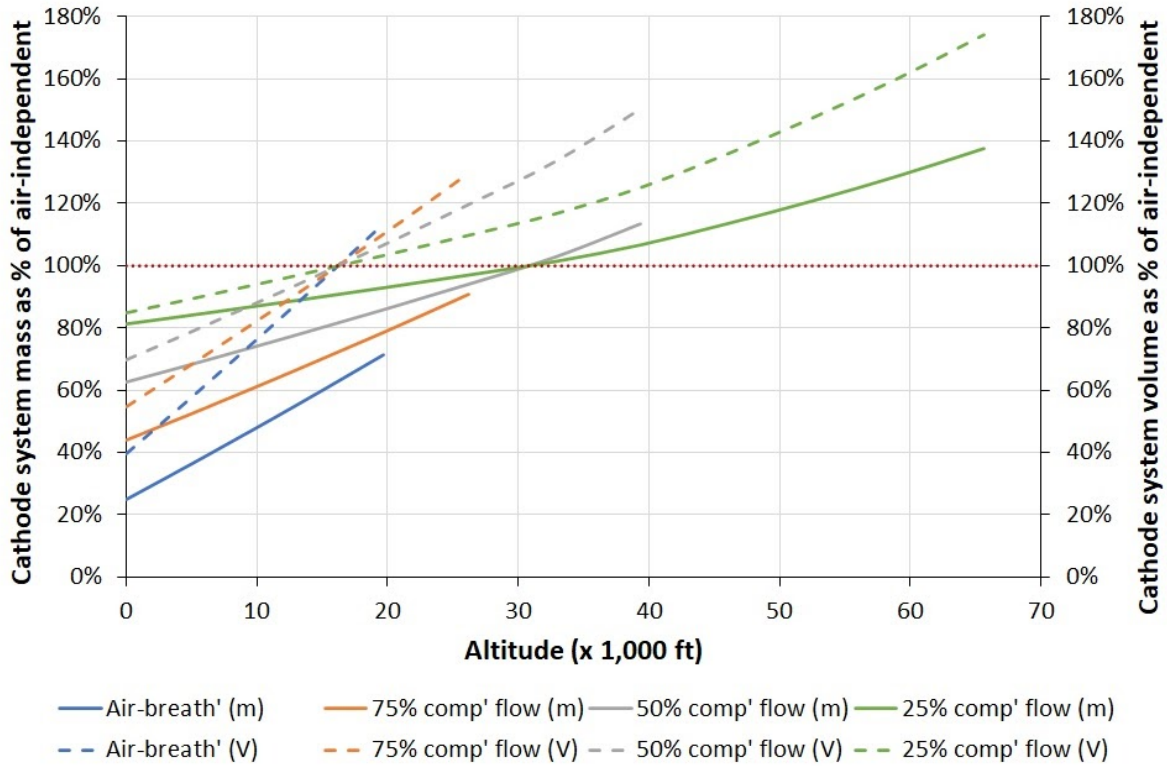

Figure 6.8: Cathode system mass and volume change with altitude as a percentage of a fully air-independent design for a 30 minute flight time

Results from the 30 minute design point show that for altitudes in excess of 30,800 ft an air-independent cathode configuration has the lowest overall mass and volume. As the altitude is decreased, the optimum configuration in terms of mass includes a larger compressor contribution until below 20,000 ft where a fully air-breathing system is most advantageous. An air-independent configuration remains the most promising in terms of volume until altitude is decreased below 17,000 ft in which case an air-breathing design is smaller.

When the flight time was doubled to one hour an air-independent configuration was only beneficial in terms of mass and volume at altitudes above 56,000 ft as shown in Figure 6.9. Below this altitude, having an air-breathing cathode topped up with stored oxygen saves both mass and space. At a typical altitude for a commercial passenger aircraft, 35,000 ft based on this study a hybrid cathode system would be most suited with the compressor supplying 50% of the required oxidant flow.

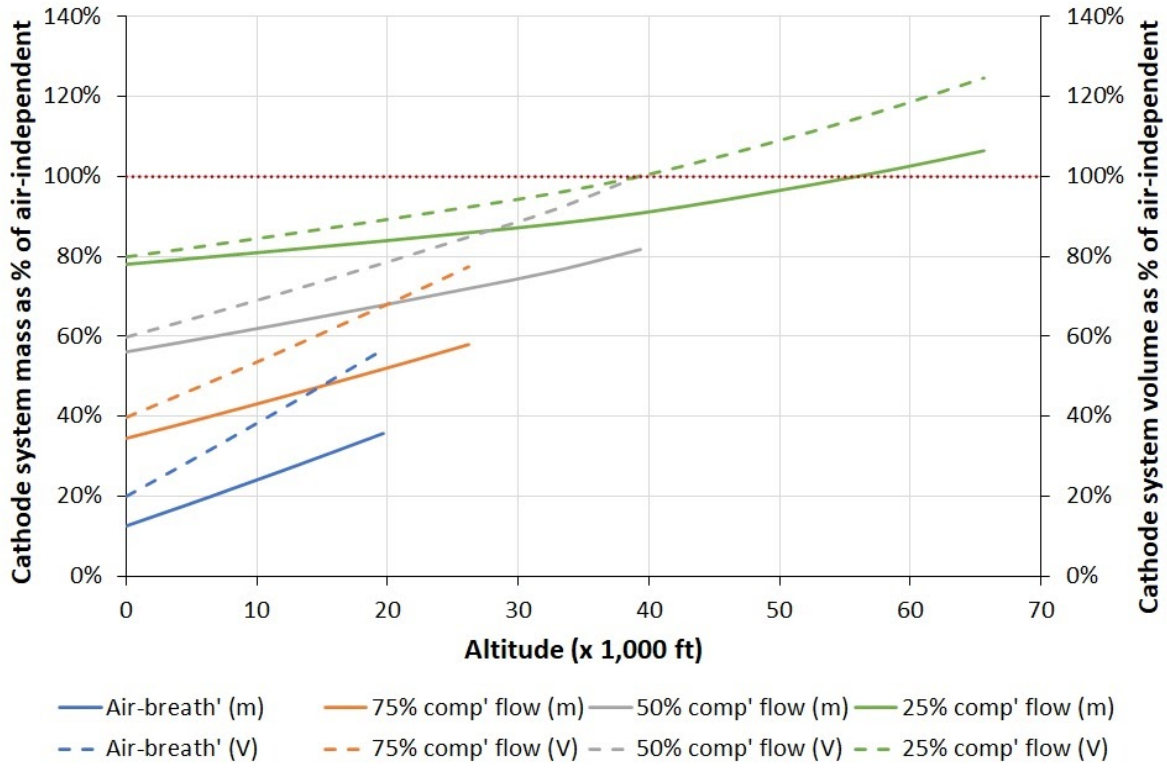

Figure 6.9: Cathode system mass and volume change with altitude as a percentage of a fully air-independent design for a one hour flight time

To demonstrate the effect of further increasing the flight time on the relative performance of the defined cathode configurations, a ten hour flight time was considered. The results, Figure 6.10 show that for extended mission durations it is always beneficial to utilise some form of hybrid or fully air-breathing cathode design. This relationship is reliant on the calculation methodology and physical relationships defined in this Chapter and may change if significant advances in either compressor design or oxygen storage are realised.

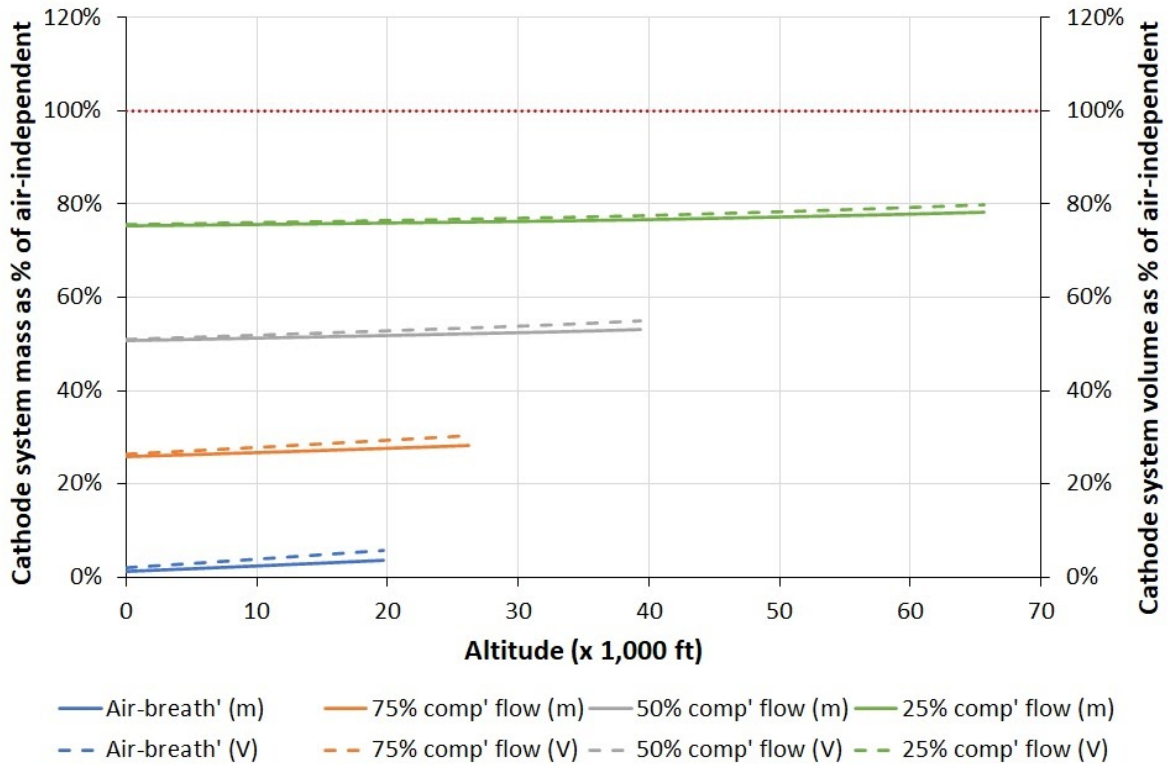

Figure 6.10: Cathode system mass and volume change with altitude as a percentage of a fully air-independent design for a ten hour flight time

6.6 Summary

In this Chapter both air-breathing and air-independent fuel cell cathode subsystems have been discussed and analysed. Both systems can be and have been used for both PEMFC and DMFC systems although commercially, air-breathing systems are nearly always preferred due to their lower cost and less difficult integration.

Key design considerations for both cathode system types have been discussed; primarily, the compressor design for an air-breathing system and consideration of oxygen storage methods for air-independent systems. How these considerations relate to system gravimetric and volumetric efficiencies have also been discussed.

It was shown that for air-independent systems, the most efficient method of storing oxygen both in terms of mass and volume is in a liquified state. It was also shown that the difference in storage efficiency between liquefied oxygen and high-pressure compressed gaseous storage was less extreme than that previously demonstrated for hydrogen.

A hypothesis was made and proven that combining elements from both air-breathing and air-independent systems into a hybrid semi-independent system might lead to gravimetric and volumetric efficiency gains. The results yielded from this investigation showed that incorporating onboard oxygen storage in the form of LO_2 (air-independent) into an air-breathing design would lead to improvements in efficiency for high altitude flights. For very short flight times, a fully air-independent system was shown to offer both mass and space savings.

Given the additional mission flexibility and performance improvements garnered from the inclusion of onboard oxygen to supplement the cathode supply to a fuel cell, it is the recommendation of this work that any mid to large scale fuel cell integration effort should include a hybrid semi-independent cathode design. This will enable flexibility for operation at higher altitudes as well as the ability to artificially boost the fuel cell performance by operating an oxygen rich cathode.

6.6 References

[1] Larminie J, Dicks A. Fuel Cell Systems Explained. 2nd ed. John Wiley & Sons; 2003. https://doi.org/10.1016/S0378-7753(00)00571-1.

[2] Ballard Power Systems Inc. FCgen-1020ACS 2015. http://ballard.com/files/PDF/Backup_Power/1020ACS_v2.pdf (accessed August 5, 2016).

[3] Ballard Power Systems Inc. FCveloCity-HD 2016. http://ballard.com/files/PDF/Bus/FCvelocity_HD_Family_of_Products_Low_Res.pdf (accessed August 5, 2016).

[4] Horizon Energy Systems. AEROSTACKS, World's lightest fuel cells for electric UAVs 2015. https://media.wix.com/ugd/047f54_8483372175ef4e1aa43edbe62aaae68e.pdf (accessed August 5, 2016).

[5] Horizon Fuel Cell Technologies. H-1000XP Designed for efficiency 2014. http://media.wix.com/ugd/047f54_d140778984ed4c61a0c5d2fc8b9df2ab.pdf (accessed August 5, 2016).

[6] Intelligent Energy Ltd. Datasheet, AC64 stack 2016. http://www.intelligent-energy.com/uploads/uploads/Datasheets/41556_ie_-_ac64_datasheet.pdf (accessed December 5, 2016).

[7] Intelligent Energy Ltd. Datasheet, FCM-801 2018.

[8] SFC Energy. Efoy Comfort Technical Data n.d. https://www.efoy-comfort.com/technical-data (accessed August 4, 2020).

[9] SFC Energy. Efoy_Comfort_210 2018. https://www.efoy-comfort.com/sites/default/files/sfc_M10_perspektive_I_18201_210_sRGB_8.png (accessed February 21, 2019).

[10] Prater K. The renaissance of the solid polymer fuel cell. J Power Sources 1990;29:239–50. https://doi.org/10.1016/0378-7753(90)80023-7.

[11] Pilatowsky I, Romero RJ, Isaza CA, Gamboa SA, Sebastian PJ, Rivera W. Thermodynamics of Fuel Cells. Cogener. Fuel Cell - Sorption Air Cond. Syst. 1st ed., London: Springer-Verlag; 2011, p. 25–36. https://doi.org/10.1007/978-1-84996-028-1.

[12] Sugawara T, Kanazawa T, Imai N, Tachibana Y. Development of Motorized Turbo Compressor for Clarity Fuel Cell. SAE Tech Pap 2017. https://doi.org/10.4271/2017-01-1187.

[13] Cheng X, Shi Z, Glass N, Zhang L, Zhang J, Song D, et al. A review of PEM hydrogen fuel cell contamination: Impacts, mechanisms, and mitigation. J Power Sources 2007;165:739–56. https://doi.org/10.1016/j.jpowsour.2006.12.012.

[14] Yu W, Sichuan X, Ni H. Air compressors for fuel cell vehicles: An systematic review. SAE Int J Altern Powertrains 2015;4:115–22. https://doi.org/10.4271/2015-01-1172.

[15] Bailey S. Development and Test of the Toroidal Intersecting Vane Management System 2005.

[16] Venturi M, Sang J, Knoop A, Hornburg G. Air supply system for automotive fuel cell application. SAE Tech Pap 2012. https://doi.org/10.4271/2012-01-1225.

[17] Rotrex. Rotrex TM EK10AA Fuel Cell Compressor Technical Datasheet n.d.:1–8. https://www.rotrex.com/wp-content/uploads/2020/01/Rotrex-Technical-Datasheet-EK10AA-Range-V1.50-1.pdf (accessed August 29, 2020).

[18] aeristech. Aeristech Electric Fuel Cell Compressor - AeFC805D n.d.:160. https://www.aeristech.co.uk/wp-content/uploads/2019/11/AeFC805D_DATASHEET_V1.1.0.pdf (accessed August 29, 2020).

[19] aeristech. Aeristech Electric Fuel Cell Compressor - AeFC806E n.d.:120. https://www.aeristech.co.uk/wp-content/uploads/2019/11/AeFC806E_DATASHEET_V1.1.0.pdf (accessed August 29, 2020).

[20] Hall N. Compressor Thermodynamics. NASA - Glenn Res Cent 2015. https://www.grc.nasa.gov/WWW/K-12/airplane/compth.html (accessed August 22, 2020).

[21] Technical Committee ISO/TC20. ISO 2533:1975 Standard Atmosphere. 1975.

[22] Thirkell A, Chen R, Harrington I. A Fuel Cell System Sizing Tool Based on Current Production Aircraft. Fort Worth, Texas: SAE International; 2017. https://doi.org/10.4271/2017-01-2135.

[23] Thiagarajan V, Karthikeyan P, Thanarajan K, Neelakrishnan S, Manoharan R, Chen R, et al. Experimental investigation on DMFCs using reduced noble metal loading with NiTiO3 as supportive material to enhance cell performances. Int J Hydrogen Energy 2019;44:13415–23. https://doi.org/10.1016/j.ijhydene.2019.03.244.

[24] Amirinejad M, Rowshanzamir S, Eikani MH. Effects of operating parameters on performance of a proton exchange membrane fuel cell. J Power Sources 2006;161:872–5. https://doi.org/10.1016/j.jpowsour.2006.04.144.

[25] Coppo M, Siegel NP, Spakovsky MR von. On the influence of temperature on PEM fuel cell operation. J Power Sources 2006;159:560–9. https://doi.org/10.1016/j.jpowsour.2005.09.069.

[26] Ko J, Chippar P, Ju H. A one-dimensional, two-phase model for direct methanol fuel cells - Part I: Model development and parametric study. Energy 2010;35:2149–59. https://doi.org/10.1016/j.energy.2010.01.034.

[27] Vasile NS, Monteverde Videla AHA, Simari C, Nicotera I, Specchia S. Influence of membrane-type and flow field design on methanol crossover on a single-cell DMFC: An experimental and multi-physics modeling study. Int J Hydrogen Energy 2017;42:27995–8010. https://doi.org/10.1016/j.ijhydene.2017.06.214.

[28] Santarelli MG, Torchio MF. Experimental analysis of the effects of the operating variables on the performance of a single PEMFC. Energy Convers Manag 2007;48:40–51. https://doi.org/10.1016/j.enconman.2006.05.013.

[29] Health and Safety Executive. Oxygen use in the workplace: Fire and explosion hazards. 2013.

[30] BOC. Oxygen Safety Data Sheet 2017. https://www.boconline.co.uk/en/images/10021701_tcm410-39599.pdf (accessed August 28, 2020).

[31] National Institute of Standards and Technology. Thermophysical Properties of Fluid Systems. NIST Chem WebBook, SRD 69 2018. https://webbook.nist.gov/chemistry/fluid/ (accessed April 17, 2021).

[32] Horizon Fuel Cell Technologies. Ultra-light composite cylinder (E-Series) 2017. http://www.fuelcellstore.com/hydrogen-equipment/hydrogen-storage/composite-storage-cylinders/ultra-light-composite-storage-cylinder-e-series (accessed January 5, 2017).

[33] Luxfer Gas Cylinders. G-StorTM H2 hydrogen-storage cylinders 2015. http://www.luxfercylinders.com/products/alternative-fuel/gstorh2 (accessed January 5, 2016).

[34] Mahytec. Hydrogen storage solutions 2016. http://www.mahytec.com/en/our-solutions/ (accessed January 5, 2017).

[35] Steelhead Composites. Hydrogen gas storage 2016. http://steelheadcomposites.com/products/gas-cylinders/hydrogen/ (accessed January 5, 2017).

[36] lapesa. Horizontal Cryogenic Tanks n.d.:10–1. www.lapesa.es/descargar.php?f=/sites/default/files/documentos/gnli_1011.pdf (accessed January 5, 2017).

[37] Quantum fuel systems. Q-LiteTM advanced CNG fuel storage tanks 2015. http://www.qtww.com/product/q-lite-lightest-cng-tanks/ (accessed January 5, 2017).

[38] Luxfer Gas Cylinders. L6X Composite inflation and aerospace cylinders 2015. http://www.luxfercylinders.com/products/l6x-composite-cylinder (accessed January 5, 2016).

[39] Chart Industries. CAIRE Liquid Oxygen Reservoirs 2017. http://www.chartindustries.com/Respiratory-Healthcare/Liquid-Oxygen-Systems/Reservoirs (accessed January 9, 2017).

Chapter 7 Thermal Management System Modelling

7.1 Introduction

It is critical to the performance and durability of the fuel cell to ensure adequate cooling to maintain the operating temperature of polymer electrolyte based fuel cells below 100 °C. This ensures adequate membrane hydration for optimum proton conductivity [1]. Zhang, G [2] gives the four main sources of heat generation in PEMFCs. These are:

1. Entropic heat of reactions
2. Irreversible heat of electrochemical reactions
3. Heat from ohmic resistances
4. Heat from condensation of water vapour

The low-quality heat produced by fuel cells [3], a result of their low operating temperature leads to added complexity in the thermal management system design. As heat transfer is fundamentally a factor of an area, a temperature difference and a thermal conductivity [4], the design complexities take the form of either an increased transfer area or the utilisation of a heat transfer medium with a higher thermal conductivity.

As cases in which the exhaust water is in liquid form are very rare [5,6] it is usual to use the Lower Heating Value (LHV) for the thermodynamic reversible voltage when calculating the heat generation rate of a fuel cell. This equates to 1.23 V for a Polymer Electrolyte Membrane Fuel Cell (PEMFC) and 1.22 V for a Direct Methanol Fuel Cell (DMFC). Fuel cell heating rate can be calculated using Equation 7.1.

$$\dot{Q}_{gen} = In\,(V_{LHV} - V_c) = P_e\left(\frac{V_{LHV}}{V_c} - 1\right) \qquad (7.1)$$

Where:

I - Current (A)

n - Number of cells

P_e - Electrical power (W)

$\dot{Q}_{gen}$ - Heat generation rate (W)

V_c - Cell potential (V)

V_{LHV} - Thermodynamic neutral voltage based on the LHV (V)

If the cells within the stack are not adequately hydrated, then the proton exchange membranes will dry out and overheat. Overheating can cause further issues such as melting of materials or a fire. This leads to the need for a robust cooling solution for the fuel cell.

Four main approaches to the thermal management of PEMFCs exist depending on the heat dissipation and system packaging requirements: physical contact, air-cooling, liquid-cooling and phase-change-cooling [1,2,5,6]. Each cooling strategy will be discussed and a modelling strategy devised for the one(s) deemed most suitable for use in aeronautical applications.

As thermal management is only a small component of this work package, a simplified approach to modelling fuel cell thermal management will be implemented. The generally accepted approach [7-9] of modelling the fuel cell as a single control volume and using average stack thermal properties (temperature, heat capacity, and thermal conductivity) will be implemented in this Chapter. This approach is a good approximation to a real fuel cell because the material balance, both in terms of mass and volume is dominated by the material used for the bipolar plates.

7.2 PEMFC Cooling Methodologies

7.2.1 Physical Contact Heat Sink

For very small, low-power fuel cells heat rejection through physical contact with some sort of heatsink may be the only feasible possibility. This is especially true if such a fuel cell was located in an area with limited direct access to an ambient airflow. Such applications of this type of fuel cell might include portable electronics such as laptops and smartphones [10,11]. It is also hypothesised by the author that this type of fuel cell architecture may also find a use as part of a distributed fuel cell system on board an aircraft. In particular, small fuel cells located in space-limited areas such as wing tips could utilise the skin of the aircraft as a heatsink in subsonic designs.

Physical contact cooling, otherwise referred to as “cooling with heat spreaders” or “edge cooling” relies on in-plane heat conduction between the fuel cell and the heat sink [2]. When implementing this cooling method, it is essential that the in-plane thermal conductivity of the cooling plates is high. Two common methods for implementing edge cooling are heat pipes and cooling plates constructed from highly conductive graphite-based materials.

The key benefit of physical contact cooling is a significant reduction in the Balance of Plant (BoP) required. There is no need for dedicated coolant delivery therefore, eliminating components including pumps reducing the overall mass, volume and parasitic current draw of the cooling system. However, major challenges with this cooling strategy include being able to control the temperature variation across the active area of the fuel cell and scalability to higher power applications.

7.2.2 Air-Cooling

Cooling by means of passing a separate airflow across the fuel cell stack is the most popular cooling method for lower power fuel cells (< 4 kW) [12]. This cooling strategy makes use of heat transfer by convection from the fuel cell assembly to the forced airflow. In addition to the balance of plant requirement, an open-cathode fuel cell design is also necessary to implement this cooling strategy. Figure 7.1 gives an example schematic of how an open cathode PEMFC design may be implemented, notice the additional cooling channels and discrete anode and cathode flow fields for each Membrane Electrode Assembly (MEA).

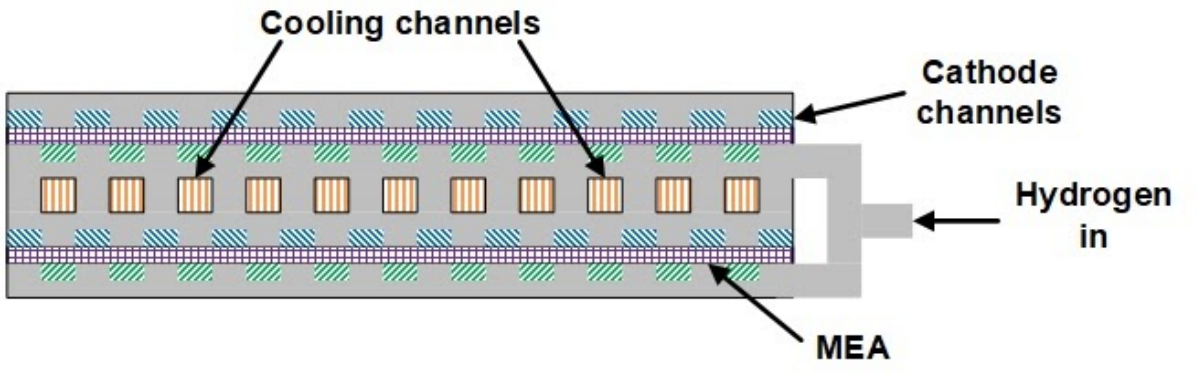

Figure 7.1: Example schematic of an open-cathode air-cooled fuel cell with a dead-ended anode fed by a common hydrogen manifold

Supporting BoP for an open-cathode air-cooled fuel cell design primarily consists of cooling fan(s), their power supply and associated ducting. As the open-cathode design does not allow for in-line humidification, care must be taken both in design and operation to ensure adequate membrane hydration.

Sizing the BoP required to support an air-cooled PEMFC is a multi-step process. The goal is to determine the mass flow of air required to maintain the desired fuel cell operating temperature. The heat generation rate, defined earlier in Equation 7.1 gives the minimum heat that must be rejected to maintain a constant temperature. Mass flow rate of air, $\dot{m}_{air}$ is directly proportional to the heating rate of the cooling airflow as defined by Equation 7.2.

$$\dot{Q}_{air} = \dot{m}_{air}\, c_p\, \Delta T_{air} \qquad (7.2)$$

Where:

c_p - Specific heat at constant pressure (J/kgK)

$\dot{m}_{air}$ - Mass flow of air (kg/s)

$\dot{Q}_{air}$ - Heat transfer rate to air (W)

ΔT_{air} - Change in air temperature (K)

Using a modified form of Equation 7.2, this time relating to the thermal properties of the fuel cell it is possible to derive a formula for the rate of temperature change of the fuel cell as a result of the energy balance between heat generation and removal by air. The final form of this is included as Equation 7.3. The average fuel cell stack heat capacity, $c_{p_{FC}}$ is determined using the heat capacity of the bulk material, usually stainless steel.

$$\dot{T}_{FC} = \frac{(\dot{Q}_{gen} - \dot{Q}_{air})}{m_{FC}\, c_{p_{FC}}} \qquad (7.3)$$

Where:

$c_{p_{FC}}$ - Average fuel cell stack heat capacity (J/kgK)

m_{FC} - Fuel cell mass (kg)

$\dot{Q}_{air}$ - Heat transfer rate to air (W)

$\dot{Q}_{gen}$ - Heat generation rate (W)

$\dot{T}_{FC}$ - Rate of change of fuel cell temperature (K/s)

Multiplying Equation 7.3 through by time and adding the initial fuel cell starting temperature, $T_{FC\,int}$ gives the fuel cell stack temperature at that particular instant. This process is described by Equation 7.4.

$$T_{FC\,t} = T_{FC\,int} + (\dot{T}_{FC}\ t) \tag{7.4}$$

Where:

T_{FC} - Fuel cell temperature at time t (K)

$T_{FC\,int}$ - Initial fuel cell temperature (K)

$\dot{T}_{FC}$ - Rate of change of fuel cell temperature (K/s)

t - Time (s)

Over recent years, significant work has been carried out in industry to improve the performance of lightweight air-cooled PEMFCs for the purpose of powering small remotely piloted Unmanned Aerial Vehicles (UAV). A selection of the most advanced modern fuel cells have been included in Table 7.1.

Table 7.1: Current state-of-the-art commercial air-cooled PEMFCs [13-16]

Fuel Cell	**Rated Power (W)**	**Specific Power (W/kg)**	**Power Density (W/L)**
Intelligent Energy AC64 [13]	2,760	2,110	670
Intelligent Energy AC10 [14]	650	1,140	595
Horizon Aerostacks [15]	1,000	444	166
Ballard FCair [16]	1,300	325	68

Based on the available data included within Table 7.1, a specific power of 2,000 W/kg and a power density of 600 W/L will be used specifically for air-cooled PEMFCs in this work. Temperature regulation using air-cooling is managed by varying cooling fan speed as a function of fuel cell temperature. This can vary from a set of simple limit switches to more refined methodologies based on predictive control. It would be typical to include a safety factor in the upper temperature limit to allow for temperature variations with the stack.

7.2.3 *Liquid-Cooling*

Liquid-cooling of a PEMFC stack works on a similar principle to the cooling of an internal combustion engine. Extra plates with embedded coolant channels are normally included in the fuel cell construction. This increases the mass and volume of the fuel cell stack, therefore decreasing the gravimetric and volumetric densities.

A liquid based thermal management strategy offers several benefits when compared with air cooling. Firstly, the increased heat capacity of the liquid coolant allows for a higher degree of heat rejection. Therefore it is not uncommon to find liquid-cooled PEMFCs stacks with rated power in excess of 5 kW [17,18]. Secondly, the use of a cooling fluid as a heat transfer medium allows the heat to be transferred more efficiently over a greater distance from where it is generated in the fuel cell to where it is exchanged with the environment. An exemplar schematic of a liquid cooled PEMFC system is shown in Figure 7.2.

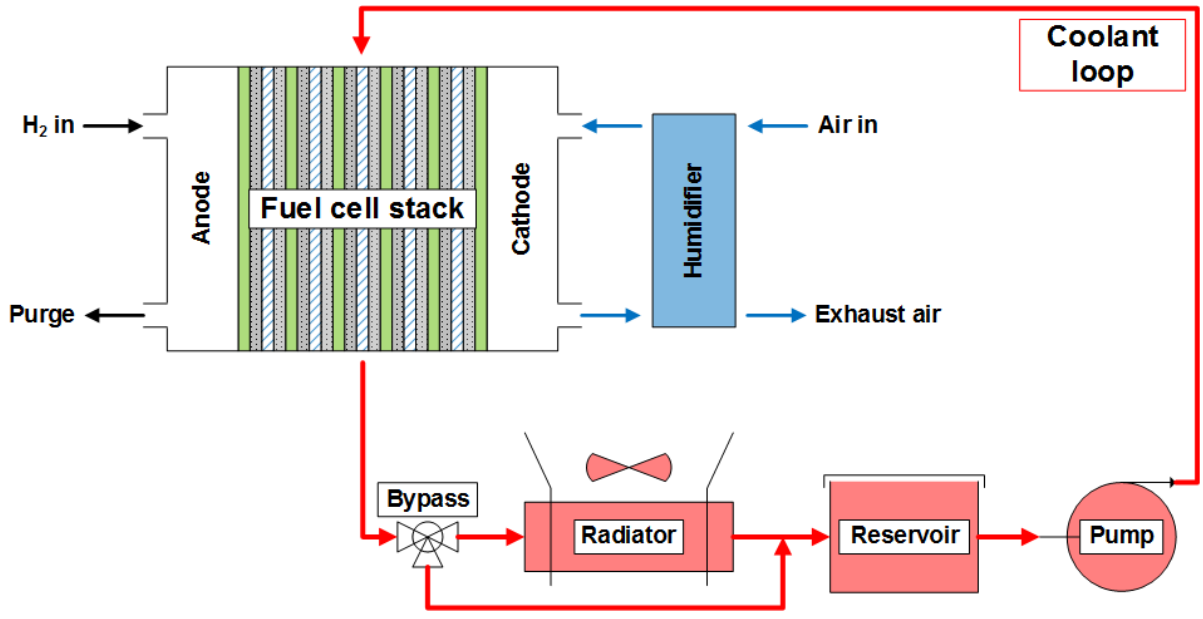

Figure 7.2: Exemplar schematic of a liquid-cooled, externally humidified PEMFC system

Ideally, De-Ionised (DI) water is used as the coolant due to its very high heat capacity (4.18 kJ/kgK) [2] and the reduced risk of contaminating the fuel cell MEA. However, generally and especially in colder climates where freezing may pose a threat, it is also common to use an antifreeze mixture of water and ethylene-glycol.

Figure 7.3 demonstrates how the freezing point of a water/ethylene glycol solution varies with the percentage composition by mass of ethylene glycol [19,20]. At a solution of 37% water / 63% ethylene-glycol by mass (40/60 by volume), the freezing point of the coolant is -53 ℃ (220 K) compared with 0 ℃ (273 K) for pure DI water.

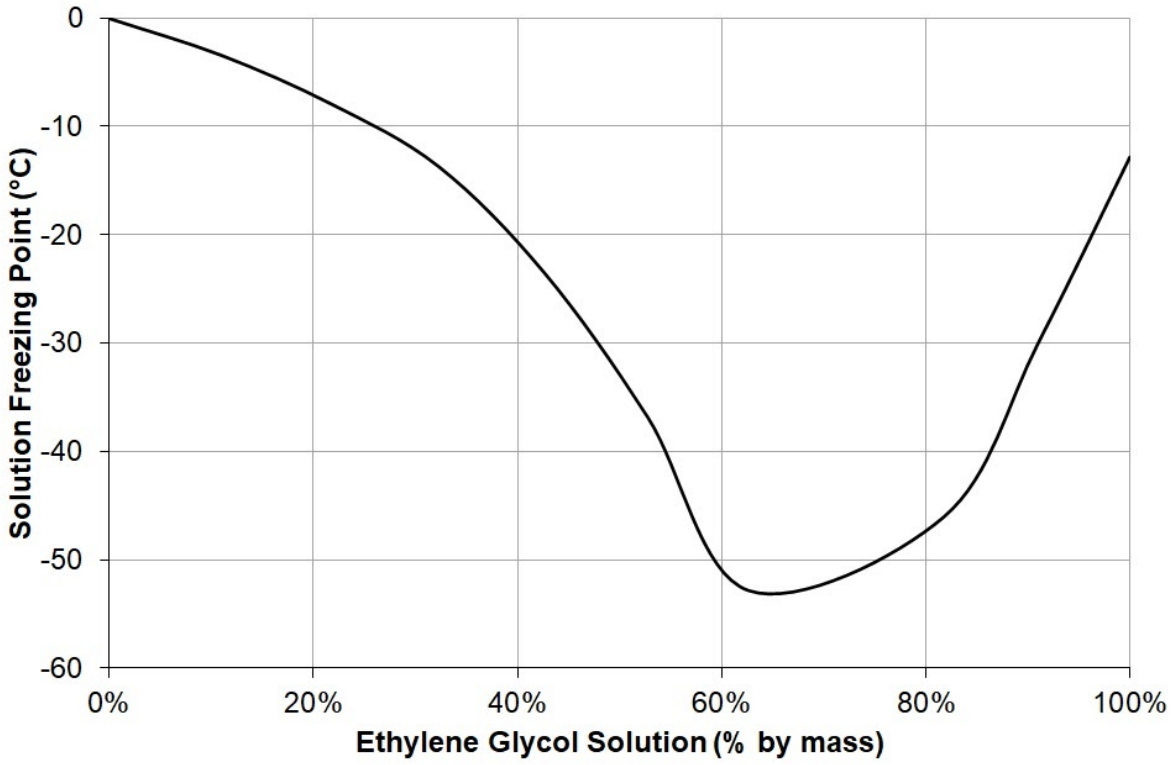

Figure 7.3: Freezing point of water/ethylene glycol solutions with varying mass compositions of ethylene glycol [19,20]

A disadvantage of a liquid-cooled system is that it requires the largest BoP of any of the cooling methodologies. This is because, as well as requiring a coolant storage and delivery system, it is also necessary to have a separate humidifier. The humidifier is required to ensure the cells remain wetted through high power operation. The key challenge is the optimisation of the coolant flow field [2]. This is usually achieved by controlling the coolant inlet temperature and the coolant flow rate [21].

Liquid-cooled PEMFCs have been the primary choice for automotive manufacturers, including Toyota and Hyundai [22]. Unfortunately, detailed information on the specific systems is not widely available due to their respective company intellectual property. However, information on other commercially available liquid-cooled PEMFCs is available and is summarised in Table 7.2.

Table 7.2: Current state-of-the-art commercial liquid-cooled PEMFCs [17,18,23,24]

Fuel Cell	**Rated Power (kW)**	**Specific Power (W/kg)**	**Power Density (W/L)**
Ballard FCvelocity-9SSL* [23]	21	1,235	1,522
Ballard FCveloCity-HD [24]	100	551	190
Hydrogenics HyPM-XR [25]	12.5	156	115
Hydrogenics HyPM-HD [26]	33	449	471

* Stack only, does not include any of the thermal system balance of plant

Specific power and power density are shown, using the data in Table 7.2, to scale with the rated power of the fuel cell. This holds true even when comparing between the different manufactures. Generally, the specific power and power density of liquid-cooled fuel cells will be lower than that of air-cooled systems due to the extra BoP required. Based on the supplied data, a specific power of 500 W/kg and a power density of 200 W/L will be used for liquid-cooled PEMFCs in the modelling work.

The solution used to model the liquid-cooled thermal management system was based heavily on the one used for air-cooled systems. The primary difference was the inclusion of a 0.37/0.63 DI water/ethylene glycol coolant to act as an energy carrier between the fuel cell and the heat exchanger. The required flow rate of liquid coolant can be found using Equation 7.5.

$$\dot{Q}_c = \dot{m}_c \, c_{p\,c} \, \Delta T_c \qquad (7.5)$$

Where:

$c_{p\,c}$ - Coolant specific heat capacity (J/kgK)

$\dot{m}_c$ - Mass flow of coolant (kg/s)

$\dot{Q}_c$ - Heat transfer rate to coolant (W)

ΔT_c - Change in coolant temperature (K)

The heat capacity of water/ethylene glycol solutions varies with both temperature and composition [20]. These relationships are outlined in Figure 7.4 with specific attention drawn to a mass composition of 37% water, 63% ethylene glycol earlier identified as the solution with the lowest freezing point.

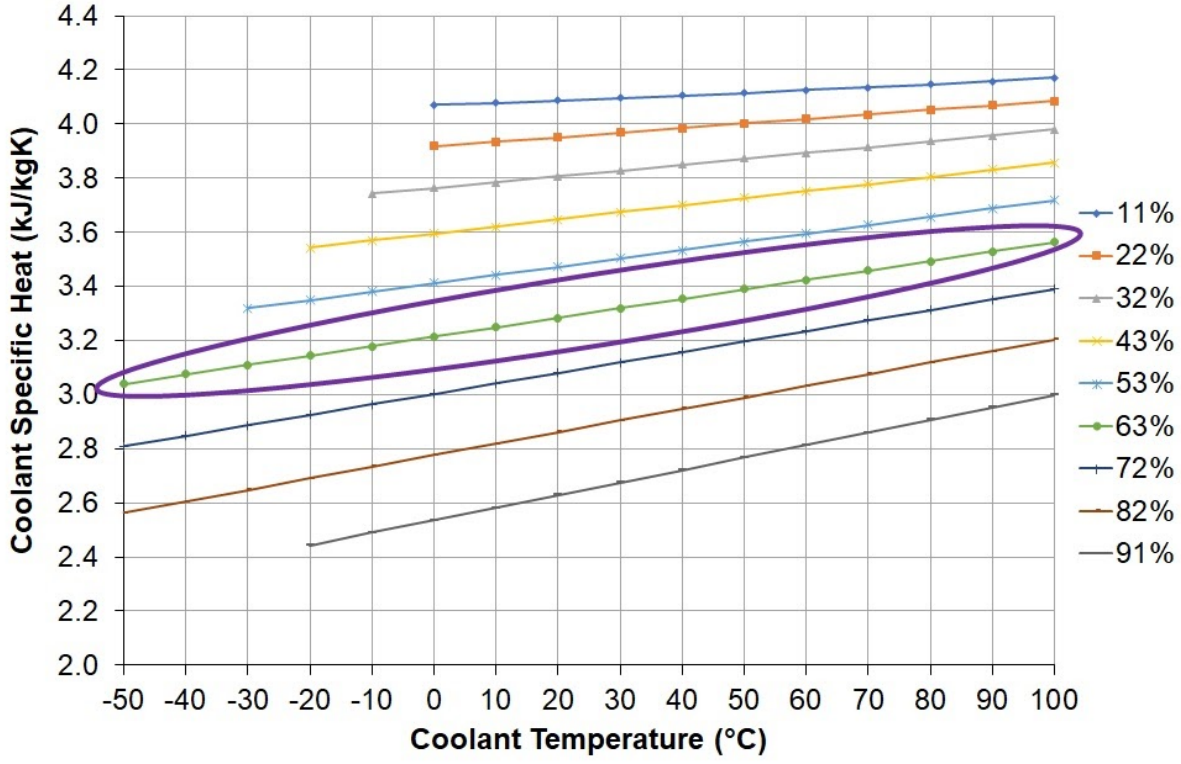

Figure 7.4: Relationships between specific heat and temperature for water/ethylene glycol solutions with mass percentages of ethylene glycol ranging from 11% to 91% [20]

Many researchers have written excellent works detailing the design process of heat exchangers, these were expertly summarised and implemented by my colleague Dr A. Fly [25]. As such it should be sufficient to use the specific power and power density relationships deduced earlier. Especially as a majority of these also include the liquid-cooling BoP such as heat exchangers and pumps.

7.2.4 Phase-Change-Cooling

Two main approaches to phase-change-cooling have been suggested [2]; evaporative and cooling through boiling. Evaporative-cooling shows more promise as cooling through boiling introduces two-phase flow instabilities. Evaporative-cooling works by the removal of heat through the evaporation of ultra pure DI within the flow channels, both cooling and humidifying the cells [21,26].

Numerous advantages of phase-change-cooling exist in relation to the performance of a PEMFC system. The coolant flow rate is reduced in comparison with liquid-cooling as phase-change-cooling utilises the latent heat of vaporisation of the cooling fluid which is usually considerably higher than the sensible heat of the fluid. An example of this is the latent heat of water, 2250 kJ/kg at 100 kPa, which is more than 500 times greater than the sensible heat absorbed by the temperature of liquid water increasing by 1 °C [2].

Phase-change-cooling also has a reduced BoP when compared with liquid-cooling due in part to its self-humidifying nature. Additionally, all of the heat rejected from the fuel cell to the cooling fluid does not need to be rejected to the atmosphere prior to reinjection into the fuel cell. Only sufficient heat needs to be rejected from the coolant stream to condense sufficient water to maintain a positive water balance. Although heat rejection from an evaporatively-cooled fuel cell system has been shown to be up to three times greater than that of a liquid-cooled system [1].

A positive water balance refers to a state where the system is producing more water than is required to be injected into the fuel cell. As water is produced as a byproduct of the electrochemical reaction inside the fuel cell, not all of the water evaporated needs to be condensed to maintain this positive water balance. An exemplar schematic for an evaporatively cooled PEMFC system is shown in Figure 7.5.

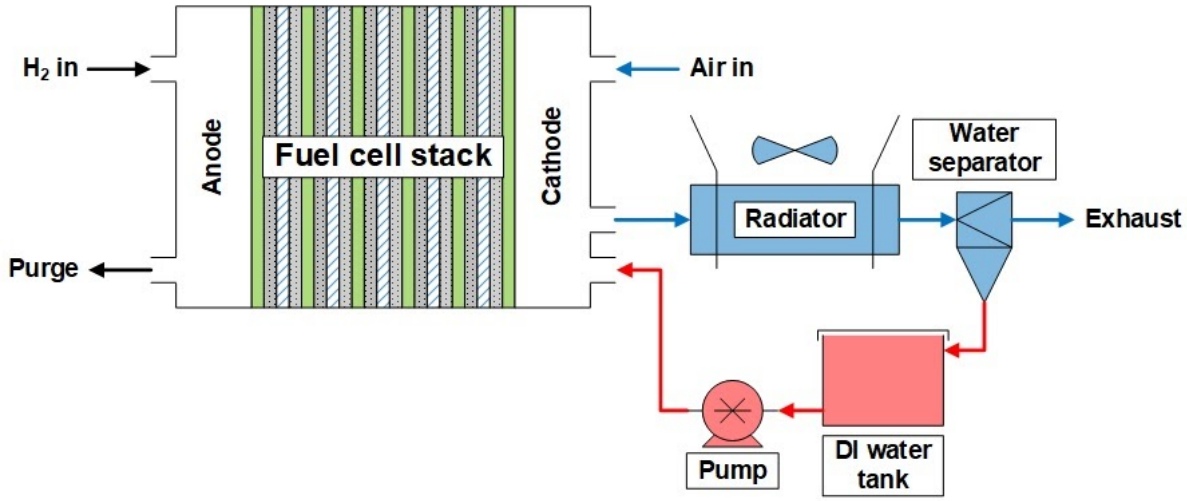

Figure 7.5: Exemplar schematic of an evaporatively-cooled PEMFC system

The key challenge with evaporative-cooling is avoiding premature degradation of the active components within the fuel cell. As the coolant is injected directly into the flow channels, it will interact with the cells and the polymer electrolyte membrane. Due to this prolonged contact with the active surfaces of the fuel cell, it is critical that the coolant remains non-conductive.

Ultra-pure DI water is non-conductive as all the charged particles are removed during the de-ionisation process. However, DI water has a very strong ionic affinity, meaning that it will readily strip ions from exposed surfaces within the fuel cell. It is therefore important to ensure that the materials which are in contact with the coolant are chosen for their compatibility with DI water.

At the time of writing, evaporatively-cooled PEMFCs are yet to garner commercial maturity. However, they have been the subject of continued research and development for at least the past 20 years [21,25-29]. As such, detailed information regarding this specific PEMFC technology remains proprietary. This fact combined with the higher confidence in mature liquid-cooled alternatives, excludes further investigation of evaporatively-cooled PEMFCs as part of this work.

7.3 DMFC Thermal Management

Heat is rejected through two processes in direct methanol fuel cells. Firstly, a small fraction of the generated heat is rejected directly from the outermost surfaces to ambient through either natural or forced convection [30]. Most of the heat generated by the electrochemical reaction in a DMFC is rejected to the reactant flows, with the temperatures of both being raised and the liquid solution on the anode being vaporised [30-34].

Unlike the typical evaporative system required for a PEMFC (Figure 7.5), DMFCs do not require additional DI water to be injected for the purpose of heat rejection. Instead, they utilise the abundance of liquid solution (methanol in water) already present on the anode as coolant. An example schematic of a DMFC system is shown in Figure 7.6. It is important to note that the primary function of a DMFC's thermal management system is enabling the recycling of unused reactants from the anode and product water from the cathode.

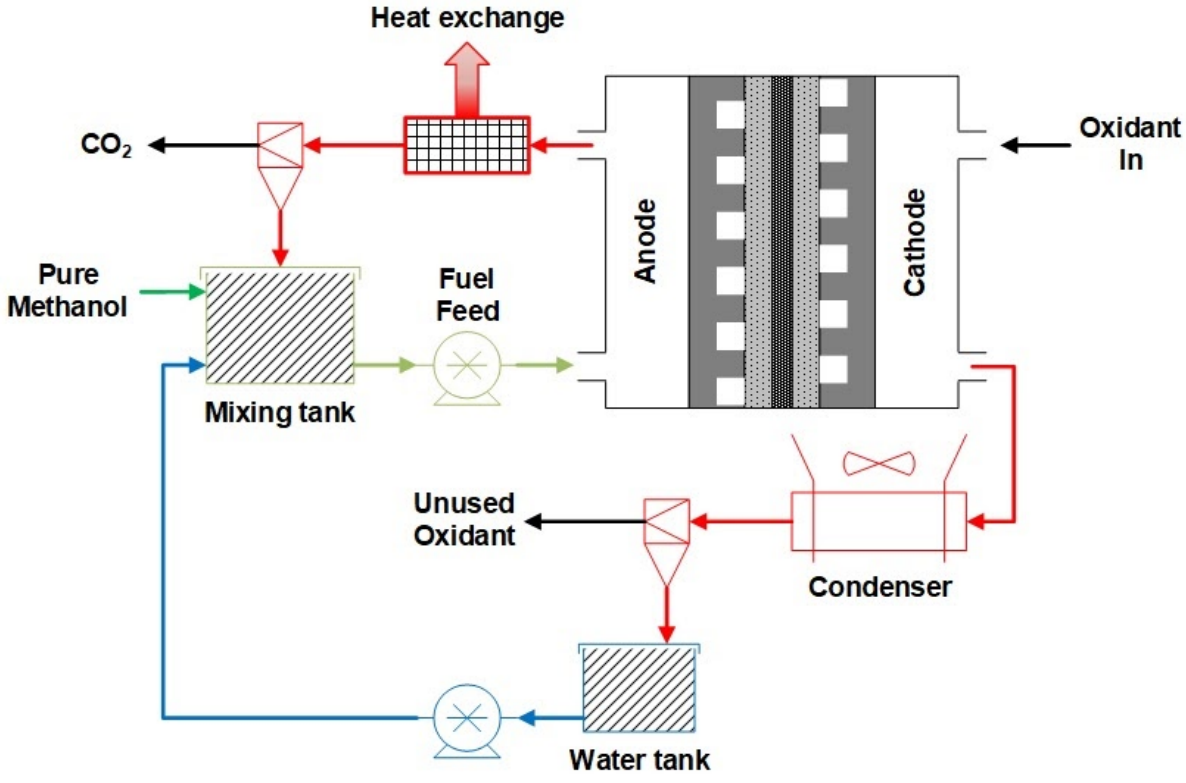

Figure 7.6: Example schematic of a DMFC system, highlighting the thermal management balance of plant

Sufficient heat must be rejected from the exhaust stream to condense all unused methanol for recirculation into the fuel cell. As the latent heat of evaporation of methanol is around 50% of that of water [35], less heat exchange is required when compared to a hydrogen fed PEMFC. Considering that a majority of the anode exhaust flow is in liquid form, heat rejection is centred predominantly around sensible cooling rather than condensing phase-change. In addition, sufficient water must be condensed from the cathode exhaust stream to maintain the desired fuel concentration in the mixing tank highlighted in Figure 7.6.

Ultimately, the thermal management of a DMFC is a complex interaction between the way the system is physically designed and the operating parameters. An excellent review of how these parameters affect the operating temperature of DMFCs was given over 20 years ago by Argyropoulos, P. et al [32], summarised in Table 7.3. They concluded in their study that DMFC operating temperature is weakly affected by inlet flow conditions and is strongly affected by the physical size and load profile.

Table 7.3: Summary of the effects of changing various DMFC design and/or operation parameters on temperature [32] reproduced with permission from Elsevier (Licence: 4916440413416)

Parameter	**Effect on DMFC Temperature**	**Comments**
Increasing the number of stacked cells	Increase	Critical effect
Increasing the ratio of active to total cross sectional area	Small	-
Increasing the current density	Increase	Critical effect
Increasing the anode side inlet temperature	Increase	Critical effect
Increasing the anode side inlet flow rate	Small Increase	Convective heat transfer not critical
Increasing the cathode side inlet temperature	Increase	Weak Effect
Increasing the cathode side inlet flow rate	Small decrease	Based on assumptions made

7.4 Effect of Altitude on Heat Removal

Fundamentally, all of the thermal management strategies outlined in this Chapter can be summarised as different techniques for moving the heat from the active sites in the fuel cell to some form of heat exchanger to be exchanged with the atmosphere. This final step in each process, the exchange of heat with the atmosphere will be affected by an aircraft's altitude in the same manner.

As discussed in Chapters 2 and 6, the variation with altitude of the properties of air are well understood. To recap, as altitude increases from sea level to 20 km (65,000 ft) the ambient air temperature decreases from 288 K to 216 K and the pressure decreases from 101 kPa to 55 kPa [2,36]. The variation of the thermal conductivity of air with increasing altitude is directly proportional to the change in temperature [36]. Finally, the density of air decreases with increasing altitude following a similar trend to that of pressure.

Using the standard equation for heat transfer and the associated relationships, Equation 7.6, it is possible to relate how the altitude variance of each of the thermal properties of air affect the potential heat transfer rate. As altitude is increased, assuming that the operating temperature of the fuel cell remains unchanged, the temperature difference, ΔT will increase. From Figure 7.7 [35,36], it can be seen that increasing altitude will reduce the heat transfer coefficient, K as both the thermal conductivity and reciprocal of thermal diffusivity decrease with increasing altitude. This results in a need for an increased heat transfer surface area to achieve the same overall heat transfer at higher altitudes.

As well as the performance of the heat exchange process at altitude, the ability of air to remove the desired heat must also be considered. As the ability of air to hold thermal energy is dominated by the change in temperature between hot and cold (Equation 7.2). This means that as the altitude is increased, and temperature decreased, less air mass flow is required to remove the same quantity of heat. This is demonstrated graphically in Figure 7.8 for a fixed heat load of 50 kW. The mas flow plateau noted in Figure 7.8 is a direct result of the ISA temperature profile in the atmosphere as shown by Figure 2.4 in Chapter 2.

$$\dot{Q} = KA_S\left(T_w - T_f\right) \;\; \& \;\; K \propto k, \; \frac{1}{\alpha_t} \;\; \& \;\; \alpha_t = \frac{k}{\rho c_p} \qquad (7.6)$$

Where:

A_S - Surface area (m^2)

c_p - Specific heat capacity at constant pressure (J/kgK)

K - Heat transfer coefficient (W/m^2K)

k - Thermal conductivity (W/mK)

$\dot{Q}$ - Heat transfer rate (W)

T_f - Flow temperature (K)

T_w - Wall temperature (K)

α_t - Thermal diffusivity (m^2/s)

ρ - Density (kg/m^3)

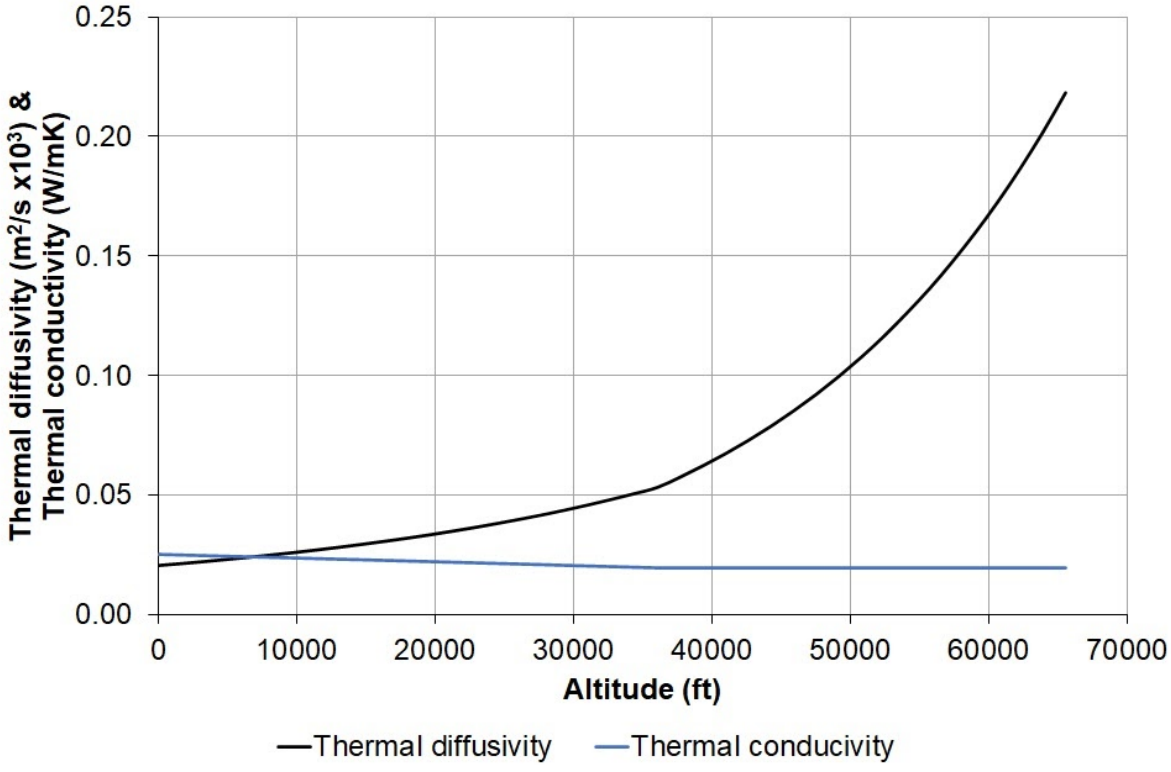

Figure 7.7: Change in thermal diffusivity and thermal conductivity of air with increasing altitude based on the International Standard Atmosphere [35,36]

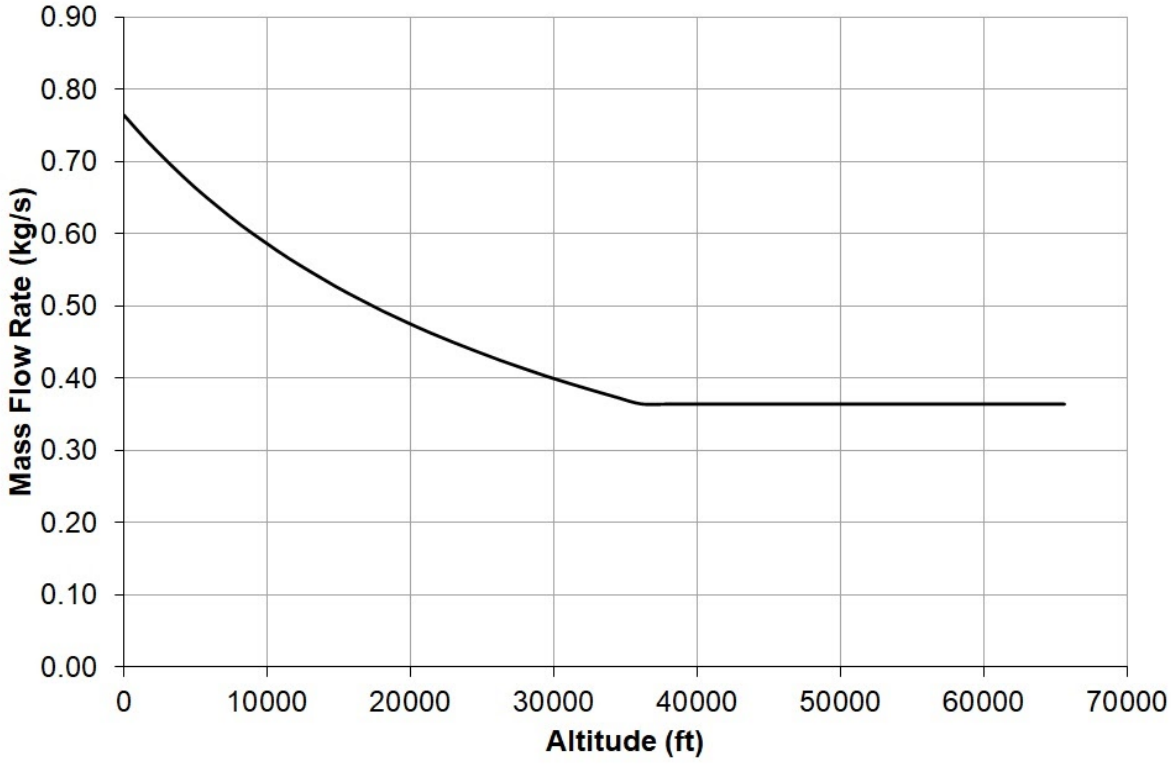

Figure 7.8: Change in mass flow rate of air required to remove a thermal load of 50 kW with altitude

Considering what has been discussed, the most suitable fuel cell thermal management system for high-altitude flight is an evaporative phase-change design. This deduction is based on the notion that the fuel cell stack temperature for both air-cooled and liquid-cooled systems is directly linked to the ability of the thermal management system to reject heat to the environment. However, in the case of phase-change systems (and DMFC systems) the purpose of the heat exchange is to recover liquid water for recycling. In these designs the bulk temperature of the cathode exit flow only needs reducing sufficiently to recover sufficient liquid water before being exhausted off the aircraft.

To its detriment, when considering the desire for a reduced heat signature and visible signature in the form of reduced contrails the evaporative-cooling designs do lose favour when compared to the closed nature of a liquid-cooled design.

7.5 Summary

In this Chapter the four primary cooling strategies for hydrogen fed polymer electrolyte membrane fuel cells have been introduced and compared. Two primary methods were identified based on net fuel cell electrical power, air-cooling and liquid-cooling. For lower power output fuel cells < 4 kW, air-cooling would be the preferred method due to its lower cost and simpler system design. Liquid-cooling has been identified as the preferred cooling methodology for higher power fuel cell systems due to higher technology maturity and more robust nature.

Simplified modelling strategies have been developed for both air-cooling and liquid-cooling scenarios. These were both based on the assumption that the fuel cell stack can be treated as a single control volume and used average stack thermal properties. This assumption produces reasonable results as the bulk material properties of a fuel cell are generally the same and relate directly to the material choice of the bipolar plates.

The current status and primary function of direct methanol fuel cell thermal management systems has been identified. In general, the literature does not suggest any active thermal management strategy for this fuel cell technology other than the initial fuel cell stack design and operating envelope. This is because, in most cases their temperature is self-regulating due to the liquid fuel supplied to the anode providing ample evaporative cooling. Therefore, the primary function of thermal management here is to enable reactant and water recycling.

As altitude is increased the ability of the ambient air to remove heat from the system is improved per unit mass. However, the heat transfer ability of the heat exchanger is reduced. Therefore, a larger heat transfer surface area is required to dissipate the same heat load at high altitude compared to at sea level.

7.6 References

[1] Soupremanien U, Le Person S, Favre-Marinet M, Bultel Y. Tools for Designing the Cooling System of a Proton Exchange Membrane Fuel Cell. Appl Therm Eng 2012;40:161–73. https://doi.org/10.1016/j.applthermaleng.2012.02.008.

[2] Zhang G, Kandlikar SG. A critical review of cooling techniques in proton exchange membrane fuel cell stacks. Int J Hydrogen Energy 2012;37:2412–29. https://doi.org/10.1016/j.ijhydene.2011.11.010.

[3] Ellamla HR, Staffell I, Bujlo P, Pollet BG, Pasupathi S. Current status of fuel cell based combined heat and power systems for residential sector. J Power Sources 2015;293:312–28. https://doi.org/10.1016/j.jpowsour.2015.05.050.

[4] Tavares S. Aerospace engineering pocket reference. Taylor & Francis; 2015.

[5] Larminie J, Dicks A. Fuel Cell Systems Explained. 2nd ed. John Wiley & Sons; 2003. https://doi.org/10.1016/S0378-7753(00)00571-1.

[6] O'Hayre R, Cha S-W, Colella W, Prinz FB. Fuel cell fundamentals. 3rd ed. John Wiley & Sons; 2016.

[7] Ferguson A, Ugursal VI. Fuel cell modelling for building cogeneration applications. J Power Sources 2004;137:30–42. https://doi.org/10.1016/j.jpowsour.2004.05.021.

[8] Wang C, Hashem Nehrir M, Shaw S. Dynamic models and model validation for PEM fuel cells using electrical circuits. IEEE Trans Energy Convers 2005;20:442–51. https://doi.org/10.1109/pes.2005.1489284.

[9] Amphlett JC, Mann RF, Peppley BA, Roberge PR, Rodrigues A. A model predicting transient responses of proton exchange membrane fuel cells. J Power Sources 1996;61:183–8. https://doi.org/10.1016/S0378-7753(96)02360-9.

[10] Agnolucci P. Economics and market prospects of portable fuel cells. Int J Hydrogen Energy 2007;32:4319–28. https://doi.org/10.1016/j.ijhydene.2007.03.042.

[11] Dailey PL. Enforcement in Mobile Devices. Computer (Long Beach Calif) 2003;36:10–2. https://doi.org/10.1109/MC.2003.1244525.

[12] Faghri A, Guo Z. Challenges and opportunities of thermal management issues related to fuel cell technology and modeling. Int J Heat Mass Transf 2005;48:3891–920. https://doi.org/10.1016/j.ijheatmasstransfer.2005.04.014.

[13] Intelligent Energy Ltd. Datasheet, AC64 stack 2016. http://www.intelligent-energy.com/uploads/uploads/Datasheets/41556_ie_-_ac64_datasheet.pdf (accessed December 5, 2016).

[14] Intelligent Energy Ltd. Datasheet, AC10 stack 2016. http://www.intelligent-energy.com/uploads/accompanying_files/41556_IE_-_AC10_datasheet_no_crops.pdf (accessed December 5, 2016).

[15] Horizon Energy Systems. AEROSTACKS, World's lightest fuel cells for electric UAVs 2015. https://media.wix.com/ugd/047f54_8483372175ef4e1aa43edbe62aaae68e.pdf (accessed August 5, 2016).

[16] Ballard. FCair ™ UAV Power Systems 2018:2. https://www.ballard.com/docs/default-source/uav/uav-data-sheet-spc5106994.pdf?sfvrsn=2 (accessed September 12, 2020).

[17] Hydrogenics. HyPM-HD power modules 2016. http://www.hydrogenics.com/wp-content/uploads/HyPM-HD-Brochure.pdf (accessed August 5, 2016).

[18] Ballard Power Systems Inc. FCveloCity-HD 2016. http://ballard.com/files/PDF/Bus/FCvelocity_HD_Family_of_Products_Low_Res.pdf (accessed August 5, 2016).

[19] MEGlobal. Ethylene Glycol Product Guide 2008:1–33. https://www.meglobal.biz/wp-content/uploads/2019/01/Monoethylene-Glycol-MEG-Technical-Product-Brochure-PDF.pdf (accessed September 19, 2020).

[20] Engineering ToolBox. Ethylene Glycol Heat-Transfer Fluid 2003. https://www.engineeringtoolbox.com/ethylene-glycol-d_146.html (accessed September 19, 2020).

[21] Fly A, Thring RH. Temperature Regulation in an Evaporatively Cooled Proton Exchange Membrane Fuel Cell Stack. Int J Hydrogen Energy 2015;40:11976–82. https://doi.org/10.1016/j.ijhydene.2015.04.086.

[22] E4tech. The Fuel Cell Industry Review 2019. 2019.

[23] Ballard Power Systems Inc. FCvelocity-9SSL 2011. http://ballard.com/files/PDF/Material_Handling/9SSL.pdf (accessed August 5, 2016).

[24] Hydrogenics. HyPM-XR power modules 2016. http://www.hydrogenics.com/wp-content/uploads/HyPM-XR-Brochure.pdf (accessed August 5, 2016).

[25] Fly A. Thermal and water management of evaporatively cooled fuel cell vehicles. Loughborough University, 2015.

[26] Meyers JP, Darling RM, Evans C, Balliet R, Perry ML. Evaporativley-Cooled PEM Fuel-Cell Stack System. ECS Trans., vol. 3, The Electrochemical Society; 2006, p. 1207–14. https://doi.org/10.1149/1.2356240.

[27] Fly A, Thring RH. A comparison of evaporative and liquid cooling methods for fuel cell vehicles. Int J Hydrogen Energy 2016;41:14217–29. https://doi.org/10.1016/j.ijhydene.2016.06.089.

[28] Warburton A, Mossop D, Burslem B, Rama P, Adcock P, Cole J, et al. Development of an evaporatively cooled hydrogen fuel cell system and its vehicle application. SAE Tech Pap 2013;2. https://doi.org/10.4271/2013-01-0475.

[29] Wood DL, Yi JS, Nguyen T V. Effect of direct liquid water injection and interdigitated flow field on the performance of proton exchange membrane fuel cells. Electrochim Acta 1998;43:3795–809. https://doi.org/10.1016/S0013-4686(98)00139-X.

[30] Cai W, Li S, Li C, Liang L, Xing W, Liu C. A model based thermal management of DMFC stack considering the double-phase flow in the anode. Chem Eng Sci 2013;93:110–23. https://doi.org/10.1016/j.ces.2013.01.040.

[31] Argyropoulos P, Scott K, Taama WM. One-dimensional thermal model for direct methanol fuel cell stacks. Part I. Model development. J Power Sources 1999;79:169–83. https://doi.org/10.1016/S0378-7753(99)00181-0.

[32] Argyropoulos P, Scott K, Taama WM. One-dimensional thermal model for direct methanol fuel cell stacks. Part II. Model based parametric analysis and predicted temperature profiles. J Power Sources 1999;79:184–98. https://doi.org/10.1016/S0378-7753(99)00182-2.

[33] Dohle H, Mergel J, Stolten D. Heat and power management of a direct-methanol-fuel-cell (DMFC) system. J Power Sources 2002;111:268–82. https://doi.org/10.1016/s0140-6701(03)91859-5.

[34] Takaguchi H, Ohashi M. 1 kW Direct Methanol Fuel Cell System. Fujikura Tech Rev 2015:1–4.

[35] National Institute of Standards and Technology. Thermophysical Properties of Fluid Systems. NIST Chem WebBook, SRD 69 2018. https://webbook.nist.gov/chemistry/fluid/ (accessed April 17, 2021).

[36] Technical Committee ISO/TC20. ISO 2533:1975 Standard Atmosphere. 1975.

Chapter 8 Dynamic Modelling

8.1 Overview of Previous Chapters

8.1.1 Aircraft Submodel - Chapter 2

In Chapter 2, a predictive aircraft model was developed in conjunction with atmospheric models for both temperature and pressure. The work carried out on the predictive aircraft model was published as an SAE Technical Paper in 2017 [1].

The rate of aircraft electrification has been shown to be growing. Combined with increasing environmental pressures a model was developed to enable efficient preliminary design decisions on fuel cell systems for aeronautical applications, a predictive tool was constructed to quickly estimate the peak electrical demand of the user's aircraft.

Fifteen aircraft categories have been defined based on the aircrafts primary function and propulsion method. A model was then developed which can predict the electrical generation capability and propulsive requirements. Validating the categorisation model against real aircraft data showed a good correlation between the real and modelled data. Generally, an error of less than 5% was obtained by the model. Certain instances, higher than this cut-off percentage arose when the model was based on a small dataset.

Variation of atmospheric properties with altitude which could affect the performance of a fuel cell system were given according to the International Standard Atmosphere (ISA) along with MIL-HDBK-310 Hot and MIL-HDBK-310 Cold. The atmospheric models provided by MIL-HDBK-310 gave the extremes of both hot and cold environments.

8.1.2 Fuel Cell Submodel - Chapter 4

Creation of a validated electrical fuel cell stack model has been detailed step-by-step in Chapter 4. Importance of the thermodynamic reversible voltage, $V_{0\,HHV}$ was discussed in relation to the modelling of fuel cell electrical behaviour.

Primary fuel cell irreversibilities: activation, fuel crossover, ohmic and mass transport have been defined, both theoretically and empirically. An empirical form of the Nernst equation was used to predict the performance of both a single cell Polymer Electrolyte Membrane Fuel Cell (PEMFC) and Direct Methanol Fuel Cell (DMFC). The model results were validated against experimental data for both fuel cell technologies. Root mean square errors in the predicted real cell voltage were 9.52 mV and 8.72 mV for the PEMFC and DMFC respectively.

8.1.3 Anode Submodel - Chapter 5

It has been shown that anode subsystem specific energy and energy density both improve for hydrogen as the storage pressure is increased, cylinder type advanced and with liquefaction. A similar trend has also been shown with methanol storage with increasing specific energy and energy density with increasing methanol concentration.

A case study was carried out to determine whether a single or multi tank methanol storage solution would be optimal for a DMFC anode feed system. It was found that although the performance of the single tank system improved dramatically with increasing methanol concentration, the twin tank design case always had higher specific energy and energy density at the same inlet feed concentration.

Finally, hydrogen and methanol storage solutions were directly compared, Figure 8.1. Liquid Hydrogen (LH_2) was found to be the most energy dense fuel cell fuel storage configuration considered. However, pure and high concentration methanol storage both showed similar performance to those for LH_2 and compressed gaseous hydrogen. Given that the material properties favoured methanol from a cost and ease of storage perspective, the potential benefits of DMFCs over PEMFCS for aviation have been shown.

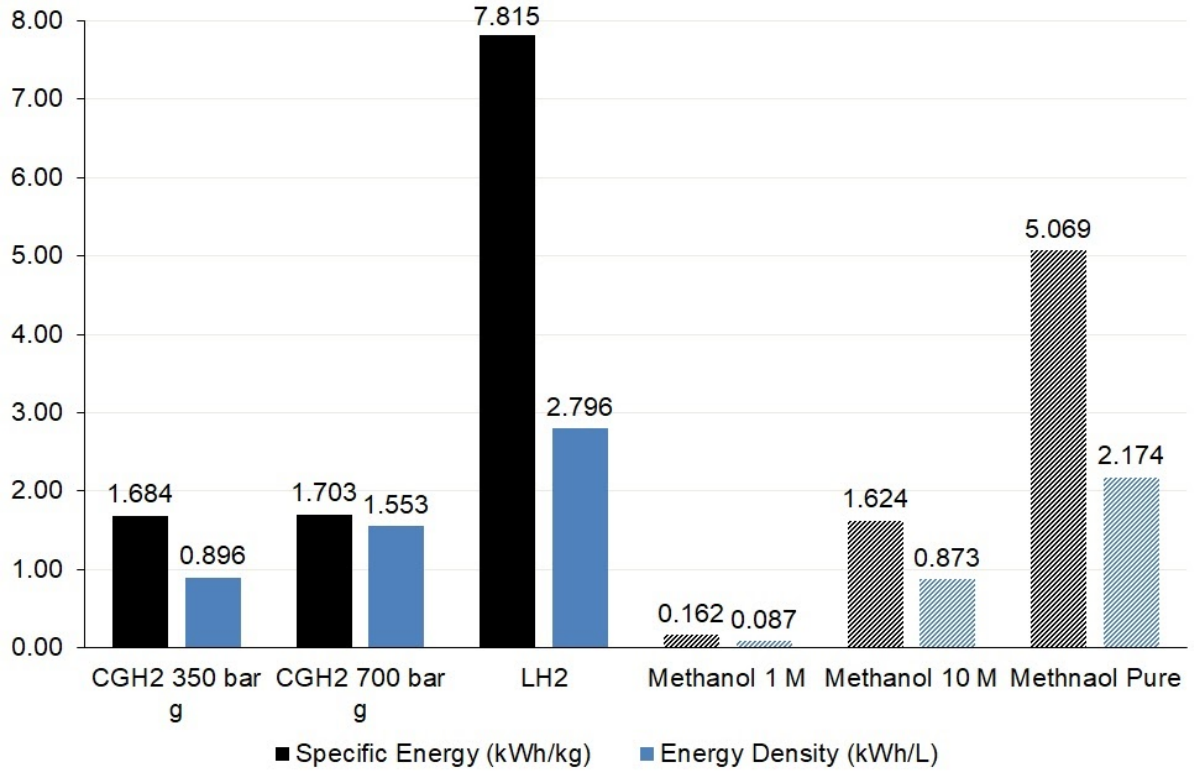

Figure 8.1: Specific energy and energy density averages for commercial hydrogen and methanol storage subsystems [2-7]

8.1.4 Cathode Submodel - Chapter 6

Key design considerations for both air-breathing and air-independant cathode systems were discussed, primarily the compressor design for an air-breathing system and consideration of oxygen storage method for air-independent systems. How these considerations relate to system gravimetric and volumetric efficiencies have also been discussed.

It was shown that for air-independent systems, the most efficient method of storing oxygen both in terms of mass and volume is in a liquified state. It was also shown that the difference in storage efficiency between liquefied oxygen and high-pressure compressed gaseous storage was less extreme than that previously demonstrated for hydrogen.

A hypothesis was made and proven that combining elements from both air-breathing and air-independent systems into a hybrid semi-independent system might lead to gravimetric and volumetric efficiency gains. The results yielded from this investigation showed that incorporating onboard oxygen storage in the form of LO_2 (air-independent) into an air-breathing design would lead to improvements in efficiency for high altitude flights. For very short flight times, a fully air-independent system was shown to offer both mass and space savings.

Given the additional mission flexibility and performance improvements garnered from the inclusion of onboard oxygen to supplement the cathode supply to a fuel cell, it is the recommendation of this work that any mid to large scale fuel cell integration effort should include a hybrid semi-independent cathode design. This will enable flexibility for operation at higher altitudes as well as the ability to artificially boost the fuel cell performance by operating an oxygen rich cathode.

8.1.5 Thermal Management Submodel - Chapter 7

Simplified modelling strategies have been developed for both air-cooling and liquid-cooling scenarios. These were both based on the assumption that the fuel cell stack can be treated as a single control volume and used average stack thermal properties.

The current status and primary function of direct methanol fuel cell thermal management systems has been identified. In general, the literature does not suggest any active thermal management strategy for this fuel cell technology other than the initial fuel cell stack design and operating envelope. This is because, in most cases their temperature is self-regulating due to the liquid fuel supplied to the anode providing ample evaporative cooling. Therefore, the primary function of thermal management here is to enable reactant and water recycling.

As altitude is increased the ability of the ambient air to remove heat from the system is improved per unit mass. However, the heat transfer ability of the heat exchanger is reduced. Therefore, a larger heat transfer surface area is required to dissipate the same heat load at altitude compared to at sea level.

8.2 Additional Submodels

8.2.1 Battery Model

High specific energy fuel cell systems have already been shown to be essential for aeronautical applications. However, in some cases the relatively poor specific power of fuel cells compared to alternative electrical power providers, batteries and capacitors calls for some form of hybridised system. Chao, C H. [8] gives an excellent comparison of the relative specific energy and specific power of the main technology options Figure 8.2.

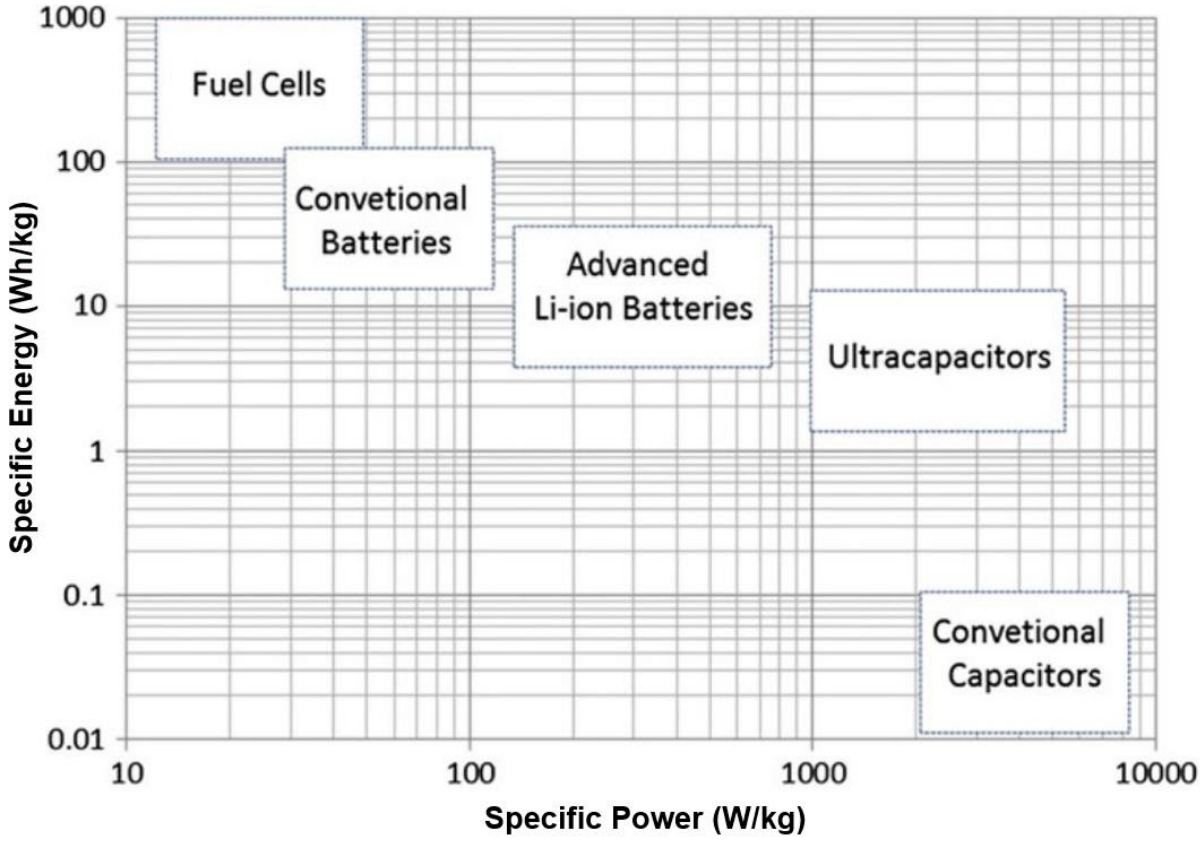

Figure 8.2: Specific Energy vs. Specific Power for various energy storage technologies, including fuel cells and advanced Li-ion batteries [8] reproduced with permission from Elsevier (Licence: 4927150372144)

A “Lithium-Ion Temperature Dependent Battery Model” [9] built into MATLAB® Simulink was adapted and used for battery simulations. This model provides an experimentally validated method of simulating a battery's charge and discharge characteristics under varying temperatures [9]. The model is based on an equivalent circuit with multiple laplace functions to represent the various compatible battery chemistries and discharge characteristics obtained from manufacturer’s published data. Model assumptions include [9]:

- Minimum battery potential is 0 V
- Discharging and charging characteristics are assumed to be equal
- Peukert effect, capacity change with current amplitude is ignored
- Batteries have no self-discharge or memory effects

Significant advances are being made every year in the field of lithium-ion battery technology however, the technology chosen for simulation was Lithium Cobalt Oxide ($LiCoO_2$) as this chemistry has been proven safe for aviation in the Boeing 787 [10]. The specific energy of this battery technology was taken as 155 Wh/kg [11] and an energy density assumed to be 240 Wh/litre.

Atmospheric temperature variation as a result of changing altitude was used as the input to the temperature dependent battery model as shown by Figure 8.3. The user was able to select which atmospheric model, from ISA and MIL-HDBK-310 Hot/Cold the temperature variation was based on.

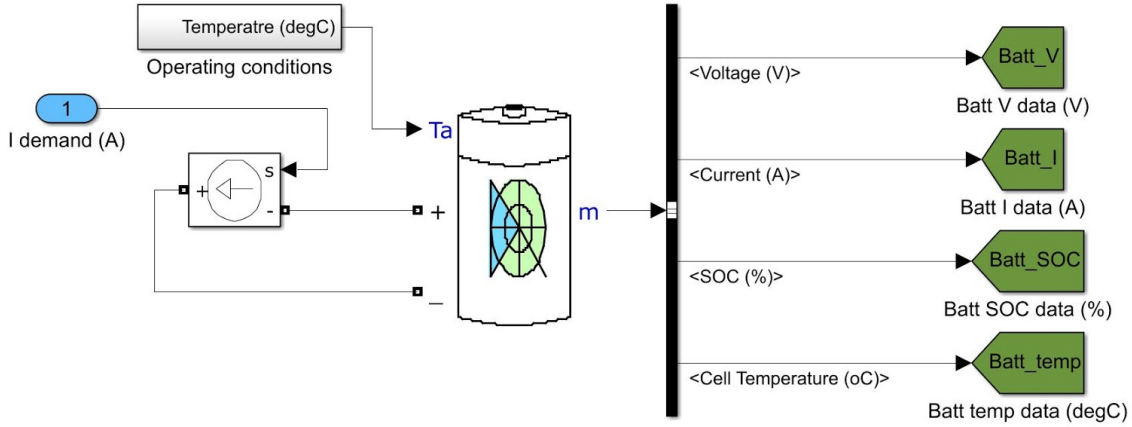

Figure 8.3: Matlab® Simulink battery submodel showing the integration of atmospheric temperature variation and output links

8.2.2 Submodel Integration

Power electronics interlink between fuel cell and battery assumed to be an dual ideal diode powerpath controller, a form of parallel hybridisation [12]. This utilises the theory of natural balancing, where the higher voltage supply supplies the initial load. As the voltage of the primary supply (fuel cell) drops (polarisation curve) the voltage will balance with that of the secondary power source (battery). From this point, both the fuel cell and battery will supply the load (with equal and 'balanced' voltage). This link is represented by the red dashed line between the two bus bars of Figure 8.4.

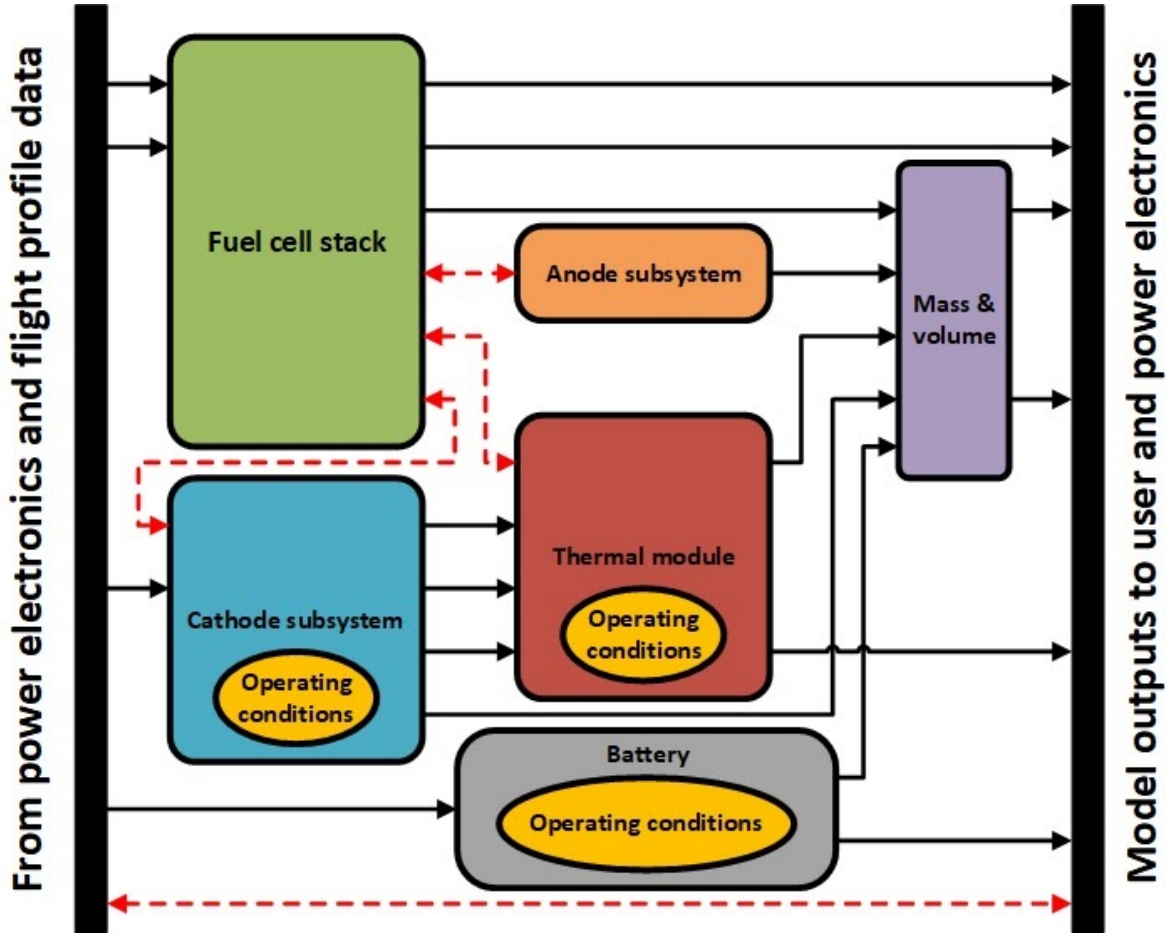

Figure 8.4: Simplified schematic for MATLAB® Simulink dynamic fuel cell system model. Fuel cell and battery assumed to be interlinked with a dual ideal diode powerpath controller.

The model schematic (Figure 8.4) also shows the dependence of each submodel on the other, represented by double-headed arrows. A key novel aspect of this model in comparison to others in the literature [13-23] is the deep integration of the dependence on ambient operating conditions. This is of vital importance for an fuel cell system integration into an aircraft designed to operate at elevated altitudes.

8.3 Model Calibration

A full cell equation (Equation 8.1) was derived in Chapter 4 by combining the effects of reactant concentration, pressure, temperature and validated irreversibilities on the temperature dependent reversible thermodynamic voltage [24-26]. Experimental data was obtained for both a PEMFC and DMFC for the purpose of calibrating the model.

$$V_c = \frac{\Delta\bar{g}}{zF} + \frac{RT}{zF} ln\left(\frac{\Pi c^M_{reactants}}{\Pi c^M_{products}}\right) + \frac{RT}{4F} ln\left(\frac{p_2}{p_1}\right) + \frac{\Delta\bar{s}_T}{zF}(T - T_0) - \\ - \frac{RT}{z\alpha F} ln\left(\frac{i + i_n}{i_0}\right) - i\Omega - xexp(yi) \quad (8.1)$$

Where:

c - Concentration of species in reaction (mol/dm^3)

F - Faraday constant (96,485 C/mol)

$\Delta\bar{g}$ - Absolute Gibbs free energy change (J/mol)

i - Current density (A/cm^2)

i_0 - Exchange current density (A/cm^2)

i_n - Internal current density (A/cm^2)

p_1 - Initial system pressure (Pa)

p_2 - Final system pressure (Pa)

R - Universal gas constant (8.314 J/molK)

$\Delta\bar{s}_T$ - Absolute entropy change at temperature “T” (J/mol.K)

T - Temperature (K)

T_0 - Reference temperature (25°C / 298.15 K)

V_c - Cell potential (V)

x - Mass transport loss empirical constant 1 (V)

y - Mass transport loss empirical constant 2 (cm^2/A)

z - Number of electrons transferred per mole of fuel

α - Charge transfer coefficient

Ω - Area specific resistance (Ωcm^2)

Literature derived [24-27] ranges were used as the starting point for the iterative determination of fit parameters for the full cell equation (Equation 8.1). These starting points were: $i_0 = 3.0E^{-6} \rightarrow 6.7E^{-5}\ A/cm^2$, $i_n = 0.003 \rightarrow 0.02\ A/cm^2$, $\Omega = 0.01 \rightarrow 0.245\ \Omega cm^2$, $x = 3.0E^{-4}\ V$, $y = 9.45\ cm^2/A$, and $\alpha = 0 \rightarrow 1$. It is expected that the values required to fit the experimental data may differ slightly from these ranges due in part to the age of available references and the experimental nature of the tested fuel cells.

8.3.1 Experimental Method

Membrane Electrode Assemblies (MEA) were manufactured for both operation with hydrogen (PEMFC) and methanol (DMFC). A MEA typically consists of seven layers: two Gas Diffusion Layers (GDL), two MicroPorous Layers (MPL), two catalyst layers and a membrane. The arrangement of these layers in a complete MEA is shown in Figure 8.5. It is also common practice to refer to the sub-assembly of GDL, MPL and catalyst layer as a Gas Diffusion Electrode (GDE).

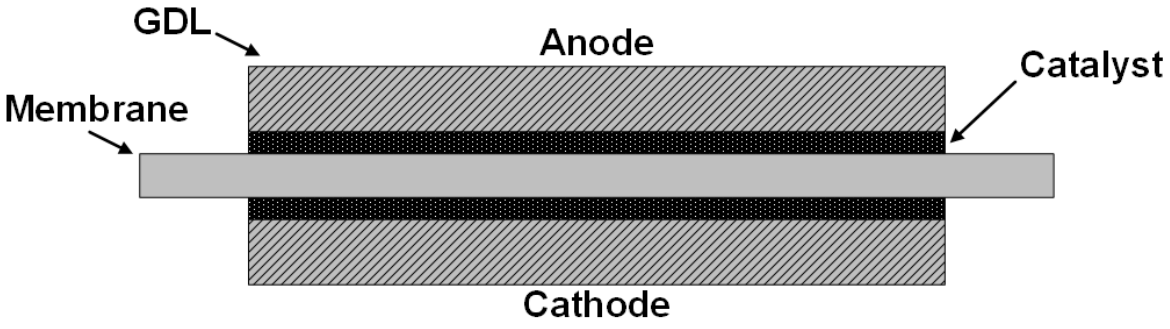

Figure 8.5: Arrangement of a seven-layer membrane electrode assembly

A commercially available GDE with a catalyst loading of 0.50 mg/cm^2 60 wt% Pt/C (FuelCellStore.com 1610004) was used for both the anode and cathode of the PEMFC MEA and the cathode of the DMFC MEA. A novel platinum nickel titanate ($Pt.NiTiO_3$) catalyst was used on the DMFC anode GDE as it has been shown to offer increased performance over traditional catalysts [28-30]. Due to its novel nature, the DMFC anode GDE had to be manufactured in-house.

Anode catalyst ink was prepared using Pt.$NiTiO_3$/C novel catalyst powder, manufactured by PSG College of Technology, India as per Thiagarajan et al. using the wet chemical method [29] with a mass breakdown of 40% platinum, 20% $NiTiO_3$ and 40% carbon support, water based D1021 Nafion™ ionomer dispersion and IsoPropyl Alcohol (IPA) ≥99.7% solvent.

Appropriate quantities of each of the catalyst ink constituents were measured out and added to a mixing vial in the following order to avoid ignition of the platinum-based catalyst powder: Catalyst powder → Ionomer → Solvent. The ratios by wet mass used were: 3% catalyst powder, 40% ionomer and 57% IPA as per [28].

The ink mixture was swirled by hand after the addition of the ionomer and before the addition of the IPA to ensure that all the catalyst powder had been wetted. The mixture was then sonicated for 120 mins using a camlab camSonix C175 digital ultrasound bath at a frequency of 37 kHz to ensure a colloidal suspension. The sonication time was based on a literature survey where two hours was found to be typical [31,32].

Catalyst ink was coated onto CeTech carbon cloth with microporous layer GDL (FuelCellStore.com 1595000) using a bar coater at a speed of 1.0 mm/s. To ensure consistency, the coating was carried out in a single layer. Single layer coating is also beneficial from a mass manufacturing perspective as it helps to simplify the process. The coating Wet-Layer Thickness (WLT) defined by Equation 8.2, was used to obtain different platinum loadings, where ρ_{Pt} is the area density of platinum, commonly given in mg/cm^2.

$$WLT = \frac{Target\ Pt\ loading \times Ink\ volume}{m_{Pt}} \qquad (8.2)$$

Where:

m_{Pt} - Mass of platinum (kg)

WLT - Wet-Layer Thickness (m)

An oversized section of GDL was used so that the uniformly coated middle section could be used in the assembly of the MEA. After coating, the catalyst ink mixture was allowed to dry for a minimum of 24 hours in ambient conditions. Once fully dry, the correct active area of GDE was cut out and its mass measured. The difference in area density between the coated GDE, ρ_{GDE} and uncoated GDL, ρ_{GDL} was used to find the final platinum loading using Equation 8.3.

$$Actual\ Pt\ loading\ =\ (\rho_{GDE}\ -\ \rho_{GDL}) \times \%Pt_{dry\ mix} \tag{8.3}$$

Where:

$\%Pt_{dry\ mix}$ - Percentage of platinum in the dry mix

ρ_{GDE} - Area density of GDE (kg/m^2)

ρ_{GDL} - Area density of GDL (kg/m^2)

Where the percentage of platinum in the dry mix, $\%Pt_{dry\ mix}$ was defined by Equation 8.4.

$$\%Pt_{dry\ mix}\ = \frac{\left(m_{catalyst\ powder} \times \%Pt_{catalyst\ powder}\right)}{m_{catalyst\ powder} + \left(vol_{ionomer} \times \rho_{dry\ ionomer}\right)} \tag{8.4}$$

Where:

$\%Pt_{catalyst\ powder}$ - Percentage of platinum in the catalyst powder

$\%Pt_{dry\ mix}$ - Percentage of platinum in the dry mix

$m_{catalyst\ powder}$ - Mass of catalyst powder (kg)

$vol_{ionomer}$ - Volume of ionomer solution (m^3)

$\rho_{dry\ ionomer}$ - Equivalent dry density of ionomer (kg/m^3)

The mass of the dry ionomer was calculated using the "equivalent dry density", $\rho_{dry\ ionomer}$ which was deduced experimentally. This was done by pipetting a known quantity of Nafion™ D1021 Dispersion liquid into a vial, allowing it to dry naturally and weighing the remaining solid. Other masses and volumes were measured experimentally.

Final assembly of both the PEMFC and DMFC MEAs was carried out by hot-pressing under a pressure of 5.0 MPa at a temperature of 120 °C for 180 s with a sheet of Nafion™ 117 membrane (FuelCellStore.com 591239). Technical specifications for both MEAs are summarised in Table 8.1.

Table 8.1: Technical specifications for PEMFC and DMFC MEAs used in experimental work

	PEMFC MEA	**DMFC MEA**
Active area	25 cm^2	25 cm^2
Anode catalyst and loading	0.5 mg/cm^2 Pt/C	0.66 mg/cm^2 $Pt.NiTiO_3$/C
Cathode catalyst and loading	0.5 mg/cm^2 Pt/C	0.5 mg/cm^2 Pt/C
Membrane	Nafion™ 117	Nafion™ 117
Gas diffusion layer	Carbon cloth with MPL	Carbon cloth with MPL

Each MEA was installed in the Scribner single cell test fixture and clamping bolts torqued to 3 Nm as per the manufacturer's instructions. Fuel cell temperature was controlled using cartridge heaters in each end plate and a closed loop temperature controlled. Electrically the fuel cell was connected to a TDI RBL488 50-150-800 electronic load, controlled digitally by in-house National Instruments™ LabVIEW software. Pressure and temperature signals were logged throughout the tests using the same LabVIEW software.

Oxidant, in the form of air, was fed via a heater/dehumidifier unit at 500 ml/min. The heater/humidifier was set such that the cathode inlet was at 60 °C and 100% Relative Humidity (RH). Hydrogen fuel was fed to the anode (when configured as a PEMFC) also via the heater/humidifier unit as was also fed at 60 °C and 100% RH. When configured as a DMFC, a dilute solution of deionised water and methanol with a molar concentration of 1.0 mol/dm^3 was fed at 3 ml/min via a MASTERflex L/S Series peristaltic pump. A schematic representation of the experimental test setup has been included as Figure 8.6 for reference.

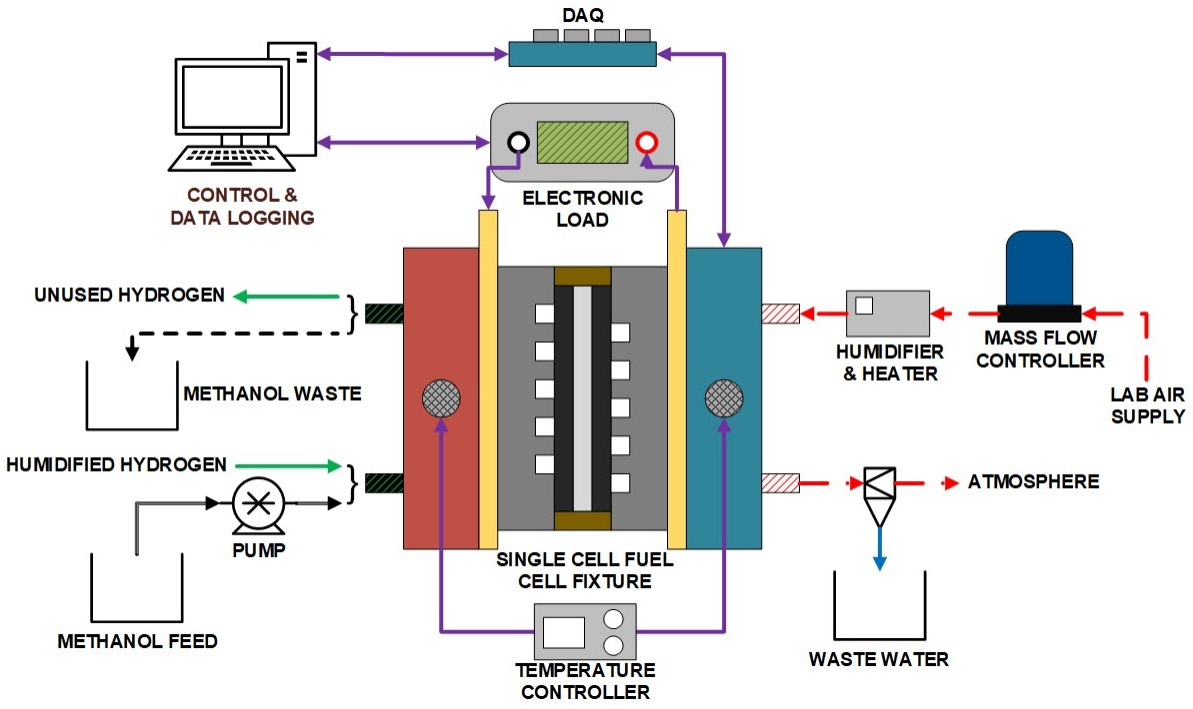

Figure 8.6: Dual-purpose experimental test setup. Anode configuration can be quickly modified to allow either PEMFC testing with hydrogen or DMFC testing with methanol.

Conditioning, sometimes "activation" is considered to play an important role in achieving the best fuel cell performance possible [33]. The protocol outlined in Table 8.2 was used to activate the MEAs in this study. Each current setpoint, $\%\ of\ I_{max}$ used was a certain percentage of the maximum possible current for that MEA.

Table 8.2: Membrane electrode assembly conditioning protocol

Step	**Setpoint (≈% of I_{max})**	**Time (s)**	**Step**	**Setpoint (≈% of I_{max})**	**Time (s)**
1	0%	300	**6**	40%	300
2	7.5%	300	**7**	50%	300
3	15%	300	**8**	75%	300
4	20%	300	**9**	0%	300
5	30%	300	**10**	Polarisation (OCV – 0.1V)	

Fuel cell performance was evaluated by holding Open Circuit Voltage (OCV) for 300 s to check stability and then running extended polarisations with a scan rate of 0.5 mV/s to ensure a pseudo steady-state response.

8.3.2 PEMFC

Empirical parameters used to fit the full cell equation to experimental data for the PEMFC operating at a temperature of 70 °C with pure hydrogen as a fuel and humidified air as the oxidant were: $i_0 = 1.0E^{-5}\ A/cm^2$, $i_n = 0.07\ A/cm^2$, $\Omega = 0.35\ \Omega cm^2$, $x = 3.5E^{-4}\ V$, $y = 11\ cm^2/A$ and the charge transfer coefficient, α was set at 0.29. Figure 8.7 contains the experimental and theoretical polarisation curves. The Root-Mean-Square Error (RMSE) for the calibrated PEMFC model was 9.52 mV. Full details on the calculation of RMSE and its advantages over other error measurements was discussed in Chapter 4.

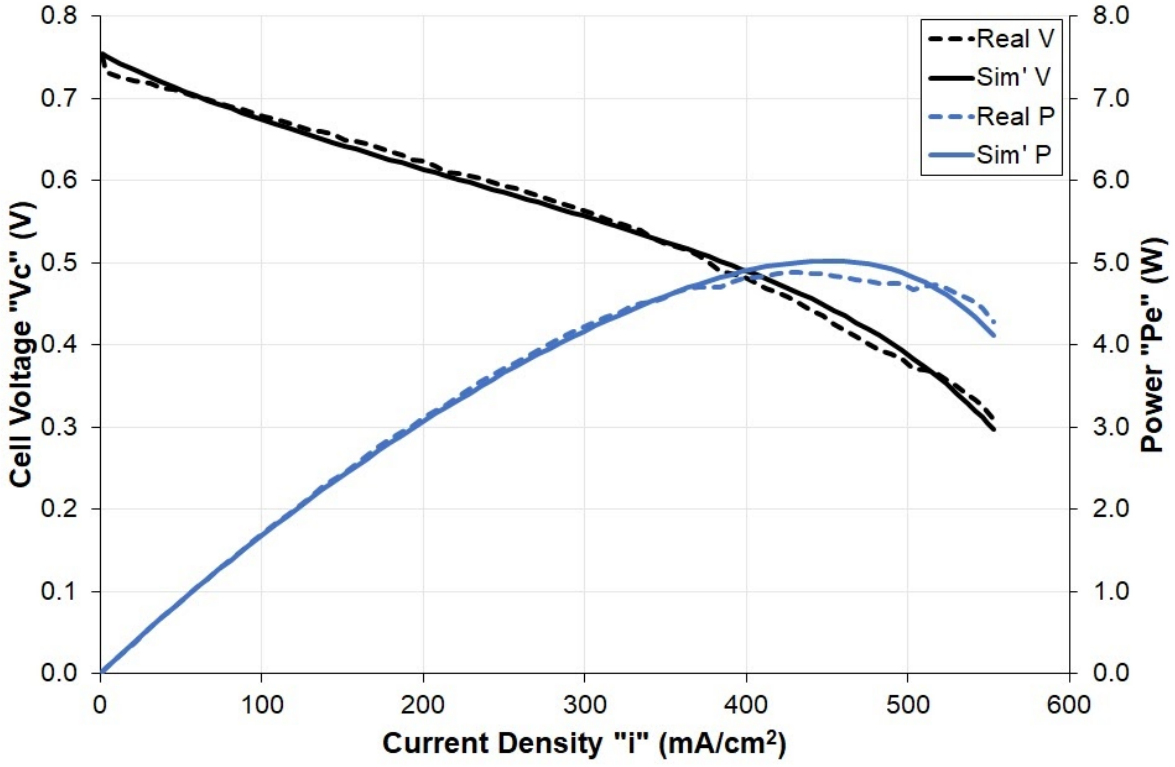

Figure 8.7: Comparison of theoretical and experimental results for a single cell 25cm² polymer electrolyte membrane fuel cell

8.3.3 DMFC

Experimental conditions were varied slightly for the DMFC MEA compared with the PEMFC. An operating temperature of 60 °C was used due to rig limitations. Humidified air was used as the oxidant and dilute methanol as the fuel. A theoretical polarisation curve was fitted to the experimental data using the following empirical parameters: $i_0 = 2.5E^{-7}\ A/cm^2$, $i_n = 0.0045\ A/cm^2$, $\Omega = 0.37\ \Omega cm^2$, $x = 1.5E^{-4}\ V$, $y = 28.9\ cm^2/A$ and $\alpha = 0.074$. Figure 8.8 contains the corresponding experimental and theoretical polarisation curves. The RMSE for the calibrated DMFC model was calculated to be 8.72 mV.

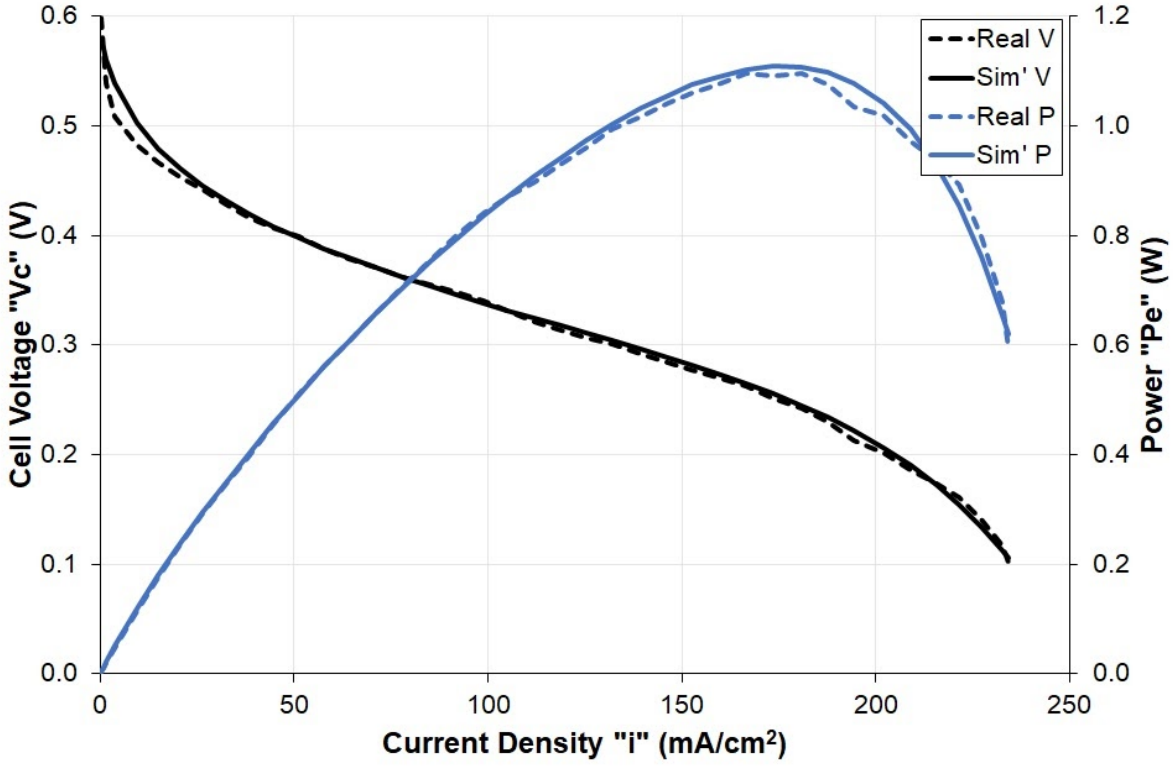

Figure 8.8: Comparison of theoretical and experimental results for a single cell 25cm² direct methanol fuel cell

8.4 Modelling Evaluation

Two aircraft were chosen as modelling case studies to test the outputs of the dynamic MATLAB® Simulink model. The first was the Skywalker X8, a small (< 7 kg) remotely operated model Unmanned Aerial Vehicle (UAV). This aircraft was chosen as a good representation of the type of small surveillance UAV used by the military which would greatly benefit from the increased range afforded by a fuel cell system over the more traditional battery only systems.

A General Atomics MQ-1 Predator was chosen as the second aircraft case study. This represents a typical military multi-role Medium-Altitude Long-Endurance (MALE) UAV. Additionally, this type of UAV could see many civilian applications, performing roles such as search and rescue and aerial mapping.

8.4.1 Aircraft 1 - Skywalker X8

A Skywalker X8 remotely piloted model UAV (Figure 8.9) was chosen as a case study to represent the growing market of small, easily transportable surveillance aircraft. This type of aircraft has multiple uses, both in the civilian and military sectors. Table 8.3 contains the standard specification for this type of aircraft. The power requirements, both propulsive and electrical were generated using the previously developed aircraft sizing tool [1].

Figure 8.9: Skywalker X8 model unmanned aerial vehicle

Table 8.3: Technical specifications of Skywalker X8 [1,34,35]

MTOW	4.5 kg	**Endurance**	25 min
Weight empty	2.0 kg	**Propulsive power requirement [1]**	250 W
Wingspan	2.1 m	**Electrical power requirement [1]**	250 W
Altitude	200 m (650 ft)	**Total power requirement**	500 W

Based on the research set out in this Thesis, the relatively low power requirement (< 500 W) and the very low payload availability for the fuel cell system (≈ 2 kg) of this aircraft an air-cooled open-cathode PEMFC system with onboard CGH_2 storage is recommended. This system will be intended to be the primary power provider to both the propulsion and auxiliary systems onboard the aircraft.

The key question to answer as part of this modelling case study is the degree of benefit which may be obtained by hybridising the fuel cell with a battery as a secondary power source. In the case of a fuel cell / battery hybrid system, the fuel cell will be sized such that it can deliver the cruise power demand. In this case the cruise power demand is 20 A at 12 VDC.

Technical data contained within Table 8.3 will be used for the physical sizing of the power system. An experimentally derived flight profile, Figure 8.10 will be used to ascertain the dynamic response of the fuel cell system. The discrepancy in current demand during straight and level flight was due to changing wind conditions during the data collection flight.

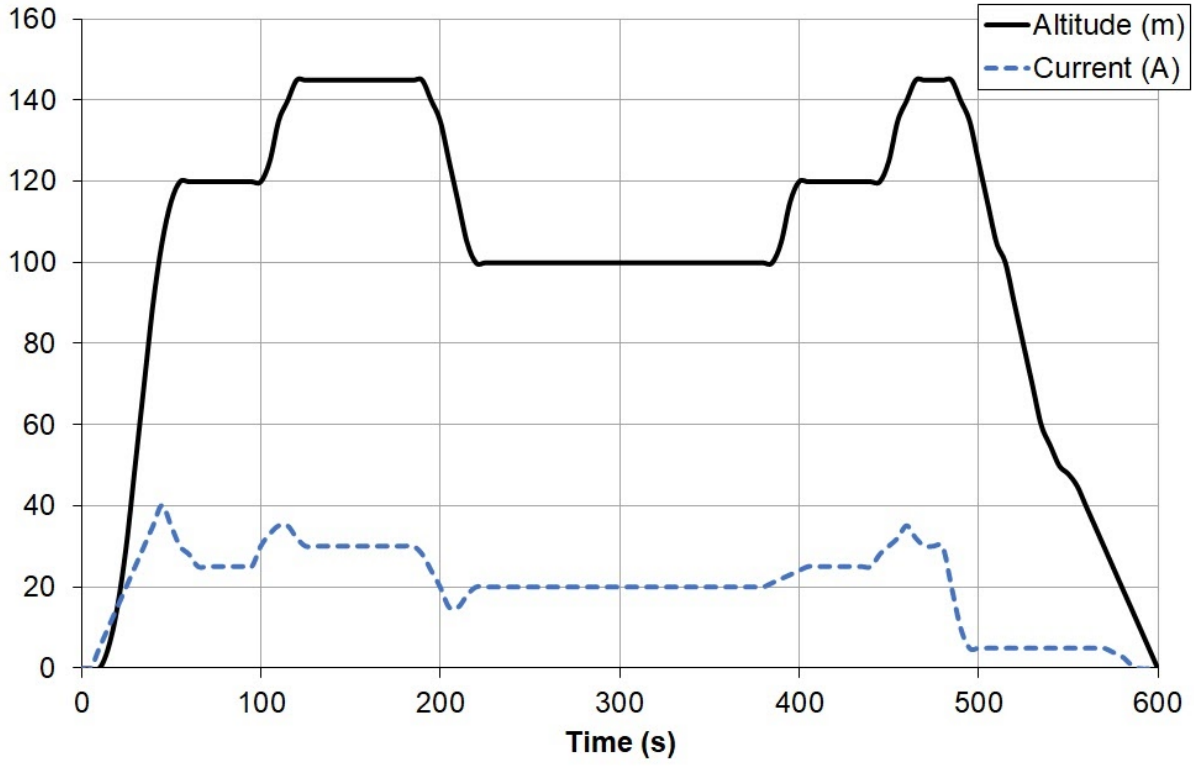

Figure 8.10: Experimentally derived flight and current demand profile for Skywalker X8 operating at a nominal voltage of 12 VDC

8.4.2 Aircraft 2 - MQ-1 Predator

The General Atomics MQ-1 Predator, Figure 8.11 is a multi-role medium-range long-endurance unmanned aerial vehicle. Its primary role is as an aerial reconnaissance aircraft for American military organisations however, it can also be fitted with offensive weaponry in order to undertake combat operations.

Figure 8.11: General Atomics MQ-1 Predator (image in Public Domain) [36]

As standard, propulsion is provided courtesy of a Rotax 914F piston engine rated at 75 kW with a 3 kW starter generator used for both starting the engine and providing electrical power to aircraft systems. The power requirements predicted by the sizing model are shown to be in good agreement with the original aircraft specification. These have been included with other key technical specifications for the aircraft in Table 8.4.

Table 8.4: Technical specifications of General Atomics MQ-1 Predator [1,37]

MTOW	1,020 kg	**Endurance**	20 hrs
Weight empty	512 kg	**Propulsive power requirement [1]**	76 kW
Wingspan	16.8 m	**Electrical power requirement [1]**	2 kW
Altitude	7,620 m (25,000 ft)	**Total power requirement**	78 kW

Of the 508 kg difference between the MTOW and weight empty, 204 kg is designated as payload leaving 304 kg for fuel and fluids. When the mass of the engine, 78 kg and necessary ancillaries are added to the equation the total mass available for the fuel cell system (without changing the range or payload) is ≈ 400 kg.

A high power density fuel cell system would be essential as it will be the primary motive power provider and it will need to physically fit inside the constraints of the small diameter highly aerodynamic high aspect ratio airframe. Combined with the power requirement of nearly 80 kW, a liquid-cooled PEMFC will be used. Based on the endurance and altitude requirements of the aircraft, hydrogen fuel will be stored in liquid form and oxidant will be supplied via an air-breathing design utilising a compressor as the additional parasitic current draw was preferential due to the associated mass and volume benefits.

This modelling evaluation exercise is primarily concerned with determining the suitability of a fuel cell system based on power, mass and volume metrics. However, additional mission benefits are associated with replacing the internal combustion powertrain with a hydrogen fuel cell system. The lower exhaust temperature of the fuel cell system will reduce the thermal signature of the aircraft in flight. Additionally, the silent, vibration free operation of the fuel cell will lower the acoustic emissions. Both of these fuel cell characteristics aid the low observability desirable during reconnaissance missions.

A theoretical flight profile for the MQ-1 Predator carrying out a reconnaissance mission with an eight hour loiter period over the target area is shown in Figure 8.12. The current demand is based on generating the total power requirements at a nominal voltage of 300 V.

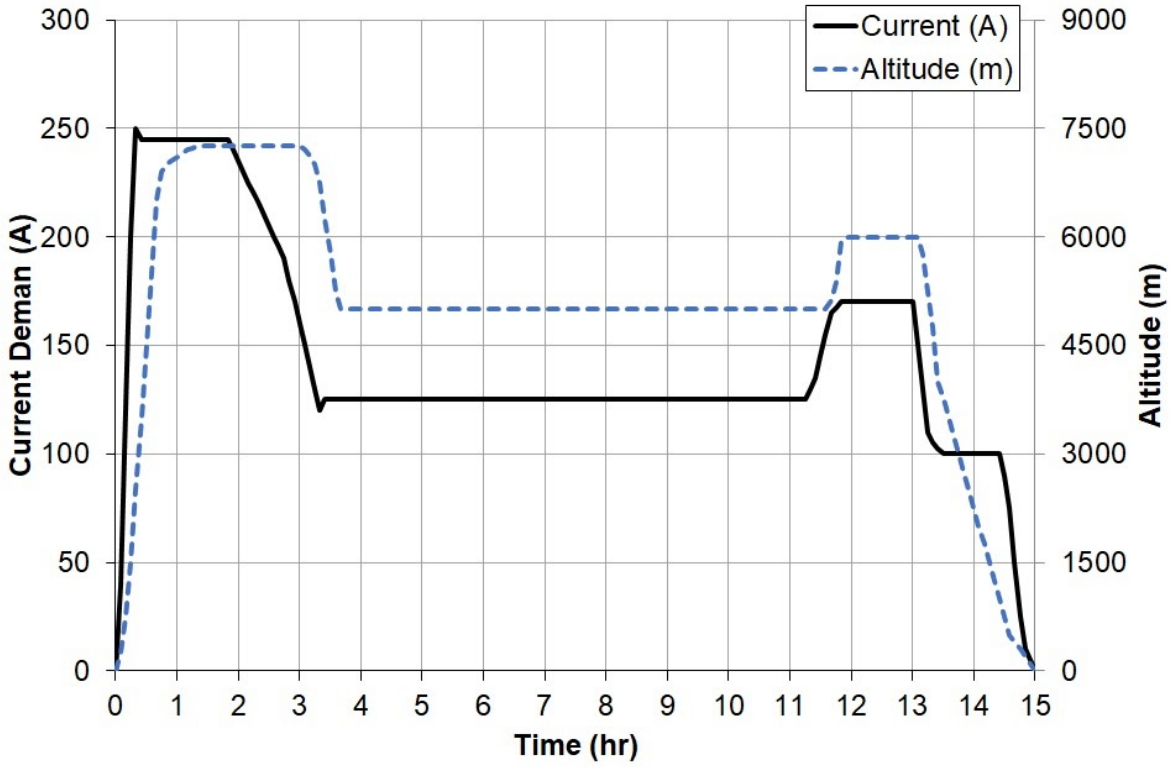

Figure 8.12: Theoretical profile for a typical reconnaissance flight for MQ-1 Predator

8.5 Results

8.5.1 Aircraft 1 - Skywalker X8

Based on the operating regime, Figure 8.12 and the physical constraints of the Skywalker X8 an air-cooled air-breathing PEMFC fuelled by gaseous hydrogen compressed to 700 barg was modelled as the solitary motive power provider for the aircraft. To allow the delivery of the full flight profile the fuel cell was based on the validated polarisation curve and an active area, A of 80 cm^2. Due to the highly modular nature of hydrogen fuel cells, this active area would likely be split into two separate stacks, each with 40 cm^2 to allow better packaging.

Each key subsystem of the complete fuel cell system was sized by the model to meet the requirements of the aircraft and mission profile. As the fuel cell is a closed cathode, air-cooled design, gravimetric and volumetric power densities of 2,000 W/kg and 600 W/l were used to assign dimensionality to the fuel cell stack. These numbers were obtained from commercial data as discussed in Chapter 7. A nominal mass of 0.125 kg and volume of 0.30 l was assigned to the air-cooling thermal management system which comprises a cooling fan and cowl.

For the fuel system, the mass of hydrogen required for the total flight was calculated using the methodology outlined in Chapter 5. The relationships: $mass = 21.228u$ and $vol = 23.356u$ which describe the total storage system mass (kg) and volume (l) where "u" is the mass of hydrogen stored were used for subsystem sizing. Derivation of these relationships was detailed in Chapter 5.

Commercial compressor data was analysed in Chapter 6 to derive gravimetric and volumetric power efficiencies of 0.45 kW/kg and 0.39 kW/l respectively. Compressor power, calculated using Equation 6.3 and the desired flow rate for the fuel cell (Equation 6.2) was used to feed these relationships..

A summary of their masses and volumes is included in Table 8.5. Note, that as the mission length is extended, only the mass and volume of the hydrogen storage and delivery subsystem will change due to the nature of the other systems' design.

Table 8.5: Subsystem sizing for a fuel cell only system suitable for a Skywalker X8

Subsystem	**Mass (kg)**	**Volume (litres)**
Fuel cell stack	0.299	0.996
Hydrogen storage and delivery	0.164	0.181
Oxidant delivery	0.125	0.144
Thermal management	0.125	0.30
Totals:	0.713	1.62

The model's dynamic response to a single 10 minute flight profile for the sized fuel cell system can be seen in Figure 8.13. Here the fuel cell delivers the full current demand according to the flight profile. As the altitude of the aircraft remained fairly low (< 200 m), there are very few altitude effects on the performance of the fuel cell system. The fuel cell upper temperature limit was set to 80 °C to enable the highest performance with minimal parastics from the thermal management system.

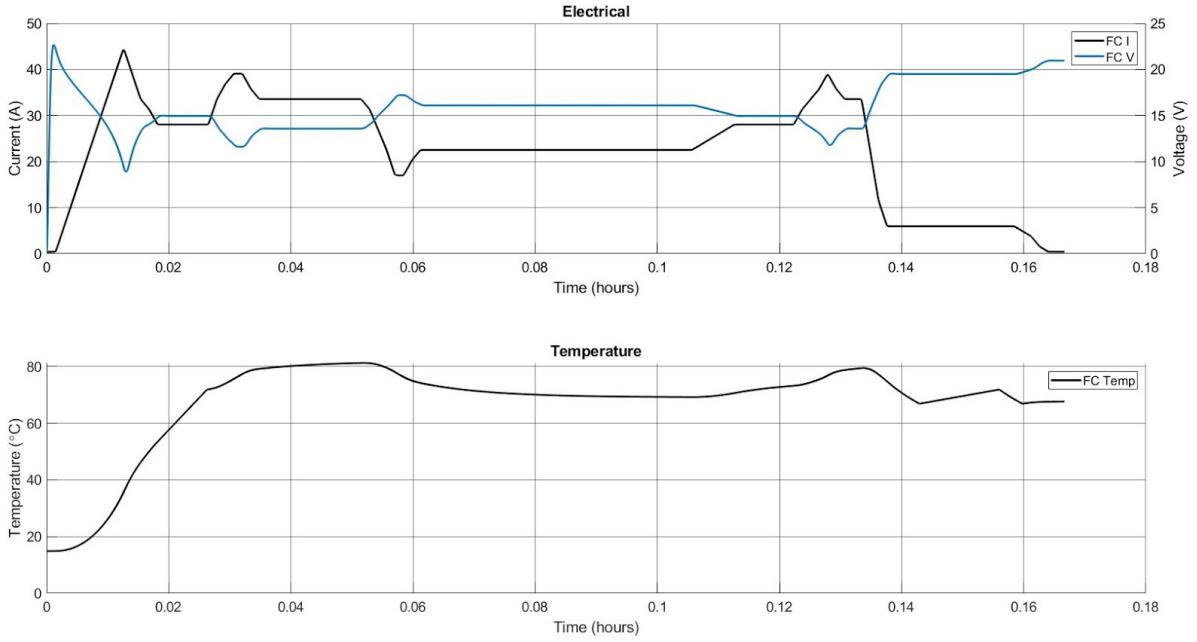

Figure 8.13: Model output in response to a single Skywalker X8 flight profile for an air-cooled air-breathing polymer electrolyte fuel cell system with 700 barg compressed hydrogen storage

It was hypothesised that the overall system energy density and specific energy could be improved by hybridising the fuel cell system with a secondary energy source in the form of a $LiCoO_2$ battery. A hybrid system of systems was designed such that the fuel cell was capable of providing the full cruise power demand (20 A at 12 V). The battery component was sized such that at the end of the flight profile, the State of Charge (SOC) was at least 30 % and that the maximum current draw was never more than 10 times the capacity. These steps were taken to prolong battery life.

An active area of 45 cm^2 and minimum cell voltage of 0.5 V were selected for the fuel cell stack subsystem. For a single 10 minute flight profile a 2.0 Ah capacity battery was required in order to ensure the discharge rate was below the predefined limit. The dynamic response of the hybrid system model, Figure 8.14 shows how the fuel cell supplies the baseline load up to 20 A. This baseline load was determined by the current the fuel cell could provide at a minimum cell voltage of 0.5 V. Peak loads above this threshold are provided by the battery.

Due to the lower power output of the fuel cell required for this design case, an upper temperature limit of 70 °C was used. This could be achieved using the same size thermal management system used for the higher output case. To achieve a core temperature of 70 °C and airflow rate of 0.03 kg/s was applied when the core temperature exceeded 72 °C, this airflow was then removed when the core temperature reduced to 67 °C.

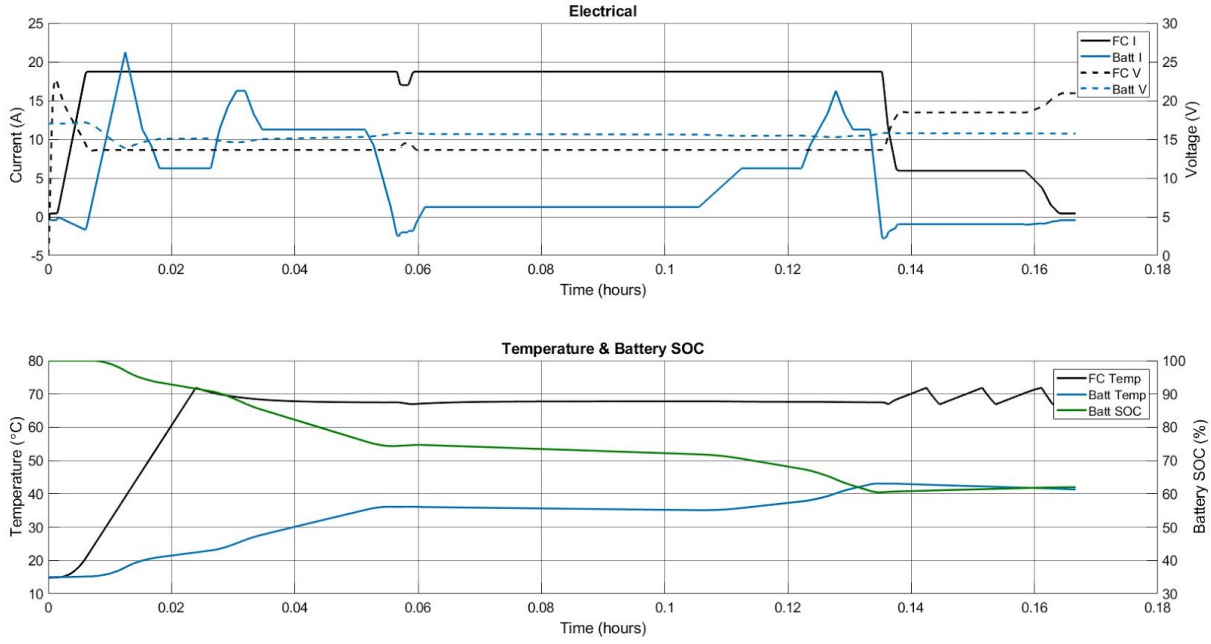

Figure 8.14: Model output in response to a single Skywalker X8 flight profile for an air-cooled air-breathing polymer electrolyte fuel cell with 700 barg compressed hydrogen storage hybridised with a 2.0 Ah $LiCoO_2$ 4-cell battery

Table 8.6 contains a sizing breakdown of the system of systems for a hybrid architecture Skywalker X8 for a single flight profile. In comparison to the similar analysis carried out on the fuel cell only system it has been shown that the hybrid system has a lower overall mass and requires less physical space within the airframe.

Table 8.6: Subsystem sizing for a fuel cell / battery hybrid system suitable for a Skywalker X8

Subsystem	**Mass (kg)**	**Volume (litres)**
Fuel cell stack	0.157	0.522
Hydrogen storage and delivery	0.114	0.125
Oxidant delivery	0.062	0.072
Thermal management	0.125	0.30
Battery	0.180	0.115
Totals:	0.64	1.13

To compare the overall performance of both the fuel cell only and fuel cell / battery hybrid system, they were compared to the battery only system traditionally used in this type of aircraft. This analysis involved re-sizing the three different power system architectures for each flight condition. Flight conditions were defined as multiples of the original giving a flight time range of 10 mins to 100 mins. Analysis results are contained within Figure 8.15.

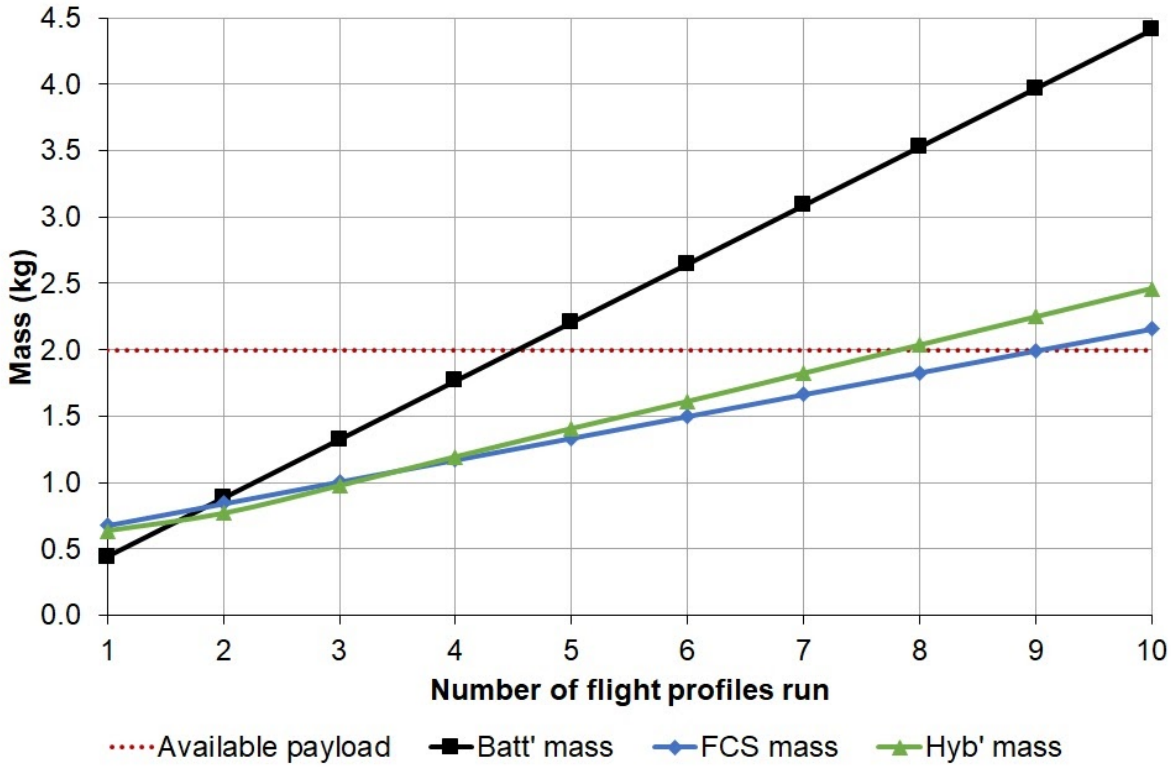

Figure 8.15: Variation of total system mass with increasing flight time for battery only, fuel cell only and fuel cell / battery hybrid systems for the Skywalker X8

System analysis results clearly show that for all but the very shortest flight times a power system containing a fuel cell is always lighter than using a battery system alone. If the power delivery system is designed for the maximum payload of the aircraft then a fuel cell only system can provide twice the energy of a battery only system.

When considering the volume occupied by the three different systems and how it evolves through increased flight time the battery only system shows, in Figure 8.16 clear advantages over the other alternatives. However, given that the available volume within the Skywalker X8 airframe is 9.55 litres [35], even a fuel cell only system can be comfortably integrated when only considering the space occupied.

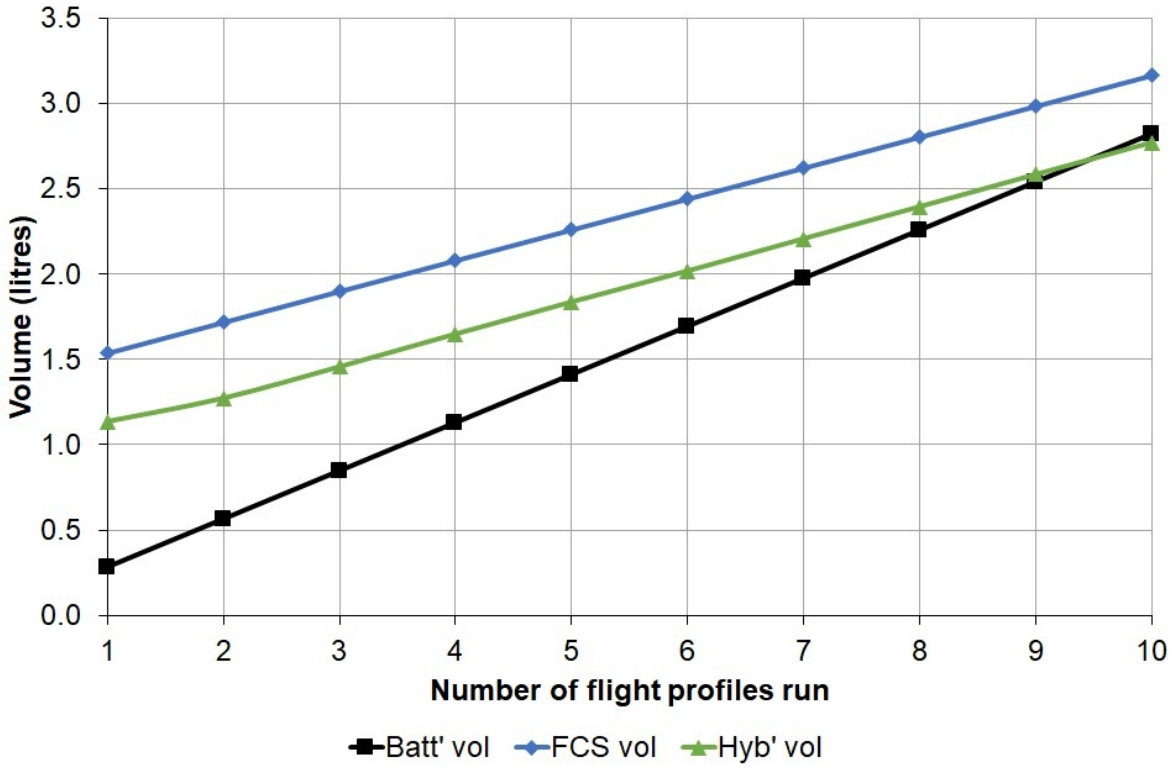

Figure 8.16: Variation of total system volume with increasing flight time for battery only, fuel cell only and fuel cell / battery hybrid systems for the Skywalker X8

The modelling results for the Skywalker X8 have shown that the benefits of fuel cell and hybrid systems over more conventional battery architecture are generally related to gravimetric efficiency. This means that for the same take-off weight, the aircraft can fly further using a fuel cell system than a battery.

8.5.2 Aircraft 2 - MQ-1 Predator

A fuel cell system was sized to suit the Predator UAV and dynamically modelled based on the flight profile and operating assumptions described in Section 8.4.2. The system was configured assuming no change in the mission requirements of the aircraft. A liquid-cooled polymer electrolyte membrane fuel cell with an active area of 700 cm^2 and 745 cells was required to meet the peak power requirement without requiring a secondary power source. Liquid hydrogen fuel was used along with an air compressor. Mass and volume breakdowns of the main fuel cell system components are given in Table 8.7.

Table 8.7: Subsystem sizing for a fuel cell system suitable for a MQ-1 Predator

Subsystem	**Mass (kg)**	**Volume (litres)**
Fuel cell stack (+ thermal management)	242	605
Hydrogen storage and delivery	414	1,455
Oxidant delivery	24	28
Totals:	680	2088

The initial mass allowance given for the fuel cell system in modelling study outline was 400 kg of which 340 kg was set aside for fuel. Unfortunately, at current technology levels based on the sizing results in Table 8.7, it is not possible to directly replace the fossil fuelled power plant with a hydrogen fuelled fuel cell system whilst maintaining the same mission endurance.

When considering the two main components in terms of mass, the fuel cell and the hydrogen storage, improvements can be made to both when compared to the legacy equipment being replaced. In this particular instance, the fuel cell stack and thermal management has more than double the mass of the Rotax 914F piston engine and associated starter / generator. Whereas the original mass allowance for fuel and fluids is around 75% of that required for the hydrogen storage system.

Using currently available technology, it would be possible to physically integrate a fuel cell system, like the one designed into a MQ-1 Predator by sacrificing the endurance requirement and therefore the amount of hydrogen storage required. Alternatively, improvements in the specific power of the fuel cell stack above 500 W/kg would also better suit the adoption of fuel cells in these types of aircraft. Although specific powers above this threshold have been readily reported in the literature, the numbers used in this work are based on real commercially available data [38-41]. A doubling of the current figure to 1,000 W/kg would allow the design architecture to fit within the original 400 kg limit.

Dynamic response plots for the modelled fuel cell to the input altitude and current profiles are shown in Figure 8.17. The upper plot shows the overall current and voltage response of the complete fuel cell system. As the boundary of the model is the fuel cell system, no details are given on how power is utilised however, it can be assumed that a majority is for propulsion.

The lower section of Figure 8.17 shows the breakdown of the three main current demands on the fuel cell stack, aircraft demand, air compressor demand and coolant pump demand and the total response of the fuel cell. It is shown that although the air compressor is a relatively high parasitic power drain on the overall system, the coolant pump is not. This is because of the low coolant flow rate when compared to air flow rate.

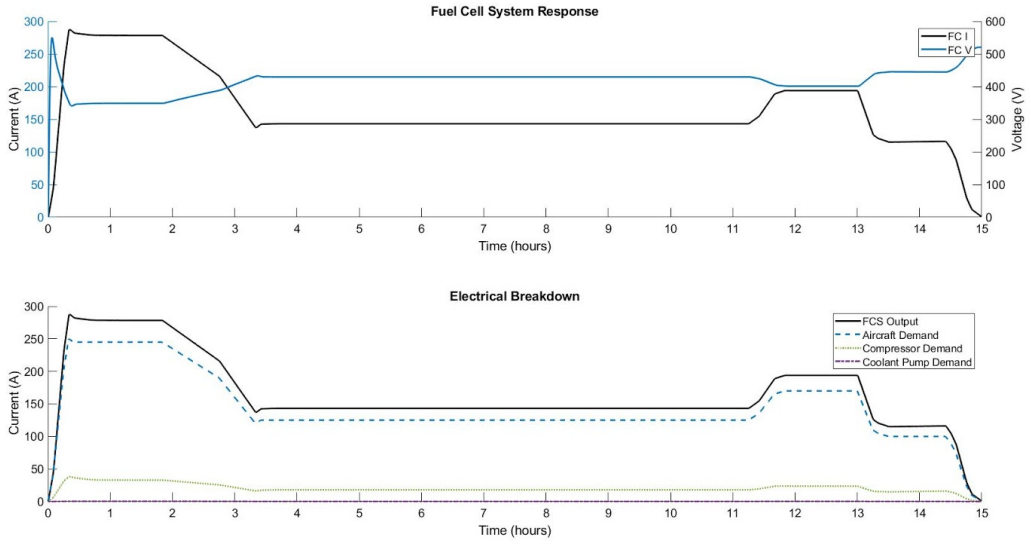

Figure 8.17: Model output response to flight profile for MQ-1 Predator described in Figure 8.12. Specific breakdown of key current demands and outputs given in lower half.

8.6 Additional Model Scope

The models and associated strategy discussed throughout this work were used to carry out a sensitivity study on potential future improvements in fuel cell stack and hydrogen storage technologies. The sensitivity study looked at three technology level scenarios. The first was using the specific power/energies and power/energy densities of today's levels which have been discussed already in this Thesis. The second level assumes the specific stack power is increased from 500 W/kg to 2.0 kW/kg and stack power density from 200 W/l to 2.5 kW/l for all fuel cell types. Thirdly, an increase in the specific energy and energy density of hydrogen storage by one third was considered. The aim of this study was to determine which area of fuel cell system design is most limiting in terms of overall system mass and volume. Five aircraft of varying types were used in the sensitivity study. Summaries of key design and mission criteria are contained in Table 8.8.

Table 8.8: Summary of aircraft used in sensitivity study

Aircraft	**MTOW (kg)**	**Flight Time (hrs)**	**Fuel Cell Power (kW)**	**Fuel Cell Cooling**	**Fuel Cell Use**
Skywalker X8	4.5	0.6	0.5	Air	Propulsion
MQ-1 Predator	1,020	15	80	Liquid	Propulsion
Medium Business	3,000	4	840	Liquid	Propulsion
Narrow Body Passenger	73,500	6	135	Liquid	APU
Wide Body Passenger	500,000	10	466	Liquid	APU

Results for the sensitivity study carried out on the aircraft in Table 8.8 using the technology levels discussed earlier are shown in Figure 8.18. The results suggest that for aircraft using fuel cells for propulsion, increasing specific power and power density of the fuel cell stack lead to significant reductions in system mass and volume. The level of system improvement appears to be fairly insensitive to flight duration. However, system configurations with higher power fuel cell stacks such as the MQ-1 Predator see significant mass and volume savings with the increase in fuel cell technology level.

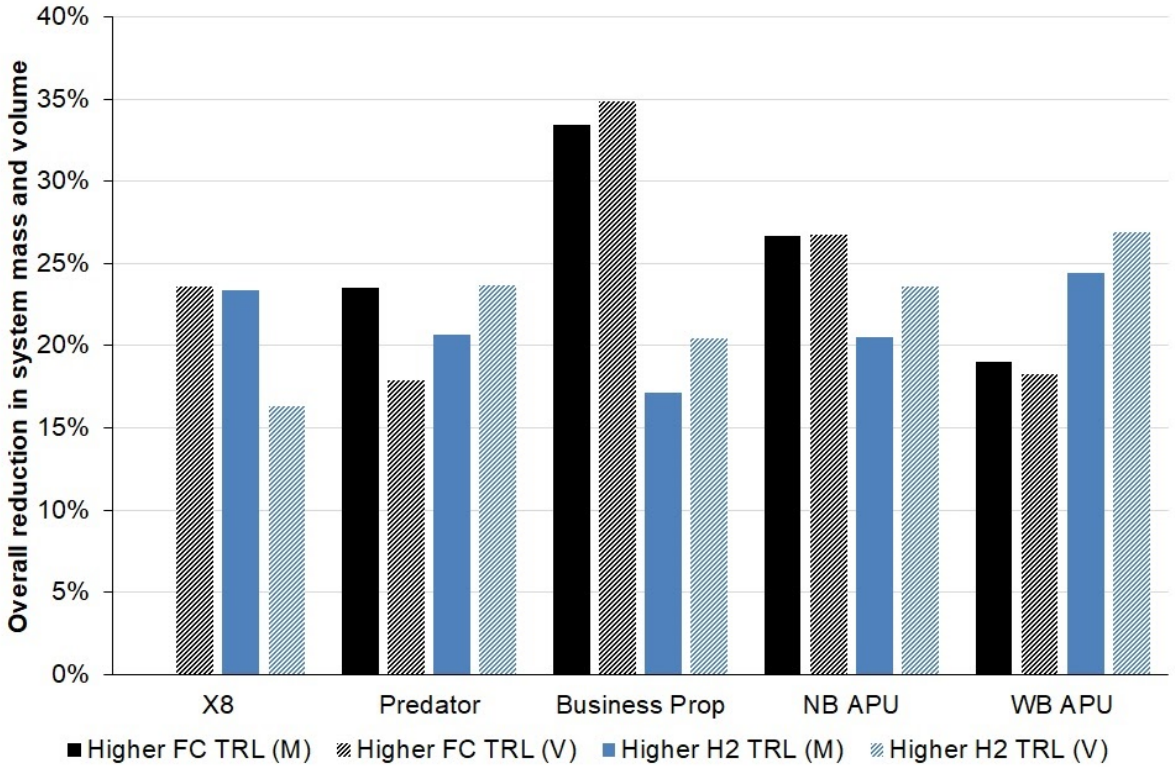

Figure 8.18: Percentage change in overall system mass and volume for doubling fuel cell sizing efficiency and doubling hydrogen storage efficiency

For systems using fuel cells as an Auxiliary Power Unit (APU), the system mass and volume savings are directly related to the relative fuel cell power and mission duration. For the Narrow Body (NB) aircraft which had a smaller fuel cell and shorter mission duration it is shown that the savings are less than the Wide Body (WB) aircraft with a more powerful fuel cell and longer range.

The results also show that for a majority of aircraft, which have relatively short flight profiles, the overall system mass and volume is currently more sensitive to changes in the fuel cell stack power density and specific power than it is the storage efficiency of hydrogen.

8.7 Summary

For both case studies used in this modelling evaluation the high specific power requirements favoured the use of a hydrogen fed polymer electrolyte fuel cell systems. It has been shown previously in this work that the specific energy of a liquid fed direct methanol fuel cell can be higher than an equivalent PEMFC fed by gaseous hydrogen. However, for the high-endurance case (MQ-1 Predator) hydrogen was stored in its liquid state therefore, providing the highest specific energy of any system described in this work.

Development of a dynamic fuel cell model which accounts for environmental conditions associated with aeronautical applications has been shown. The developed model was used in conjunction with a simple battery model from the Simulink library and an experimentally derived flight profile to investigate the consequences of hybridisation on a Skywalker X8 model aircraft

Three system architectures were derived for testing: fuel cell only, battery only and fuel cell/battery hybrid. The flight profile, which is representative of a 10 minute flight, was used as the input to each modelled architecture. Using the battery only model as a baseline, the gravimetric and volumetric performance of the fuel cell and hybrid systems were shown for a varying number of looped flight profiles.

The modelling work has shown that substantial mass and volume savings can be made by replacing a battery system with a fuel cell system. Hybridising a fuel cell with a battery has also been shown to offer improvements in volumetric efficiency when compared to a solely fuel cell system. However, these observations are dependent on mission flight time. For shorter flights a fully battery system is suggested to be more suitable. Whereas, for longer flights a fuel cell or hybrid system gives the advantages of lower mass and volume.

For a medium-range long-endurance unmanned aerial vehicle such as the MQ-1 Predator the use of hydrogen fed liquid-cooled fuel cells has been shown to be feasible using current technology levels if the mission requirements of the aircraft are modified. It was also clear from the results that hydrogen storage is not the only limiting factor. Commercialisation of higher specific power liquid-cooled fuel cell systems in the region of 1,000 W/kg would allow full integration with no performance limitations.

Reference was made to the additional mission benefits associated with replacing the internal combustion powertrain with a hydrogen fuel cell system in particular, the reduced acoustic and thermal emissions from the aircraft. Both of which aid the low observability desirable during reconnaissance missions.

A study was carried out using the model to determine the sensitivity of overall system mass and volume to changes in the technology level of fuel cell stacks and hydrogen storage. The results across a range of aircraft types and mission durations show that based on the current liquid-cooled fuel cell technology levels presented in this work, the overall system is more sensitive to improvements in this than it is in hydrogen storage efficiency.

8.8 References

[1] Thirkell A, Chen R, Harrington I. A Fuel Cell System Sizing Tool Based on Current Production Aircraft. Fort Worth, Texas: SAE International; 2017. https://doi.org/10.4271/2017-01-2135.

[2] Luxfer Gas Cylinders. G-Stor H2 Fuel Cell Vehicle Cylinders. Prod Specific Sheet 2018.https://www.luxfercylinders.com/img/luxfer/products_upload/G-Stor-H2-spec-sheet-2018.pdf (accessed July 12, 2020).

[3] Luxfer Gas Cylinders. G-StorTM H2 hydrogen-storage cylinders 2015. http://www.luxfercylinders.com/products/alternative-fuel/gstorh2 (accessed January 5, 2016).

[4] Mahytec. Hydrogen storage solutions 2016. http://www.mahytec.com/en/our-solutions/ (accessed January 5, 2017).

[5] Villalonga S, Nony F, Magnier C, Yvernes JL, Thomas C, Delmas B, et al. Composite 700 Bar-Vessel for on-Board Compressed Gaseous Hydrogen Storage. ICCM17, Edinburgh: International Committee on COmposite Materials; 2009.

[6] lapesa. Horizontal Cryogenic Tanks n.d.:10–1. www.lapesa.es/descargar.php?f=/sites/default/files/documentos/gnli_1011.pdf (accessed January 5, 2017).

[7] Pressol HDPE Jerrycan. RS-Online Datasheet 2010:2010. https://docs.rs-online.com/ab22/0900766b80e0f376.pdf (accessed July 31, 2020).

[8] Chao CH, Shieh JJ. A new control strategy for hybrid fuel cell-battery power systems with improved efficiency. Int J Hydrogen Energy 2012;37:13141–6. https://doi.org/10.1016/j.ijhydene.2012.03.143.

[9] MathWorks. Battery - Generic battery model. Co Website 2008. https://www.mathworks.com/help/physmod/sps/powersys/ref/battery.html (accessed October 24, 2020).

[10] Boeing. Batteries and Advance Airplanes 2013. http://787updates.newairplane.com/787-Electrical-Systems/Batteries-and-Advanced-Airplanes (accessed March 7, 2018).

[11] Battery University. BU-205: Types of Lithium-ion 2019. https://batteryuniversity.com/learn/article/types_of_lithium_ion#:~:text=Li-cobalt excels on high,power%2C safety and life span.&text=150–200Wh%2Fkg.,provide up to 240Wh%2Fkg.&text=0.7–1C%2C charges to 4.20,cells)%3B 3h charge typical. (accessed November 21, 2020).

[12] Howroyd S, Chen R. Powerpath controller for fuel cell & battery hybridisation. Int J Hydrogen Energy 2016;41:4229–38. https://doi.org/10.1016/j.ijhydene.2016.01.038.

[13] Fathabadi H. Combining a proton exchange membrane fuel cell (PEMFC) stack with a Li-ion battery to supply the power needs of a hybrid electric vehicle. Renew Energy 2019;130:714–24. https://doi.org/10.1016/j.renene.2018.06.104.

[14] Xun Q, Liu Y, Holmberg E. A Comparative Study of Fuel Cell Electric Vehicles Hybridization with Battery or Supercapacitor. Int. Symp. Power Electron. Electr. Drives, Autom. Motion, IEEE; 2018, p. 389–94. https://doi.org/10.1109/SPEEDAM.2018.8445386.

[15] Kadyk T, Winnefeld C, Hanke-Rauschenbach R, Krewer U. Analysis and Design of Fuel Cell Systems for Aviation. Energies 2018;11:375. https://doi.org/10.3390/en11020375.

[16] Oh TH. Conceptual design of small unmanned aerial vehicle with proton exchange membrane fuel cell system for long endurance mission. Energy Convers Manag 2018;176:349–56. https://doi.org/10.1016/j.enconman.2018.09.036.

[17] Saleh IM, Ali R, Zhang H. Environmental Impact of High Altitudes on the Operation of PEM Fuel Cell Based UAS. Energy Power Eng 2018;10:87–105. https://doi.org/10.4236/epe.2018.103007.

[18] Donateo T, Ficarella A, Spedicato L, Arista A, Ferraro M. A new approach to calculating endurance in electric flight and comparing fuel cells and batteries. Appl Energy 2017;187:807–19. https://doi.org/10.1016/j.apenergy.2016.11.100.

[19] Gong A, Palmer JL, Brian G, Harvey JR, Verstraete D. Performance of a hybrid, fuel-cell-based power system during simulated small unmanned aircraft missions. Int J Hydrogen Energy 2016;41:11418–26. https://doi.org/10.1016/j.ijhydene.2016.04.044.

[20] Mobariz KN, Youssef AM, Abdel-Rahman M. Long endurance hybrid fuel cell-battery powered UAV. World J Model Simul 2015;11:69–80.

[21] Pratt JW, Klebanoff LE, Munoz-Ramos K, Akhil AA, Curgus DB, Schenkman BL. Proton exchange membrane fuel cells for electrical power generation on-board commercial airplanes. Appl Energy 2013;101:776–96. https://doi.org/10.1016/j.apenergy.2012.08.003.

[22] Nishizawa A, Kallo J, Garrot O, Weiss-Ungethüm J. Fuel cell and Li-ion battery direct hybridization system for aircraft applications. J Power Sources 2013;222:294–300. https://doi.org/10.1016/jjpowsour.2012.09.011.

[23] Outeiro MT, Chibante R, Carvalho AS, de Almeida AT. A parameter optimized model of a Proton Exchange Membrane fuel cell including temperature effects. J Power Sources 2008;185:952–60. https://doi.org/10.1016/j.jpowsour.2008.08.019.

[24] Larminie J, Dicks A. Fuel Cell Systems Explained. 2nd ed. John Wiley & Sons; 2003. https://doi.org/10.1016/S0378-7753(00)00571-1.

[25] O'Hayre R, Cha S-W, Colella W, Prinz FB. Fuel cell fundamentals. 3rd ed. John Wiley & Sons; 2016.

[26] Barbir F. PEM Fuel Cells Theory and Practice. Elsevier Academic Press; 2005.

[27] Kumaresan T, Velumani T, Chandran M, Palaniswamy K, Thirkell A, Fly A, et al. Effect of Nafion loading and the novel flow field designs on Innovative anode electrocatalyst for improved DMFCs performance. Mater Lett 2020;276. https://doi.org/10.1016/j.matlet.2020.128222.

[28] Thiagarajan V, Manoharan R, Karthikeyan P, Nikhila E, Hernández-Ramírez A, Rodriguez-Varela FJ. Pt nanoparticles supported on NiTiO 3 /C as electrocatalyst towards high performance Methanol Oxidation Reaction. Int J Hydrogen Energy 2017;42:9795–805. https://doi.org/10.1016/j.ijhydene.2017.01.017.

[29] Thiagarajan V, Karthikeyan P, Thanarajan K, Neelakrishnan S, Manoharan R, Chen R, et al. Experimental investigation on DMFCs using reduced noble metal loading with NiTiO3 as supportive material to enhance cell performances. Int J Hydrogen Energy 2019;44:13415–23. https://doi.org/10.1016/j.ijhydene.2019.03.244.

[30] Su K, Yao X, Sui S, Wei Z, Zhang J, Du S. Ionomer content effects on the electrocatalyst layer with in-situ grown Pt nanowires in PEMFCs. Int J Hydrogen Energy 2014;39:3219–25. https://doi.org/10.1016/j.ijhydene.2013.12.117.

[31] Ngo TT, Yu TL, Lin HL. Influence of the composition of isopropyl alcohol/water mixture solvents in catalyst ink solutions on proton exchange membrane fuel cell

performance. J Power Sources 2013;225:293–303. https://doi.org/10.1016/j.jpowsour.2012.10.055.

[32] Inoue M, Iwasaki T, Sayama K, Umeda M. Effect of conditioning method on direct methanol fuel cell performance. J Power Sources 2010;195:5986–9. https://doi.org/10.1016/j.jpowsour.2009.11.015.

[33] skywalkermodel.com. Skywalker X8 Technical Data 2015. http://skywalkermodel.com/en/76.html (accessed October 25, 2020).

[34] Airelectronics. X8 Flying Wing 2021. https://www.airelectronics.es/products/x8_brochure.pdf (accessed May 9, 2021).

[35] Pratt L. MQ-1 Predator, armed with AGM-114 Hellfire missiles. Wikimedia Commons 2008. https://upload.wikimedia.org/wikipedia/commons/c/c7/MQ-1_Predator%2C_armed_with_AGM-114_Hellfire_missiles.jpg (accessed October 24, 2020).

[36] Streetly M, editor. Jane's all the world's aircraft: unmanned 2015-2016. IHS; 2015.

[37] Ballard Power Systems Inc. FCvelocity-9SSL 2011. http://ballard.com/files/PDF/Material_Handling/9SSL.pdf (accessed August 5, 2016).

[38] Ballard Power Systems Inc. FCveloCity-HD 2016. http://ballard.com/files/PDF/Bus/FCvelocity_HD_Family_of_Products_Low_Res.pdf (accessed August 5, 2016).

[39] Hydrogenics. HyPM-XR power modules 2016. http://www.hydrogenics.com/wp-content/uploads/HyPM-XR-Brochure.pdf (accessed August 5, 2016).

[40] Hydrogenics. HyPM-HD power modules 2016. http://www.hydrogenics.com/wp-content/uploads/HyPM-HD-Brochure.pdf (accessed August 5, 2016).

Chapter 9 Conclusions

In response to the increased demand for aircraft electrification and growing interest in fuel cell technology, a comprehensive study has been carried out to assess the suitability of fuel cells for a range of aircraft. The aim of this study was to explore the applicability and limitations of utilising fuel cells for the purpose of aircraft electrification with key objectives to:

1. Define a methodology to predict the electrical requirements, propulsive or auxiliary of any aircraft based on the highest level design information.
2. Critically analyse existing fuel cell technologies and down-select to two technologies. Assess the required balance of plant for the down-selected fuel cell technologies.
3. Produce and evaluate a dynamic fuel cell system sizing model to assist aircraft designers during an aircraft's preliminary design phase.

For Objective 1, fifteen aircraft categories were defined based on the aircrafts primary function and propulsion method. A model was then developed to predict the electrical generation capability and propulsive requirements. Validating the categorisation model against real aircraft data showed a good correlation between the real and modelled data. Generally, an error of less than 5% was obtained by the model. Certain instances, higher than this cut-off percentage arose when the model was based on a small dataset. The results for this section of work were published as a peer reviewed technical paper by SAE International in 2017 (Appendix 1, Entry 1).

Six commercially available fuel cell technologies were reviewed for use in aeronautical applications. Key decision factors for the down-selection of two technologies from the six were operating temperature and technology maturity. A low operating temperature of < 100 °C was seen as advantageous to minimising an aircraft thermal signature, a key requirement for most military aircraft. Combined with the high maturity level of the solid polymer membrane, hydrogen fed Polymer Electrolyte Membrane and liquid fed Direct Methanol Fuel Cells (PEMFC & DMFC) were selected as the best solutions for further study.

A system of systems design approach was adopted for each of the down-selected fuel cell technologies. This holistic approach was vital as both PEMFC and DMFC systems have distinct advantages over each other and the full system must always be considered to avoid bias. Primary fuel cell subsystems were grouped into four categories to aid comparison. Each of these categories also represents a distinct submodel of the complete dynamic model shown in Figure 8.4 in Chapter 8.

An electrochemical submodel, Equation 9.1, was developed which allowed maximum flexibility in that it could be used for either fuel cell technology and incorporated performance effects of altitude related flight conditions. It combined the effects of reactant concentration, pressure, temperature and validated irreversibilities on the temperature dependent reversible thermodynamic voltage. This full cell model is a combination of equations published separately in the literature.

$$V_c = \frac{\Delta \bar{g}_{HHV}}{zF} + \frac{RT}{zF} ln\left(\frac{\Pi c^M_{reactants}}{\Pi c^M_{products}}\right) + \frac{RT}{4F} ln\left(\frac{p_2}{p_1}\right) + \frac{\Delta \bar{s}_T}{zF}(T - T_0) - \\ - \frac{RT}{z\alpha F} ln\left(\frac{i + i_n}{i_0}\right) - i\Omega - xexp(yi) \qquad (9.1)$$

Fuel, or anode reactant, is the primary area of divergence between PEMFC and DMFC systems. Polymer electrolyte membrane fuel cells require a supply of purified hydrogen for optimum performance and durability. Although hydrogen has the highest specific energy of any fuel, it has one of the lowest energy densities. This means that its usefulness as a fuel is dependent on high pressure compression or complex liquefaction.

Direct methanol fuel cells on the other hand utilise methanol as a fuel without prior reformation. As a result, a potential 140 % rise in energy density can be realised. Additional benefits arise from the use of liquid methanol as a fuel as its storage and handling requirements are very similar to traditional hydrocarbon fuels. Meaning that integration into existing aircraft designs and adoption by both civilian and military aircraft operators will be seamless when compared to that of hydrogen. A summary of the key findings are shown in Figure 9.1.

Direct methanol fuel cells are known to have a much lower specific power than PEMFCs at today's technology levels. However, the advantages of the fuel type mean it will still be a suitable choice for auxiliary electrical generation onboard larger aircraft.

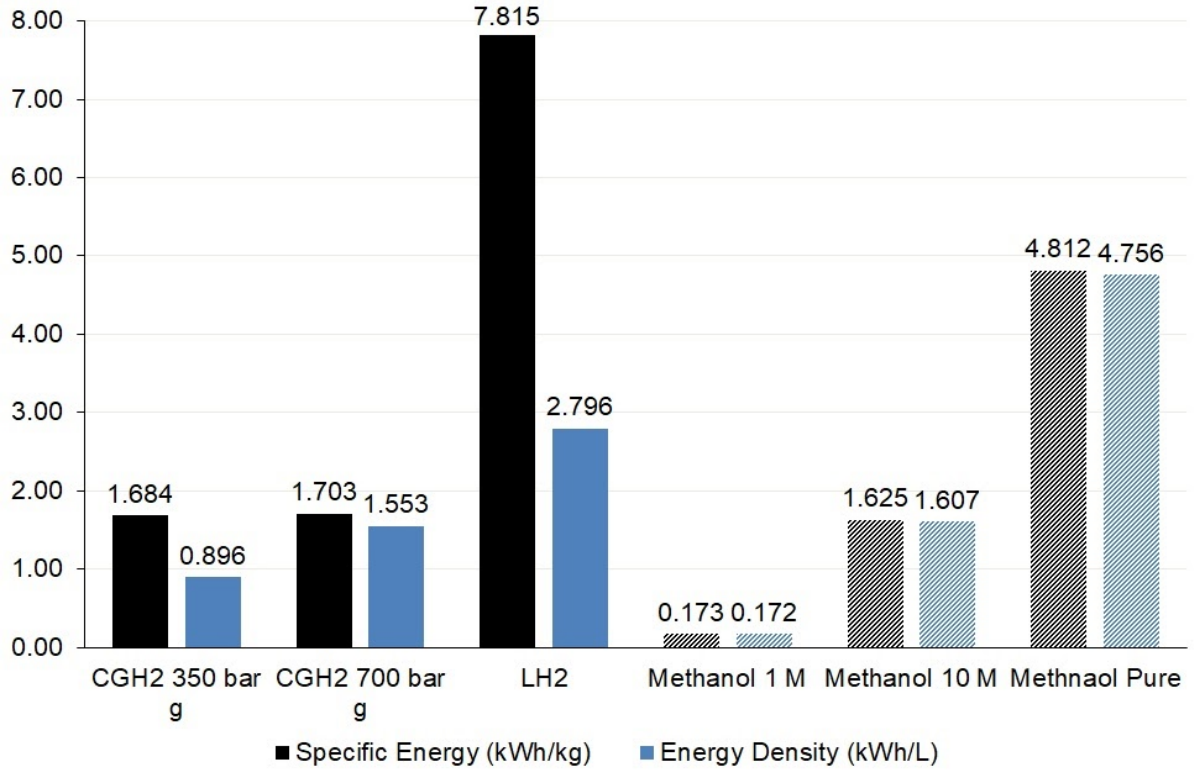

Figure 9.1: Summary of low-temperature fuel cell, aircraft suitable fuel storage technologies

Both down-selected fuel cell technologies have the same oxidant requirements at the cathode. Either an air-breathing or air-independent design can be implemented where an air-breathing solution would utilise some form of atmospheric air compression whereas, air-independent uses an onboard oxygen supply.

A hypothesis was made and proven that combining elements from both air-breathing and air-independent systems into a hybrid semi-independent system might lead to gravimetric and volumetric efficiency gains. The results yielded from this investigation showed that incorporating onboard oxygen storage in liquid form (air-independent) into an air-breathing design would lead to improvements in efficiency for high altitude mission profiles.

However, for missions at an altitude below 20,000 ft it was shown that an air-breathing system would be the most efficient from both a gravimetric and volumetric perspective. Ultimately, future advances in either compressor or oxygen storage technologies may alter these findings.

The final component of Objective 2 was the thermal management subsystem. When choosing the appropriate cooling strategy for a hydrogen fed fuel cell the primary consideration is the rate of heat generation. For lower power output fuel cells < 4 kW, air-cooling would be the preferred method due to its lower cost and simpler system design. Liquid-cooling has been identified as the preferred cooling methodology for higher power fuel cell systems due to higher technology maturity and more robust nature.

The current status and primary function of direct methanol fuel cell thermal management systems has been identified. In general, the literature does not suggest any active thermal management strategy for this fuel cell technology other than the initial fuel cell stack design and operating envelope. This is because, in most cases their temperature is self-regulating due to the liquid fuel supplied to the anode providing ample evaporative cooling. Therefore, the primary function of thermal management here is to enable reactant and water recycling.

As altitude is increased the ability of the ambient air to remove heat from the system is improved per unit mass. However, the heat transfer ability of the heat exchanger is reduced. Therefore, a larger heat transfer surface area is required to dissipate the same heat load at altitude compared to at sea level.

A dynamic fuel cell sizing model was created by combining the previously discussed submodels. It was calibrated using both a single-cell PEMFC and DMFC each with an active area of 25cm^2. The model was shown to be in excellent agreement with errors in the region of 5 % and predominantly in the difficult to simulate mass transport region.

Model evaluation was carried out using two case study aircraft, a Skywalker X8 and a General Atomics MQ-1 Predator. Results from the Skywalker X8 study showed the benefit of fuel cell systems over modern Li-ion batteries. A fuel cell system was shown to offer mass savings for all but the shortest flights with the potential for volumetric savings on longer flight times. The larger MQ-1 Predator case study showed that the integration of current commercially available fuel cell technology is feasible with small mission modifications. Commercialisation of higher specific power liquid-cooled fuel cell systems in the region of 1,000 W/kg would allow full integration with no performance limitations.

A study was carried out using the model to determine the sensitivity of overall system mass and volume to changes in the technology level of fuel cell stacks and hydrogen storage. The results across a range of aircraft types and mission durations show that based on the current liquid-cooled fuel cell technology levels presented in this work, the overall system is more sensitive to improvements in this than it is in hydrogen storage efficiency.

Future Work

An alternative compressor design which could be considered for use in this application is a turbo compressor. For this design, some of the energy contained within the cathode exhaust is used to help compress and feed oxygen to the inlet. This type of compressor has not been considered here as it would require a separate detailed study on the behaviour of turbine wheels in fully humidified and super-saturated flows.

More detailed sensitivity studies could be carried out using the model and associated aircraft database to test how changing system components can affect the overall mass and volume. If detail, in the form of increased component resolution was added into the model then these sensitivity studies could theoretically be run on anything down to the type of valve used to actuate the purge valve of a hydrogen fuel cell system.

Continual updating of the models parameters will allow it to better represent changing technology levels in all of the systems mentioned in this work. Of particular interest to the author would be an increase in research effort on the improving of direct methanol fuel cell power densities. Or alternative systems which would allow the utilisation of a liquid, methanol like fuel by a fuel cell system. This would have profound effects on the adoption of low and/or zero emission fuel cell technology by the aviation industry.

Reference List

Abdin Z, Webb CJ, Gray EMA. PEM fuel cell model and simulation in Matlab–Simulink based on physical parameters. Energy 2016;116:1131–44. https://doi.org/10.1016/j.energy.2016.10.033.

aeristech. Aeristech Electric Fuel Cell Compressor - AeFC805D n.d.:160. https://www.aeristech.co.uk/wp-content/uploads/2019/11/AeFC805D_DATASHEET_V1.1.0.pdf (accessed August 29, 2020).

aeristech. Aeristech Electric Fuel Cell Compressor - AeFC806E n.d.:120. https://www.aeristech.co.uk/wp-content/uploads/2019/11/AeFC806E_DATASHEET_V1.1.0.pdf (accessed August 29, 2020).

Agnolucci P. Economics and market prospects of portable fuel cells. Int J Hydrogen Energy 2007;32:4319–28. https://doi.org/10.1016/j.ijhydene.2007.03.042.

Aguiar P, Brett DJL, Brandon NP. Solid oxide fuel cell/gas turbine hybrid system analysis for high-altitude long-endurance unmanned aerial vehicles. Int J Hydrogen Energy 2008;33:7214–23. https://doi.org/10.1016/j.ijhydene.2008.09.012.

Ahluwalia RK, Peng JK. Dynamics of Cryogenic Hydrogen Storage in Insulated Pressure Vessels for Automotive Applications. Int J Hydrogen Energy 2008;33:4622–33. https://doi.org/10.1016/j.ijhydene.2008.05.090.

Air Liquide (Paris). Division Scientifique. Encyclopedie des gaz. Amsterdam, New York: Elsevier; 1976.

Airbus Training. A320-Electrical n.d.:38. http://www.smartcockpit.com/docs/A320-Electrical.pdf (accessed March 8, 2017).

Airbus Training. A330-Electrical n.d.:44, http://www.smartcockpit.com/docs/A330-Electrical.pdf (accessed March 8, 2017).

Airbus Training. A340-Electrical n.d.:46, http://www.smartcockpit.com/docs/FCOM_A340-Electrical.pdf (accessed March 8, 2017).

Airelectronics. X8 Flying Wing 2021. https://www.airelectronics.es/products/x8_brochure.pdf (accessed May 9, 2021).

Amirinejad M, Rowshanzamir S, Eikani MH. Effects of operating parameters on performance of a proton exchange membrane fuel cell. J Power Sources 2006;161:872–5. https://doi.org/10.1016/j.jpowsour.2006.04.144.

Amphlett JC, Mann RF, Peppley BA, Roberge PR, Rodrigues A. A model predicting transient responses of proton exchange membrane fuel cells. J Power Sources 1996;61:183–8. https://doi.org/10.1016/S0378-7753(96)02360-9.

Argyropoulos P, Scott K, Taama WM. One-dimensional thermal model for direct methanol fuel cell stacks. Part I. Model development. J Power Sources 1999;79:169–83. https://doi.org/10.1016/S0378-7753(99)00181-0.

Argyropoulos P, Scott K, Taama WM. One-dimensional thermal model for direct methanol fuel cell stacks. Part II. Model based parametric analysis and predicted temperature profiles. J Power Sources 1999;79:184–98. https://doi.org/10.1016/S0378-7753(99)00182-2.

Astronics. COREPOWER 1425 400 Amp Power Conversion Unit n.d. https://www.astronics.com/docs/default-source/aes-docs/tier-iii/data-sheets/1425-pcu.pdf?sfvrsn=6f2eab58_12 (accessed March 24, 2020).

Babac G, Sisman A, Cimen T. Two-Dimensional Thermal Analysis of Liquid Hydrogen Tank Insulation. Int J Hydrogen Energy 2009;34:6357–63. https://doi.org/10.1016/j.ijhydene.2009.05.052.

Bailey S. Development and Test of the Toroidal Intersecting Vane Management System 2005.

Ballard Power Systems Inc. FCgen-1020ACS 2015. http://ballard.com/files/PDF/Backup_Power/1020ACS_v2.pdf (accessed August 5, 2016).

Ballard Power Systems Inc. FCvelocity-9SSL 2011. http://ballard.com/files/PDF/Material_Handling/9SSL.pdf (accessed August 5, 2016).

Ballard Power Systems Inc. FCveloCity-HD 2016. http://ballard.com/files/PDF/Bus/FCvelocity_HD_Family_of_Products_Low_Res.pdf (accessed August 5, 2016).

Ballard. FCair TM UAV Power Systems 2018:2. https://www.ballard.com/docs/default-source/uav/uav-data-sheet-spc5106994.pdf?sfvrsn=2 (accessed September 12, 2020).

Barbir F, Görgün H. Electrochemical hydrogen pump for recirculation of hydrogen in a fuel cell stack. J Appl Electrochem 2007;37:359–65. https://doi.org/10.1007/s10800-006-9266-0.

Barbir F. PEM Fuel Cells Theory and Practice. Elsevier Academic Press; 2005.

Bard AJ, Faulkner L. Electrochemical methods: fundamentals and applications. 2nd ed. New York, London: Wiley-Interscience; 2000.

Barsi S, Kassemi M. Numerical and Experimental Comparisons of the Self-Pressurization Behavior of an LH2 Tank in Normal Gravity. Cryogenics (Guildf) 2008;48:122–9. https://doi.org/10.1016/j.cryogenics.2008.01.003.

Barthelemy H, Weber M, Barbier F. Hydrogen storage: Recent improvements and industrial perspectives. Int J Hydrogen Energy 2017;42:7254–62. https://doi.org/10.1016/j.ijhydene.2016.03.178.

Battery University. BU-205: Types of Lithium-ion 2019. https://batteryuniversity.com/learn/article/types_of_lithium_ion#:~:text=Li-cobalt excels on high,power%2C safety and life span.&text=150–200Wh%2Fkg.,provide up to 240Wh%2Fkg.&text=0.7–1C%2C charges to 4.20,cells)%3B 3h charge typical. (accessed November 21, 2020).

BOC. Hydrogen. Factsheet 2017. https://www.boconline.co.uk/en/legacy/attachment?files=tcm:t410-116758,tcm:410-116758,tcm:10-116758 (accessed June 29, 2020).

BOC. Oxygen Safety Data Sheet 2017. https://www.boconline.co.uk/en/images/10021701_tcm410-39599.pdf (accessed August 28, 2020).

Boccaletti C, Duni G, Fabbri G, Santini E. Simulation models of fuel cell systems. Proc ICEM, Electr Mach … 2006:1–6.

Boeing. Batteries and Advance Airplanes 2013. http://787updates.newairplane.com/787-Electrical-Systems/Batteries-and-Advanced-Airplanes (accessed March 7, 2018).

Boeing. F-15 Strike Eagle 2016, http://www.boeing.com/defense/f-15-strike-eagle/ (accessed March 8, 2017).

Bradley TH, Moffitt BA, Mavris DN, Parekh DE. Development and experimental characterization of a fuel cell powered aircraft. J Power Sources 2007;171:793–801. https://doi.org/10.1016/j.jpowsour.2007.06.215.

Braun-Unkhoff M, Riedel U. Alternative fuels in aviation. CEAS Aeronaut J 2014;6:83–93. https://doi.org/10.1007/s13272-014-0131-2.

Bresciani F, Rabissi C, Casalegno A, Zago M, Marchesi R. Experimental investigation on DMFC temporary degradation. Int J Hydrogen Energy 2014;39:21647–56. https://doi.org/10.1016/j.ijhydene.2014.09.072.

Cai W, Li S, Li C, Liang L, Xing W, Liu C. A model based thermal management of DMFC stack considering the double-phase flow in the anode. Chem Eng Sci 2013;93:110–23. https://doi.org/10.1016/j.ces.2013.01.040.

Cambridge Dictionary. performance. Cambridge Dict n.d. https://dictionary.cambridge.org/dictionary/english/performance (accessed April 23, 2020).

Chai T, Draxler RR. Root mean square error (RMSE) or mean absolute error (MAE)? -Arguments against avoiding RMSE in the literature. Geosci Model Dev 2014;7:1247–50. https://doi.org/10.5194/gmd-7-1247-2014.

Chao CH, Shieh JJ. A new control strategy for hybrid fuel cell-battery power systems with improved efficiency. Int J Hydrogen Energy 2012;37:13141–6. https://doi.org/10.1016/j.ijhydene.2012.03.143

Chao CH, Shieh JJ. A new control strategy for hybrid fuel cell-battery power systems with improved efficiency. Int J Hydrogen Energy 2012;37:13141–6. https://doi.org/10.1016/j.ijhydene.2012.03.143.

Chart Industries. CAIRE Liquid Oxygen Reservoirs 2017. http://www.chartindustries.com/Respiratory-Healthcare/Liquid-Oxygen-Systems/Reservoirs (accessed January 9, 2017).

Chen C-CC, Shaw D, Hsueh K-LL. Optimization of the electrodes humidification temperature and clamping pressure to achieve uniform current density in a commercial-sized proton exchange membrane fuel cell. Int J Hydrogen Energy 2017;42:3185–96. https://doi.org/10.1016/j.ijhydene.2016.09.178.

Cheng X, Shi Z, Glass N, Zhang L, Zhang J, Song D, et al. A review of PEM hydrogen fuel cell contamination: Impacts, mechanisms, and mitigation. J Power Sources 2007;165:739–56. https://doi.org/10.1016/j.jpowsour.2006.12.012.

Clark WW, Rifkin J. A green hydrogen economy. Energy Policy 2006;34:2630–9. https://doi.org/10.1016/j.enpol.2005.06.024.

Colleen Spiegel. PEM Fuel Cell: Modeling and Simulation using MATLAB. ElsevierAcademic Press; 2008. https://doi.org/10.1016/B978-012374259-9.50006-9.

Coppo M, Siegel NP, Spakovsky MR von. On the influence of temperature on PEM fuel cell operation. J Power Sources 2006;159:560–9. https://doi.org/10.1016/j.jpowsour.2005.09.069.

Cunningham JM, Hoffman MA, Friedman DJ. A Comparison of High-Pressure and Low-Pressure Operation of PEM Fuel Cell Systems. SAE Tech Pap Ser 2010;1. https://doi.org/10.4271/2001-01-0538.

Daggett D, Hadaller O, Hendricks R, Walther R. Alternative fuels and their potential impact on aviation. 25th Congr. Int. Counc. Aeronaut. Sci. 2006, vol. 5, Hamburg: 2006, p. 2888–97.

Dailey PL. Enforcement in Mobile Devices. Computer (Long Beach Calif) 2003;36:10–2. https://doi.org/10.1109/MC.2003.1244525.

Datasheet Micropumps. RS-Online Datasheet n.d. https://docs.rs-online.com/facd/0900766b815814c9.pdf (accessed July 31, 2020).

DeSilva U, Bunce RH, Claussen H. Novel gas turbine exhaust temperature measurement system. ASME Turbo Expo, vol. 4, 2013, p. 1–8. https://doi.org/10.1115/GT2013-95152.

Dincer I. Green methods for hydrogen production. Int J Hydrogen Energy 2012;37:1954–71. https://doi.org/10.1016/j.ijhydene.2011.03.173.

Dohle H, Mergel J, Stolten D. Heat and power management of a direct-methanol-fuel-cell (DMFC) system. J Power Sources 2002;111:268–82. https://doi.org/10.1016/s0140-6701(03)91859-5.

Donateo T, Ficarella A, Spedicato L, Arista A, Ferraro M. A new approach to calculating endurance in electric flight and comparing fuel cells and batteries. Appl Energy 2017;187:807–19. https://doi.org/10.1016/j.apenergy.2016.11.100.

Dougherty AJ, Bartholet ZT, Chumsky RJ, Delano KC, Huang X, Morris DK. The Liquidus Temperature for Methanol-Water Mixtures at High Pressure and Low Temperature, With Application to Titan. J Geophys Res Planets 2018;123:3080–7. https://doi.org/10.1029/2018JE005707.

Dudek M, Tomczyk P, Wygonik P, Korkosz M, Bogusz P, Lis B. Hybrid fuel cell - battery system as a main power unit for small unmanned aerial vehicles (UAV). Int J Electrochem Sci 2013;8:8442–63.

Durbin DJ, Malardier-Jugroot C. Review of hydrogen storage techniques for on board vehicle applications. Int J Hydrogen Energy 2013;38:14595–617. https://doi.org/10.1016/j.ijhydene.2013.07.058.

E4tech. The Fuel Cell Industry Review 2019. 2019.

Edwards PP, Kuznetsov VL, David WIF, Brandon NP. Hydrogen and fuel cells: Towards a sustainable energy future. Energy Policy 2008;36:4356–62. https://doi.org/10.1016/j.enpol.2008.09.036.

Ellamla HR, Staffell I, Bujlo P, Pollet BG, Pasupathi S. Current status of fuel cell based combined heat and power systems for residential sector. J Power Sources 2015;293:312–28. https://doi.org/10.1016/j.jpowsour.2015.05.050.

Endres GG, Gething MJ. Jane's aircraft recognition guide. 5th ed. Collins; 2007.

Engineering ToolBox. Ethylene Glycol Heat-Transfer Fluid 2003. https://www.engineeringtoolbox.com/ethylene-glycol-d_146.html (accessed September 19, 2020).

Epstein AH, O'Flarity SM. Considerations for reducing aviation's CO2 with aircraft electric propulsion. J Propuls Power 2019;35:572–82. https://doi.org/10.2514/1.B37015.

Faghri A, Guo Z. Challenges and opportunities of thermal management issues related to fuel cell technology and modeling. Int J Heat Mass Transf 2005;48:3891–920. https://doi.org/10.1016/j.ijheatmasstransfer.2005.04.014.

Fathabadi H. Combining a proton exchange membrane fuel cell (PEMFC) stack with a Li-ion battery to supply the power needs of a hybrid electric vehicle. Renew Energy 2019;130:714–24. https://doi.org/10.1016/j.renene.2018.06.104.

Feiner AS, McEvoy AJ. The Nernst Equation. J Chem Educ 1994;71:493–4. https://doi.org/10.1021/ed071p493.

Ferguson A, Ugursal VI. Fuel cell modelling for building cogeneration applications. J Power Sources 2004;137:30–42. https://doi.org/10.1016/j.jpowsour.2004.05.021.

FIBA Technologies. High Pressure Hydrogen Type II Vessel 2018. https://www.fibatech.com/2014/11/24/type-2-hydrogen-vessel/#:~:text=Our new%2C Type 2%2C hoop,on board hydrogen-fueled vehicles. (accessed July 12, 2020).

Flojet Triplex Series Pump Datasheet. RS-Online Datasheet 2013. https://docs.rs-online.com/a85f/0900766b8144b750.pdf (accessed July 31, 2020).

Fly A, Thring RH. A comparison of evaporative and liquid cooling methods for fuel cell vehicles. Int J Hydrogen Energy 2016;41:14217–29. https://doi.org/10.1016/j.ijhydene.2016.06.089.

Fly A, Thring RH. Temperature Regulation in an Evaporatively Cooled Proton Exchange Membrane Fuel Cell Stack. Int J Hydrogen Energy 2015;40:11976–82. https://doi.org/10.1016/j.ijhydene.2015.04.086.

Fly A. Thermal and water management of evaporatively cooled fuel cell vehicles. Loughborough University, 2015.

Garceau NM, Kim SY, Lim CM, Cho MJ, Kim KY, Baik JH. Performance test of a 6 L liquid hydrogen fuel tank for unmanned aerial vehicles 2015;101. https://doi.org/10.1088/1757-899X/101/1/012130.

General Atomics - Aeronautical Systems Inc. MQ-9 Reaper/Predator 2015:2, http://www.ga-asi.com/Websites/gaasi/images/products/aircraft_systems/pdf/MQ9 Reaper_Predator_B_032515.pdf (accessed March 8, 2017).

General Atomics - Aeronautical Systems Inc. Predator B 2015:2, http://www.ga-asi.com/Websites/gaasi/images/products/aircraft_systems/pdf/Predator_B021915.pdf (accessed March 8, 2017).

Gong A, Palmer JL, Brian G, Harvey JR, Verstraete D. Performance of a hybrid, fuel-cell-based power system during simulated small unmanned aircraft missions. Int J Hydrogen Energy 2016;41:11418–26. https://doi.org/10.1016/j.ijhydene.2016.04.044.

Green DW, Perry RH. Perry's Chemical Engineers' Handbook. 8th ed. London: McGraw-Hill; 2008.

Gunston B, Willis D, Munson K, Peacock L, Jackson P, Bushell S, editors. Jane's all the world's aircraft: development & production 2016-2017. IHS; 2016.

Gunston B, Willis D, Munson K, Peacock LT, Jackson P, Bushell S, editors. Jane's all the world's aircraft: development & production 2015-2016. IHS; 2015.

Gunston B, Willis D, Munson K, Peacock LT, Jackson PA, Bushell S, editors. Jane's all the world's aircraft: development & production 2014-2015. IHS; 2014.

Guo Z, Faghri A. Vapor feed direct methanol fuel cells with passive thermal-fluids management system. J Power Sources 2007;167:378–90. https://doi.org/10.1016/j.jpowsour.2007.02.024.

Guynn MD, Freh JE, Olson ED. Evaluation of a hydrogen fuel cell powered blended-wing-body aircraft concept for reduced noise and emissions. NASA 2004;NASA/TM-20.

Gwak G, Kim D, Lee S, Ju H. Studies of the methanol crossover and cell performance behaviors of high temperature-direct methanol fuel cells (HT-DMFCs). Int J Hydrogen Energy 2018;43:13999–4011. https://doi.org/10.1016/j.ijhydene.2017.11.029.

Haberbusch MS, Hui TY, Lobo S. No-Vent TM Liquid Hydrogen Storage System. AIAA/ASME/SAE/ASEE Jt. Propuls. Conf. Exhib., Denver: AIAA; 2009, p. 1–8. https://doi.org/10.2514/6.2009-5331.

Haberbusch MS, Nguyen CT, Stochl RJ, Hui TY. Development of No-VentTM Liquid Hydrogen Storage System for Space Applications. Cryogenics (Guildf) 2010;50:541–8. https://doi.org/10.1016/j.cryogenics.2010.02.025.

Halim FA, Hasran UA, Masdar MS, Kamarudin SK. Study on a Passive Vapor Feed Direct Methanol Fuel Cell with High Methanol Concentration. J Clean Energy Technol 2013;1:292–4. https://doi.org/10.7763/JOCET.2013.V1.66.

Hall N. Compressor Thermodynamics. NASA - Glenn Res Cent 2015. https://www.grc.nasa.gov/WWW/K-12/airplane/compth.html (accessed August 22, 2020).

Hamnett A. Mechanism and electrocatalysis in the direct methanol fuel cell. Catal Today 1997;38:445–57. https://doi.org/10.1016/S0920-5861(97)00054-0.

Han J, Park ES. Direct methanol fuel-cell combined with a small back-up battery. J Power Sources 2002;112:477–83. https://doi.org/10.1016/S0378-7753(02)00441-X.

Hasan MM, Balasubramaniam R. Analysis of the pressure rise in a partially filled liquid tank in microgravity with low wall heat flux and simultaneous boiling and condensation. 50th AIAA Aerosp Sci Meet Incl New Horizons Forum Aerosp Expo 2012. https://doi.org/10.2514/6.2012-760.

Health and Safety Executive. Oxygen use in the workplace: Fire and explosion hazards. 2013.

Heinzel A, Barragán VM. Review of the state-of-the-art of the methanol crossover in direct methanol fuel cells. J Power Sources 1999;84:70–4. https://doi.org/10.1016/S0378-7753(99)00302-X.

Herwerth C, Chiang C, Ko A, Matsuyama S, Choi SB, Mirmirani M, et al. Development of a small long endurance hybrid PEM fuel cell powered UAV. SAE Tech Pap 2007. https://doi.org/10.4271/2007-01-3930.

Hirscher M, editor. Handbook of Hydrogen Storage: New Materials for Future Energy Storage. Wiley-VCH; 2010. https://doi.org/10.1002/9783527629800.

Horizon Energy Systems. AEROSTACKS, World's lightest fuel cells for electric UAVs 2015. https://media.wix.com/ugd/047f54_8483372175ef4e1aa43edbe62aaae68e.pdf (accessed August 5, 2016).

Horizon Fuel Cell Technologies. H-1000XP Designed for efficiency 2014. http://media.wix.com/ugd/047f54_d140778984ed4c61a0c5d2fc8b9df2ab.pdf (accessed August 5, 2016).

Horizon Fuel Cell Technologies. Ultra-light composite cylinder (E-Series) 2017. http://www.fuelcellstore.com/hydrogen-equipment/hydrogen-storage/composite-storage-cylinders/ultra-light-composite-storage-cylinder-e-series (accessed January 5, 2017).

Howroyd S, Chen R. Powerpath controller for fuel cell & battery hybridisation. Int J Hydrogen Energy 2016;41:4229–38. https://doi.org/10.1016/j.ijhydene.2016.01.038.

Hydrogenics. HyPM-HD power modules 2016. http://www.hydrogenics.com/wp-content/uploads/HyPM-HD-Brochure.pdf (accessed August 5, 2016).

Hydrogenics. HyPM-XR power modules 2016. http://www.hydrogenics.com/wp-content/uploads/HyPM-XR-Brochure.pdf (accessed August 5, 2016).

Im JY, Kim BS, Choi HG, Cho SM. Effect of pressure for direct fuel cells using DME-based fuels. J Power Sources 2008;179:301–4. https://doi.org/10.1016/j.jpowsour.2007.12.046.

Inoue M, Iwasaki T, Sayama K, Umeda M. Effect of conditioning method on direct methanol fuel cell performance. J Power Sources 2010;195:5986–9. https://doi.org/10.1016/j.jpowsour.2009.11.015.

Intelligent Energy Ltd. Datasheet, AC10 stack 2016. http://www.intelligent-energy.com/uploads/accompanying_files/41556_IE_-_AC10_datasheet_no_crops.pdf (accessed December 5, 2016).

Intelligent Energy Ltd. Datasheet, AC64 stack 2016. http://www.intelligent-energy.com/uploads/uploads/Datasheets/41556_ie_-_ac64_datasheet.pdf (accessed December 5, 2016).

Intelligent Energy Ltd. Datasheet, FCM-801 2018.

International Air Transport Association. IATA 2015 Report on Alternative Fuels. Montreal-Geneva: 2015.

Kadyk T, Winnefeld C, Hanke-Rauschenbach R, Krewer U. Analysis and Design of Fuel Cell Systems for Aviation. Energies 2018;11:375. https://doi.org/10.3390/en11020375.

Kandaramath Hari T, Yaakob Z, Binitha NN. Aviation biofuel from renewable resources: Routes, opportunities and challenges. Renew Sustain Energy Rev 2015;42:1234–44. https://doi.org/10.1016/j.rser.2014.10.095.

Kang K, Lee G, Gwak G, Choi Y, Ju H. Development of an advanced MEA to use high-concentration methanol fuel in a direct methanol fuel cell system. Int J Hydrogen Energy 2012;37:6285–91. https://doi.org/10.1016/j.ijhydene.2011.06.114.

Khan F, Nawaz A, Muhammad MA, Khadim MA. Review And Analysis Of MATLAB® Simulink Model Of PEM Fuel Cell Stack. Int J Eng Comput Sci 2013;13:31–4.

Kim J, Lee S, Srinivasan S, Chamberlin CE, Kim J, Lee S, et al. Modeling of Proton Exchange Membrane Fuel Cell Performance with an Empirical Equation. J Electrochem Soc 1995;142:2670–4. https://doi.org/10.1149/1.2050072.

Kim K, Kim T, Lee K, Kwon S. Fuel cell system with sodium borohydride as hydrogen source for unmanned aerial vehicles. J Power Sources 2011;196:9069–75. https://doi.org/10.1016/j.jpowsour.2011.01.038.

Kim S, Hong I. Effects of humidity and temperature on a proton exchange membrane fuel cell (PEMFC) stack. J Ind Eng Chem 2008;14:357–64. https://doi.org/10.1016/j.jiec.2008.01.007

Kim T, Kwon S. Design and development of a fuel cell-powered small unmanned aircraft. Int J Hydrogen Energy 2012;37:615–22. https://doi.org/10.1016/j.ijhydene.2011.09.051.

Klell M, Kindermann H, Jogl C. Thermodynamics of gaseous and liquid hydrogen storage. Proc. Int. Hydrog. Energy Congr. Exhib. IHEC 2007, Istanbul: 2007, p. 13–5.

Ko J, Chippar P, Ju H. A one-dimensional, two-phase model for direct methanol fuel cells - Part I: Model development and parametric study. Energy 2010;35:2149–59. https://doi.org/10.1016/j.energy.2010.01.034.

Kongkanand A, Subramanian NP, Yu Y, Liu Z, Igarashi H, Muller DA. Achieving High-Power PEM Fuel Cell Performance with an Ultralow-Pt-Content Core-Shell Catalyst. ACS Catal 2016;6:1578–83. https://doi.org/10.1021/acscatal.5b02819.

Kumar L, Jain S. Electric propulsion system for electric vehicular technology: A review. Renew Sustain Energy Rev 2014;29:924–40. https://doi.org/10.1016/j.rser.2013.09.014.

Kumaresan T, Velumani T, Chandran M, Palaniswamy K, Thirkell A, Fly A, et al. Effect of Nafion loading and the novel flow field designs on Innovative anode electrocatalyst for improved DMFCs performance. Mater Lett 2020;276. https://doi.org/10.1016/j.matlet.2020.128222.

Lapeña-Rey N, Mosquera J, Bataller E, Ortí F, Dudfield C, Orsillo A. Environmentally friendly power sources for aerospace applications. J Power Sources 2008;181:353–62. https://doi.org/10.1016/j.jpowsour.2007.11.045.

lapesa. Horizontal Cryogenic Tanks n.d.:10–1. www.lapesa.es/descargar.php?f=/sites/default/files/documentos/gnli_1011.pdf (accessed January 5, 2017).

Larminie J, Dicks A. Fuel Cell Systems Explained. 2nd ed. John Wiley & Sons; 2003. https://doi.org/10.1016/S0378-7753(00)00571-1.

Laurencelle F, Chahine R, Hamelin J, Agbossou K, Fournier M, Bose TK, et al. Characterization of a Ballard MK5-E Proton Exchange Membrane Fuel Cell Stack. Fuel Cells 2001;1:66–71. https://doi.org/10.1002/1615-6854(200105)1:1<66::AID-FUCE66>3.0.CO;2-3.

Lee JH, Lalk TR, Appleby a. J. Modeling electrochemical performance in large scale proton exchange membrane fuel cell stacks. J Power Sources 1998;70:258–68. https://doi.org/10.1016/S0378-7753(97)02683-9.

Liu J, Zhao T, Chen R, Wong C. The effect of methanol concentration on the performance of a passive DMFC. Electrochem Commun 2005:288–94. https://doi.org/10.1016/j.elecom.2005.01.011.

Luxfer Gas Cylinders. G-Stor H2 Fuel Cell Vehicle Cylinders. Prod Specific Sheet 2018.https://www.luxfercylinders.com/img/luxfer/products_upload/G-Stor-H2-spec-sheet-2018.pdf (accessed July 12, 2020).

Luxfer Gas Cylinders. G-StorTM H2 hydrogen-storage cylinders 2015. http://www.luxfercylinders.com/products/alternative-fuel/gstorh2 (accessed January 5, 2016).

Luxfer Gas Cylinders. L6X Composite inflation and aerospace cylinders 2015. http://www.luxfercylinders.com/products/l6x-composite-cylinder (accessed January 5, 2016).

Mahytec. Hydrogen storage solutions 2016. http://www.mahytec.com/en/our-solutions/ (accessed January 5, 2017).

Makridis SS. Hydrogen storage and compression. In: Carriveau R, Ting DS-K, editors. Methane Hydrog. Energy Storage. 1st ed., IET Digital Library; 2016. https://doi.org/10.1049/pbpo101e_ch1.

MathWorks. Battery - Generic battery model. Co Website 2008. https://www.mathworks.com/help/physmod/sps/powersys/ref/battery.html (accessed October 24, 2020).

McAllister S, Chen J-Y, Fernandez-Pello AC. Fundamentals of Combustion Processes. 1st ed. New York: Springer-Verlag; 2011. https://doi.org/10.1007/978-1-4419-7943-8.

McConnell VP. Military UAVs claiming the skies with fuel cell power. Fuel Cells Bull 2007;2007:12–5. https://doi.org/10.1016/S1464-2859(07)70438-8.

McGrath KM, Surya Prakash GK, Olah G a. Direct Methanol Fuel Cell. J Ind Eng Chem 2004;10:1063–80.

McKinsey & Company, Clean Sky 2 JU, Fuel Cells and Hydrogen 2 JU. Hydrogen-powered aviation A fact-based study of hydrogen technology, economics, and climate impact by 2050. 1st ed. McKinsey & Company; 2020. https://doi.org/10.2843/471510.

McLean GF, Niet T, Djilali N. An assessment of AFC technology. Int J Hydrogen Energy 2002;27:507–26.

MEGlobal. Ethylene Glycol Product Guide 2008:1–33. https://www.meglobal.biz/wp-content/uploads/2019/01/Monoethylene-Glycol-MEG-Technical-Product-Brochure-PDF.pdf (accessed September 19, 2020).

Mehta V, Cooper JS. Review and analysis of PEM fuel cell design and manufacturing 2002;114.

Methanol Institute. Compatibility of Elastomers in Neat Methanol. 2016

Methanol Institute. Compatibility of Metals & Alloys in Neat Methanol Service. 2016.

Methanol Institute. Freezing Points of Methanol. Methanol Prop 2016. http://www.methanol.org/wp-content/uploads/2016/06/FreezingPointsMethanol-WaterSolutions.pdf (accessed March 25, 2020).

Meyers JP, Darling RM, Evans C, Balliet R, Perry ML. Evaporativley-Cooled PEM Fuel-Cell Stack System. ECS Trans., vol. 3, The Electrochemical Society; 2006, p. 1207–14. https://doi.org/10.1149/1.2356240.

Microsoft. LINEST function 2017. https://support.office.com/en-us/article/LINEST-function-84d7d0d9-6e50-4101-977a-fa7abf772b6d?NS=EXCEL&Version=16&SysLcid=1033&UiLcid=1033&AppVer=ZXL160&HelpId=xlmain11.chm60097&ui=en-US&rs=en-US&ad=US (accessed March 10, 2017).

Middleton M. Better Exponential Curve Fitting Using Excel. Decis. Sci. Inst. Annu. Meet. 41st, San Diego: 2010.

Mills GL, Buchholtz BW, Olsen A. Design, fabrication and testing of a liquid hydrogen fuel tank for a long duration aircraft. AIP Conf Proc 2012;1434:773–80. https://doi.org/10.1063/1.4706990.

Ministry of Defence. Joint Doctrine Note 2/11 the UK Approach To Unmanned Aircraft. 2011.

Ministry of Defence. Joint Doctrine Publication 0-30.2: Unmanned Aircraft Systems. 2017.

Ministry of Defence. Securing Britain in an Age of Uncertainty : The Strategic Defence and Security Review Securing Britain in an. 2010.

Mobariz KN, Youssef AM, Abdel-Rahman M. Long endurance hybrid fuel cell-battery powered UAV. World J Model Simul 2015;11:69–80.

Moir I, Seabridge A, Jukes M. Electrical Systems. Civ. Avion. Syst. 2nd ed., John Wiley & Sons; 2013, p. 235–90.

Monem AA A El, M Azmy A. Dynamic Modelling of Proton Exchange Membrane Fuel Cells for Electric Vehicle Applications. J Pet Environ Biotechnol 2014;5. https://doi.org/10.4172/2157-7463.1000169.

Munoz-ramos K, Pratt JW, Akhil AA, Schenkman, Benjamin L. Klebanoff LE, Curgus DB. Electrical Analysis of Proton Exchange Membrane Fuel Cells for Electrical Power Generation On-Board Commercial Airplanes. IEEE Transp. Electrif. Conf. Expo, 2012, p. 1–6.

Nakagawa N, Tsujiguchi T, Sakurai S, Aoki R. Performance of an active direct methanol fuel cell fed with neat methanol. J Power Sources 2012;219:325–32. https://doi.org/10.1016/j.jpowsour.2012.07.062.

Nakagawa N, Xiu Y. Performance of a direct methanol fuel cell operated at atmospheric pressure. J Power Sources 2003;118:248–55. https://doi.org/10.1016/S0378-7753(03)00090-9.

National Institute of Standards and Technology. Saturation Properties for Hydrogen — Pressure Increments. NIST Chem WebBook, SRD 69 n.d. https://webbook.nist.gov/cgi/fluid.cgi?Action=Load&ID=C1333740&Type=SatT&Digits=5&PLow=.5&PHigh=1.5&PInc=.1&RefState=DEF&TUnit=K&PUnit=atm&DUnit=kg/m3&HUnit=kJ/mol&WUnit=m/s&VisUnit=uPa*s&STUnit=N/m (accessed June 24, 2020).

National Institute of Standards and Technology. Thermophysical Properties of Fluid Systems. NIST Chem WebBook, SRD 69 2018. https://webbook.nist.gov/chemistry/fluid/ (accessed April 17, 2021).

Ngo TT, Yu TL, Lin HL. Influence of the composition of isopropyl alcohol/water mixture solvents in catalyst ink solutions on proton exchange membrane fuel cell performance. J Power Sources 2013;225:293–303. https://doi.org/10.1016/j.jpowsour.2012.10.055.

Nishizawa A, Kallo J, Garrot O, Weiss-Ungethüm J. Fuel cell and Li-ion battery direct hybridization system for aircraft applications. J Power Sources 2013;222:294–300. https://doi.org/10.1016/jjpowsour.2012.09.011.

Notardonato WU, Swanger AM, Fesmire JE, Jumper KM, Johnson WL, Tomsik TM. Zero boil-off methods for large-scale liquid hydrogen tanks using integrated refrigeration and storage. IOP Conf Ser Mater Sci Eng 2017;278. https://doi.org/10.1088/1757-899X/278/1/012012.

O'Hayre R, Cha S-W, Colella W, Prinz FB. Fuel cell fundamentals. 3rd ed. John Wiley & Sons; 2016.

Oh TH. Conceptual design of small unmanned aerial vehicle with proton exchange membrane fuel cell system for long endurance mission. Energy Convers Manag 2018;176:349–56. https://doi.org/10.1016/j.enconman.2018.09.036.

Outeiro MT, Chibante R, Carvalho AS, de Almeida AT. A parameter optimized model of a Proton Exchange Membrane fuel cell including temperature effects. J Power Sources 2008;185:952–60. https://doi.org/10.1016/j.jpowsour.2008.08.019.

Pan YH. Advanced air-breathing direct methanol fuel cells for portable applications. J Power Sources 2006;161:282–9. https://doi.org/10.1016/j.jpowsour.2006.03.048.

Park GG, Yang TH, Yoon YG, Lee WY, Kim CS. Pore size effect of the DMFC catalyst supported on porous materials. Int J Hydrogen Energy 2003;28:645–50. https://doi.org/10.1016/S0360-3199(02)00140-4.

Pathapati PR, Xue X, Tang J. A new dynamic model for predicting transient phenomena in a PEM fuel cell system. Renew Energy 2005;30:1–22. https://doi.org/10.1016/j.renene.2004.05.001.

Petrinić M, Jakopović Ž. Modeling and simulation of PEM fuel cell - Power converter system. MIPRO 2007 - 30th Jubil Int Conv Proc Microelectron Electron Electron Technol Hypermedia Grid Syst MEE /HGS 2007;1:151–6.

Pilatowsky I, Romero RJ, Isaza CA, Gamboa SA, Sebastian PJ, Rivera W. Thermodynamics of Fuel Cells. Cogener. Fuel Cell - Sorption Air Cond. Syst. 1st ed., London: Springer-Verlag; 2011, p. 25–36. https://doi.org/10.1007/978-1-84996-028-1.

Plachta DW, Guzik MC. Cryogenic Boil-Off Reduction System. Cryogenics (Guildf) 2014;60:62–7. https://doi.org/10.1016/j.cryogenics.2013.12.006.

Plachta DW, Johnson WL, Feller JR. Zero Boil-Off System Testing. Cryogenics (Guildf) 2016;74:88–94. https://doi.org/10.1016/j.cryogenics.2015.10.009.

Prater K. The renaissance of the solid polymer fuel cell. J Power Sources 1990;29:239–50. https://doi.org/10.1016/0378-7753(90)80023-7.

Pratt JW, Brouwer J, Samuelsen GS. Performance of Proton Exchange Membrane Fuel Cell at High-Altitude Conditions. J Propuls Power 2007;23:437–44. https://doi.org/10.2514/1.20535.

Pratt JW, Brouwer J, Samuelsen GS. Performance of Proton Exchange Membrane Fuel Cell at High-Altitude Conditions. J Propuls Power 2012;23:437–44. https://doi.org/10.2514/1.20535.

Pratt JW, Klebanoff LE, Munoz-Ramos K, Akhil AA, Curgus DB, Schenkman BL. Proton exchange membrane fuel cells for electrical power generation on-board commercial airplanes. Appl Energy 2013;101:776–96. https://doi.org/10.1016/j.apenergy.2012.08.003.

Pratt L. MQ-1 Predator, armed with AGM-114 Hellfire missiles. Wikimedia Commons 2008. https://upload.wikimedia.org/wikipedia/commons/c/c7/MQ-1_Predator%2C_armed_with_AGM-114_Hellfire_missiles.jpg (accessed October 24, 2020).

Pressol HDPE Jerrycan. RS-Online Datasheet 2010:2010. https://docs.rs-online.com/ab22/0900766b80e0f376.pdf (accessed July 31, 2020).

Preuster P, Alekseev A, Wasserscheid P. Hydrogen Storage Technologies for Future Energy Systems. Annu Rev Chem Biomol Eng 2017;8:445–71. https://doi.org/10.1146/annurev-chembioeng-060816-101334.

Qin Y, Du Q, Fan M, Chang Y, Yin Y. Study on the operating pressure effect on the performance of a proton exchange membrane fuel cell power system. Energy Convers Manag 2017;142:357–65. https://doi.org/10.1016/j.enconman.2017.03.035.

Quantum fuel systems. Q-LiteTM advanced CNG fuel storage tanks 2015. http://www.qtww.com/product/q-lite-lightest-cng-tanks/ (accessed January 5, 2017).

Rayment C, Sherwin S. Introduction to Fuel Cell Technology. 2003. https://doi.org/10.1.1.129.3231&rep=rep1&type=pdf.

Reid A. The Composition of Earth's Atmosphere With Elevation. MrReidOrg 2014. http://wordpress.mrreid.org/2014/08/01/the-composition-of-earths-atmosphere-with-elevation / (accessed June 15, 2020).

Renau J, Lozano A, Barroso J, Miralles J, Martin J, Sanchez F, et al. Use of fuel cell stacks to achieve high altitudes in light unmanned aerial vehicles. Int J Hydrogen Energy 2015;40:14573–83. https://doi.org/10.1016/j.ijhydene.2015.02.071.

Renouard-Vallet G, Saballus M, Schumann P, Kallo J, Friedrich KA, Müller-Steinhagen H. Fuel Cells for Civil Aircraft Application: On-Board Production of Power, Water and Inert Gas. Chem Eng Res Des 2012;90:3–10. https://doi.org/10.1016/j.cherd.2011.07.016.

Rohland B, Eberle K, Ströbel R, Scholta J, Garche J. Electrochemical hydrogen compressor. Electrochim Acta 1998;43:3841–6. https://doi.org/10.1016/S0013-4686(98)00144-3.

Roth B, Iii RG. Fuel cell hybrid propulsion challenges and opportunities for commercial aviation 2010:1–15. https://doi.org/doi:10.2514/6.2010-6537.

Rotrex. Rotrex TM EK10AA Fuel Cell Compressor Technical Datasheet n.d.:1–8. https://www.rotrex.com/wp-content/uploads/2020/01/Rotrex-Technical-Datasheet-EK10AA-Range-V1.50-1.pdf (accessed August 29, 2020).

Saleh IM, Ali R, Zhang H. Environmental Impact of High Altitudes on the Operation of PEM Fuel Cell Based UAS. Energy Power Eng 2018;10:87–105. https://doi.org/10.4236/epe.2018.103007.

SALEH IMM, ALI R, ZHANG H. Simplified mathematical model of proton exchange membrane fuel cell based on horizon fuel cell stack. J Mod Power Syst Clean Energy 2016;4:668–79. https://doi.org/10.1007/s40565-016-0196-5.

Santarelli MG, Torchio MF. Experimental analysis of the effects of the operating variables on the performance of a single PEMFC. Energy Convers Manag 2007;48:40–51. https://doi.org/10.1016/j.enconman.2006.05.013.

Scheelhaase J, Maertens S, Grimme W. Synthetic fuels in aviation - Current barriers and potential political measures. Transp Res Procedia 2019;43:21–30. https://doi.org/10.1016/j.trpro.2019.12.015.

Schlapbach L, Züttel a. Hydrogen-storage materials for mobile applications. Nature 2001;414:353–8. https://doi.org/10.1038/35104634.

Scott K, Taama WM, Argyropoulos P. Engineering aspects of the direct methanol fuel cell system. J Power Sources 1999;79:43–59. https://doi.org/10.1016/S0378-7753(98)00198-0.

SFC Energy. Efoy Comfort Technical Data n.d. https://www.efoy-comfort.com/technical-data (accessed August 4, 2020).

SFC Energy. Efoy_Comfort_210 2018. https://www.efoy-comfort.com/sites/default/files/sfc_M10_perspektive_I_18201_210_sRGB_8.png (accessed February 21, 2019).

Shen KY, Park S, Kim YB. Hydrogen utilization enhancement of proton exchange membrane fuel cell with anode recirculation system through a purge strategy. Int J Hydrogen Energy 2020;45:16773–86. https://doi.org/10.1016/j.ijhydene.2020.04.147.

Sigma-Aldrich. Methanol Safety Data Sheet 2018. https://www.sigmaaldrich.com/MSDS/MSDS/DisplayMSDSPage.do?country=GB&language=en&productNumber=322415&brand=SIAL&PageToGoToURL=https%3A%2F%2Fwww.sigmaaldrich.com%2Fcatalog%2Fproduct%2Fsial%2F322415%3Flang%3Den (accessed August 17, 2018).

skywalkermodel.com. Skywalker X8 Technical Data 2015. http://skywalkermodel.com/en/76.html (accessed October 25, 2020).

Sliwinski J, Gardi A, Marino M, Sabatini R. Hybrid-electric propulsion integration in unmanned aircraft. Energy 2017;140:1407–16. https://doi.org/10.1016/j.energy.2017.05.183.

Soupremanien U, Le Person S, Favre-Marinet M, Bultel Y. Tools for Designing the Cooling System of a Proton Exchange Membrane Fuel Cell. Appl Therm Eng 2012;40:161–73. https://doi.org/10.1016/j.applthermaleng.2012.02.008.

Springer TE. Modeling and Experimental Diagnostics in Polymer Electrolyte Fuel Cells. J Electrochem Soc 1993;140:3513. https://doi.org/10.1149/1.2221120.

Steelhead Composites. Hydrogen gas storage 2016. http://steelheadcomposites.com/products/gas-cylinders/hydrogen/ (accessed January 5, 2017).

Streetly M, editor. Jane's all the world's aircraft: unmanned 2015-2016. IHS; 2015.

Su K, Yao X, Sui S, Wei Z, Zhang J, Du S. Ionomer content effects on the electrocatalyst layer with in-situ grown Pt nanowires in PEMFCs. Int J Hydrogen Energy 2014;39:3219–25. https://doi.org/10.1016/j.ijhydene.2013.12.117.

Sugawara T, Kanazawa T, Imai N, Tachibana Y. Development of Motorized Turbo Compressor for Clarity Fuel Cell. SAE Tech Pap 2017. https://doi.org/10.4271/2017-01-1187.

Takaguchi H, Ohashi M. 1 kW Direct Methanol Fuel Cell System. Fujikura Tech Rev 2015:1–4.

Tang Y, Yuan W, Pan M, Wan Z. Experimental investigation on the dynamic performance of a hybrid PEM fuel cell/battery system for lightweight electric vehicle application. Appl Energy 2011;88:68–76. https://doi.org/10.1016/j.apenergy.2010.07.033.

Tavares S. Aerospace engineering pocket reference. Taylor & Francis; 2015.

Technical Committee ISO/TC20. ISO 2533:1975 Standard Atmosphere. 1975.

Thiagarajan V, Karthikeyan P, Thanarajan K, Neelakrishnan S, Manoharan R, Chen R, et al. Experimental investigation on DMFCs using reduced noble metal loading with NiTiO3 as supportive material to enhance cell performances. Int J Hydrogen Energy 2019;44:13415–23. https://doi.org/10.1016/j.ijhydene.2019.03.244.

Thiagarajan V, Manoharan R, Karthikeyan P, Nikhila E, Hernández-Ramírez A, Rodriguez-Varela FJ. Pt nanoparticles supported on NiTiO 3 /C as electrocatalyst towards

high performance Methanol Oxidation Reaction. Int J Hydrogen Energy 2017;42:9795–805. https://doi.org/10.1016/j.ijhydene.2017.01.017.

Thirkell A, Chen R, Harrington I. A Fuel Cell System Sizing Tool Based on Current Production Aircraft. Fort Worth, Texas: SAE International; 2017. https://doi.org/10.4271/2017-01-2135.

Thirkell A, Chen R. Comparison of Gaseous and Liquid Fuel Cells for Automotive Applications. In: Razi Nalim M, Vasudevan R, Rahetekar S, editors. Adv. Automot. Technol. 1st ed., Springer Singapore; 2020. https://doi.org/10.1007/978-981-15-5947-1.

Toghyani S, Baniasadi E, Afshari E. Performance analysis and comparative study of an anodic recirculation system based on electrochemical pump in proton exchange membrane fuel cell. Int J Hydrogen Energy 2018;43:19691–703. https://doi.org/10.1016/j.ijhydene.2018.08.194.

Tzimas E, Filiou C, Peteves SD, Veyret J. Hydrogen Storage : State-of-the-Art and Future Perspective. 2003.

U.S. Department of Defense. Department of Defense Handbook: Global Climatic Data for Developing Military Products MIL-HDBK-310. vol. MIL-STD-31. 1997.

United Nations. Paris Agreement. 2015. https://doi.org/FCCC/CP/2015/L.9.

Vasile NS, Monteverde Videla AHA, Simari C, Nicotera I, Specchia S. Influence of membrane-type and flow field design on methanol crossover on a single-cell DMFC: An experimental and multi-physics modeling study. Int J Hydrogen Energy 2017;42:27995–8010. https://doi.org/10.1016/j.ijhydene.2017.06.214.

Venturi M, Sang J, Knoop A, Hornburg G. Air supply system for automotive fuel cell application. SAE Tech Pap 2012. https://doi.org/10.4271/2012-01-1225.

Vidal-Iglesias FJ, Solla-Gullón J, Rodes A, Herrero E, Aldaz A. Understanding the Nernst equation and other electrochemical concepts: An easy experimental approach for students. J Chem Educ 2012;89:936–9. https://doi.org/10.1021/ed2007179.

Villalonga S, Nony F, Magnier C, Yvernes JL, Thomas C, Delmas B, et al. Composite 700 Bar-Vessel for on-Board Compressed Gaseous Hydrogen Storage. ICCM17, Edinburgh: International Committee on COmposite Materials; 2009.

Walker N, Garraway A, Brooke-Holland L, Mills C. Combat Air Strategy progress and next steps Compiled by : 2019.

Wang C, Hashem Nehrir M, Shaw S. Dynamic models and model validation for PEM fuel cells using electrical circuits. IEEE Trans Energy Convers 2005;20:442–51. https://doi.org/10.1109/pes.2005.1489284.

Wang L, Husar A, Zhou T, Liu H. A parametric study of PEM fuel cell performances. Int J Hydrogen Energy 2003;28:1263–72. https://doi.org/10.1016/S0360-3199(02)00284-7.

Wang Y, Chen KS, Mishler J, Cho SC, Adroher XC. A review of polymer electrolyte membrane fuel cells: Technology, applications, and needs on fundamental research. Appl Energy 2011;88:981–1007. https://doi.org/10.1016/j.apenergy.2010.09.030.

Warburton A, Mossop D, Burslem B, Rama P, Adcock P, Cole J, et al. Development of an evaporatively cooled hydrogen fuel cell system and its vehicle application. SAE Tech Pap 2013;2. https://doi.org/10.4271/2013-01-0475.

Ward TA, Jenal N. Design and initial flight tests of a hydrogen fuel cell powered unmanned air vehicle (UAV). Electrochem Soc 2010;26:433–44. https://doi.org/10.1149/1.3429016.

Wei Z, Wang S, Yi B, Liu J, Chen L, Zhou WJ, et al. Influence of electrode structure on the performance of a direct methanol fuel cell. J Power Sources 2002;106:364–9. https://doi.org/10.1016/S0378-7753(01)01023-0.

Wilberforce T, El-Hassan Z, Khatib FN, Al Makky A, Baroutaji A, Carton JG, et al. Modelling and simulation of Proton Exchange Membrane fuel cell with serpentine bipolar plate using MATLAB. Int J Hydrogen Energy 2017;42:25639–62. https://doi.org/10.1016/j.ijhydene.2017.06.091.

Willmott CJ, Matsuura K. Advantages of the mean absolute error (MAE) over the root mean square error (RMSE) in assessing average model performance. Clim Res 2005;30:79–82. https://doi.org/10.3354/cr030079.

Winnefeld C, Kadyk T, Bensmann B, Krewer U, Hanke-Rauschenbach R. Modelling and Designing Cryogenic Hydrogen Tanks for Future Aircraft Applications. Energies 2018;11:105. https://doi.org/10.3390/en11010105.

Wood DL, Yi JS, Nguyen T V. Effect of direct liquid water injection and interdigitated flow field on the performance of proton exchange membrane fuel cells. Electrochim Acta 1998;43:3795–809. https://doi.org/10.1016/S0013-4686(98)00139-X.

Xu C, Zhao TS, Yang WW. Modeling of water transport through the membrane electrode assembly for direct methanol fuel cells. J Power Sources 2008;178:291–308. https://doi.org/10.1016/j.jpowsour.2007.11.098.

Xu C, Zhao TS. A new flow field design for polymer electrolyte-based fuel cells. Electrochem Commun 2007;9:497–503. https://doi.org/10.1016/j.elecom.2006.10.031.

Xun Q, Liu Y, Holmberg E. A Comparative Study of Fuel Cell Electric Vehicles Hybridization with Battery or Supercapacitor. Int. Symp. Power Electron. Electr. Drives, Autom. Motion, IEEE; 2018, p. 389–94. https://doi.org/10.1109/SPEEDAM.2018.8445386.

Yan Q, Toghiani H, Causey H. Steady state and dynamic performance of proton exchange membrane fuel cells (PEMFCs) under various operating conditions and load changes. J Power Sources 2006;161:492–502. https://doi.org/10.1016/j.jpowsour.2006.03.077.

Yu W, Sichuan X, Ni H. Air compressors for fuel cell vehicles: An systematic review. SAE Int J Altern Powertrains 2015;4:115–22. https://doi.org/10.4271/2015-01-1172.

Zhang G, Kandlikar SG. A critical review of cooling techniques in proton exchange membrane fuel cell stacks. Int J Hydrogen Energy 2012;37:2412–29. https://doi.org/10.1016/j.ijhydene.2011.11.010.

Zhang J, Fisher TS, Ramachandran PV, Gore JP, Mudawar I. A Review of Heat Transfer Issues in Hydrogen Storage Technologies. J Heat Transfer 2005;127:1391. https://doi.org/10.1115/1.2098875.

Zhao TS, Xu C, Chen R, Yang WW. Mass transport phenomena in direct methanol fuel cells. Prog Energy Combust Sci 2009;35:275–92. https://doi.org/10.1016/j.pecs.2009.01.001.

Zuttel A. Materials for hydrogen storage. Mater Today 2003;6:24–33. https://doi.org/10.1016/S1369-7021(03)00922-2.

Appendix 1 - Publications

---

1. **Thirkell A**, Chen R, Harrington I. A Fuel Cell System Sizing Tool Based on Current Production Aircraft. Fort Worth, Texas: SAE International; 2017. https://doi.org/10.4271/2017-01-2135.
2. **Thirkell A**, Chen R. Comparison of Gaseous and Liquid Fuel Cells for Automotive Applications. In: Razi Nalim M, Vasudevan R, Rahetekar S, editors. Adv. Automot. Technol. 1st ed., Springer Singapore; 2020. https://doi.org/10.1007/978-981-15-5947-1_5.
3. Kumaresan T, Velumani T, Chandran M, Palaniswamy K, **Thirkell A**, Fly A, et al. Effect of Nafion loading and the novel flow field designs on Innovative anode electrocatalyst for improved DMFCs performance. Mater Lett 2020. https://doi.org/10.1016/j.matlet.2020.128222.

Appendix 2 - Aircraft Categorisation Empirical Correlations

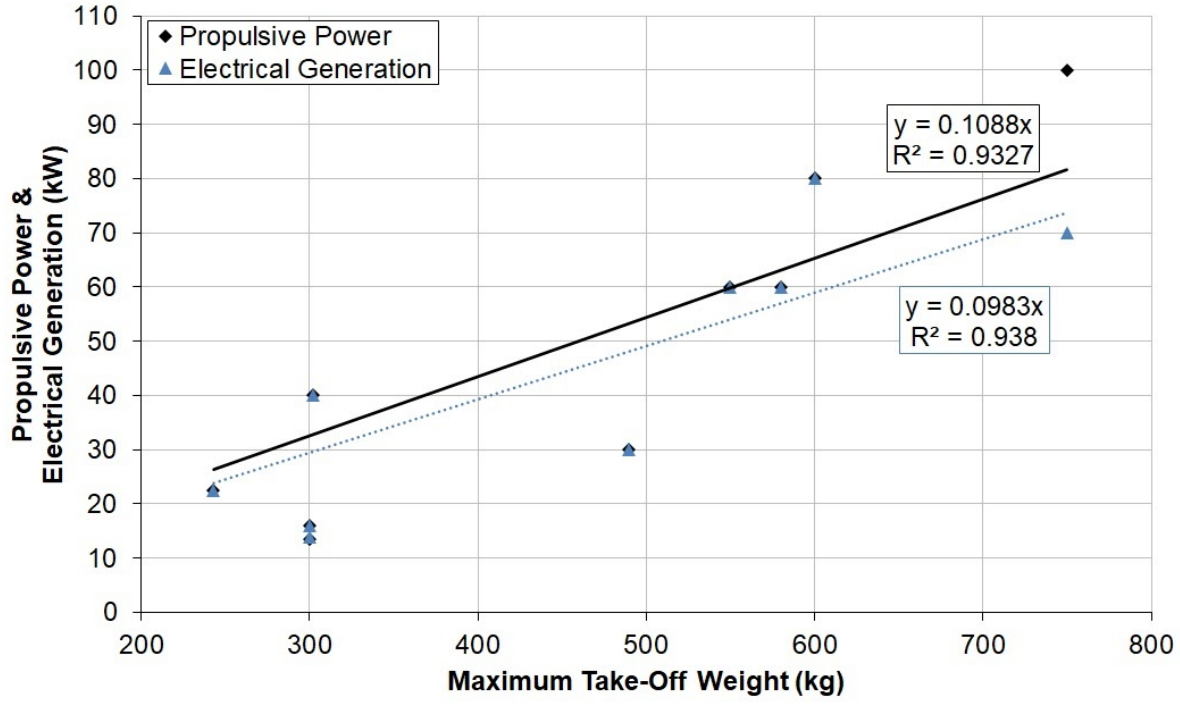

Figure A2.1: Refined correlations for existing propeller driven all electric aircraft

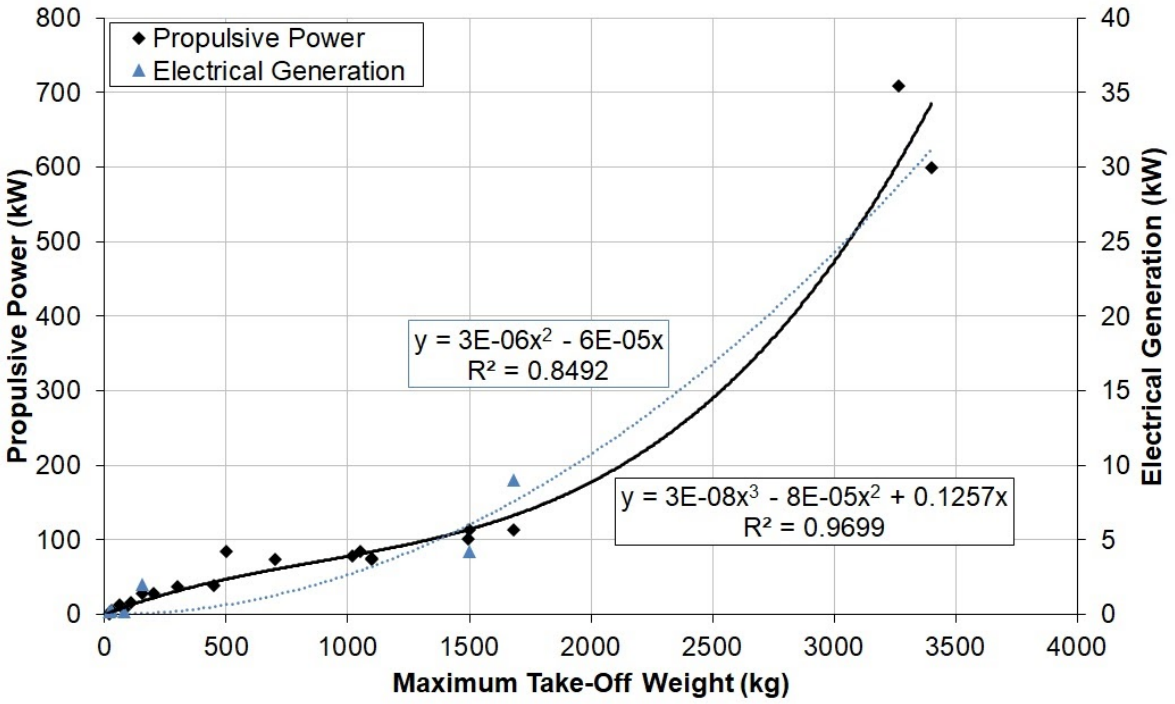

Figure A2.2: Refined correlations for existing propeller driven unmanned aerial vehicles

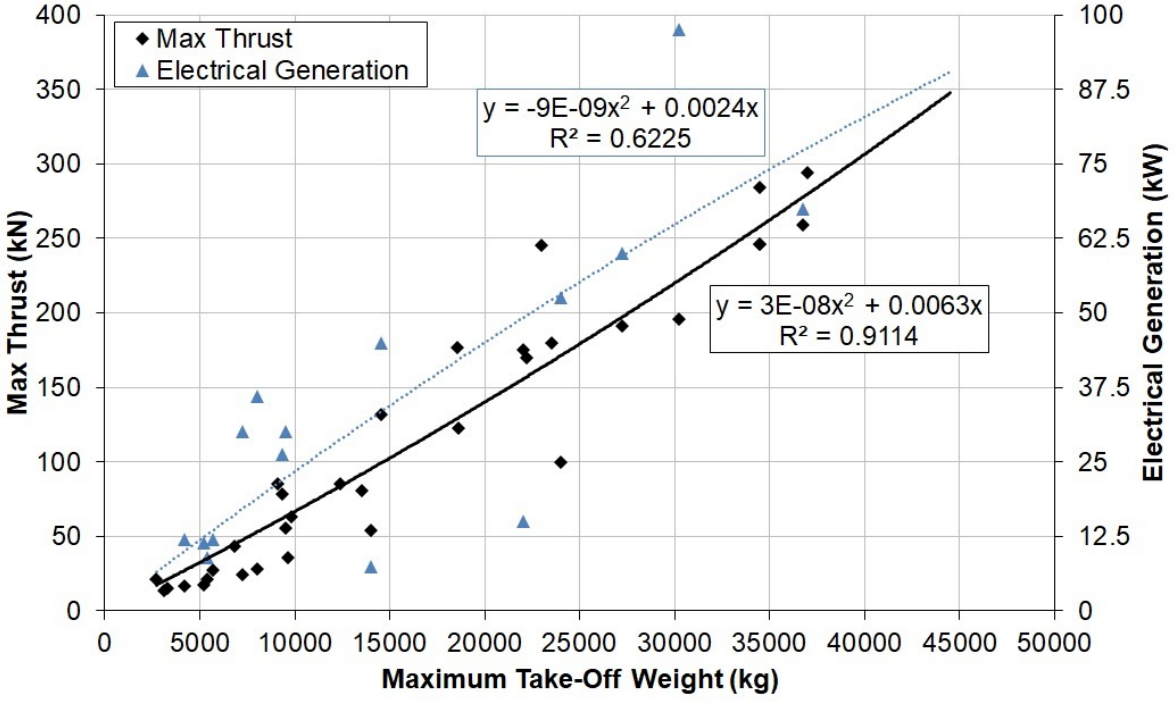

Figure A2.3: Refined correlations for existing jet propelled fighter and trainer aircraft

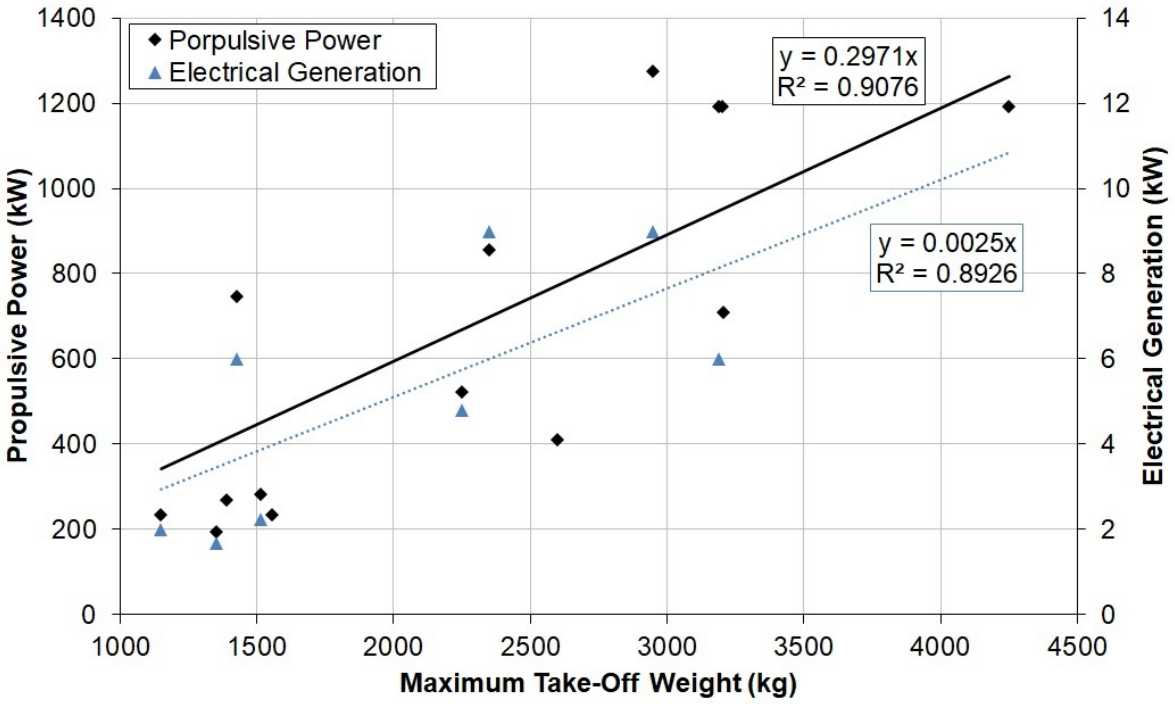

Figure A2.4: Refined correlations for existing propeller driven fighter and trainer aircraft

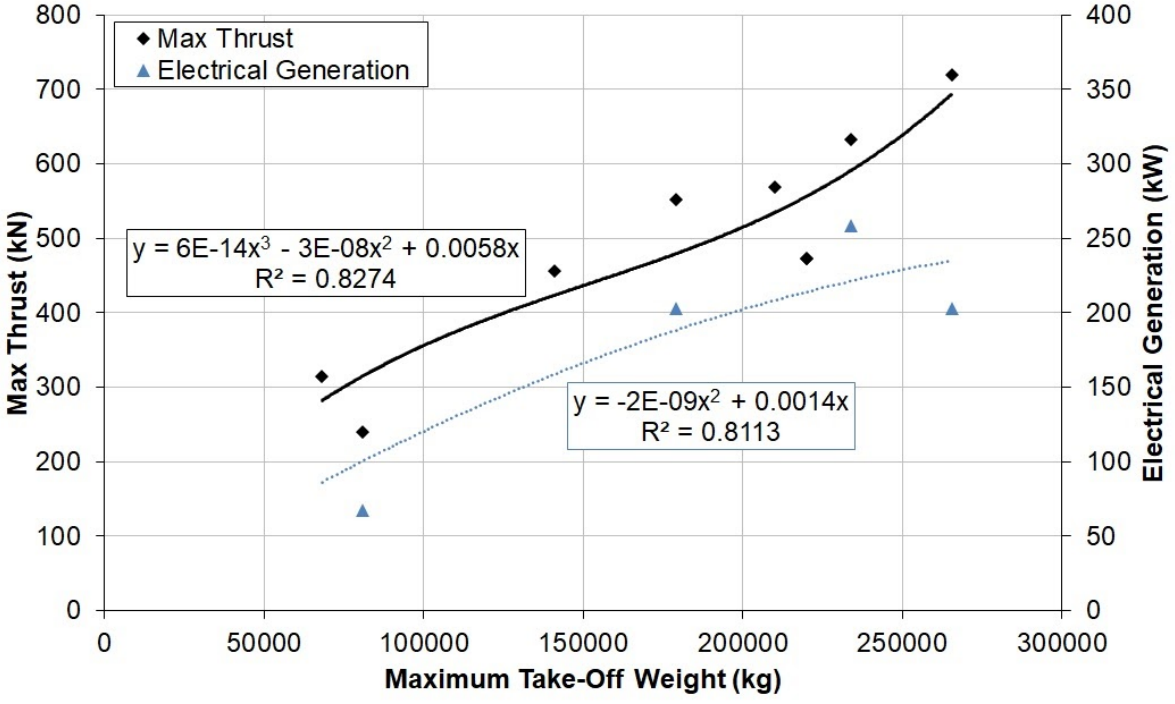

Figure A2.5: Refined correlations for existing jet propelled transport aircraft

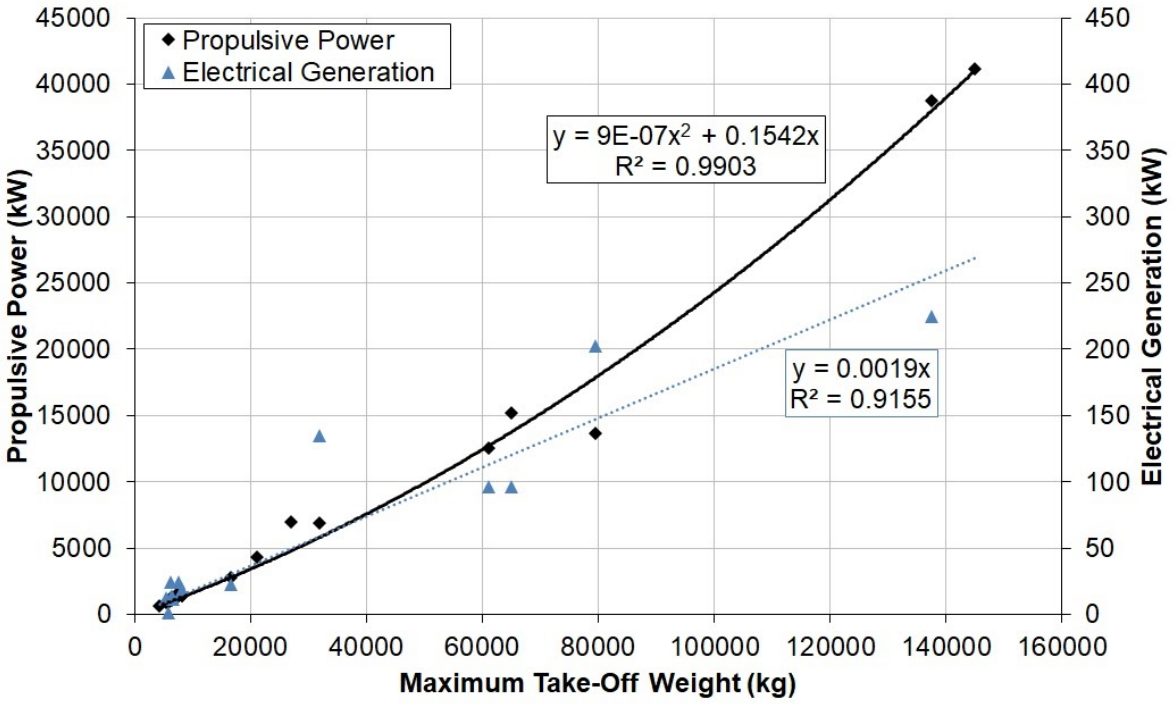

Figure A2.6: Refined correlations for existing propeller driven transport aircraft

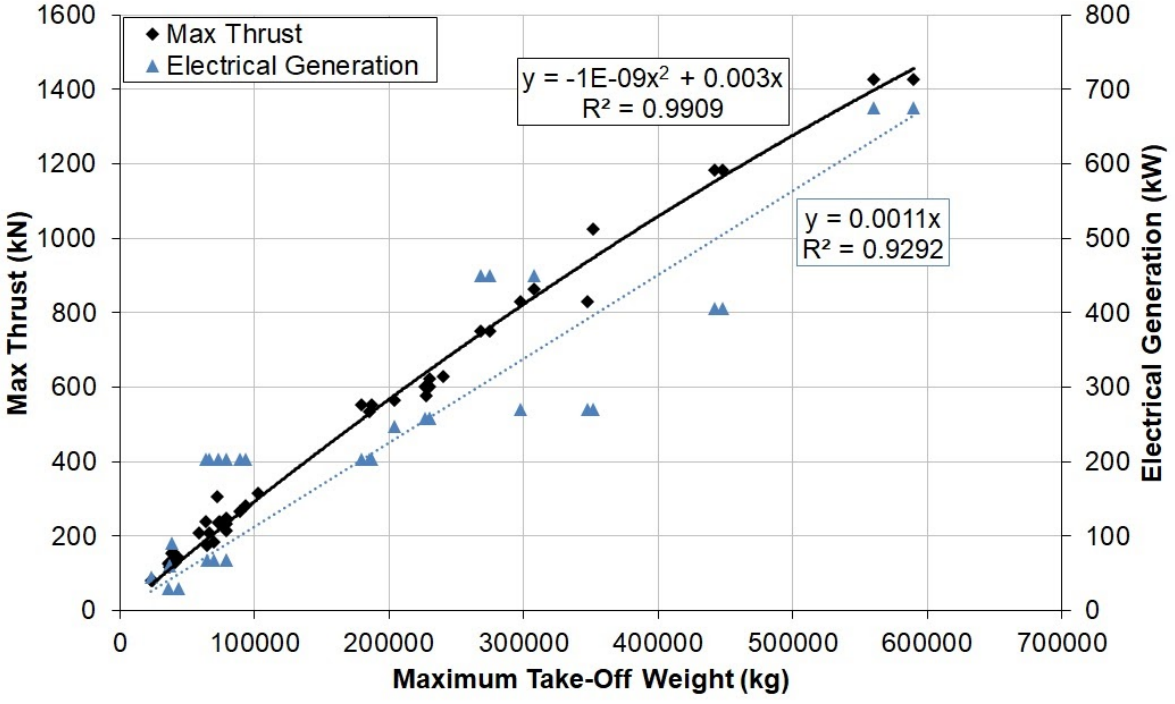

Figure A2.7: Refined correlations for existing jet propelled airliner and freighter aircraft

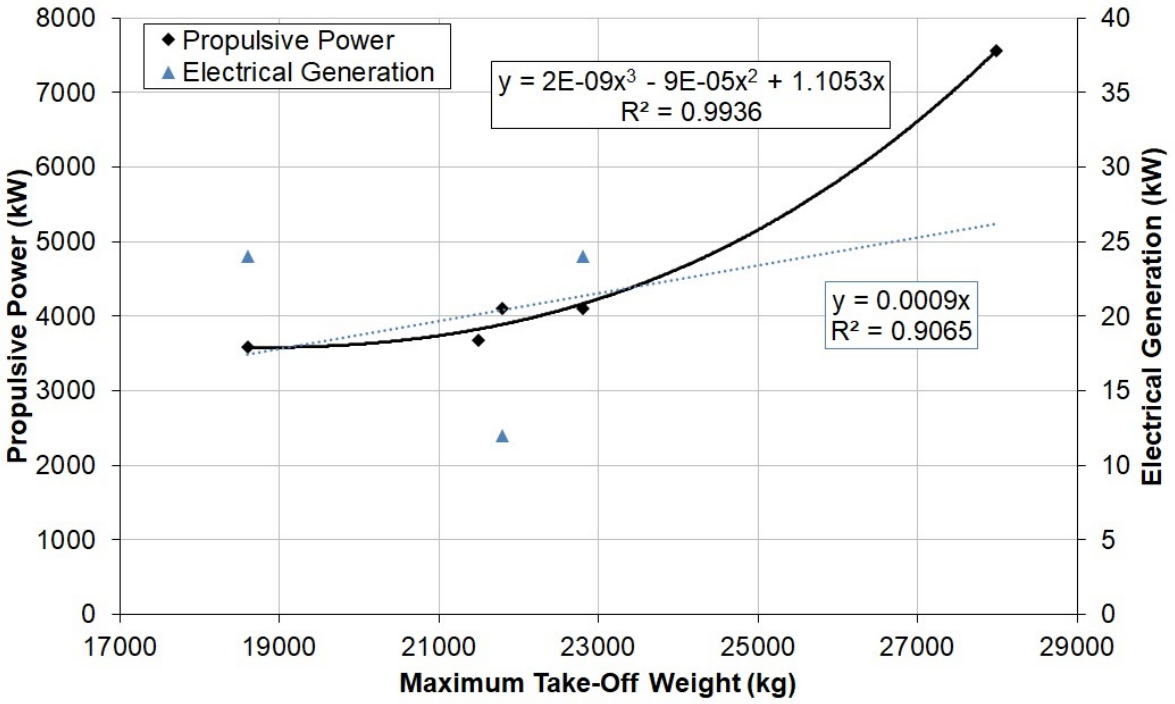

Figure A2.8: Refined correlations for existing propeller driven airliner and freighter aircraft

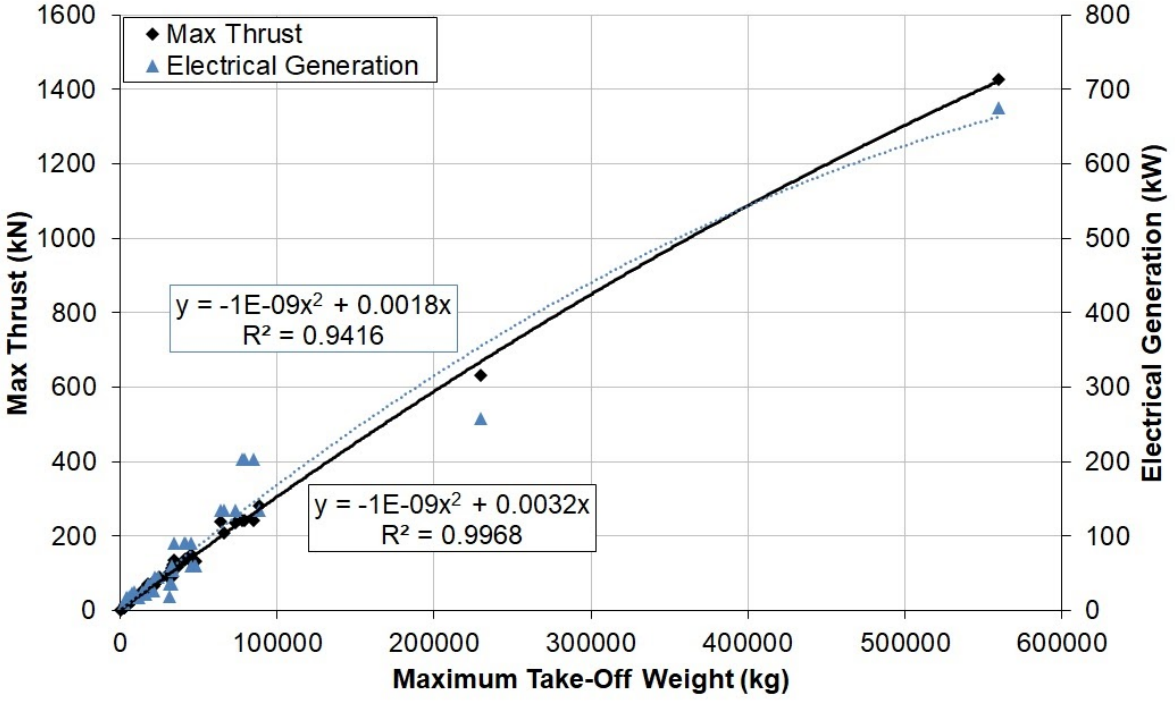

Figure A2.9: Refined correlations for existing jet propelled business aircraft

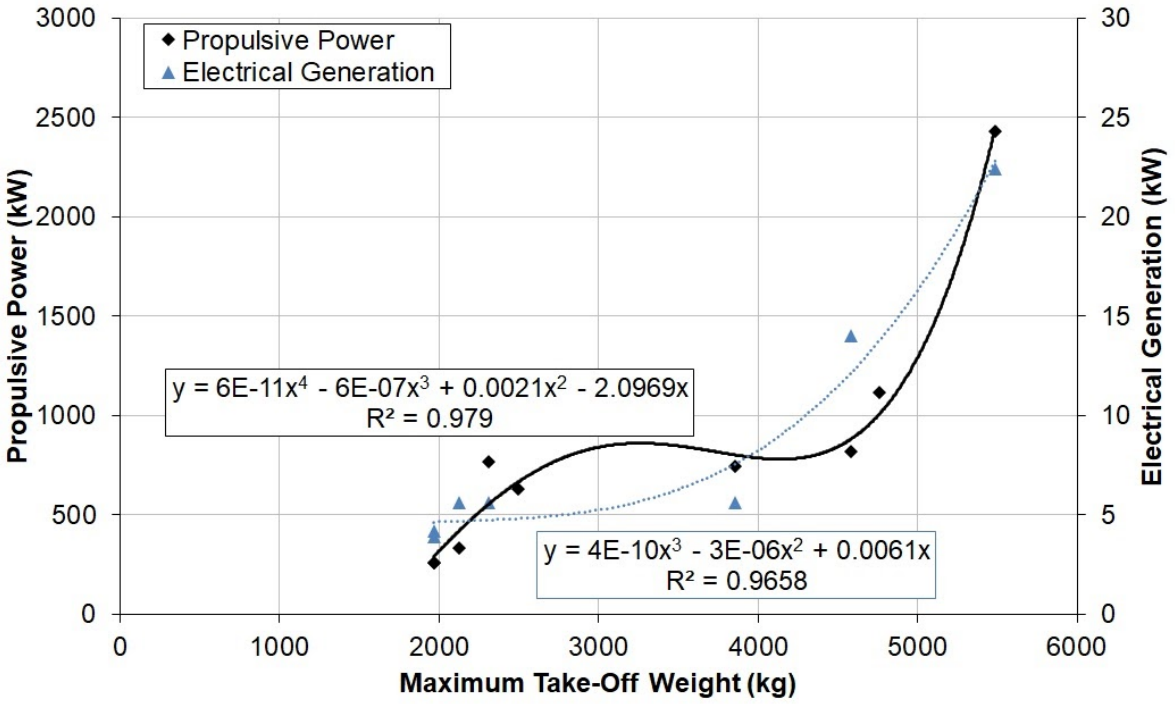

Figure A2.10: Refined correlations for existing propeller driven business aircraft

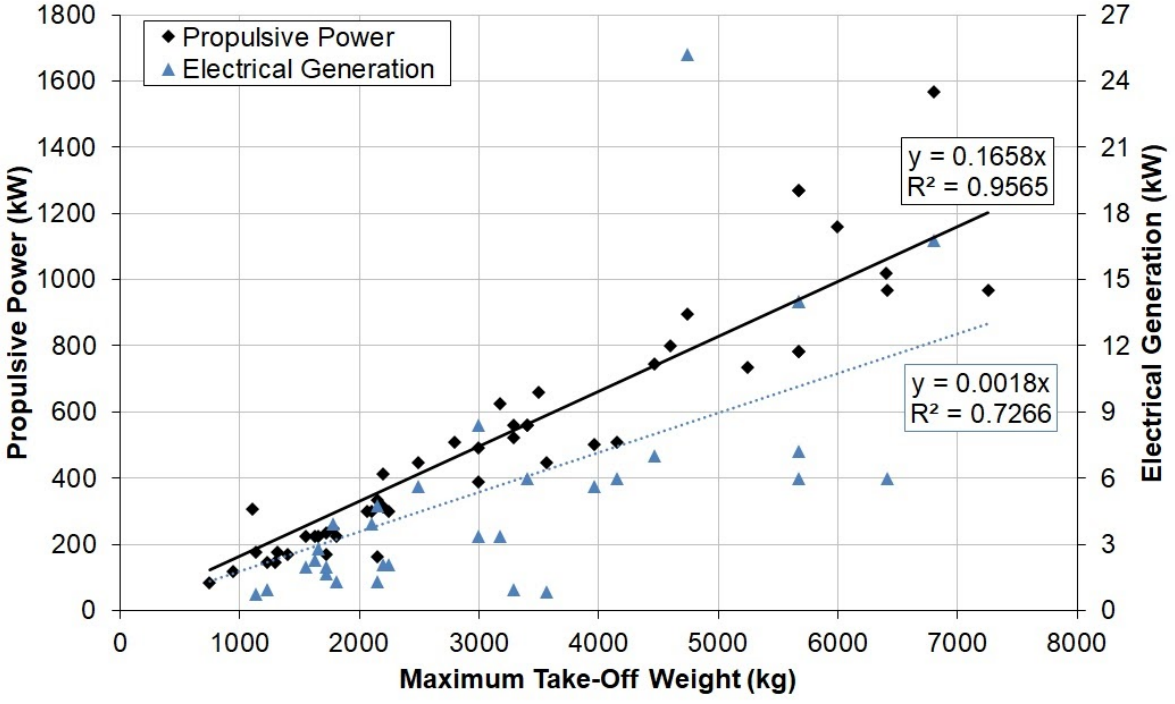

Figure A2.11: Refined correlations for existing propeller driven utility aircraft

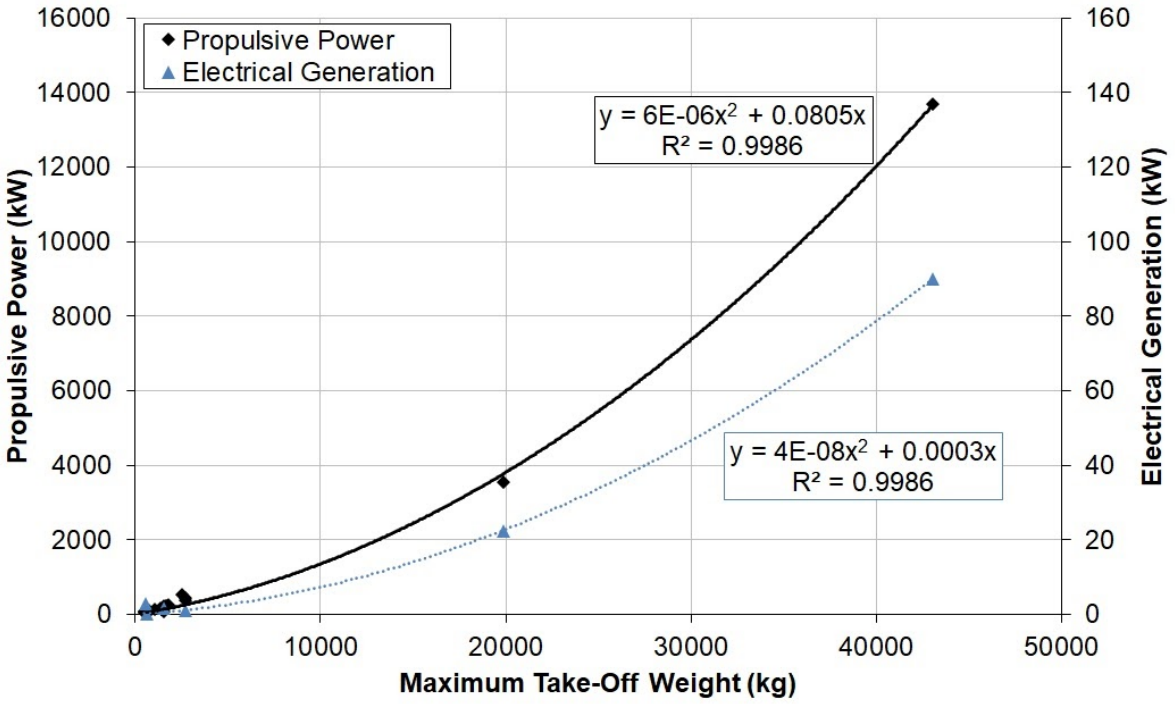

Figure A2.12: Refined correlations for existing propeller driven amphibian aircraft

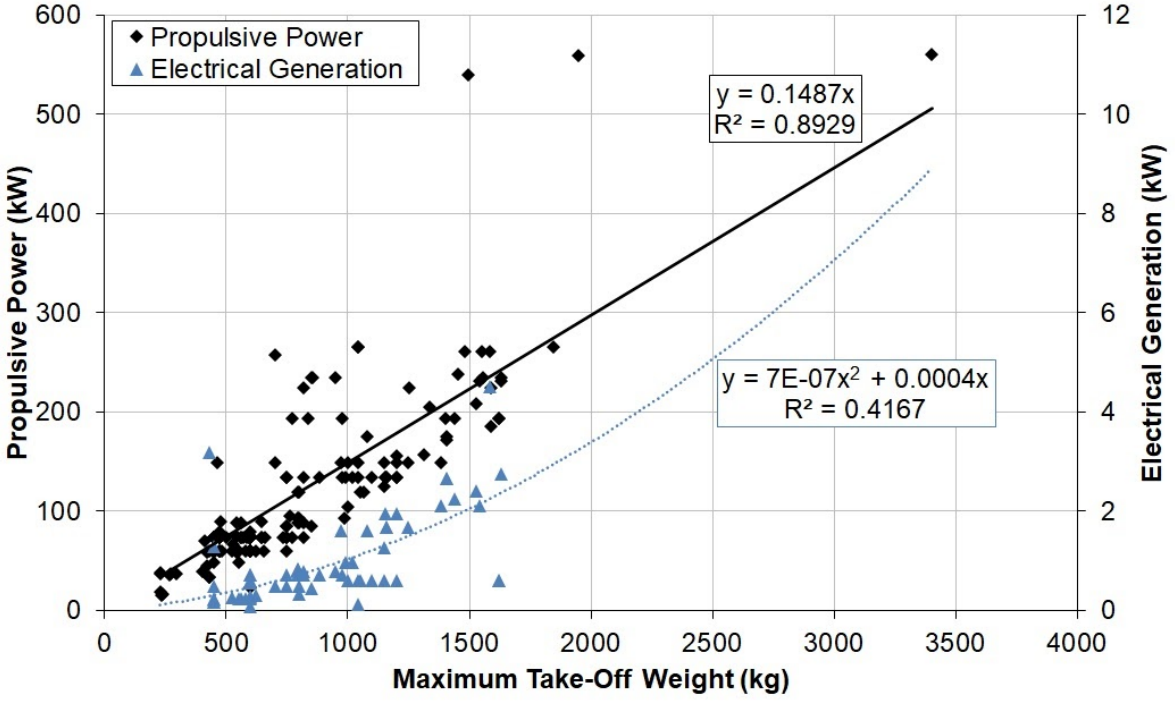

Figure A2.13: Refined correlations for existing propeller driven light aircraft

Appendix 3 - Chemical Information

A3.1 Hydrogen

Thermodynamic data from O'Hayre, R (2016)

Temperature (K)	**$\hat{g}_T$ (J/mol)**	**$\hat{h}_T$ (J/mol)**	**$\hat{s}_T$ (J/mol.K)**	**Cp_T (J/molK)**
200	-26660	-2770	119.42	27.26
220	-29070	-2220	122.05	27.81
240	-31540	-1660	124.48	28.21
260	-34050	-1090	126.75	28.49
280	-36610	-520	128.87	28.7
298	-38960	0	130.68	28.84
300	-39200	50	130.86	28.85
320	-41840	630	132.72	28.96
340	-44510	1210	134.38	29.04
360	-47220	1790	136.14	29.1
380	-49960	2380	137.72	29.15
400	-52730	2960	139.22	29.18

A3.2 Methanol

Thermodynamic data from O'Hayre, R (2016)

Liquid

Temperature (K)	**$\hat{g}_T$ (J/mol)**	**$\hat{h}_T$ (J/mol)**	**$\hat{s}_T$ (J/mol.K)**	**Cp_T (J/molK)**
298	-276370	-238500	127.19	81.59
300	-276610	-238420	127.28	81.59
400	-290560	-230260	150.75	81.59

Gas

Temperature (K)	**$\hat{g}_T$ (J/mol)**	**$\hat{h}_T$ (J/mol)**	**$\hat{s}_T$ (J/mol.K)**	**Cp_T (J/molK)**
280	-268110	-201730	237.08	42.95
298	-272440	-200940	239.81	44.04
300	-272880	-200860	240.08	44.15
320	-277710	-199960	242.97	45.46
340	-282600	-199040	245.77	46.85
360	-287540	-198090	248.49	48.31
380	-292540	-197110	251.14	49.83
400	-297590	196090	253.74	51.4

A3.3 Water

Thermodynamic data from O'Hayre, R (2016)

Liquid

Temperature (K)	**$\hat{g}_T$ (J/mol)**	**$\hat{h}_T$ (J/mol)**	**$\hat{s}_T$ (J/mol.K)**	**Cp_T (J/molK)**
273	-305010	-287730	63.28	76.1
280	-305460	-287200	65.21	75.81
298	-306690	-285830	69.95	75.37
300	-306820	-285690	70.42	75.35
320	-308270	-284180	75.28	75.27
340	-309820	-282680	79.85	75.41
360	-311460	-281170	84.16	75.72
373	-312580	-280180	86.85	75.99

Gas

Temperature (K)	**$\hat{g}_T$ (J/mol)**	**$\hat{h}_T$ (J/mol)**	**$\hat{s}_T$ (J/mol.K)**	**Cp_T (J/molK)**
280	-294720	-242440	186.73	33.53
298	-298130	-241830	188.84	33.59
300	-298480	-241770	189.04	33.6
320	-302280	-241090	191.21	33.69
340	-306130	-240420	193.26	33.81
360	-310010	-239740	195.2	33.95
380	-313940	-239060	197.04	34.1
400	-317890	-238380	198.79	34.26

A3.4 Oxygen

Thermodynamic data from O'Hayre, R (2016)

Temperature (K)	**$\hat{g}_T$ (J/mol)**	**$\hat{h}_T$ (J/mol)**	**$\hat{s}_T$ (J/mol.K)**	**Cp_T (J/molK)**
200	-41540	-2710	194.16	25.35
220	-45450	-2190	196.63	26.41
240	-49410	-1660	198.97	27.25
260	-53410	-1100	201.18	27.93
280	-57450	-540	203.27	28.48
298	-61120	0	205	28.91
300	-61540	30	205.25	28.96
320	-65660	620	207.13	29.36
340	-69820	1210	208.92	29.71
360	-74020	1810	210.63	30.02
380	-78250	2410	212.26	30.3
400	-82510	3020	213.82	30.56

A3.5 Carbon Dioxide

Thermodynamic data from O'Hayre, R (2016)

Temperature (K)	**$\hat{g}_T$ (J/mol)**	**$\hat{h}_T$ (J/mol)**	**$\hat{s}_T$ (J/mol.K)**	**Cp_T (J/molK)**
200	-436930	-396900	200.1	31.33
220	-440950	-396250	203.16	32.77
240	-445040	-395590	206.07	34.04
260	-449190	-394890	208.84	35.19
280	-453390	-394180	211.48	36.24
298	-457250	-393510	213.79	37.13
300	-457650	-393440	214.02	37.22
320	-461950	-392690	216.45	38.13
340	-466310	-391920	218.79	39
360	-470710	-391130	221.04	39.81
380	-475150	-390330	223.21	40.59
400	-479630	-389510	225.31	41.34